An Engineering Study of Key Interactions within the Process for Antibody Fragment Production

A thesis submitted to University College London for the degree of Doctor of Engineering

By

Andrew David Tustian

Department of Biochemical Engineering
University College London
Torrington Place
London
WC1E 7JE

2008

ProQuest LLC
789 East Eisenhower Parkway
P.O. Box 1346
Ann Arbor, MI 48106-1346

I, Andrew David Tustian, confirm that the work presented in this thesis is my own. Where information has been derived from other sources, I confirm that this has been indicated in the thesis.

Date..07..OCT..2008...

Abstract

This thesis illustrates the need for biologics manufacturing processes to be considered as a whole, as the operation of the upstream process can greatly alter the performance of downstream steps. It develops methods to allow this to be done at minimal cost and with the minimum requirement for process material. The industrial bioprocess for antibody fragment (Fab') production in *E. coli* is used as the case study.

Two variations of the antibody production process were examined. In the first lactose was used both to induce Fab' production and to provide the post-induction energy source. Cell growth was controlled by phosphate limitation. The second process used isopropyl β-D-1-thiogalactopyranoside (IPTG) for Fab' induction, with a glycerol feed providing energy post-induction. Both variations produced high cell density broths (ca. 20% solids w/v), and industrially relevant quantities of Fab' (ca. 1 g/L). However, the IPTG-induced fermentation was chosen for detailed study as it was the most controllable and reproducible of the two. The fermentation was investigated together with the initial unit operations of broth centrifugation, heat/chemical Fab' extraction, and spheroplast centrifugation.

Methods were developed to allow all aspects of the two centrifugation steps in the initial process to be mimicked at small-scale. Loss of cell integrity upon entry and exit to the industrial centrifuge was mimicked through the use of a rotating disc and capillary jet device respectively. Clarification was mimicked through the adaptation of an existing method to high cell density feeds (>10% w/v) by the addition of a dilution step and a mathematical correction based on the Richardson-Zaki equation. Dewatering of the solids cake was predicted to within ± 8% at small-scale using a novel method that maintains industrial spin speed, spin time, and height of the sediment cake at millilitre-scale. All small-scale methods developed were verified at pilot-scale.

The heat/chemical Fab' extraction step was mimicked in microfuge tubes. Outputs, in terms of % total protein and Fab' release, were shown to be within ± 6% of pilot-scale results in all cases tested. Any differences between pilot- and small-scale performances were shown not to be statistically significant. Product quality, as

assessed by SDS-PAGE, was shown to be very similar to pilot-scale. As the periplasmic extraction was identified as the step most detrimental to overall yield of the initial DSP the microfuge method was used in a 2-factor statistical design of experiments study to analyse the robustness of the extraction procedure.

The process was then considered as a whole. Post-induction glycerol feed rate was varied and the impacts upon subsequent processing analysed using both the methods developed and pilot-scale data. This demonstrated the usefulness and accuracy of the small-scale methods developed, and also showed that optimizing the feed rate for maximum Fab' production during fermentation did not result in optimum Fab' production after initial DSP. Instead a higher feed rate should be used to produce cells with weaker periplasmic membranes to facilitate more effective Fab' release upon heat/chemical extraction.

The thesis concludes with a discussion of the business relevance of the small-scale methods developed. Their general applicability for candidate screening, process development and process understanding is suggested, and the regulatory issues relevant to their use are explored.

Acknowledgements

Firstly I would like to thank my academic supervisor Nigel Titchener-Hooker, my industrial supervisor Leigh Bowering, and my academic advisor Frank Baganz for their help and advice throughout the project.

During my doctorate I have also received much help and support from the whole Biochemical Engineering Department at UCL. Specific acknowledgement to Mike Hoare, Inass Hassan and Michael Rose for help with the USD and pilot-scale comparison work; Steve Doig, Jonny Betts, Jean Aucamp, Samir Ujam, Alex Berrill and Balasundarum Bangaru for assistance with fermentation operation and sterilisation; Ioannis Papantoniou for the CFD data; and Gareth Mannell and Andy Tait for their enthusiastic help in general matters concerning the pilot plant.

Special thanks also must go to my student Shahrukh Shiraz for his help with periplasmic extraction unit operation studies, through the Nuffield Bursary scheme.

Financial support from UCB and the Engineering and Physical Sciences Research Council (EPSRC) under the Innovative Manufacturing Research initiative is gratefully acknowledged.

Table of Contents

Abstract 3
Acknowledgements 5
Table of Contents 6
List of figures 14
List of tables 19
Nomenclature 20
1. Introduction 23
1.1 Project significance 23
1.2 Antibodies and antibody fragments 24
1.2.1 Biological function of antibodies 24
1.2.2 Antibody structure 25
1.2.3 Antibodies in biotechnology 28
1.2.4 Biotechnological applications of antibodies and antibody fragments 31
1.2.5 Biotechnological production of antibodies and antibody fragments 33
1.3 Production and purification of Fab' in *E. coli* 37
1.3.1 The upstream process - *E. coli* fermentation strategies relevant to antibody fragment production 37
1.3.1.1 High cell-density culture of E coli 37
1.3.1.2 Increasing recombinant protein production in E. coli 39
1.3.2 The downstream process – purification strategies relevant to antibody fragment production in *E. coli* 42
1.3.2.1 Separation of biomass 43
1.3.2.1.1 Centrifugation 43
1.3.2.1.2 Microfiltration 46
1.3.2.1.3 Expanded bed chromatography 47
1.3.2.2 Release of product from biomass 47
1.3.2.2.1 Mechanical cell disruption 47
1.3.2.2.2 Periplasmic extraction 48
1.3.2.3 Purification, finishing and formulation 49
1.3.2.3.1 Purification 49
1.3.2.3.2 Finishing/viral clearance 50
1.3.2.3.3 Formulation 50

1.3.3 Whole process considerations 50
1.3.4 UCB protocol for purification of A33 Fab' 51
1.4 Techniques for rapid process evaluation and interaction analysis 52
1.4.1 Ultra scale-down (USD) methodology 52
1.4.2 Computer modelling 53
1.4.2.1 Process modelling 54
1.4.2.2 Decisional tools 54
1.4.3 Statistical design of experiments (DoE) 54
1.5 Project objectives 56
1.6 Thesis layout 56
2. Materials and methods 59
2.1 Materials 59
2.1.1 Chemicals 59
2.1.2 *Escherichia coli* strain and plasmid 59
2.1.3 *Saccharomyces cerevisiae* 59
2.2 Fermentation methods 59
2.2.1 Culture media 59
2.2.1.1 2xPY complex media 59
2.2.1.2 SM6F defined media 59
2.2.1.3 SM6G$_c$ defined media 60
2.2.1.4 100 x SM6 trace elements solution 60
2.2.2 Lactose-induced fermentations 60
2.2.2.1 Inoculum preparation 60
2.2.2.3 75 L lactose fermentation 60
2.2.3 IPTG-induced fermentations 61
2.2.3.1 Inoculum preparation 61
2.2.3.2 75 L IPTG fermentation 61
2.2.3.3 20 L IPTG fermentation 62
2.3 Downstream processing 62
2.3.1 Centrifugation 62
2.3.1.1 Pilot-scale disc-stack centrifugation 62
2.3.1.2 Pilot-scale advanced tubular-bowl centrifugation 63
2.3.2 Pilot-scale periplasmic extraction 63
2.4 USD methods 64
2.4.1 USD assessment of centrifugal entry damage 64

2.4.2 USD assessment of centrifugal exit damage 64
2.4.2.1 Sample preparation 64
2.4.2.2 USD exit damage assessment 65
2.4.2.3 Assessment of complete cell breakage 65
2.4.3 USD centrifugal clarification 65
2.4.3.1 Wet solids content determination 65
2.4.3.2 Sample preparation – USD method for dilute suspensions 66
2.4.3.3 Sample preparation – USD method for high solids suspensions 66
2.4.3.4 Clarification test 66
2.4.4 USD dewatering prediction 67
2.4.5 USD periplasmic extraction 67
2.5 Production of A33 Fab' standard 68
2.6 Analytical methods 69
2.6.1 Particle size distribution data 69
2.6.2 Metabolite analysis 69
2.6.3 Protein G HPLC assay for Fab' quantification 70
2.6.3.1 Sample preparation 70
2.6.3.1.1 Total fermentation samples 70
2.6.3.1.2 Periplasmic fermentation samples 70
2.6.3.1.3 Supernatant fermentation samples 71
2.6.3.2 Fab' quantification 71
2.6.4 Determination of total protein concentration 71
2.6.5 Viscosity measurements 72
2.6.6 Determination of biomass 72
2.6.6.1 Optical density (OD_{600}) 72
2.6.6.2 Dry cell weight (DCW) 72
2.6.7 Total sample disruption 72
2.6.7.1 Homogenisation of E. coli cells 72
2.6.7.2 Sonication of E. coli spheroplasts 73
2.6.8 SDS-PAGE 73
2.6.9 Numeration of colony forming units 73
2.6.10 Cell damage analysis using flow cytometry 73
2.7 Computational methods 74
2.7.1 CFD analysis 74
2.7.2 Statistical design of experiments 75

2.7.3 Creation of process model 75

3. Choice, characterisation and analysis of upstream process for production of antibody fragments 76

3.1 Abstract 76

3.2 Introduction 77

3.3 Results and discussion 79

3.3.1 Large pilot-scale process exploratory studies 79

3.3.1.1 Large pilot-scale process exploratory studies – the lactose-induced process 79

3.3.1.2 Large pilot-scale process exploratory studies – the IPTG-induced process 81

3.3.1.3 Discussion of 75 L fermentations and choice of upstream process case study 83

3.3.2 IPTG-induced process characterisation at 20 L scale 84

3.3.3 Investigation of upstream critical process parameter: post-induction carbon feed rate 89

3.4 Conclusions 94

4. Evaluation of centrifugation-induced cell damage 96

4.1 Abstract 96

4.2 Introduction 97

4.2.1 Performance indicators of centrifugal unit operations 97

4.2.2 Centrifugation-induced cell damage 97

4.2.2.1 Cell damage during separation 98

4.2.2.2 Cell damage during centrifugal exit 100

4.2.3 Quantifying cell damage 101

4.3 Theoretical considerations 102

4.3.1 Consideration of centrifugal entry damage 102

4.3.1.1 Maximum energy dissipations in industrial centrifuges 102

4.3.1.2 Maximum energy dissipations in USD rotating disc device 103

4.3.1.2 Residence time 105

4.3.2 Consideration of centrifugal exit damage 105

4.3.2.1Exit damage in pilot-scale disc-stack centrifuge 105

4.3.2.2 Forces generated in mimic 107

4.3.2.3 Impact effects 108

4.3.3 Assessment of cell damage 109

4.4 Results and discussion 110
4.4.1 Consideration of centrifugal entry damage 110
4.4.1.1 CFD of rotating disc shear device 110
4.4.1.2 Assessing the shear sensitivity of pre-extraction E. coli cells 111
4.4.2 Consideration of centrifugal exit damage 111
4.5 Conclusions 118
5. Ultra scale-down methodology for predicting the centrifugal separation behaviour of high cell density cultures 119
5.1 Abstract 119
5.2 Introduction 119
5.3 Theoretical considerations 121
5.3.1 USD centrifugation theory 121
5.3.2 Compensation for entry zone shear forces 123
5.3.3 Settling of high cell density cultures 123
5.3.4 Correcting sedimentation rate for the effect of suspended particle concentration 124
5.3.5 Proposed generic USD methodology 126
5.4 Results and discussion 126
5.4.1 Method verification using high cell density *E. coli* fermentations 126
5.4.2 Method verification using Baker's Yeast 130
5.5 Conclusions 132
6. Ultra scale-down approach for predicting the dewatering of cellular sediments in industrial centrifuges 133
6.1 Abstract 133
6.2 Introduction 133
6.3 Theoretical considerations 135
6.3.1 Factors affecting centrifugal dewatering 135
6.3.1.1 Spin Time and Spin Speed 135
6.3.1.2 Sediment height 136
6.3.1.3 Feed properties and the effects of shear 137
6.3.1.4 Other factors 138
6.3.2 Definition and assessment of dewatering 138
6.3.3 The effect of shape on maximal levels of dewatering 138
6.4 Results: method development 139
6.4.1 Preparation of feed material 139

6.4.2 Determination of dry mass content of cells 140
6.4.3 Baker's Yeast studies 140
6.4.4 *E. coli* pre- and post-extraction studies 143
6.5 Generic USD method 147
6.6 Results: method verification 149
6.6.1 Preparation of feed material 149
6.6.2 Performance of USD mimic for the Baker's Yeast cells 150
6.6.3 Performance of USD mimic for pre-extraction *E. coli* cells 150
6.6.4 Performance of USD mimic for post-extraction *E. coli* cells 153
6.7 Discussion 153
6.7.1 Wider application of the proposed USD method 153
6.7.2 Relating the experimental levels of dewatering obtained to theoretical maximum packing densities 153
6.8 Conclusions 155
7. Periplasmic extraction characterisation and scale-down 157
7.1 Abstract 157
7.2 Introduction 157
7.3 Results and discussion 160
7.3.1 Creation of USD mimic of extraction unit operation 160
7.3.1.1 Calibration of USD equipment 161
7.3.1.2 Verification of USD methodology 161
7.3.1.3 Product quality variations between pilot and USD extractions 166
7.3.2 Identification of critical process parameters in the periplasmic extraction unit operation 167
7.4 Conclusions 172
8. Case study of the use of USD methods to gain whole process information: The effect of post-induction carbon feed rate on yield after initial DSP in the antibody fragment production process 174
8.1 Abstract 174
8.2 Introduction 174
8.3 Results and discussion 175
8.3.1 Overview of pilot and USD process flowsheets 175
8.3.2 Fermentation unit operation 178
8.3.3 Centrifugal cell harvest 179
8.3.3.1 Pilot-scale prediction of clarification efficiency 179

8.3.3.2 USD prediction of clarification efficiency 179
8.3.3.3 Interaction between USP and yield during cell harvest 179
8.3.4 Periplasmic extraction 184
8.3.4.1 Pilot-scale prediction of extraction efficiency 184
8.3.4.2 USD prediction of extraction efficiency 185
8.3.4.3 Interaction between USP and yield during periplasmic extraction 185
8.3.5 Centrifugal spheroplast removal 186
8.3.5.1 Pilot-scale prediction of centrifugal dewatering efficiency 186
8.3.5.2 USD prediction of centrifugal dewatering efficiency 187
8.3.3.3 Interaction between USP and yield during spheroplast removal 187
8.3.6 Interaction between post-induction carbon feed rate and product yield after initial DSP 191
8.4 Conclusions 193
9. Discussion of cryopreservation as a mechanism of long-term storage of upstream cell material for later downstream process development 195
9.1 Abstract 195
9.2 Introduction 195
9.2.1 Motivation for assessment of cryopreservation as a mechanism of long-term storage of upstream cell material 195
9.2.2 Mechanisms of cell damage during freezing 196
9.2.3 Determinants of the extent of cell damage induced by a freeze-thaw cycle 197
9.2.4 Freeze-thaw issues specific to industrial process under consideration . 199
9.2.5. Flow cytometry as a method for assessing bacterial cell damage 200
9.3 Results and discussion 201
9.3.1 Flow cytometry controls 201
9.3.2 Assessment of freeze/thaw protocol to IPTG-induced process 203
9.3.3 Cryopreservation protocol optimisation studies 204
9.4 Conclusions 211
10. Conclusions and future work 212
10.1 Conclusions 212
10.2 Future work 216
10.2.1 Extend USD process coverage 216
10.2.2 Increase understanding of the periplasmic extraction unit operation 216
10.2.3 Further cryopreservation work 216

10.2.4 Increase small-scale throughput 217
11. EngD requirements: Bioprocess management and regulatory implications of USD technology 218
11.1 Introduction 218
11.2 Commercial and management relevance of USD methodology 218
11.2.1 Traditional pharmaceutical process development 218
11.2.2 Current challenges in bioprocess development 219
11.2.3 The role of increased process optimisation 219
11.2.4 Strategies for applying USD methodologies during bioprocess development 220
11.2.4.1 USD methodology for pre-pilot plant studies 220
11.2.4.2 USD methodology for increased process understanding 221
11.3 Validation and regulatory issues 223
11.3.1 General validation strategies 223
11.3.1.1 Stage 1: process pre-qualification 224
11.3.1.2 Stage 2: manufacturing qualification 224
11.3.1.3 Stage 3: life-cycle qualification 224
11.3.2 Facilitation of validation by USD methodology 225
11.3.3 Validation of USD methodology 225
11.4 Conclusions 225
12. References 227
Appendix A1: Bacterial growth rate calculations 252
Appendix A2: Relative centrifugal force 254
Appendix A3: MATLAB code and curve-fit equations used to create process model 255
Appendix A4: Publication 262
Appendix A5: Conference Presentations 270

List of figures

Fig. 1-1: 3D Protein Strucuture of IgG2a Murine Antibody 26
Fig. 1-2: Schematic diagram of an Ig monomer. 28
Fig. 1-3: Examples of antibody-based constructs and respective routes for their generation. 30
Fig. 1-4: Outline of the liquid flow direction and form of a typical disc-stack centrifuge 44
Fig. 1-5: Outline of the liquid flow direction and form of a typical tubular bowl centrifuge 45
Fig. 1-6: Mechanism of action of a multi-chamber bowl centrifuge 46
Fig. 1-7: Overview of process used for producing A33 antibody fragments in *E. coli*.. 52
Fig. 3-1: Data from 75L pilot scale run of the lactose-induced fermentation. 80
Fig. 3-2: Metabolite levels in the external medium during the time course of the lactose-induced fermentation 80
Fig. 3-3: Fab' production and compartmentalisation during the induction period of the lactose-induced fermentation 81
Fig. 3-4: Data from 75L pilot scale run of the IPTG-induced fermentation 82
Fig. 3-5: Fab' production and compartmentalisation during the induction period of the IPTG-induced fermentation 83
Fig. 3-6: Data from 20L pilot scale run of the IPTG-induced fermentation 86
Fig. 3-7: Online measurements of OUR, CER and RQ from 20L pilot scale run of the IPTG-induced fermentation 87
Fig. 3-8: Correlation between OD_{600} and DCW prior to induction 87
Fig. 3-9: Correlation between OD_{600} and DCW post-induction 88
Fig. 3-10: Fab' production and compartmentalisation during the induction period of the 20 L IPTG-induced fermentation. 88
Fig. 3-11: Total Fab' production during the induction period of five 20 L IPTG-induced fermentations 90
Fig. 3-12: Supernatant Fab' production during the induction period of five 20 L IPTG-induced fermentations 91
Fig. 3-13: Periplasmic (internal) Fab' concentrations during the induction period of five 20 L IPTG-induced fermentations 91

Fig. 3-14: The effect of post-induction carbon feed upon Fab' production and compartmentalisation 36 h after induction 92
Fig. 3-15: Fab' production and compartmentalisation during the induction period of a 20 L IPTG-induced fermentation 92
Fig. 4-1: Rotating disc shear device used to mimic centrifugal entry shear in the thesis 99
Fig. 4-2: Schematic diagram of the capillary device used to mimic centrifugal exit shear in the thesis 102
Fig. 4-3: Schematic representation of a typical fluid stream exiting from a capillary nozzle 109
Fig. 4-4: Comparison of maximum energy dissipations found in the rotating disc shear device 110
Fig. 4-5: The effect of similar energy dissipation rates to that found in the entry zone of industrial centrifuges upon cell integrity 113
Fig. 4-6: The effect of similar energy dissipation rates to that found in the entry zone of industrial centrifuges upon periplasmic integrity 113
Fig. 4-7: The effect of ejection speed from the small-scale capillary device upon the % of total protein lost to the extracellular medium after small-scale periplasmic extraction 114
Fig. 4-8: The effect of ejection speed from the small-scale capillary device upon the % of total Fab' present in the extracellular medium after small-scale periplasmic extraction 114
Fig. 4-9: The effect of ejection speed from the small-scale capillary device upon the % of total protein lost to the extracellular medium after small-scale periplasmic extraction 115
Fig. 4-10: The effect of ejection speed from the small-scale capillary device upon the % of total Fab' present in the extracellular medium after small-scale periplasmic extraction 115
Fig. 4-11: The effect of ejection speed from the small-scale capillary device upon the % of total protein lost to the extracellular medium after small-scale periplasmic extraction 116
Fig. 4-12: The effect of ejection speed from the small-scale capillary device upon the % of total Fab' present in the extracellular medium after small-scale periplasmic extraction 116

Fig. 5-1: Clarification plotted against equivalent flowrate/settling area for *E. coli* cells obtained with a specific growth rate of 0.0026 h^{-1} after induction 127
Fig. 5-2: Cumulative particle size distributions of *E. coli* cells..... 128
Fig. 5-3: Clarification plotted against equivalent flowrate/settling area for *E. coli* cells obtained with a specific growth rate of 0.0037 h^{-1} after induction 129
Fig. 5-4: Clarification plotted against equivalent flowrate/settling area for *E. coli* cells obtained with a specific growth rate of 0.0044 h^{-1} after induction 130
Fig. 5-5: Clarification plotted against equivalent flowrate/settling area for Baker's Yeast cells 131
Fig. 5-6: Cumulative particle size distributions of resuspended Baker's Yeast cells... 131
Fig. 6-1: Examples of calculations of sediment height for a variety of industrial and laboratory centrifuges..... 137
Fig. 6-2: The effect of spin time upon % dewatering and % clarification for Baker's Yeast..... 141
Fig. 6-3: The effect of RCF upon % dewatering for Baker's Yeast 142
Fig. 6-4: The effect of sediment height upon % dewatering for Baker's Yeast 142
Fig. 6-5: The cumulative size distribution on volume basis of *E. coli* 145
Fig. 6-6: The effect of spin time upon % dewatering 145
Fig. 6-7: The effect of RCF upon % dewatering 146
Fig. 6-8: The effect of sediment height upon % dewatering 146
Fig. 6-9: Proposed generic USD methodology for predicting industrial-scale dewatering. 148
Fig. 6-10: Successful prediction of the dewatering performance of the Carr Powerfuge™ P6 with Baker's Yeast 150
Fig. 6-11: Parity plot comparing USD dewatering performance with that of the Carr Powerfuge P6 with pre- and post-extraction *E. coli*..... 152
Fig. 7-1: Structure of a generic lipopolysaccharide of gram-negative bacteria..... 158
Fig. 7-2: Photographic reproduction of the Eppendorf Thermomixer R 160
Fig. 7-3: Parity plot illustrating the equivalence of the actual temperature in microfuge tubes incubated in the Eppendorf Thermomixer R with the set-point, at a broad range of temperatures..... 162
Fig. 7-4: Parity plot illustrating the equivalence of the actual temperature in microfuge tubes incubated in the Eppendorf Thermomixer R with the set-point, at around the standard temperature at which the extraction is performed (60°C)..... 162

Fig. 7-5: Protein release over time for thawed resuspended *E. coli* cells incubated at 60°C in a 3 L vessel and an Eppendorf Thermomixer R 163
Fig. 7-6: Fab' release over time for thawed resuspended *E. coli* cells incubated at 60°C in a 3 L vessel and an Eppendorf Thermomixer R 164
Fig. 7-7: Protein release over time for thawed resuspended *E. coli* cells incubated at 60°C in a 20 L vessel and an Eppendorf Thermomixer R 165
Fig. 7-8: Fab' release over time for thawed resuspended *E. coli* cells incubated at 60°C in a 20 L vessel and an Eppendorf Thermomixer R 166
Fig. 7-9: Non-reducing 8-16 % SDS-PAGE gel showing protein profile of periplasmic extractions performed using a variety of pilot and USD equipment 169
Fig. 7-10: Half-normal plot illustrating the critical process parameters affecting the level of total protein found in the extracellular medium after extraction. 171
Fig. 7-11: Half-normal plot illustrating the critical process parameters affecting the amount of Fab' found in the extracellular medium after extraction. 172
Fig. 8-1: Process flowsheet for initial DSP of antibody fragment production in *E. coli*. 177
Fig. 8-2: The effect of post-induction carbon feed upon Fab' production and compartmentalisation 36 h after induction 178
Fig. 8-3: Clarification plotted against equivalent settling area for *E. coli* cells harvested in the disc stack centrifuge after fermentations 181
Fig. 8-4: Clarification plotted against predicted equivalent settling area for *E. coli* cells analysed by the adapted USD clarification method after fermentations 183
Fig. 8-5: Clarification levels during cell harvest at a fixed equivalent settling area of 1.1×10^{-8} m/s 184
Fig. 8-6: Efficiency of periplasmic extraction unit operation in terms of % total Fab' released into the cellular media after extraction 186
Fig. 8-8: % Dewatering during centrifugal spheroplast removal at constant compaction time, sediment height and RCF 190
Fig. 8-9: Yield during centrifugal spheroplast removal at constant compaction time, sediment height and RCF 190
Fig. 8-10: The variation in Fab' yield at different post-induction carbon feed rates at harvest and after initial downstream processing, as indicated by pilot-scale and USD data 191
Fig. 9-1: Control samples illustrating functionality of flow cytometric method used.. 202

Fig. 9-2: Schematic of flow cytometry spectrograph showing the different categories of cell population that can be identified by PI and BOX. 203
Fig. 9-3: PI/BOX stained flow cytometry spectrograph indicating physiological state of cells from the IPTG-induced process at harvest and after a freeze/thaw cycle. ... 205
Fig. 9-4: Survival of cells frozen under a variety of conditions in mid-growth and stationary phase, determined by dilution plating. 207
Fig. 9-5: Survival of cells frozen under a variety of conditions in mid-growth and stationary phase, determined by PI/BOX multi-parameter flow cytometry. 208
Fig. 9-6: Representative PI/BOX stained flow cytometry spectrographs indicating physiological state of mid-growth phase cells frozen under conditions detailed in Table 9-2. 209
Fig. 9-7: Representative PI/BOX stained flow cytometry spectrographs indicating physiological state of stationary phase cells frozen under conditions detailed in Table 9-2. 210
Fig. 11-1: USD allows bioprocess development to begin earlier in the discovery process 221
Fig. 11-2: Illustration of the creation of design space from process characterisation studies 222
Fig. A1-1: The determination of the initial growth rate as part of the IPTG-induced process characterisation 253
Fig. A5-1: Poster presented at 2nd Singapore Biologics Manufacturing Conference' and the 'Society of Biological Engineering's First Conference on Accelerating Biopharmaceutical Development 271
Fig. A5-2: Poster presented at the 'Annual bioProcessUK Conference 2006' 272

List of tables

Table 1-1: Function of the five different antibody isotypes found in vertebrates. 25
Table 1-2: FDA approved monoclonal antibody therapies. 32
Table 1-3: Examples of nutrients that inhibit *E. coli* growth when present in high concentrations 38
Table 1-4: Feeding methods in fed-batch culture 39
Table 3-1: Post-induction growth rates of the five 20 L fermentations undertaken to investigate the effect of post-induction carbon feed rate. 89
Table 4-1: Discharge velocities at shear rates of CSA-1 disc-stack centrifuge at a range of spin speeds 106
Table 4-2: Features of the CSA-1 disc-stack centrifuge 106
Table 4-3: Exit velocities and residence times used in capillary device 108
Table 6-1: Successful prediction of the dewatering performance of the Carr Powerfuge P6 with pre- and post-extraction *E. coli* 152
Table 6-2: Comparison of the maximal lattice and maximal random jammed (MRJ) packing densities for shapes of the cells 156
Table 7-1: Comparison of the performance of the USD mimic with pilot-scale extraction in the 20 L vessel with three different *E. coli* cell populations. 168
Table 7-2: Input variables and corresponding high/low limits used for 2-factor DoE study of periplasmic extraction process robustness 170
Table 8-1: The material savings allowed by the USD methods 192
Table 9-1: The percentage of total cells within each of the five cell sub-population boundaries defined in Fig. 9-2 for the fermentation endpoint and freeze/thawed samples. 206
Table 9-2: Conditions used in cryopreservation protocol optimisation studies. 206

Nomenclature

A	Absorbance
B	Cell number
B_0	Cell number at time zero
B_L	Caulk width (m)
$\%C$	Percentage clarification
c	Fab' concentration (mg/mL)
c_{IS}	Sigma value correction factor for an industrial-scale disc-stack centrifuge
c_{USD}	Sigma value correction factor for an ultra scale-down laboratory centrifuge
D	Solids concentration in sedimented paste, level of dewatering
$\%D$	The percentage of solids in the sedimented paste
D_{noz}	Nozzle depth (m)
d_p	Particle size (m)
dw_r	Dry weight to wet weight ratio of a particular cell type
DCW	Dry cell weight (g/L)
DW_{sed}	Weight of solids paste removed from a centrifuge when dried to a constant weight (g)
F	Fractional recovery of solids
f_l	Correction factor for spacer caulks
g	Gravitational acceleration ($m.s^{-2}$)
l	Length of light path (cm)
Lc	Capillary length (m)
N	Rotational speed (rps)
n	Slope obtained from a plot of log U versus log ε
n_d	Number of active discs
OD_f	Optical density of the feed (@ 600 nm)
OD_r	Optical density of the well-spun reference (@ 600 nm)
OD_s	Optical density of the supernatant (@ 600 nm)
P	Power input (W)
P_d	Discharge pressure (Pa)

$p_{(x)}$	The drag force exerted on the particles by the upward flow of liquid through the settled solids at position 'x' (N)
Q	Volumetric flow rate ($m^3.s^{-1}$)
Q_c	Volumetric flow rate through the capillary ($m^3.s^{-1}$)
r_1	Inner disc radius (m)
r_2	Outer disc radius (m)
r_l	Radius of the inner liquid ring (m)
R_c	Capillary radius (m)
R_i	Distance between the centre of rotation and the top of the liquid in a laboratory centrifuge (m)
R	Disc radius (m)
R_o	Distance between the centre of rotation and the bottom of the tube in a laboratory centrifuge (m)
Re_p	Particle Reynolds number
RT	Residence time in capillary (s)
t	Time (h)
t_d	Generation or doubling time (h)
T	Applied torque ($kg\ m^2\ s^{-2}$)
T_l	Total liquid proportion in the feed
T_s	Total solids proportion in the feed
$t_{95\%}$	Time taken for 95% clarification to be achieved in the laboratory centrifuge (s)
t_{comp}	Time for compaction (s)
$t_{compUSD}$	Time for compaction in USD mimic (s)
t_{delay}	Time centrifuge is spun with a full bowl prior to solids ejection (s)
t_{total}	Total laboratory centrifuge set time (s)
t_{USD}	Residence time in the ultra scale-down laboratory centrifuge (s)
U	Settling velocity of suspension ($m.s^{-1}$)
U_t	Settling velocity at $\varepsilon = 1$
V	Volume of process material in a laboratory tube (m^3)
V_s	Solids holding capacity of centrifuge bowl (m^3)
V_{bl}	Volume of the laminar flow boundary layer (m^3)
v	Discharge velocity (m/s)

v_∞	Tangential tip velocity (m/s)
WW_{sed}	Weight of the solids paste recovered from a centrifuge (g)
x	Chapters 4 and 5: Fractional time for acceleration of the laboratory centrifuge Elsewhere: Post-induction glycerol feed rate during fermentation (mL h^{-1} L^{-1})
X	The distance from the edge of the rotating disc (m)
X_i	Operator set plunger drive speed (m/s)
X_b	Jet break up point
X_c	Jet core zone
y	Fractional time for deceleration of the laboratory centrifuge
Z_L	Number of caulks on a disc

Greek letters

Σ	Centrifuge equivalent settling area (m^2)
δ	Laminar flow boundary layer over a rotating disc (m)
ε	Chapter 2 : Extinction coefficient (mg^{-1} mL cm^{-1}) Elsewhere : Voidage
ε_{max}	Maximum energy dissipation (W/kg)
μ	Chapter 3 and Appendix: Specific growth rate (h^{-1}) Elsewhere: Fluid viscosity (Pa.s)
φ	Cellular solids fraction
ρ	Density ($kg.m^{-3}$)
ρ_f	Fluid density ($kg.m^{-3}$)
θ	Half disc angle
ω	Angular velocity ($rad.s^{-1}$)
ϕ	Volumetric solids fraction entering the bowl
τ_{max}	Maximum shear stress (Pa)

1. Introduction

An industrial biopharmaceutical process for the production of antibody fragments in *E. coli* has been studied and a complete small-scale process mimic of the initial downstream process (DSP) generated. Its ability to provide process insights with only millilitres of material is demonstrated by its application to quantify interactions between the upstream and downstream process.

1.1 Project significance

The goal of biopharmaceutical process development is to design and test a production process that can economically, rapidly and robustly produce a drug entity of consistent high quality. This must be done at minimal cost while at sufficient speed to keep process development off the critical path to market as far as possible (Hausner, 1998; Levin and Papageorgiou, 2004). Drivers for these goals arise from the demands of governments and health care providers for lower drug prices, increasing global competition, and the rapid onset of generic biopharmaceuticals (Shah, 2004). Furthermore, regulatory authorities such as the U.S. Food and Drug Administration (FDA) are increasing pressure on the biopharmaceutical industry to understand fully their processes and for early stage material to be closer in quality to that of final manufacture (Nail and Searles, 2008; U.S. Food and Drug Administration, 2006; Yu, 2006). The thesis developed here is that careful consideration of not just individual unit operations, but also of the interactions between multiple unit operations, is necessary to understand a process fully. This knowledge will aid both regulatory approval and economic process design. Ultra scale-down (USD) methodology is developed and demonstrated as a tool to achieve rapidly the data necessary to fulfil this aim whilst minimising the use of process material, which is usually in short supply early in the development train.

A system for the production of recombinant antibody fragments has been chosen as the case study due to their extreme importance to the biopharmaceutical sector. At the time of writing, 21 monoclonal antibody FDA-approved therapies exist, mainly targeted towards oncology and immunological targets, and this number is likely to increase in the following years as antibody based therapies currently dominate the biologics drug discovery pipeline. There are currently > 200 antibody products undergoing clinical

trials (Low et al., 2007). These constitute 20-30% of all biopharmaceutical products currently in development (Glennie and Johnson, 2000; Roque et al., 2004). The organism used for antibody fragment production in this work is the bacterium *E. coli*. The high cell densities (~ 20% wet w/v) produced by this system creates an additional challenge during cell harvesting and initial downstream processing operations.

The following section (1.2) provides general theory about antibodies and antibody fragments, describing their structure, function, biotechnological applications, and the production methods used. This is followed by a discussion of strategies for the upstream production and downstream purification of antibody fragments in *E. coli*, with focus on the fermentation and primary recovery steps that are the subject of this thesis (1.3). Section 1.4 introduces the scale-down, statistical and computational techniques that are being developed to enable more rapid, economical and thorough bioprocess development. Finally, the main thesis goals and aims are presented (1.5) and an overview of the thesis layout is given (1.6).

1.2 Antibodies and antibody fragments

1.2.1 Biological function of antibodies

Antibodies are a major protein component of the vertebrate adaptive immune system. This system can be roughly divided into two types of immunity. Cellular immunity is mediated by T lymphocytes or T cells (so called because their development occurs in the thymus). This system guards against intracellular pathogens such as viruses and some bacteria, and threats such as fungi, parasites, cancerous cells, and foreign tissue. In contrast, humoral immunity is mediated by the group of proteins of interest: antibodies. Antibodies are also known as immunoglobulins. This protein group is produced by B lymphocytes or B cells (so called as they mature in the bone marrow). Humoral immunity is most effective against bacterial infections and the extracellular phases of viral infection (Voet and Voet, 1995).

Antibodies fulfil their biological function by specifically binding to pathogenic or foreign material. Each antibody can bind a particular target, called its antigen, with great specificity and strength. Antibodies can bind their targets with affinities between 10^8 and 10^{11} M^{-1}. Once bound to the target antigen, antibodies contribute to immunity in three main ways, depending on the antibody isotype. Firstly, they can halt pathogens from entering or damaging host cells by binding to them and blocking contact with cells

and tissues. This structural mode of action is known as neutralization. Secondly, they can trigger the pathogen's destruction by activating the complement pathways (Ravetch and Bolland, 2001). Thirdly, they can coat the pathogen and trigger a range of effector functions such as phagocytosis by phagocytes, degranulation by mast cells and neutrophils, and release of cytokines and cytotoxic molecules by natural killer cells (Janeway et al., 2001). The appropriate immune mechanisms for distinct pathogens are selected by the isotype of antibody.

Human antibodies come in five different isotypes or classes: IgA, IgD, IgE, IgG, and IgM. These are described in Table 1-1. There are also four further subclasses of IgG and two of IgA. Although different isotypes have different effector functions and biological functions, mediated by differences in the struture of specific constant region of the protein, they all bind antigens in the same way and share a common immunoglobulin fold.

Table 1-1: Function of the five different antibody isotypes found in vertebrates.

Isotype	Function	No. of Ig monomers
IgA	Prevents colonization of mucosal zones by pathogens (Underdown and Schiff, 1986)	Two (dimer)
IgD	Functions mainly as an antigen receptor on B cells (Geisberger et al., 2006)	One (monomer)
IgE	Protects against parasitic worms. Also has a role in allergy by binding to allergens and inducing histamine release by mast cells (Pier et al., 2004)	One (monomer)
IgG	Provides majority of antibody-based immunity against invading pathogens. Found in four subtypes (Pier et al., 2004)	One (monomer)
IgM	Is expressed on the surface of B cells as well as in secreted form. Eliminates pathogens in early phase of adaptive immune response before sufficient IgG can be produced (Geisberger et al., 2006; Pier et al., 2004)	Five (pentamer)

1.2.2 Antibody structure

The basic unit of each antibody is the immunoglobulin (Ig) monomer. This is a Y-shaped tetrameric molecule consisting of four polypeptide chains: two identical heavy (H) chains and two identical light (L) chains. These are connected by disulphide bonds. Each chain is composed of a number of domains known as Ig domains, each consisting of about 70-110 amino acid residues. They fold in a characteristic β-sheet pattern known as the Ig fold, where two domains are held together in a sandwich shape by

conserved cysteines and non-covalent bonds The 3-dimensional structure is shown in Fig. 1-1. The H and L chains consist of a mixture of constant (C) and variable domains (V). Each H chain has three constant regions (C_H1, C_H2, and C_H3) and a single variable region (V_H). Each L chain has a single constant region (C_L) and a single variable region (V_L) (Voet and Voet, 1995).

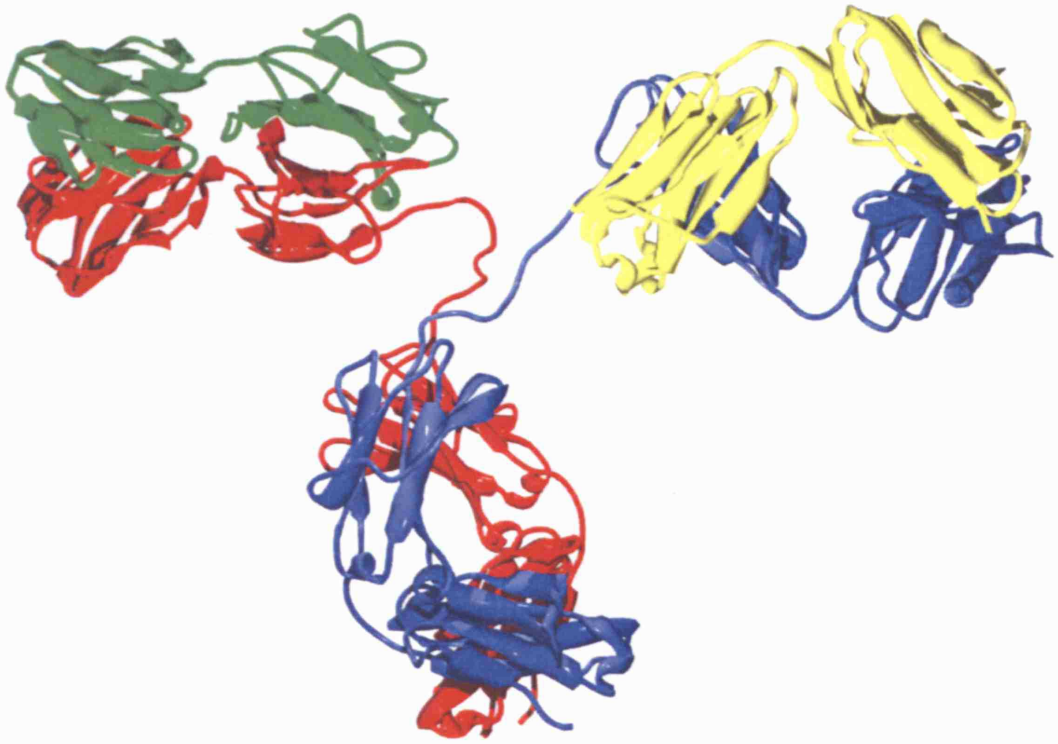

Fig. 1-1: 3D Protein Strucuture of IgG2a Murine Antibody (Harris et al., 1997). The two heavy chains are coloured red and blue, while the light chains are green and yellow. The distinctive β-sheet structure immunoglobulin fold of the Ig domains can clearly be seen. Glycosylation not shown. Created from file PDN 1IGT in www.rcsb.org/pdb.

The variable domains, located at the N-terminal tip of the Ig monomer, are extremely variable in amino acid sequence, and form the unique antigen-recognition site of each antibody. V_L and V_H are not uniformly variable however, as all variable chains share conserved amino acid residues to form the Ig fold. Variability is focused into three short hypervariable sequences, each a few residues in length. These hypervariable sequences line the antigen-binding site, and determine the antibodies binding specificity. Therefore they are also known as complementarity-determining regions (CDRs) (Janeway et al., 2001).

There are two measures of the strength of binding of any particular antibody for its antigen: affinity and avidity. Affinity measures the strength with which a single Fab binds to an antigen. However, as an antibody, and indeed antigen, may possess multiple binding sites that may contribute to increase the strength of antibody-antigen binding, the term avidity is used to describe the total strength at which a particular antibody binds its antigen. An antibodies avidity may be several orders of magnitude higher than its affinity, especially in the case of multimeric antibody isotypes such as IgM. Indeed, this is the reason for the pentameric structure of the non-affinity matured 'first response' IgM isotype.

The constant regions are different between antibody isotypes and determine the antibodies structure and effector functions. For example, IgM constant region cause association of five Ig monomers to form a pentamer. The IgE constant region can initiate mast cell degranulation when complexed with an antigen.

A typical Ig monomer is depicted in Fig. 1-2, illustrating all the regions discussed above. Also depicted are the three regions of the protein: Fc, Fab, and Fv. These are defined by proteolytic digestion of the Ig monomer. Treatment of the Ig monomer with the enzyme papain results in the cleavage of the molecule at the hinge region (also shown) into two Fab fragments and one Fc fragment. The Fc region contains only constant domains, and is named historically '**f**ragment **c**rystallisable'. The Fab fragments, which each consist of one complete light chain and C_H1 and V_H from the heavy chain, contain the antibody binding site. Hence they are known as '**f**ragment **a**ntigen **b**inding'. The Fab fragment can be further cleaved by enzymatic approaches, yielding the Fv (**f**ragment **v**ariable) fragment. This fragment contains only the variable domains of the H and L chains (Brinkmann et al., 1997). It is the smallest antibody fragment that retains antigen binding activity, but generally Fv fragments by themselves are unstable as the V_H and V_L domains can dissociate, often accompanied by aggregation (Glockshuber et al., 1990).

Fig. 1-2 also shows that antibodies, as produced by the vertebrate immune system, are glycosylated at conserved positions on their constant domains. Glycosylation is variable and its role complex. The structure of attached carbohydrate can be critical for antibody effector functions such as complement activation, and can also increase the protein's

stability by decreasing sensitivity to proteases (Jefferis and Lund, 1997; Wright and Morrison, 1997).

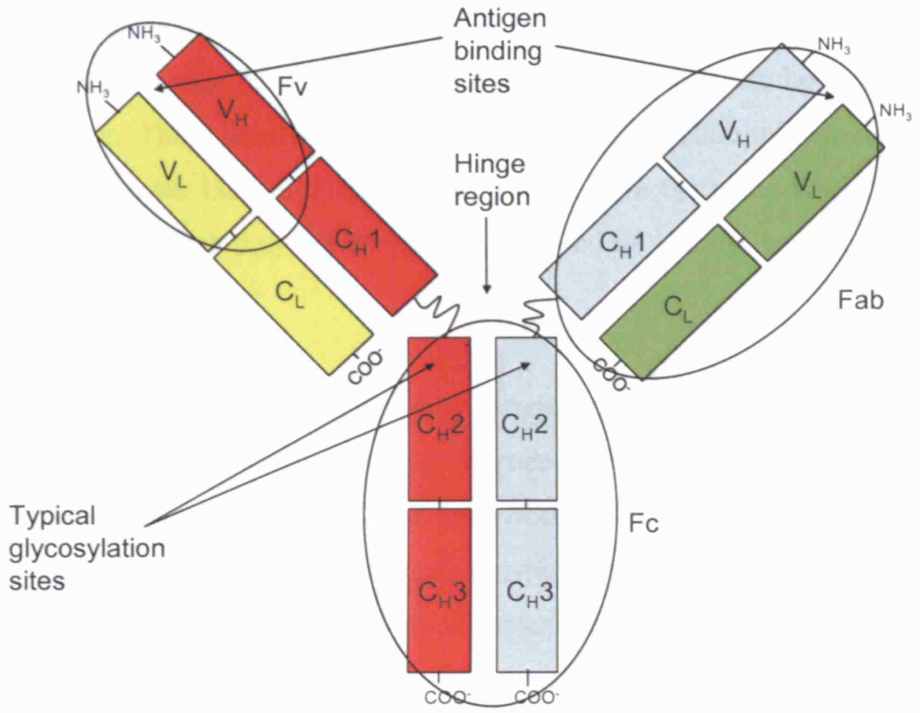

Fig. 1-2: Schematic diagram of an Ig monomer. Note that different isotypes may contain multiple copies of each monomer and more complex Fc regions. Disulphide bonds not shown.

1.2.3 Antibodies in biotechnology

Antibodies have many structural and functional features that make them valuable reagents for research, therapy, and other biotechnological applications. Their key property is their ability to form highly specific interactions with a wide variety of ligands. Functional domains providing specific antigen-binding (Fab or Fv) or effector functions (Fc) can be exchanged between molecules, expressed as separate biologically active fragments, or expressed as components of novel fusion proteins (Chester and Hawkins, 1995; Morrison, 1992).

Both polyclonal or monoclonal antibodies are used in biotechnology. Polyclonal antibodies are multiple variant forms of antibody binding the same target; produced by different V(D)J recombination in different producing cells, or clones. Monoclonal antibodies are identical in their protein 1^{o} structure, all produced from a single clone.

Monoclonal antibodies are more commonly used in biotechnology as they can be fully characterised, defined and optimised.

As well as whole antibodies, antibody fragments, such as Fab or Fv, are also commonly used in biotechnology (Joosten et al., 2003) as they can be more easily produced in recombinant systems, have reduced molecular weight, and lack the effector functions of the Fc region. These usually have a single binding interaction with an antigen: they tend to be monovalent. Hence, although they would have the same binding affinity as the antibody from which they are derived, they have less avidity than whole antibody with multiple Fab regions.

Antibody fragments were historically produced by enzymatic cleavage of whole antibodies, but are now more commonly produced by recombinant organisms. A variety of antibody fragment configurations have been developed. For example, the basic Fab region can be produced as two separate polypeptide chains. Fab' fragments are standard Fab fragments but with the heavy chain extended to include one or more hinge region cysteine residues. In order to increase binding avidity the di-Fab ($F(ab')_2$) can be created by linking two Fab' arms with a disulphide bond (Carter et al., 1992) or thioester bridge (Rodrigues et al., 1993), or by constructing a linear $F(ab')_2$ comprising tandem repeats of the heavy chain fragment V_H-C_H1-V_H-C_H1 (Zapata et al., 1995). The Fv region has also been produced recombinantly, although the lack of cross-linking cysteine residues causes a tendency to dissociate into V_H and V_L upon dilution (Glockshuber et al., 1990). Therefore both a single chain Fv (scFv), with a polypeptide linker inserted between the V_H and V_L domains, and a disulphide stabilised Fv have been designed to increase stability (Raag and Whitlow, 1995).

As well as simple antibody fragments, the basic antibody monomer has been rearranged and engineered to form a myriad of different structures. Fig. 1-3 illustrates some of the more common variants that have been produced.

The creation and isolation of specific antibodies to specific antigens in biotechnology is a complex matter. Antibodies were first produced in a polyclonal form, purified from the blood of animals immunised against the desired antigen. The development of hybridoma technology allowed the conversion of B cells from immunised mice into cell lines that can proliferate and produce monoclonal antibody indefinitely (Kohler and

Milstein, 1975). The immunogenicity of these antibodies in humans, and the complexity of protein engineering in mammalian cells then lead to the development of antibody genetic manipulation in bacteria. Although the complex structure and large size of IgG molecules makes expression in bacteria exceedingly difficult, the Fab region (Better et al., 1988) or a single chain Fv fragment (Skerra and Pluckthun, 1988) can be produced. These methods allowed antibodies to be cloned, expressed, and optimised with respect to affinity, stability, and specificity. They can also be 'humanised' by the transfer of antigen binding sites into a human antibody framework (Carter, 2006). This retains antibody binding specificity while reducing the potential of immunogenicity. The development of display technologies permitted precise control over antibody selection conditions by the use of bacteriophages or yeast to create antibodies, rather than mice. These techniques rely on rapid cloning of immunoglobulin gene segments to create libraries of antibodies with slightly different amino acid sequences. These are then 'displayed' at the surface of the yeast or bacteriophage to allow affinity selection of the desired antibodies (Hoogenboom, 2005; Sidhu and Fellouse, 2006). Most recently, a bacterial *E. coli* system has been developed that allows combination of full-length IgG and surface-displayed molecules, to further speed antibody development (Mazor et al., 2007).

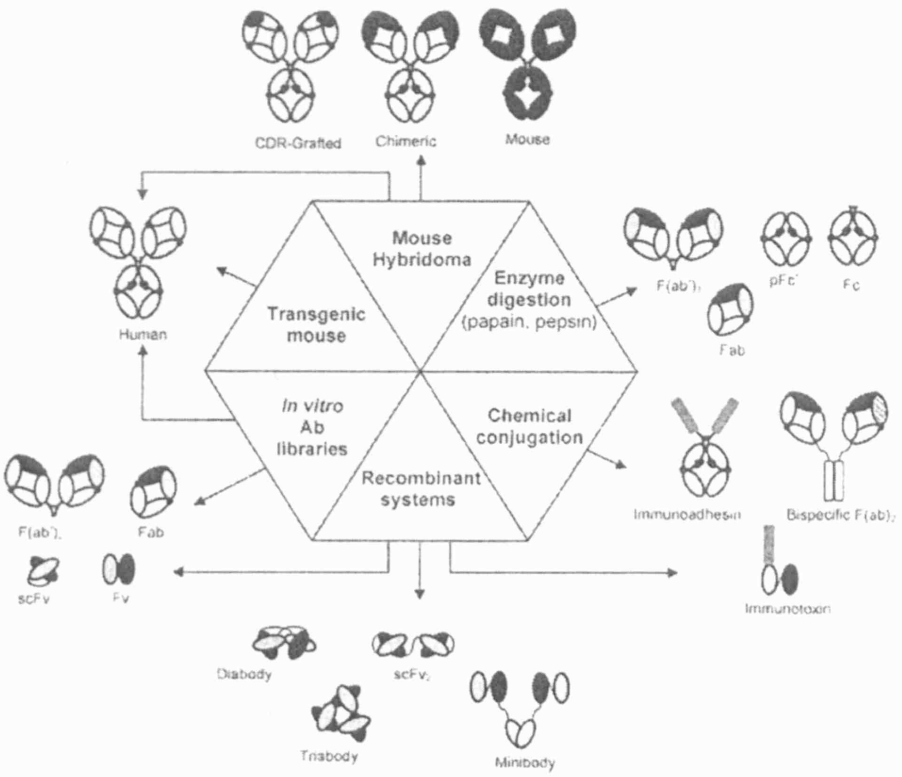

Fig. 1-3: Examples of antibody-based constructs and respective routes for their generation. Taken from Roque et al., 2004.

1.2.4 Biotechnological applications of antibodies and antibody fragments

The three major areas of application of antibodies are medical diagnosis, medical therapy, and scientific research. Several immunodiagnostic methods based on detection of typical disease biomarkers are used to diagnose infectious diseases, for example ELISA, immunofluorescence, Western blot, immunodiffusion, and immunoelectrophoresis. Two examples are the detection of indicators of cancer (Krauss, 2003) and rhumatoid arthritis (Bizzaro, 2007).

The ability of antibodies to bind to a single antigen with high specificity leads to their therapeutic power. There are currently over 200 antibody based biopharmaceuticals under development, and 21 monoclonal antibody FDA-approved therapies (Table 1-2).

Research applications stem around identification, location, and quantification of proteins of interest. For example, antibodies are used in flow cytometry to differentiate cell types and life stage by the type of proteins they express (Brehm-Stecher and Johnston, 2004). They are used in immunoprecipitation to identify binding partners of a protein of interest from crude cell lysate (Williams, 2000). They are used in Western blot analysis to identify proteins separated by electrophoresis (Kurien and Scofield, 2006). ELISA assays use antibodies to quantify proteins (Reen, 1994). The techniques of immunohistochemistry and immunofluorescence can be used to examine protein expression in tissue sections or to locate proteins within cells (Brehm-Stecher and Johnston, 2004; Scanziani, 1998).

Other suggested applications are: treatment of wastewater, counter-bioterrorism and bio-defence, biosensors, and the food industry. Antibodies (Joosten et al., 2003) and antibody fragments are also considered as components of a variety of consumer goods. For example, antibody fragments could be used in shampoos to prevent formation of dandruff, or in toothpaste to protect against cavities (Frenken et al., 1998).

Table 1-2: FDA approved monoclonal antibody therapies. Note this does not include polyclonal antibody therapies such as CryoFab™, a treatment for snake bites.

Antibody	Brand name	Approval date (FDA)	Type	Target	Approved treatments
Abciximab	ReoPro	1994	Chimeric	Inhibition of glycoprotein IIb/IIa	Cardiovascular disease
Adalimumab	Humira	2002	Human	Inhibition of TNF-α signalling	Inflammatory diseases (mostly auto-immune disorders)
Alemtuzumab	Campath	2001	Humanised	CD52	Chronic lymphocytic leukemia
Basiliximab	Simulect	1998	Chimeric	IL-2 receptor	Tranplant rejection
Bevacizumab	Avastin	2004	Humanised	Vascular endothelial growth factor	Colorectal cancer
Cetuximab	Erbitux	2004	Chimeric	Epidermal growth factor receptor	Colorectal cancer
Daclizumab	Zenapax	1997	Humanised	IL-2 receptor	Transplant rejection
Eculizumab	Soliris	2007	Humanised	Complement system protein C5	Inflammatory diseases including paroxysmal nocturnal hemoglobinuria
Efalizumab	Raptiva	2002	Humanised	CD11a	Inflammatory diseases (psoriasis)
Ibritumomab	Zevalin	2002	Murine	CD20	Non-Hogdkin lymphoma (with yttrium-90 or indium-111)
Infliximab	Remicade	1998	Chimeric	Inhibition of TNF-α signalling	Inflammatory disorders (mostly auto-immune disorders)
Muromonab-CD3	Orthoclone OKT3	1986	Murine	T cell CD3 receptor	Transplant rejection

Natalizumab	Tysabri	2006	Humanised	T cell VLA4 receptor	Inflammatory diseases (mainly autoimmune-related multiple sclerosis therapy)
Omalizumab	Xolair	2004	Humanised	IgE	Inflammatory diseases (mainly allergy-related asthma therapy)
Palivizumab	Synagis	1998	Humanised	Epitope of the F protein of Respiratory Syncytial Virus (RSV)	Viral infection (especially RSV)
Panitumumab	Vectibix	2006	Human	Epidermal growth factor receptor	Colorectal cancer
Ranibizumab	Lucentis	2006	Humanised Fab	Vascular endothelial growth factor	Macular degeneration
Gemtuzumab ozogamicin	Mylotarg	2000	Humanised	CD33	Acute myelogenous leukemia (with calicheamicin)
Rituximab	Rituxan, Mabthera	1997	Chimeric	CD20	Non-Hodgkin lymphoma
Tositumomab	Bexxar	2003	Murine	CD20	Non-Hodgkin lymphoma
Trastuzumab	Herceptin	1998	Humanised	ErbB2	Breast cancer

1.2.5 Biotechnological production of antibodies and antibody fragments

There is currently a large demand for monoclonal antibodies and antibody fragments, and the number of monoclonal antibody therapies under development suggests that this demand will only increase in the future. However, antibodies are expensive to produce. Monoclonal antibody therapies are amongst the most expensive of all drugs, where the annual cost per patient can reach US$35,000 for antibodies treating cancer conditions (Farid, 2007). These high prices, due to the expensive recombinant production process, are also a reflection of the fact that as antibodies are now marketed for chronic conditions and have relatively low potency there is a need for high cumulative doses

(grams rather than milligrams). As such, antibody production has been attempted with almost all common expression systems (Farid, 2007).

Most of the approved monoclonal antibody processes are manufactured using similar processes: batch/fed-batch culture using mammalian cells, usually Chinese hamster ovary (CHO) but also mouse myeloma (NS0) cell lines. Purification usually relies primarily on chromatography with intermediate filtration and viral clearance operations (Farid, 2006). These cells have the ability to produce correctly folded and glycosylated full length antibodies, currently not possible in bacterial systems. Although there are some differences in the glycosylation patterns, no clinical data suggest that these structural differences have any effect on antibody activity *in vivo* or in the induction of antigenic responses (Roque et al., 2004). The major disadvantage of mammalian cell culture is the associated high cost of goods during the manufacturing process both at large and small-scale (for a full cost analysis of different antibody production systems see Farid, 2007). Also, mammalian cell lines are much more labour intensive to create and maintain than bacterial ones.

A multitude of transgenic systems have been considered for the production of antibodies. The secretion of the antibodies into the milk of transgenic dairy animals shows potential to produce large amounts of therapeutic proteins (Pollock et al., 1999). It may even be more cost-effective than fermentative mammalian cell culture (Farid, 2007). However, animal systems suffer from several drawbacks: the success rate to obtain live births is below 10%, the development timeline is too long (to produce a sufficient herd for commercial production takes a number of years), and the possibility of contamination by viruses and prions can not be discounted (Larrick and Thomas, 2001). Transgenic plants can also be used to produce antibodies, with the advantages over transgenic animals of easy scalability, freedom from human pathogens, and ease of growth within existing infrastructures. However, there are significant differences in the composition and structures of glycosylation, although a strategy to overcome this problem has been to engineer host cells in order to produce aglycosyl antibodies or to modify the carbohydrate synthesis pathways. Recently a tobacco plant has been genetically modified to express GalT (β-1,4-galactosyltransferase) resulting in galactosylation of 'plantibodies' similar to those observed in mammals (Bakker et al., 2001).

Antibody production has been considered in yeasts such as *Pichia pastoris*. Being single-celled eukaryotes these systems form somewhat of a half-way house between mammalian and bacterial cell culture. They can carry out some post-translational modifications performed by higher eukaryotic cells, such as proteolytic processing, folding, disulphide bond formation and some glycosylation. The ability to express correctly folded secreted proteins provides a distinct advantage. However, problems related to the *P. pastoris* expression system includes inefficient secretion of some proteins > 30 kDa, proteolysis of secreted proteins during high cell density (HCD) fermentations, non-mammalian glycosylation patterns, low transformation frequencies and toxicity of some antibodies to *P. pastoris* (Fisher et al., 1999). Other yeast systems such as *Hansenuela polymorpha* (Abdel-Salam et al., 2001), and *Saccharomyces cerevisiae* (Shusta et al., 1998) have also been considered.

This work uses production of antibody fragments in the bacterium, *E. coli*, as the main process case study. Historically, whole antibodies have not been produced in *E. coli* due to folding difficulties, although recent work using improved understanding of antibody structure and folding has enabled expression systems that permit assembly of full length antibodies (Simmons et al., 2002). Antibody fragments have been successfully produced in large numbers for many years using *E. coli*. Advantages are the ability to grow rapidly and to high cell density on inexpensive substrates and the production of proteins in relatively large amounts. Also the bacterium is well characterised, genetic manipulation is facile, and production can easily be scaled-up.

High-level expression of antibody fragments in the cytoplasm of *E. coli* generally results in extensive aggregation and formation of inclusion-bodies. The complexity of the process needed to purify from homogenised whole cells and then refold these inclusion bodies means that cytoplasmic production is more costly than mammalian cell systems (Farid, 2007). Therefore antibody fragments are usually designed with a periplasmic signal sequence to direct them to the periplasm. This allows stable folding of the antibody fragments as the periplasmic environment is less reducing, allowing oxidation of cysteine thiols into disulphide bonds. In this way it resembles the endoplasmic reticulum of mammalian cells where antibodies are folded *in vivo*. Moreover, there are fewer proteases present in the periplasm compared to the cytoplasm, so proteolytic degredation is less of an issue.

A major drawback of *E. coli* as a production system for monoclonal antibody therapies is the lack of mammalian post-translational modification, specifically glycosylation. Also, not all antibodies can be produced in *E. coli* as some Fv domains can be toxic to the bacterium (Joosten et al., 2003), and some antibody fragments are intrinsically unstable in *E. coli* (Demarest et al., 2006). Finally, as currently only antibody fragments can be produced in large amounts in *E. coli*, there is the problem that these have a much reduced therapeutic half-life due to increased blood clearance and so are required therapeutically in much higher amounts. However, the half-life of the antibody fragment in the body can be extended by the specific attachment of PEG (polyethylene glycol). PEGylation of proteins increases their molecular size and generally confers increased half-life in the circulation, as well as potentially reducing immunogenicity and increasing solubility. The half-life of the antibody fragment can be tailored according to therapeutic need by the addition of different sized PEG moieties (Veronese and Pasut, 2005).

E. coli is the most well-understood bacterial system, hence its industrial dominance. However, alternative prokaryotic systems available for antibody fragment production are *Lactobacillus, Bacillus,* and *Streptomyces* strains (Joosten et al., 2003).

Currently only one FDA-approved antibody therapy is produced in *E. coli*: Lucentis (ranibizumab) is a 48 kDa humanised Fab (Table 1-2) targeted at vascular endothelial growth factor A (VEGF-A). It was approved by the FDA in 2006 and EMEA in 2007 for the treatment of neovascular (wet) age-related macular degeneration (wet AMD), a progressive condition causing blurred vision and blindness mainly in people over 75. The manufacturing process involves periplasmic expression in *E. coli.* Soluble protein is released from the *E. coli* via initial homogenisation and a subsequent heating step that precipitates cellular debris. High-resolution purification is achieved by a combination of four subsequent chromatographic steps, followed by the addition of trehalose, histidine, and polysorbate 20 as excipients (Walsh, 2007).

Although currently only one *E. coli* produced antibody therapy is approved by the FDA, more are in late-stage development. For example, Cimzia™, a PEG-lyated Fab' TNF-α suppressor for the treatment of Crohn's disease and rheumatoid arthritis, which is in late stage III clinical trials, is produced in *E. coli.* In the next section the production of monoclonal antibodies such as Cimzia™ in *E. coli* is examined in detail.

1.3 Production and purification of Fab' in *E. coli*

The following is a brief introduction to some of the fermentation and bioprocessing options for the production of antibody fragments in *E. coli*. More details and theoretical considerations will be provided in the following results chapters when appropriate. After discussion of the individual unit operations a holistic overview is given focussing on the relevance of intra-process interactions and the recent FDA initiative to increase Quality by Design principles in industrial biopharmaceutical processes. Finally an overview is given of the particular bioprocess that is the case study of this thesis.

1.3.1 The upstream process - *E. coli* fermentation strategies relevant to antibody fragment production

The primary aim of the fermentation unit operation in antibody fragment production in *E. coli* is the cost-effective production of the antibody fragment by high productivity low-cost fermentation, where productivity is the amount of product formed per unit volume per time. A secondary aim, which will be discussed in more detail later in this section, is the design of the fermentation to allow facile and inexpensive downstream processing (DSP). The usual strategy to fulfil this primary goal is the growth of the *E. coli* cells to high cell densities (HCD), and the optimization of the amount of Fab' produced per cell. In this sub-section firstly strategies that can be used to grow *E. coli* to HCD are examined, before ways in which individual cell productivity can be increased are discussed.

1.3.1.1 High cell-density culture of E coli

The maximal dry cell weight (DCW) of *E. coli* culture is estimated to be ~ 200 g/L, as culture fluidity is lost when the DCW is higher than ~ 220 g/L (Lee, 1996). The current highest reported *E. coli* cell density is 190 g/L (Fuchs et al., 2002; Nakano et al., 1997). There are two approaches used to keep bacteria multiplying as close to this limit as possible: the physical control of culture conditions; and modification of the molecular biology of the bacteria used.

In order to grow cells to HCD it is necessary to meet all nutritional needs while ensuring no toxic or inhibitory factors are excreted by the cells during growth. A major problem with HCD production of *E. coli* is the accumulation of secreted acetate. Acetate is produced when carbon flux into the central metabolic pathway exceeds the

biosynthetic demands and the capacity for energy generation within the cell. Saturation of the tricarboxylic acid (TCA) cycle and/or the electron transport chain are the main causes (Lee, 1996). Acetate accumulation above 2-5 g/L at pH 7 in the growth media slows down growth, may stop biomass build up and may inhibit recombinant protein biosynthesis (Shiloach and Fass, 2005). Hence it is necessary to run the fermentation so as to minimise acetate production. There are a variety of means by which this can be achieved. Oxygen should not be limited, as oxygen is the major electron acceptor in oxidative phosphorylation. Therefore oxygen enriched air or even pure oxygen has been used to increase oxygen transfer. Temperature reduction from 37°C to 25-30°C can also reduce acetate formation by reducing nutrient uptake and metabolic rate. Lower temperature will also reduce the generation of metabolic heat and help prevent fermenter heating due to stirrer mechanical heat and metabolic heat outstripping the capacity of the fermenter cooling system. Concentration and type of carbon source will affect acetate production. For example, presence of glucose in high concentrations will cause acetate formation, while glycerol has been shown to generally not lead to acetate formation in aerated cultures due to the lower rate that *E. coli* can transport glycerol into the cytoplasm (Holms, 1986). Alternatively, fed-batch techniques can be used to lower acetate accumulation by reducing growth rate through supplying glucose slowly. Moreover, in order to reach cell densities higher than ~ 50 g/L DCW a fed-batch method is vital as *E. coli* growth is inhibited when the nutrients outlined in Table 1-3 are present above the concentrations listed. Different feeding methods in fed-batch culture are detailed in Table 1-4.

Table 1-3: Examples of nutrients that inhibit *E. coli* growth when present in high concentrations (Lee, 1996).

Nutrient	Inhibitory Concentration (g/L)
Glucose	50
Ammonia	3
Iron	1.15
Magnesium	8.7
Phosphorous	10
Zinc	0.038

It is also possible to modify the bacteria rather than the culture conditions in order to achieve HCD cultures. For example, a Clostridial constitutive acetone operon has been cloned into *E. coli* K12, thus continuously activating a process that converts acetate to acetone that can be stripped off by aeration and agitation due to its high volatility

(Bermajo et al., 1998). Examples of other molecular genetics approaches are: down-regulation of the stress response (Wang and Lee, 1998); and diversion of carbon flow away from the TCA cycle (Dedhia et al., 1994).

Table 1-4: Feeding methods in fed-batch culture. Adapted from Lee, 1996.

Without feedback control
• **Constant feeding** – feeding nutrient at predetermined (constant) rate. The specific growth rate continuously decreases.
• **Increased feeding** – feeding nutrient at an increasing (gradual, stepwise, or linear) rate. The decrease in specific growth rate can be compensated.
• **Exponential feeding** – feeding nutrient at an exponential rate. Constant specific growth rate can be attained.
With feedback control
Indirect feedback control
• **DO-stat** – feeding nutrient when there is a rise in the concentration of dissolved oxygen (DO), which results from depletion of the substrate.
• **pH-stat** – feeding nutrient when pH rises as a result of depletion of the principal carbon source.
• **CO_2 evolution rate (CER)** – this is estimated on-line using a mass-spectrophotometer, and is used to control nutirent feeding. The CER is roughly proportional to the rate of consumption of the carbon source. This method is most frequently used to control the specific growth rate.
• **Cell concentration** – the nutrient feeding rate is determined from the cell concentration, which is measured on-line using a laser turbidometer.
Direct feedback control
• **Substrate concentration control** – nutrient feeding is directly controlled by the on-line concentration of the principal carbon source.

1.3.1.2 Increasing recombinant protein production in E. coli

Here seven factors that increase the efficiency of recombinant protein production and folding are considered. These are: expression vector used, gene dosage, transcriptional regulation, translational regulation, codon usage and protein engineering, host molecular genetic modification and physical fermentation considerations. In addition to these factors, location of expression can also alter recombinant protein expression, as discussed in section 1.2.5.

Most recombinant protein expression vectors used in *E. coli* are medium to high copy number plasmids, although low-copy number plasmids or expression cassettes are sometimes used. As well as the coding sequence, promoter, regulatory sequence elements etc., which will be discussed later, there are a number of key elements to any expression plasmid. Vectors must contain an origin of replication, which will also

determine the copy number. They also require some means of selection, usually by the inclusion of an antibiotic resistance gene. However, some industrial processes forgo antibiotic selection in order to reduce media cost and later purification needs. For example, a method has been patented for the production of recombinant protein in the absence of antibiotic through the use of an expression vector that stably maintains a medium copy number between 6 and 50 (Weir and Mountain, 1999).

The gene dosage will be determined by the plasmid copy number. High copy number will increase gene dosage and this is generally desired for maximum gene expression. However, the metabolic burden and protein aggregation effects that usually result from multiple copies could prove to be detrimental for maximum productivity in certain metabolic engineering applications (Hagg et al., 2004).

Level of transcription of the recombinant genes is regulated in part via the choice of promoter and regulatory elements. There are three main requirements for a promoter. It must be reasonably strong, resulting in the accumulation of protein making up 10-30% or more of the total cellular protein. It should exhibit the lowest possible level of uninduced transcriptional activity – i.e. it should not be 'leaky'. The tight regulation of a promoter is essential for the synthesis of proteins, which may be detrimental to cell growth (Guzman et al., 1995). Finally, induction must be simple and cost-effective.

The most widely used promoters for large-scale protein expression use chemical inducers or thermal induction (Jana and Deb, 2004). The *E. coli lac* promoter and its variants are some of the most commonly used promoters for producing recombinant proteins in bacteria. These promoters are well understood and have been extensively characterised. Especially useful are the synthetic *tac* and *trc* promoters. These consist of the -35 region of the *trp* promoter and the -10 region of the *lac* promoter. They only differ by 1 b.p. in the length of the spacer region between these elements. These promoters are stronger than the native *lac* promoter (routinely allowing accumulation of polypeptides up to 15-30% of the total cell protein), and are not subject to catabolite repression (Donovan et al., 1996). The major drawbacks of these *lac*-based promoters are the cost and potential toxicity to humans of their inducer, the non-hydrolysable lactose analogue isopropyl-β-D-1-thiogalactopyranoside (IPTG). These drawbacks are less important for high-value-added products, which need extensive purification anyway. Recent research has also demonstrated that as little as 50-100 μM IPTG is necessary for

induction, as opposed to the 1mM previously commonly used (Shibui and Nagahari, 1992).

It is possible to utilise lactose as an inducer to circumvent these problems. Lactose can also double up as a carbon source after induction. However, lactose is not without its problems as an inducer (see Gombert and Kilikian, 1998 for review). Its cost for biopharmaceutical processes has risen significantly recently due to FDA insistence on it being sourced from certified prion-free herds. Its low solubility in water requires large liquid volumes to be added to the culture, meaning fewer bacteria can be grown in a fixed fermenter size. The fact it is a carbon source means carbon restriction cannot be used to control cell growth after induction. Finally, the nongenetic heterogeneity of the amount of lactose permease in the cell membrane results in a long and variable lag phase between lactose addition and induction (Menzella et al., 2003). Two examples of lactose's use as an inducer are: the production of the kringle fragments of human apolipoprotein(a) (Lim et al., 2004b) and the carboxyltransferase component of a propionyl-CoA carboxylase complex from *Streptomyces coelicolor* (Menzella et al., 2003).

There are multiple temperature controlled promoters available. The best characterised cold-shock promoter is that of the major *E. coli* cold-shock protein CspA (Baneyx, 1999). The *cspA* promoter is rather well repressed at and above 37°C, compares favourably to the *tac* promoter for the expression of an aggregation-prone fusion protein at reduced temperatures, and remains functional at 10°C. The major problem with the *cspA* system is that it becomes repressed 1-2 hours after temperature downshift, a time period too short to allow high-level expression. Other temperature controlled promoters include the strong bacteriophage pL promoter, and adapted versions of the *lac* system with the *lac* repressor mutated to become thermosensitive (Jana and Deb, 2004).

Consideration of codon usage can increase recombinant protein expression in *E. coli*. The recombinant gene can be poorly expressed if contains many codons rarely found in *E. coli*, i.e. ones that *E. coli* has low numbers of the corresponding tRNAs for. Also, *E. coli* contains certain codon pair biases, coding for temporary pausing of the translational machinery to allow time for correct domain folding. If the recombinant gene by chance contains these pairs, translation and folding may be inhibited. It may even be beneficial

to engineer certain codon pairs between domains of recombinant proteins to allow time for correct folding (Gutman and Hatfield, 1989).

The protein of interest can also be engineered to increase its stability and ease of folding in the host organism. For example, the effect of specific framework residue substitutions on expression and location of a Fab-fusion protein in *E. coli* has been studied (Forsberg et al., 1997). A fifteen-fold increase in the level of product in the growth medium was achieved using only five light chain substitutions.

Multiple *E. coli* strains have been created to improve specific types of recombinant protein production. *E. coli* have been engineered to lack certain proteases or modified to allow more efficient recombinant protein folding. An example of a protease deficient commercially available *E. coli* strain is K12 KS1000, which is deficient in the Prc protease, a periplasmic protease formerly known as Tsp (Silber et al., 1992).

Physical control of the fermentation conditions can greatly affect recombinant protein production. This is mainly as protein folding can easily become the rate determining step in protein production, and this can lead to aggregation of the protein of interest in inclusion bodies (Baneyx, 1999). Consequently, reduction of temperature during induction can enhance functional protein formation by reducing rates at which the protein is formed. This has also been found to increase product retention in the periplasm when a periplasmic locator sequence is being utilised. Lower expression rates reduce the concentration of the unfolded intermediate in the cell, thereby favouring correct folding over aggregation. Many other fermentation conditions including: specific growth rate after induction (Glick, 1995), post-induction feeding strategies (Wong et al., 1997), pH (Huang et al., 2002), dissolved oxygen concentration (Bhattacharya and Dubey, 1997), concentration of inducer (Bowering, 2000) duration of induction, and salt concentration (Vaara, 1992) can also affect the compartmentalisation of the protein product, product titre, and cell viability.

1.3.2 The downstream process – purification strategies relevant to antibody fragment production in *E. coli*

Design of downstream processing is highly dependant on the expression system, protein of interest, and location of expression. Here we will only consider processing steps relevant to the production of antibody fragments in the *E. coli* periplasm: the system of

interest. Cytosolic production and the extensive solubilisation and renaturation stages required for protein recovery from exclusion bodies are not considered as this has been found to be less cost-effective than periplasmic production (Farid, 2007).

Processing may be divided into a number of stages including primary recovery and release of intracellular product, purification, finishing and formulation. Here focus is given to HCD primary recovery, as these steps form the focus of the thesis.

1.3.2.1 Separation of biomass

Recovery of proteins from fermentation broths usually begins with separation of the solids from the liquid phase of the fermentation broth. The leading methods for this are centrifugation and microfiltration. Expanded bed chromatography can also be considered once the product is released into the liquid phase.

1.3.2.1.1 Centrifugation

Centrifugation separates on the basis of the particle size and/or density difference between solids and liquids or two liquids. The density gradient is amplified through the application of centrifugal force by high-speed rotation. In bioprocessing, centrifugation can be used for the removal of whole cells, cell debris, spheroplasts, and inclusion bodies from the liquid phase. Therefore it can be used both for initial recovery of the cells/liquid from the raw fermentation broth, and also later on for separation post intracellular product release. In the biotechnology industry three different types of centrifuge are commonly used: disc-stack, multi-chamber bowl, and tubular bowl centrifuges (Boychyn et al., 2004).

Disc-stack centrifugation has emerged as the most widely used form of centrifugation in biotechnology (Low et al., 2007). A typical disc-stack centrifuge is illustrated in Fig. 1-4. A stack of hollow truncated discs increases the area available for separation. Spacer caulks keep the discs separated and the disc angle is between 35-50°. The feed enters the centrifuge through a central feed pipe leading to the feed chamber at the bottom of the stack. Solids settle on the lower surface of each disc and slide downwards into the conical holding space where dewatering and compaction occur. The clarified liquid moves upward and inward, and is discharged at pressure from the centrifuge. Solids are discharged intermittently at a fixed time interval, or continuously through nozzles.

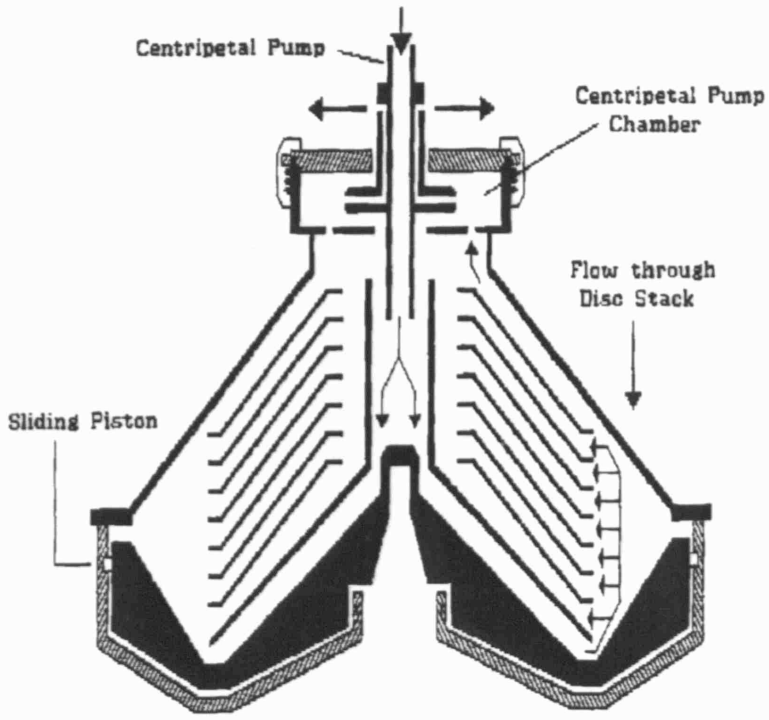

Fig. 1-4: Outline of the liquid flow direction and form of a typical disc-stack centrifuge.

Disc-stack centrifuges can apply high shear forces to solids both at centrifuge entry and exit, although entry shear can be reduced through the use of hermetic inlets. Other drawbacks with disc-stack machines are their reduced dewatering ability and ease of cleaning, especially compared to tubular bowl machines. However, disc-stack machines allow discharge during bowl rotation.

Tubular bowls (Fig. 1-5) are some of the simplest centrifuges in design terms, formed from a tube rotating between bearings at each end. The feed is pumped into one end, the separated liquid leaving at the other, while solids in the feed will separate to the wall of the bowl.

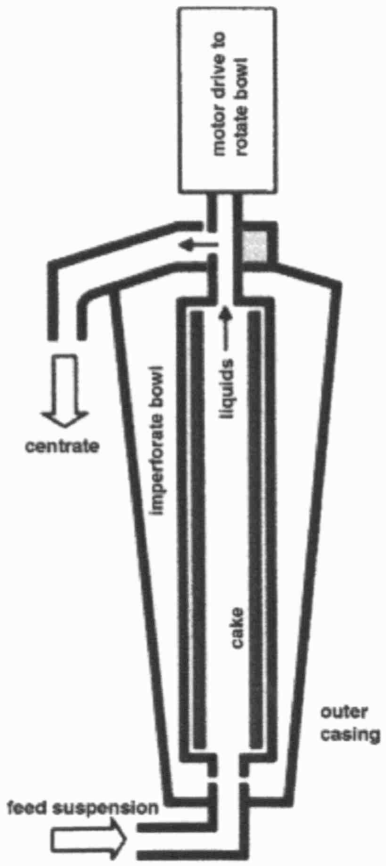

Fig. 1-5: Outline of the liquid flow direction and form of a typical tubular bowl centrifuge. Taken from Sutherland (2005).

The simple construction of tubular bowl centrifuges allows faster rotation speeds, thereby increasing the dewatering that can be achieved. On the other hand tubular bowl centrifuges have longer operating times due to the need for dismantling for solids removal. However, the advanced tubular bowl Carr Powerfuge™ allows solids removal without dismantling by the aid of an internal scraper, although bowl rotation must be fully halted.

Among other types of continuous-flow centrifuges sometimes used by the biopharmaceutical industry are the multi-chamber bowl centrifuges, also known as chamber bowl centrifuges. They are solid bowl centrifuges used for the recovery of fine biological material (Boychyn et al., 2000). The feed enters the rotating bowl through the individual chambers, from the inner chamber to the outer. The large particles will be deposited in the inner chamber, whereas the lighter, smaller particles are deposited progressively in the outer chambers (Fig. 1-6). The clarified liquid is discharged under pressure (Salte, 2006). A major drawback of this type of centrifuge is that the machine

must be stopped and dismantled for solids removal. Therefore it is usually only used for a low solids content liquid (Sutherland, 2005).

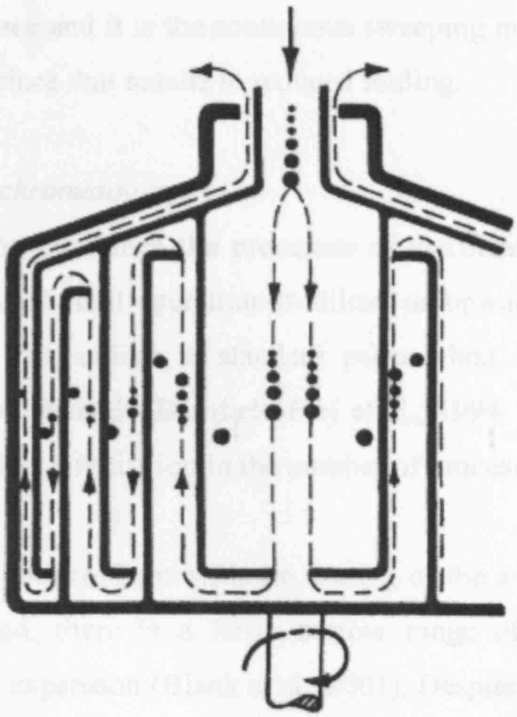

Fig. 1-6: Mechanism of action of a multi-chamber bowl centrifuge. Taken from Sutherland (2005).

One common drawback with industrial centrifugation is the large capital cost needed. Centrifugation alone also cannot guarantee 100% clarification, and usually requires a depth filtration step prior to chromatography (Low et al., 2007).

1.3.2.1.2 Microfiltration

Microfiltration can also be used for biomass separation. It is also commonly used to remove any remaining particulate matter after centrifugation. It is also used for biomass separation without centrifugation, although this is less common. When compared with centrifugation alone, microfiltration results in better clarification (Berthold and Kempken, 1994), and has the advantage of requiring less capital costs. However, it suffers from the inability to be a platform unit operation, one that can be used without much optimization over a wide range of feed conditions (Voisard et al., 2003).

Dead-end filtration is operated with the filter perpendicular to the flow. Cell debris and cells build up on the filter over time, fouling the filter, increasing the pressure needed to maintain flow rate, and eventually blocking the filter.

For industrial applications cross-flow filtration is often preferred to dead-end operation because of the lower rate of membrane fouling, especially where filtration is replacing centrifugation rather than supplementing it. In cross-flow filtration, the feed flow is parallel to the filter surface and it is the continuous sweeping motion of the feed-stream across the membrane surface that results in reduced fouling.

1.3.2.1.3 Expanded bed chromatography

Expanded bed adsorption combines the processes of clarification, concentration, and initial purification in a single unit operation. It utilises an upward liquid stream through a chromatography bed that, unlike in standard packed bed chromatography, allows particulate matter to pass through (Barnfield-Frej et al., 1994; Thommes et al., 1996). As such, the main benefit is a reduction in the number of process steps required.

The technique suffers from problems with the fouling of the adsorbent due to cell and cell debris binding. Also, there is a fairly narrow range of usable flow rates for acceptable values of bed expansion (Blank et al., 2001). Despite recent improvements to partially negate these problems (Dainiak et al., 2004; Viloria-Cols et al., 2004), expanded beds are not commonly used in industry. Rather a hybrid centrifugation-filtration system has become the industry standard for primary recovery (Low et al., 2007).

1.3.2.2 Release of product from biomass

Periplasmically-located proteins can be released by a variety of methods, including mechanical cell disruption and periplasmic extraction.

1.3.2.2.1 Mechanical cell disruption

Mechanical cell disruption, or homogenisation, destroys cell integrity and therefore releases recombinant product from the cells into solution. Industrial-scale cell homogenisation usually involves forcing cell suspension through a restricted orifice at high pressure. Several mechanisms are believed to be involved in cell disruption: fluid mechanical stresses caused by turbulent flow, rapid acceleration in the homogeniser valve unit, and jet impingement (Keshavarz-Moore et al., 1990).

There are major disadvantages to using this method for the release of periplasmic protein. Firstly, it liberates both periplasmic and cytosolic contents, thus exposing the

recombinant protein to host cytosolic proteases and also increasing subsequent process contaminant load and negating a major benefit of periplasmic expression. Secondly, homogenisation generates a large number of fine particles that will reduce the efficiency of subsequent biomass removal unit operations.

1.3.2.2.2 Periplasmic extraction

Periplasmic extraction is preferable to homogenisation if it allows efficient release of periplasmic material while maintaining cell or spheroplast integrity. This reduces host protease degradation of the recombinant protein as only 7 of the 25 known *E. coli* proteases are located in the periplasm (Swamy and Goldberg, 1982). Also, contaminant load is greatly reduced, as the periplasm contains only 4-8% of cell proteins and no DNA (Nossal and Heppel, 1966).

Multiple techniques have been used for periplasmic release including: physical methods such as osmotic shock (Zimmermann et al., 1991), freeze/thaw (Johnson and Hecht, 1994), heat treatment (Tsuchido et al., 1985); enzymatic methods (Neu and Heppel, 1964) such as lysozyme treatment; and chemical methods such as addition of triton X-100 and guanidine (Naglak and Wang, 1990), chloroform (Ames et al., 1984), and EDTA (Ryan and Parulekar, 1991). Many of these methods are not easily scalable. For example, the use of enzymes will greatly increase process cost and purification load.

One scalable and effective method for the periplasmic release of antibody fragments involves the combination of chemical and heat extraction (Weir and Bailey, 1997). Trishydroxymethylaminomethane (TRIS) and ethylenediamine tetraacetic acid (EDTA) are used synergistically to permeablise the outer membrane. EDTA acts by stripping stabilising divalent cations off the lipopolysaccharide (LPS) layer (Marvin et al., 1989), while each TRIS molecule binds multiple LPS and induces clumping and therefore destabilization of the membrane (Irvin et al., 1981). The inner membrane maintains stability due to the small number of LPS it contains. The elevated temperature both enhances periplasmic release by inducing membrane blebbing (Katsui et al., 1982), and also acts as a heat extraction step, degrading contaminating membrane proteins less thermally stable than antibody fragments. Increased temperatures have also been shown to increase product quality by selectively degrading misfolded Fab's (Weir and Bailey, 1997).

1.3.2.3 Purification, finishing and formulation

Only primary recovery and product release DSP unit operations are studied in this thesis. Therefore, despite being topics of intense interest, purification, finishing and formulation are only discussed briefly.

1.3.2.3.1 Purification

Chromatographic separations are the workhorse purification methods of antibodies and antibody fragments.

Affinity chromatography, based on highly specific interactions between an immobilised ligand and the protein of interest, dominates antibody purification, especially for mammalian cell derived antibodies. Protein A, a Staphylococcal antibody binding protein, is by far the most common ligand used. However, the significant expense of protein A resins and possible leaching of the protein from the column has lead to a search for alternative ligands (Rongxiu et al., 1998).

Ion-exchange chromatography, separating proteins on the basis of charge, is frequently used as a second chromatographic step. It is especially useful for the purification of Fab's due to their generally high pI. It has also been used as the primary purification step, for example, in the commercial process for the production of the monoclonal antibody therapy Humira® (Walsh, 2007).

In many purification schemes, a polishing chromatography step is used for final purification. Hydrophobic interaction chromatography is commonly used for this purpose, separating protein based on variations in hydrophobicity.

Despite the current dominance of antibody purification by chromatographic separation, recent increases in upstream yields have led to talk of a purification 'bottleneck'. Therefore multiple other purification technologies are being considered for antibody purification including: precipitation, membrane chromatography, high-resolution ultrafiltration, crystallization, and high-pressure refolding (Thommes and Etzel, 2007). However, chromatographic separation looks like remaining the purification paradigm for the rest of the decade at least.

1.3.2.3.2 Finishing/viral clearance

Viral clearance is required to be a two stage process by the regulatory authorities. It usually involves a low pH hold stage for viral inactivation, and then a viral filtration.

1.3.2.3.3 Formulation

At the end of the DSP train before bottling, it is necessary to ultrafilter/diafilter the protein into the required formulation buffer.

1.3.3 Whole process considerations

The performance of a biopharmaceutical production process will not simply be a function of the individual operation yields but will also depend on interactions that exist between these unit operations. Therefore, for the realisation of best process output it is necessary both to understand the nature of such interactions and ideally be able to quantify them.

Some examples of the necessity of considering interactions between process steps have already been given. For example, homogenisation is less useful than specific periplasmic extraction due to increased contaminant load hindering purification and the increase in fines hindering biomass separation. However, many intra-process interactions are less obvious and require detailed analysis to elucidate. A recent example of this comes from the purification of Fab' produced in the *E. coli* periplasm. Here, ion-exchange chromatography (IEX) was used as the main purification step. However, a second purification step was required due to the co-purification of host proteins with similar functional pI's during the IEX step. Analysis found that the major co-purifying protein was the periplasmic phosphate binding protein PhoS/PstS. Genetic modification of the host *phoS/pstS* gene to lower the protein's functional pI prevented its co-purification with Fab' fragments during IEX, thereby completely eliminating the need for a second purification step (Humphreys et al., 2004).

The need to consider process interactions has been stressed by the key regulatory authorities. The FDA has recently released guidelines upon applying Quality by Design (QbD) to biological processes. QbD is defined as "designing and developing formulations and manufacturing processes to ensure predefined product quality" (Yu, 2006). QbD constitutes the definition of a desired product quality profile early in drug development. The product and manufacturing process is then designed to meet the

target quality profile. This is facilitated by the identification and control of critical raw material attributes, critical process parameters, and sources of variability such as intra-process interactions. In this way quality is designed into the process. QbD can be difficult to apply to a biological process however. This is due to the difficulty of fully characterising complicated biological products: indeed, the product is defined by the process! The multitude of ways product quality can be assessed means the choice of the most critical product attributes for safety and efficacy of product can be exceedingly difficult to define. QbD also ties in with recent FDA and EMEA initiatives towards process analytical technology (PAT) in that in both QbD and PAT the process is monitored and adapted over time to produce consistent quality.

The FDA defines PAT as "a system for designing, analyzing, and controlling manufacturing through timely measurements (i.e. during processing) of critical quality and performance attributes of raw and in-process materials and processes, with the goal of ensuring final product quality" (Low et al., 2007). PAT aims to allow real time process monitoring to faciliate appropriate responses to deviations before batch rejection is necessary. PAT is facilitated by increased knowledge of process interactions, as the effect of deviations in one unit operation on another will be known and can be taken into account during PAT design. Conversely, process monitoring by PAT can also facilitate interaction identification.

1.3.4 UCB protocol for purification of A33 Fab'

This thesis is based around an industrial process for the production of 'A33' antibody fragments in *E. coli*, as used by UCB Group (Slough, UK). A process overview is given in Fig. 1-7. The A33 Fab' produced is a 47.4 kDa protein, with a typically high pI for a Fab' fragment of ~ 8.3. It is a humanised, univalent Fab dimer of V_L-C_L and V_H-C_H chains with linker region, stabilised by disulphide bonds between the two chains. In this thesis research is focussed upon the fermentation and the initial DSP steps (centrifugation, periplasmic extraction and subsequent spheroplast removal via centrifugation). Specific process information is given in subsequent results chapters.

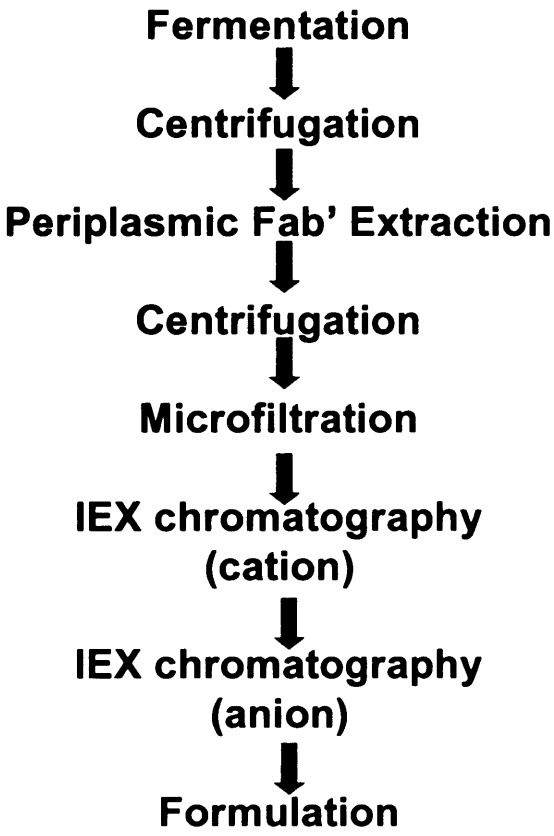

Fig. 1-7: Overview of process used for producing A33 antibody fragments in *E. coli*.

1.4 Techniques for rapid process evaluation and interaction analysis

Techniques that increase the speed at which information can be gained about a bioprocess, or decrease the material necessary to generate these data, will reduce the cost of process development. This will thus allow more process information to be determined, at an earlier stage, and so allow quality to be designed into a process using QbD principles. In this section we examine three interrelated approaches that can be used to achieve this aim: ultra scale-down methodology, computer modelling, and statistical design of experiments.

1.4.1 Ultra scale-down (USD) methodology

With the development of high-value, low volume biopharmaceutical products, large quantities of test material are rarely available for timely process development without substantially increased financial investment and risk. The conventional approach of geometric scale-down for process development studies is limited to the litre range by the practicalities of producing process equipment capable of operating at smaller scales. USD techniques take scale-down one step further by allowing the prediction of

industrial-scale operations using only millilitre quantities of material. They combine the use of standard lab equipment with mimics of the engineering environment. These mimics may be experimental (e.g. shear devices) or mathematical (e.g. computational fluid dynamics). While the USD approach must always be complemented by actual pilot and large-scale studies, it can greatly aid in screening, process development, and process understanding, and also crucially allow process development to be commenced earlier in the discovery process.

USD methods have been developed to mimic multiple process steps including depth filtration (Reynolds et al., 2003) and expanded bed adsorption (Willoughby et al., 2005). Centrifugal clarification of protein precipitates and mammalian cell cultures < 2% solids (wet w/v) has been predicted using USD (Hutchinson et al., 2006), as has the shear damage caused upon feed entry to (Boychyn et al., 2001) and exit (Chan et al., 2006) from various centrifuges. There are also ongoing efforts to mimic chromatographic steps at small-scale, with some success (Wenger et al., 2007).

Similar methods capable of providing process insights with only millilitres of feed material have also been developed outside of UCL, although usually the term 'USD' is not applied. For example, the use of crystallisation for the large scale recovery of proteins has been stimulated by the use of small-scale methods to determine optimal crystallisation conditions (Bard et al., 2004; Cumbaa et al., 2003). However, USD-type methods have mainly been developed to aid the determination of optimal chromatography conditions. These are often automated high-throughput protocols (Bensch et al., 2005; Booth et al., 2008; Lacki et al., 2008). SELDI-TOF mass spectrophometry has also been applied for millilitre-scale chromatographic analysis (Wierling et al., 2007).

1.4.2 Computer modelling

Although the USD methods presented above can reduce the time and material necessary to perform experimental process studies, an *in silico* approach can yield much process information, theoretically with a zero requirement for process material, although experimental studies are always vital to confirm computational conclusions. There are two main types of bioprocess simulation: process modelling and decisional tools.

1.4.2.1 Process modelling

Process modelling approaches apply mathematical design equations to unit operations in order to evaluate the likely values of outputs such as product yield or contaminant clearance as functions of process or feed properties such as flow rates or product titres. Process models have been created for unit operations such as filtration (Reynolds et al., 2003), centrifugation (Maybury et al., 1998), homogenisation (Siddiqi et al., 1996), and chromatography (Ngiam et al., 2001). These models are based upon mathematically rigorous design equations such as centrifugal grade efficiency expressions and are used to predict the operating conditions needed to satisfy target levels for outputs such as product yield or purity. Studies have also linked unit operations together to simulate the performance of whole processes and explore intra-process interactions (Zhou and Titchener-Hooker, 1999).

1.4.2.2 Decisional tools

Decisional tools simulations integrate business and process factors together when evaluating flowsheet options and operating conditions. Hence these tools add a financial and commercial dimension to technical process design and optimisation. Typical business factors considered include cost analysis, resource utilisation, and facility studies, in order to determine the best overall strategy for product manufacture. Examples of the use of these tools include: comparing perfusion and fed-batch modes of cell culture (Lim et al., 2006); evaluating the relative merits of packed and expanded bed protein capture (Mustafa et al., 2004); and using disposable technologies as an alternative to stainless steel vessels (Farid et al., 2005).

1.4.3 Statistical design of experiments (DoE)

DoE, experimental design, was invented during the 1950's for designing experiments in systems with several important variables as an alternative to the traditional 'one-factor-at-a-time' approach. DoE experiments alter multiple variables between single experimental runs in a statistical manner. This allows determination of the effects of both individual variables and in addition any interactions between them, with a minimum number of experimental runs.

DoE has a number of uses, and the statistical approach used will be determined by the experimental aim. It can be used to survey a large number of factors (e.g. pH, temperature etc.), or to identify key variables that determine an output (e.g. yield,

contaminant load, etc.). Another use is statistical analysis of variation (ANOVA), or testing process robustness by analysing sensitivity to input variables. These experiments are done by varying all factors over two 'levels' (extreme high and extreme low). Although a full factorial design will try all high/low combinations of variables and therefore identify all variable and interaction affects, the number of experimental runs can be drastically cut down by utilizing a fractional factorial design. These are based on the assumption that 3+ multivariate effects are rare, with interactions mostly involving only two variables. The exact determination of these multivariate interactions in sacrificed to reduce the number of experimental runs required. The effects are said to be 'aliased' with more likely single variable or two variable effects.

Statistical design can also be used to help optimise processes. Multiple variables are varied over 3+ values and a response surface created from which an optimum can be derived if the correct range of values is chosen. Examples of this kind of experimental design are central composite design (CCD), central composite facing (CCF), and central composite inscribed (CCI). CCD searches for an optimum area, CCF can confirm an optimum is in a specific location in the response surface and CCI can then be used to give an accurate determination of optimum conditions for highest, or lowest, output as desired.

Statistical design of experiments can become especially powerful when combined with methods that allow process scale-down and/or automation, as a large number of runs can then be performed whilst minimising time and process material requirements. It is especially useful for integrating QbD principles into a complex bioprocess.

There are many different examples of work in biochemical engineering where DoE methodology has been applied. For example, the optimization of medium components for the production of clavulanic acid by *Streptomyces clavuligerus* was performed using both fractional factorial design and response surface methodology (Wang et al., 2004). DoE has been found to be especially useful for determining the optimum conditions for protein crystallisation (Shaw Stewart and Baldock, 1999). A DSP example of the use of DoE is given by its application to the characterization and optimization of acoustic filter performance for solids separation from perfusion mammalian cell culture (Gorenflo et al., 2005).

1.5 Project objectives

This project aims to demonstrate the worth of ultra-scale down process mimics for candidate screening, early stage pre-pilot-scale process development and expanding knowledge of the design space of a finalised process. This aim is achieved by application of the USD approach to the industrial process for antibody fragment production in *E. coli.* After transfer from UCB to UCL, a complete USD mimic of the initial downstream process will be designed.

Firstly the initial centrifugal cell harvest unit operation is examined. In order to yield a full data set at millilitre-scale it is necessary to split centrifugal unit operations into four parameters: cell damage during exit and entry, clarification efficiency, and dewatering efficiency. These can then be individually mimicked using different USD techniques.

The second stage of the initial DSP under investigation is a heat/chemical periplasmic permeabilisation operation. A USD mimic is developed in order to both predict the performance of this unit operation and also provide sufficient material for study of the third unit operation in the initial DSP, centrifugal spheroplast removal, without the need to use DSP pilot equipment. The centrifugal spheroplast removal unit operation is then mimicked at USD level using the same techniques as developed for the centrifugal cell harvest unit operations.

This project aims to demonstrate the utility of USD studies by using the techniques developed to rapidly assess interactions between the USP and DSP, with the use of minimal process material. Therefore both the necessity for consideration of intra-process interactions for optimal process performance, and the utility of USD methodology to determine these interactions, is demonstrated. Finally the business and regulatory relevance of USD approaches are made clear.

1.6 Thesis layout

In the next chapter, details are provided about the materials and methods used throughout the project. The results of experimental studies are then presented in chapters 3 to 8.

Chapter 3 describes and characterises two HCD fermentations for the production of Fab' antibody fragments in *E. coli.* The two fermentation protocols were supplied by

UCB, where both are used for the large scale production of therapeutic antibody fragments. Both fermentations were transferred to UCL and characterised in depth. The IPTG-induced fermentation was chosen as the specific case study for the thesis, and the reasons for this choice are given, followed by in depth characterisation of the fermentation at pilot-scale.

Chapters 4-6 aim to provide a comprehensive approach to characterise the industrial centrifugation of HCD feeds. Chapter 4 considers the whole centrifugation unit operation and determines likely damage caused by industrial centrifuges upon the HCD cellular feed. Chapter 5 describes the adaptation of the USD method of Hutchinson et al. (2006) for determining centrifugal clarification to HCD cultures. This adaptation was necessary as the original method was found to greatly overpredict centrifugal clarification of HCD feeds. Chapter 6 describes the development of a novel USD method for rapid prediction of the dewatering of bioprocess feeds during industrial centrifugation.

Chapter 7 describes a millilitre-scale approach for characterisation of the periplasmic extraction of Fab'. It is used to elucidate the industrial robustness of the periplasmic extraction, using a DoE approach. This method completes the USD portfolio of the initial DSP for antibody fragment production in *E. coli*.

Chapter 8 demonstrates the utility of the USD methods developed by using them to determine interactions between the fermentation, specifically changes in the post-induction carbon feed rate, and the initial DSP. It is demonstrated that merely optimizing the fermentation unit operation will not optimise whole process output, as a non-optimum post-induction feed rate in terms of the fermentation is needed to produce optimum levels of Fab' after initial downstream processing.

Chapter 9 investigates cryopreservation techniques as an option for the long term storage of upstream material, to facilitate its use for later downstream process development.

Chapter 10 provides a summary of the main observations and conclusions of the project, and gives recommendations for future work.

Finally, Chapter 11 fulfils the compulsory business requirements of the EngD, discussing bioprocess management issues arising from the thesis, both in terms of economics and regulation.

2. Materials and methods

2.1 Materials

2.1.1 Chemicals

All chemicals, unless specified otherwise, were obtained from Sigma Chemical Co. Ltd. (Dorset, UK) and were of analytical grade.

2.1.2 *Escherichia coli* strain and plasmid

The industrial *E. coli* strain W3110 (ATCC 27325) containing plasmid pTTOD A33 IGS2 used was kindly donated by UCB (Slough, UK). pTTOD A33 IGS2 produces the A33 Fab' antibody fragment under control of the *tac* promoter. Each antibody chain was preceded by the *E. coli* OmpA signal peptide to direct secretion to the periplasmic space. A working cell bank was prepared as described elsewhere (Bowering et al., 2002).

2.1.3 *Saccharomyces cerevisiae*

Baker's Yeast was obtained in packed block form from J.W. Pike Ltd. (London, UK). Cells were suspended in phosphate buffered saline (PBS) pH 7.0 to the desired packed wet weight per volume before use in USD method development studies.

2.2 Fermentation methods

2.2.1 Culture media

2.2.1.1 2xPY complex media

This media contained 16 g/L Phytone (obtained from Becton-Dickinson Life Science Research Ltd., UK), 10 g/L yeast extract, and 5 g/L NaCl.

2.2.1.2 SM6F defined media

This media contained 5.2 g/L $(NH_4)SO_4$, 3.86 g/L $NaH_2PO_4.H_2O$, 4.025 g/L KCl, 1.04 g/L $MgSO_4.7H_2O$, 4.16 g/L citric acid monohydrate, 0.25 g/L $CaCl.2H_2O$, 112 g/L glycerol anhydrous, and 0.01% (v/v) 100 x SM6 trace elements solution. The pH was adjusted to 6.95 with 15% (w/v) ammonia solution. Care was taken not to exceed pH 7.1 as this was found to induce salt precipitation.

2.2.1.3 SM6G_c defined media

This media contained 5.2 g/L $(NH_4)SO_4$, 4.4 g/L $NaH_2PO_4.H_2O$, 4.03 g/L KCl, 1.04 g/L $MgSO_4.7H_2O$, 4.16 g/L citric acid monohydrate, 0.25 g/L $CaCl.2H_2O$, 112 g/L glycerol anhydrous, and 0.01% (v/v) 100 x SM6 trace elements solution. The pH was adjusted to 6.95 with 15% (w/v) ammonia solution. Care was taken not to exceed pH 7.1 as this was found to induce salt precipitation.

2.2.1.4 100 x SM6 trace elements solution

This solution contained 104 g/L citric acid monohydrate, 5.22 g/L $CaCl_2.2H_2O$, 2.06 g/L $ZnSO_4.7H_2O$, 2.72 g/L $MnSO_4.4H_2O$, 0.81 g/L $CuSO_4.5H_2O$, 0.42 g/L $CoSO_4.7H_2O$, 10.06 g/L $FeCl_3.6H_2O$, 0.03 g/L H_3BO_3, and 0.02 g/L Na2$MoO_4.2H_2O$.

2.2.2 Lactose-induced fermentations

2.2.2.1 Inoculum preparation

Starter cultures were grown from the contents of a single vial of WCB (Bowering et al., 2002) in shake flasks containing 2xPY media supplemented with 10 μg/mL tetracycline for ~ 8 h at 30°C, 200 rpm, to a final optical density at 600 nm (OD_{600}) of 1.0-1.5. This was used as a 10% (v/v) inoculum for shake flasks containing SM6F medium and 10 μg/mL tetracycline. These defined shakes were incubated for ~ 20 h at 30°C, 200 rpm to an OD_{600} of 3-4.

2.2.2.3 75 L lactose fermentation

3 L of culture from the defined media shakes described above was used to inoculate 30 L of SM6F media in a 75 L LH high category vessel fermenter (LH 1075 series stainless steel vessel, Ingeltech UK Ltd., Berkshire, UK). pH was maintained at 6.95 using 15% (w/v) ammonia solution and 10% H_2SO_4 (v/v) solution. Polypropylene glycol, average molecular weight 2025 Da, was used to control foaming as necessary. Dissolved oxygen was maintained at 30%, using gas blending with 40:60 O_2:N_2 when necessary. The culture temperature was maintained at 30°C until the OD_{600} reached ~ 40 (after ~ 22 h), after which it was reduced to 25°C for the duration of the culture. Online data were logged using the Propac software package (Acquisition Systems Ltd, Sandhurst, UK). At the point of temperature reduction, 375.6 mL of 1M $MgSO_4.7H_2O$ was added to stabilise the outer membrane and reduce Fab' leakage. When an OD_{600} of ~ 55 was achieved, 2.4 L of 50% (w/w) lactose, at 70°C for solubility reasons, was added. Approximately 2 h after lactose addition DOT spiking and demand for acid

indicated the entire glycerol carbon source in the culture had been utilised. This was termed the induction point of the culture. After induction 50% (w/w) lactose was fed batch-wise in order to maintain lactose concentration between 20-50 g/L. This was facilitated by offline lactose quantification as detailed in section 2.6.2. The culture was harvested 36 h after induction.

2.2.3 IPTG-induced fermentations

2.2.3.1 Inoculum preparation

Starter cultures were grown from the contents of a single vial of WCB (Bowering et al., 2002) in shake flasks containing 2xPY media containing 10 μg/mL tetracycline for ~ 4 h at 37°C, at 200 rpm, to a final OD_{600} of 1.0-1.5. This was used as a 10% (v/v) inoculum for shake flasks containing $SM6G_c$ medium and 10 μg/mL tetracycline. These defined shakes were incubated for ~ 20 h at 30°C, at 200 rpm to an OD_{600} of ~ 4.0.

2.2.3.2 75 L IPTG fermentation

3 L of culture from the defined media shakes described above was used to inoculate 30 L of $SM6G_c$ media in a 75 L LH high category vessel fermenter (LH 1075 series stainless steel vessel, Ingeltech UK Ltd., Berkshire, UK). pH was maintained at 6.95 using 15% (w/v) ammonia solution and 10% H_2SO_4 (v/v) solution. Polypropylene glycol, average molecular weight 2025 Da, was used to control foaming as necessary. Dissolved oxygen was maintained at 30%, using gas blending with 40:60 O_2:N_2 when necessary. The culture temperature was maintained at 30°C until the OD_{600} reached ~ 40 (after ~ 25 h), after which it was reduced to 25°C for the duration of the culture. Online data were logged using the Propac software package (Acquisition Systems Ltd, Sandhurst, UK). Between OD_{600} of 40-88 multiple salt additions were given: at OD_{600} ~ 40, 240 mL of 1M $MgSO_4.7H_2O$ was added; at OD_{600} ~ 56, 180 mL of a 232.8 g/L solution of $NaH_2PO_4.H_2O$ was added; at OD_{600} ~ 80, a further 240 mL of the $NaH_2PO_4.H_2O$ solution was added. When an OD_{600} of ~ 95 was achieved, DOT spiking and demand for acid indicated the entire glycerol carbon source in the culture had been utilised. At this point Fab' production was induced by addition of 75 mL of 15.31 g/L of isopropyl β-D-thiogalactopyranoside (IPTG). After induction carbon was supplied to the culture for Fab' synthesis and cell maintenance by a 49.5 mL h^{-1} constant glycerol feed. This is equivalent to 1.65 mL h^{-1} (L of starting media)$^{-1}$. The culture was harvested ~ 38 h after induction, measured from the time of IPTG addition.

2.2.3.3 20 L IPTG fermentation

1 L of culture from the defined media shakes described above was used to inoculate 10 L of $SM6G_c$ media in a 20 L LH 2000 series fermenter (Ingeltech UK Ltd., Berkshire, UK). pH was maintained at 6.95 using 15% (w/v) ammonia solution and 10% H_2SO_4 (v/v) solution. Polypropylene glycol, average molecular weight 2025 Da, was used to control foaming as necessary. Dissolved oxygen was maintained at 30%, using gas blending with 40:60 O_2:N_2 when necessary. The culture temperature was maintained at 30°C until the OD_{600} reached ~ 40 (after ~ 25 h), after which it was reduced to 25°C for the duration of the culture. Fermenter exit gases were monitored by mass spectrophotometry (MM8-80 Instrument, VG Gas Analysis Ltd., Middlewich, UK). Exhaust gas compositions and online data were logged using Bioview software (Adaptive Biosystems, Watford, UK). Between OD_{600} of 40-88 multiple salt additions were given: at OD_{600} ~ 40, 80 mL of 1M $MgSO_4.7H_2O$ was added; at OD_{600} ~ 56, 60 mL of a 232.8 g/L solution of $NaH_2PO_4.H_2O$ was added; at OD_{600} ~ 80, a further 80 mL of the $NaH_2PO_4.H_2O$ solution was added. When an OD_{600} of ~ 95 was achieved, DOT spiking and demand for acid indicated the entire glycerol carbon source in the culture had been utilised. At this point Fab' production was induced by addition of 25 mL of 15.31 g/L of IPTG. After induction carbon was supplied to the culture for Fab' synthesis and cell maintenance by a 10-25 mL/h constant glycerol feed. This is equivalent to 1.0-2.5 mL h^{-1} (L of starting media)$^{-1}$. The culture was harvested 36 h after induction, measured from the time of IPTG addition.

2.3 Downstream processing

2.3.1 Centrifugation

2.3.1.1 Pilot-scale disc-stack centrifugation

A CSA-1 centrifuge (Westphalia Separator, AG, Oelde, Germany) was used for pilot-scale disc-stack centrifugation. Feed flow rates of between 10-432 L h^{-1} were used. The maximal spin speed of this centrifuge is 9800 rpm, which gives a Sigma-factor (Σ) of 1602 m^2. Clarification efficiency was estimated by taking the mean OD_{600} of supernatant samples after 1 L of fluid had entered the centrifuge bowl. Optical density of a well spun sample and of the feed were measured at lab scale as described in section 2.4.3.4, and % clarification (*%C*) determined from Equation 2-1 below:

$$\%C = \frac{OD_f - OD_s}{OD_f - OD_r} \times 100 \qquad [2\text{-}1]$$

where OD_f, OD_s and OD_r are the optical density, measured at 600 nm, of the feed, the sample supernatant and the supernatant of a reference sample, respectively (Boychyn et al., 2000). The standard deviation of replicate measurements was used to assess error, which was typically < 1%.

2.3.1.2 Pilot-scale advanced tubular-bowl centrifugation

Feed suspension was pumped into a Carr Powerfuge™ P6 centrifuge (Carr Centritech Separation Systems, Clearwater, FL, USA) at flow rates from 10-50 L/h. Temperature was maintained at ~ 10°C using glycol cooling circulating at -4°C. Solids were discharged upon the bowl reaching capacity (indicated by breakthrough of solids to supernatant). When dewatering was assessed, approximately 10 g samples of the paste discharge were taken, weighed (WW_{sed}), and then dried at 100°C to a constant mass (~ 24 h). The weight of the dried sediment was then recorded (DW_{sed}). Five separate samples were taken and averaged for each paste discharge to compensate for incomplete mixing post-ejection. The standard deviation of the samples was used for estimation of the error, found to be at most %D ± 8.5%.

2.3.2 Pilot-scale periplasmic extraction

The patented method of Weir and Bailey (1997) was used to achieve Fab' release by selective periplasmic permeablisation and simultaneous heat denaturation of protein contaminants. Cell paste was resuspended to its pre-centrifugation volume in extraction buffer to achieve a final concentration of 100mM Tris, 10mM EDTA at pH 7.4 and heated to 60°C for 16 h in either the 75 L LH 1075 series high category vessel fermenter (dewatering verification studies only), a 3 L LH 500 series fermenter (periplasmic extraction studies with internal heating element), or an Applikon Type-20 Bioreactor (Applikon, Schiedam, Holland) (all other studies). After 16 h the cells were cooled to ~ 15°C in the fermenter used for extraction. The level of reproducibility was generally high with average coefficients of variance of 1.7 and 6.6 for Fab' and total protein concentration determinations respectively.

2.4 USD methods

2.4.1 USD assessment of centrifugal entry damage

E. coli cells from an IPTG-induced fermentation run using a post-induction glycerol flow rate of 1.46 mL h^{-1} L^{-1} were taken 36 h after induction. In order to mimic the impact of high-shear regions in the inlet of centrifuges, 20 mL portions of these cells were sheared in the shear cell device described in Hutchinson et al. (2006) for 20 s at spin speeds from 0-20,000 rpm to yield maximum energy dissipations between 0 and $1.6x10^6$ W/kg. Samples were sheared at room temperature. Within 10 min of application of the shear force in the shear cell device three 2.0 mL samples of the sheared material was spun for 10 min at 13,200 rpm in an Eppendorf 5415R centrifuge, rotor F45-24-11 (Eppendorf UK Ltd., Cambridge, UK) at 4°C. The supernatant portion was then aspirated and filtered through a 0.22 μm syringe filter before being analysed for total protein and Fab' concentration. Three separate samples of the homogenate were analysed and the average Fab' concentration recorded. Error was calculated from the standard deviation of the three separate samples from each shear rate. 100% cell breakage samples were produced by high pressure homogenisation of 40 mL of the *E. coli* feed material. After homogenisation the 40 mL homogenate was treated exactly as the samples sheared in the rotating disc shear device. The level of reproducibility was found to be high, with average coefficients of variance of 1.4 and 3.3 for Fab' and total protein respectively.

2.4.2 USD assessment of centrifugal exit damage

2.4.2.1 Sample preparation

400 mL of cell broth from the relevant fermentation was spun in an Avanti JE Centrifuge System (Beckman Coulter, High Wycombe, UK) using a JS-13.1 swing-bucket rotor (N = 300-13000 rpm, relative centrifuge force (RCF) max = 26750 g) at 13,000 rpm, 4°C for 20 min. The sediment was then gently resuspended in sufficient quantity of the supernatant to generate an ~ 40% (packed wet weight/volume) suspension with a viscosity from 4-6 mPa s: approximately the same concentration and viscosity as can be expected in the collection zone of the disc-stack centrifuge used. The suspension was kept on ice for a maximum of 1 h until USD damage assessment could be performed.

2.4.2.2 USD exit damage assessment

The Instron capillary rheometer (Instron Ltd., High Wycombe, UK) was modified in-house and used as shown in Fig. 4-2. The plunger and barrel are constructed from an aluminium alloy, Durell (Smith Ltd., London, UK) with a barrel diameter and length of 20 mm and 60 mm respectively. The plunger speed is controlled by a discrete series of cog combinations, and is capable of drive speeds from 50-800 mm min^{-1}. A stainless steel capillary with an internal diameter of 0.25 mm and length 20 mm was supplied by Coopers Needle Works Ltd (Birmingham,UK). The cylindrical impingement target, constructed of stainless steel, had a diameter and height of 30 mm, and was positioned 90 mm vertically below the capillary. During trials, the target was positioned inside a collection beaker, with a lid to contain aerosol release. 15 mL samples were added to the barrel of the device and ejected from the capillary at the desired speed. After sample collection in the collection beaker, 9.3 mL of UHP water followed by 2.7 mL of 10 x Extraction Buffer (1M TRIS, 100mM EDTA, pH 7.4) was added to the 15 mL sample to yield a 20% (packed wet weight/volume) suspension in extraction buffer identical to that which would be used for pilot-scale Fab' extraction. USD periplasmic extraction was subsequently undertaken. Each ejection speed measurement was performed in triplicate and error is presented as the standard deviation of triplicate experiments. The level of reproducibility was found to be moderate, with average coefficients of variance of 4.5 and 7.8 for Fab' and total protein concentrations respectively.

2.4.2.3 Assessment of complete cell breakage

Complete cell breakage was estimated by high pressure homogenisation of 40 mL of the 40% (packed wet weight/volume) suspension. Periplasmic extraction was performed using a 15 mL aliquot of this homogenised sample exactly as described above for the samples that had passed though the Instron device.

2.4.3 USD centrifugal clarification

2.4.3.1 Wet solids content determination

The dry cell weight (DCW) of each cell suspension was determined as follows. 2 mL samples were spun for 30 min at 14,000 rpm in a pre-weighed microfuge tube using an Eppendorf 5810R centrifuge, rotor T-60-11, and the supernatant was aspirated. Cell pellets were then dried to a constant weight at 100°C. All measurements were performed in triplicate. The wet cell weight (WCW) was then calculated by dividing the DCW measurement by the DCW:WCW ratio for the particular cell type. This ratio was

determined from literature (Watson, 1965; Zierold, 1988) as 0.35 for Baker's Yeast and 0.30 for *Escherichia coli*. This method is more accurate than directly calculating WCW from the undried pellet due to the significant levels of interstitial water in a centrifugally dewatered paste.

2.4.3.2 Sample preparation – USD method for dilute (< 2% w/v) suspensions

One 100 mL sample of cell suspension was designated to be the undiluted sample, representative of the original USD method. This was sheared in the shear cell device described in Hutchinson et al. (2006) for 20 sec at 13,000 rpm and 20°C in order to mimic the impact of high-shear regions in the inlet of centrifuges leading to potential cell and cell aggregate disruption and carry over of solid contaminants. OD_{600} was then assessed and used as OD_f (Equation 2-1).

2.4.3.3 Sample preparation – USD method for high solids suspensions (> 2% w/v)

The diluted feed was created as follows. Approximately 120 mL of cell suspension was sheared in 6 batches in the shear cell device as described above. This was then spun for 30 min in an Eppendorf 5810R centrifuge, using rotor A-4-81 (N = 1000-4000 rpm, RCF max = 3250 g) and the resulting supernatant used to dilute a 10 mL portion of the original feed 1:10 (v/v). This diluted feed sample was subsequently itself sheared in the same way as the undiluted sample. OD_{600} was then assessed and used as OD_f (Equation 2-1).

2.4.3.4 Clarification test

Clarification was mimicked in both the diluted and undiluted feeds by adding 2 mL of freshly prepared sheared material to 2.2 mL microfuge tubes and spinning these in an Eppendorf 5810R centrifuge, rotor T-60-11 at a variety of spin speeds for a variety of spin times to give the desired range of $V/ct\Sigma$. All samples were spun at 10°C in order to maintain a similar temperature to that found in the settling region of the disc-stack centrifuge used. The entire supernatant was removed by pipetting and OD_{600} measured. A well-spun sample (rotor T-60-11, 13,000 rpm, 30 minute spin time) was prepared as a clarification reference sample, and the OD_{600} of the supernatant was taken to be representative of 100% clarification. All experimental points were carried out in triplicate and standard deviation used to assess error. This was typically moderate with an average coefficient of variance of 2.4. Percentage clarification was calculated using Equation 2-1.

2.4.4 USD dewatering prediction

For each type of feed used, a calibration curve was created to determine the relationship between the concentration of the cell suspension and sediment height. This was achieved by spinning five different concentrations of cells to steady-state clarification. The height of the liquid above the sediment was held constant through careful variation of the volume and concentration of feed added. % Clarification, *(%C),* was calculated as described in section 2.4.3 for the feed to be used in the dewatering experiments. A range of Q/cΣ values were used so as to gain at least four %C values of between 90-99%. These were then plotted on a probability-log graph and the Q/cΣ value for %C = 95 determined. This value was then used to determine $t_{95\%}$ for the operating conditions in the USD dewatering test, via Sigma theory. Samples were spun in pre-weighed centrifuge tubes of various sizes in either an Eppendorf 5810R centrifuge, rotor T-60-11 (N = 2000-14000 rpm) or swing-bucket rotor A-4-81 (N = 1000-4000 rpm, RCF max = 3250 x g) or an Avanti JE Centrifuge System (Beckman Coulter, High Wycombe, UK), JS-13.1 swing-bucket rotor (N = 300-13000 rpm, RCF_{max} = 26750 x g) with 15 mL tube adaptors. The Avanti JE Centrifuge System has negligible acceleration and deceleration times as used.

Upon completion of a spin the majority of the supernatant was removed from the centrifuge tubes by careful pipetting, and the remaining fluid removed from the walls of the tube by absorption to a cotton bud stick. The weight of the wet sediment was recorded (WW_{sed}). The tube was then dried at 100°C to constant mass and the weight of the dried sediment recorded (DW_{sed}).

All centrifugation runs were performed at a constant temperature of 10°C, and all experiments were performed at least in triplicate with standard deviation used to estimate the error for these laboratory determinations, found to be at most %D ± 2.5%.

2.4.5 USD periplasmic extraction

A 1 mL sample of fermentation broth was spun for 10 min at 13,200 rpm, 4°C, in an Eppendorf 5415R centrifuge, rotor F45-24-11. The supernatant was discarded by careful aspiration and immediately resuspended as follows. 0.5 mL of ultrapure water was added, followed by 0.2 mL of 5 x extraction buffer (0.5 M TRIS, 50 mM EDTA, pH 7.4) before the total volume was increased to 1 mL using ultrapure water. Pellet

resuspension was achieved through the use of a vortex mixer. The suspension was then held at 60°C for 16 h at 1000 rpm using an Eppendorf Thermomixer R. Subsequently the sample was spun for 10 min at 13,200 rpm in the Eppendorf 5415R centrifuge, rotor F45-24-11 held at 4°C. The supernatant portion was then aspirated and filtered through a 0.22 μm syringe filter before analysis. Standard deviation of triplicate experiments was used to assess error, which was usually found to be low with average coefficients of variance of 1.7 and 3.1 for Fab' and total protein release respectively.

2.5 Production of A33 Fab' standard

A A33 Fab' standard of known concentration was necessary for the calibration of the protein G Fab' quantification assay and for use in SDS-PAGE. The A33 Fab' standard was purified from cells obtained during a 75 L IPTG-induced fermentation (section 2.2.3) using a post-induction glycerol feed rate of 1.65 mL h^{-1} L^{-1}. Cells were harvested using disc-stack centrifugation (section 2.3.1.1) with a feed flow rate of 25 L/h. Cells were resuspended to original concentration in periplasmic extraction buffer (100 mM Tris HCl, 10 mM EDTA, pH 7.4) and held at 60°C for 16 h at 250 rpm in an Applikon Type-20 Bioreactor (Applikon, Schiedam, Holland). Following extraction, spheroplasts were removed by centrifugation at 10,000 rpm, 4°C, for 1.5 h using a Beckmann J2-M1 centrifuge (Beckman Instruments UK Ltd., High Wycombe, UK) with a JA-10 rotor. The supernatant was then microfiltrated through a 90 mm diameter 0.22 μm polyethersulphone membrane.

Fab' was purified from this extractant supernatant by packed bed Protein A affinity chromatography using a AKTAprime system (Amersham Biosciences UK Ltd., Little Chalfont, UK) and a XK50 column (50 mm by 70 mm, 50 mL column volume) packed with Protein A Sepharose® 4 Fast Flow matrix (column and matrix obtained from GE Healthcare UK Ltd., Bucks, UK). An operating flow rate of 35 mL min^{-1} was used throughout the purification. Glycine/glycinate was added to a final concentration of 1 M (pH 7.5) to the extractant. The column was equilibrated with 15 column volumes of equilibration buffer (1 M glycine, pH 8.0) before extractant application. The column was then washed with 5 column volumes of equilibration buffer before Fab' elution was performed using ~ 3 column volumes of 0.1 M sodium citrate pH 3.0. 35 mL fractions were collected in tubes containing 10.5 mL of 1M TRIS (pH 9.0) to adjust pH of eluted Fab' to 5.5. Fractions containing the concentrated Fab' were then pooled together to create the purified Fab' solution.

The purified Fab' solution was buffer exchanged into storage buffer (100 mM sodium acetate, 125 mM NaCl, 0.02% (w/v) sodium azide, pH 5.5) using an Amicon stirred ultrafiltration cell 8400 (Amicon Inc., Beverly, MA, USA) with an Ultracel YM regenerated cellulose membrane with a 20 kDa Mw cut-off (Millipore, Billerica, MA, USA).

The concentration of the resulting solution was determined from the absorbance (A) at 280 nm, using Equation 2-2.

$$A = \varepsilon.c.l \qquad [2\text{-}2]$$

Where c is the concentration of the Fab' (mg mL^{-1}), l is the light path (cm), and ε is the extinction coefficient. For A33 Fab', ε is equal to 1.38 mg^{-1} mL cm^{-1} (Bowering, 2004). Purity and quality of the Fab' standard was assessed using the Agilent 2100 Bioanalyser (section 2.6.8) and also by SDS-PAGE (section 2.6.9).

2.6 Analytical methods

2.6.1 Particle size distribution data

Particle size distribution (PSD) was determined by laser diffraction using a Mastersizer 2000 with a Hydro SM(A) manual small volume sample dispersion unit (Malvern Instruments Ltd., Malvern, UK) at a detecting range of 0.02-2000 μm. Size distribution in terms of % of total particle volume was recorded. Each cell suspension to be analysed was well mixed before being added dropwise to the small volume dispersion unit until an obscurance of 11-13% was reached. Measurements were repeated in triplicate and the average particle size range recorded.

2.6.2 Metabolite analysis

For analysis of lactose, glycerol and acetate concentrations in fermentation supernatant, a Dionex summit HPLC system with UV and refractive index detection was used (Dionex Corp., Sunnyvale, CA, USA). Fresh fermentation broth was spun for 10 min at 13,200 rpm in an Eppendorf 5415R centrifuge, rotor F45-24-11. The supernatant portion was then aspirated and filtered through a 0.22 μm syringe filter before being added to the HPLC multi-sampler.

A 300 x 7.8 mm Aminex ion-exclusion HPX-87H column (BioRad, Hercules, CA, USA) was used at 60°C. The mobile phase was 5 mM H_2SO_4 pumped at 0.6 ml/min. Acetate was detected by UV absorbance at 215 nm. Glycerol and lactose were detected by refractive index. Quantification was performed using peak area based on standard solutions of the analytes. Injection volume was constant at 20 µL for both samples and standards.

2.6.3 Protein G HPLC assay for Fab' quantification

2.6.3.1 Sample preparation

2.6.3.1.1 Total fermentation samples

A 40 mL sample was withdrawn from the fermentation at each timepoint and stored for a maximum of 4 days at -20°C. Samples were rapidly thawed in at 37°C and immediately homogenised as described in section 2.6.7.1. A 2.0 mL sample of the homogenate was spun for 20 min at 13,200 rpm in an Eppendorf 5415R centrifuge, rotor F45-24-11 at 4°C. The supernatant portion was then aspirated and filtered through a 0.22 µm syringe filter before being added to the HPLC multi-sampler. Three separate samples of the homogenate were analysed and the average Fab' concentration recorded.

2.6.3.1.2 Periplasmic fermentation samples

A 1 mL sample of fermentation broth was spun for 10 min at 13,200 rpm, 4°C, in an Eppendorf 5415R centrifuge, rotor F45-24-11. The supernatant was discarded by careful aspiration and the pellet stored in the microfuge tube at -20°C for a maximum of 4 days. The pellet was then rapidly thawed at 37°C and immediately resuspended as follows. 0.5 mL of UHP water was added, followed by 0.2 mL of 5 x extraction buffer (0.5 M TRIS, 50 mM EDTA, pH 7.4) before the total volume was increased to 1 mL using UHP water. Pellet resuspension was achieved through the use of a vortex mixer. The suspension was then held at 60°C for 16 h at 1000 rpm using an Eppendorf Thermomixer R. Subsequently the sample was spun for 10 min at 13,200 rpm in an Eppendorf 5415R centrifuge, rotor F45-24-11 (Eppendorf UK Ltd., Cambridge, UK) held at 4°C. The supernatant portion was then aspirated and filtered through a 0.22 µm syringe filter before being added to the HPLC multi-sampler. Three separate samples were analysed and the average Fab' concentration recorded.

2.6.3.1.3 Supernatant fermentation samples

A 1 mL sample of fermentation broth was spun for 10 min at 13,200 rpm, 4°C, in an Eppendorf 5415R centrifuge, rotor F45-24-11. The supernatant portion was then aspirated and filtered through a 0.22 µm syringe filter before being added to the HPLC multi-sampler. Three separate samples were analysed and the average Fab' concentration recorded.

2.6.3.2 Fab' quantification

Fab' quantification was achieved by a HPLC-based method, utilizing the fact that streptococcal protein G specifically binds both whole IgG and also Fc and Fab (Lian et al., 1994). A Protein G Hi-Trap column (GE Healthcare, Uppsala, Sweden) of 1 mL volume was connected to a modified Agilent 1100 series HPLC system (Agilent Technologies UK Ltd., West Lothian, UK). Column temperature was maintained at 23°C. The column was equilibrated in buffer A (20 mM sodium phosphate, pH 7.4). Injection volume was kept constant at 50 µL. Elution was performed using buffer B (20 mM sodium phosphate, pH 2.5). Protein elution was measured at 220 nm. Peak integration was performed and the resulting Fab' concentration determined from a standard curve generated from standards of pure A33 Fab' in known concentration. Samples were diluted in extraction buffer (100 mM TRIS, 10 mM EDTA, pH 7.4) to be in the linear range of the assay (20-600 mg/L), if required. The level of reproducibility was high with less than 5% variation in Fab' concentration.

2.6.4 Determination of total protein concentration

Samples were spun for 10 min at 13,200 rpm in an Eppendorf 5415R centrifuge, rotor F45-24-11. The supernatant portion was then aspirated and filtered through a 0.22 µm syringe filter to remove particulate matter. Protein concentration of the supernatant was then assayed at 595 nm after treatment with Coomassie Brilliant Blue (Bio-Rad Laboratories, GmbH, Munich, Germany) according to Bradford (Bradford, 1976) with bovine serum albumin (BSA) as a standard, although in most applications relative rather than actual protein concentration was assessed. Samples were diluted in extraction buffer (100 mM TRIS, 10 mM EDTA, pH 7.4) to be in the linear range of the assay (0.1-1.5 g/L), if required.

2.6.5 Viscosity measurements

Sample viscosities were measured with a concentric cylinder Rheomat 115 viscometer (Contraves Industrial Products, Middlesex, UK). Samples of ~ 20 mL were exposed to a range of set torque speeds that generate a shear rate ranging between 24.3-877 s^{-1}. Preset speeds above 11 were not used because of the occurrence of turbulent conditions that result in deviation of viscosity properties. Recorded readings were plotted on a shear stress versus shear rate graph and the corresponding viscosity calculated from the gradient of the correlation. Temperature was maintained at ~ 4°C by circulating cold water through the housing via a water bath. All viscosity measurements were recorded in duplicate.

2.6.6 Determination of biomass

2.6.6.1 Optical density (OD_{600})

Measurements of optical density were performed using a Genesys™ 10 series spectrophotometer (ThermoSpectronic, Cambridge, UK) at 600 nm. The sample to be analysed was, if necessary, diluted in saline solution (8.5 g/L NaCl) order to keep the absorbance reading (A) within the linear range of the spectrophotometer ($A < 0.9$). Saline solution was used as a blank. Measurements were performed in triplicate and standard deviation used to assess error.

2.6.6.2 Dry cell weight (DCW)

The dry cell weight (DCW) of each cell suspension was determined as follows. 2 mL samples were spun for 15 min at 14,000 rpm in a dried pre-weighed microfuge tube using an Eppendorf 5810R centrifuge, rotor T-60-11 and the supernatant was aspirated. Cell pellets were then dried to a constant weight at 100°C. All measurements were performed in triplicate.

2.6.7 Total sample disruption

2.6.7.1 Homogenisation of E. coli cells

Complete cell disruption was achieved using a Gaulin Micron Lab 40 homogeniser (APV Gaulin GmbH, Lubeck, Germany). 40 mL samples of broth were passed twice through the homogenising valve at an operating pressure of 1200 bar. Glycol cooling was supplied to the equipment to reduce the disruption temperature to 4°C.

2.6.7.2 Sonication of E. coli spheroplasts

Complete spheroplast disruption was necessary with smaller volumes than could be processed by high pressure mechanical homogenisation. Therefore spheroplast disruption was achieved by sonication. 1 mL samples of post-extraction samples containing suspended spheroplasts were held on ice in a 1.5 mL No Stick™ microfuge tube and subjected to 10 s on/10 s off pulses of 10 μm amplitude for 2 min using a Soniprep 150 bench mounted ultrasonic disintegrator with exponential probe (MSE (UK) Ltd., London, UK).

2.6.8 SDS-PAGE

Non-reducing SDS-PAGE electrophoresis was carried out using Novex® Bis-Tris Gels using the XCell *SureLock™* Mini-Cell. Samples were diluted in Extraction Buffer (10mM EDTA, 100mM Tris, pH 7.4) and denatured by mixing with 5 μL of Tris-Glycine SDS Sample Buffer (2x) and heating at 85°C for 3 min. Samples were subsequently subjected to electrophoresis on Novex® polyacrylamide Bis-Tris gels at a constant voltage of 125 V for 90 min. Gels were stained with SimplyBlue™ SafeStain and destained in UHP water. Pre-stained BenchMark™ Protein Ladder was used for estimation of molecular weight of protein bands. All reagents were obtained from Invitrogen (Carlsbad, CA, USA). For detailed instructions refer to the Novex Pre-Cast Gel Electrophoresis Guide available at www.invitrogen.com.

2.6.9 Numeration of colony forming units

For measurement of the number of dividing cells per mL (colony forming units, CFU) samples were serially diluted by adding 0.1 mL to 0.9 mL PBS pH 7.0. 0.1 mL of the resulting cell suspension was then plated onto 2xPY complex media (16 g/L Phytone, 10 g/L yeast extract, 5 g/L NaCl and 20 g/L technical agar) and incubated at 37°C for 48 h until single colonies could be resolved. Triplicate samples were diluted and analysed and error estimated by standard deviation. Errors were typically in the range of one order of magnitude.

2.6.10 Cell damage analysis using flow cytometry

All flow cytometry analysis was undertaken using a Coulter EPICS XL MCL analyser (Beckman Coulter UK Ltd., High Wycombe, UK) with a 15 mW argon-ion LASER tuned at 488nm. The instrument was set to measure forward angle light scatter (FS), side angle light scatter (SS), and the optical filters were set so as to measure Bis-(1,3-

dibutylbarbituric acid)trimethine oxonol (BOX) fluorescence at 525 nm (FL1) and propidium iodide (PI) fluorescence at 630 nm (FL3). Since there is a spectral overlap between BOX- and PI-emitted fluorescence, the software compensation was set up in such a way that BOX-emitted fluorescence was eliminated from the PI-emitted fluorescence detector and vice-versa.

A working flow cytometry solution of 4 mM EDTA, 2 μg/mL PI, and 5 μg/mL BOX in PBS pH 7.0 was produced. PI and BOX were obtained from Invitrogen (Carlsbad, CA, USA) and stock solutions of the two dyes were prepared as follows: PI was made up at 200 μg/mL in UHP water and stored at 4°C and BOX was made up at 10 mg/mL in dimethyl sulphoxide (DMSO) and stored at -20°C. The working solution was passed through a 0.2 μm filter prior to the addition of the BOX to remove particulate matter (the anion BOX may adhere to filter membranes).

Samples for analysis were diluted to OD_{600} of 0.1 in PBS pH 7.0. Subsequently 10 μL of diluted sample was mixed with 1 mL of working flow cytometry solution, vortexed for 10 s, and incubated at room temperature for 15 min. The sample was then analysed at a flow rate of 100-300 cells s^{-1}. Samples were analysed in triplicate and error estimated by standard deviation of the percentage of healthy cells observed. Between each sample a control containing 1 mL of working flow cytometry solution only was analysed to ensure background counts (due to dust particles etc.) were minimal.

2.7 Computational methods

2.7.1 CFD analysis

Note: all CFD experiments were performed by Ioannis Papantoniou, Department of Biochemical Engineering, UCL, and the methods and results supplied.

The flow engineering environment in the rotational disc USD device was characterised by solving the Navier-Stoke equations with specified boundary conditions. The numerical solution was carried out by using a commercial CFD package, Ansys CFX 5.7.1 (ANSYS, PA, USA, 2003). The geometry for both devices was drawn on Workbench 9.0 and the unstructured mesh was generated from CFX-Mesh. The CFX Solver was used to solve the mass and momentum equations simultaneously to obtain local information for velocity and turbulence. The k-ω based Shear-Stress-Transport (SST) model was employed in this study as it was designed to give a highly accurate

prediction of the onset and the amount of flow separation under adverse pressure gradients by the inclusion of transport effects into the formulation of the eddy-viscosity (Menter, 1996), which results in a major improvement in terms of flow separation predictions compared to the general k– ε turbulence model. The density and viscosity of the cell suspension was assumed to be the same as water. The CFX-Analysis was used to interpret the simulation results after the CFX-Solver. The biological materials in both devices may subject to both tangential (shear) and normal stress. To represent the real flow intensity, the shear rate was defined to include the normal and tangential velocity gradients (Equation 2-3).

$$sstrnr = \left[2\left\{\left(\frac{\partial U_x}{\partial x}\right)^2 + \left(\frac{\partial U_y}{\partial y}\right)^2 + \left(\frac{\partial U_z}{\partial z}\right)^2\right\} + \left(\frac{\partial U_x}{\partial y} + \frac{\partial U_y}{\partial x}\right)^2 + \left(\frac{\partial U_x}{\partial z} + \frac{\partial U_z}{\partial x}\right)^2 + \left(\frac{\partial U_y}{\partial z} + \frac{\partial U_z}{\partial y}\right)^2\right]^{\frac{1}{2}} \quad [2\text{-}3]$$

Within the rotating disc device breakage is considered to happen within the area of the boundary layer. The energy dissipation rate (ε) within the boundary layer can be calculated by Equation 2-4.

$$\varepsilon = sstrnr^2 \times \frac{\mu}{\rho} \quad [2\text{-}4]$$

2.7.2 Statistical design of experiments

Experimental design was formulated according to a resolution V 2-factor design, where main affects are aliased with 4-factor interactions and 2-factor interactions are aliased with 3-factor interactions, using DESIGN EXPERT 7.0 software (Statease, USA). 8 input variables were varied and two responses measured.

2.7.3 Creation of process model

The process model created to calculate the effect of variations in the upstream process parameter post-induction glycerol feed rate upon Fab' yield both before and after initial downstream processing was created using MATLAB® 7.1 (The MathWorks Inc., Natick, MA, USA) using the equations defined in Chapter 8 and a matrix containing values of feed rate from 1.00 to 2.00 mL h^{-1} L^{-1}, with an interval length of 0.01 mL h^{-1} L^{-1}.

3. Choice, characterisation and analysis of upstream process for production of antibody fragments

3.1 Abstract

This chapter investigated two upstream process protocols for the production of antibody fragments in *E. coli*. Both are of a batch/fed-batch design and utilise a W3110 *E. coli* strain containing a high-copy number plasmid encoding a polycistronic operon coding for the production of A33 Fab' light and heavy chains, targeted to the bacterial periplasm, under the control of the *tac* promoter. However, one method utilised lactose to both induce Fab' production and act as a carbon and energy source post-induction while the other used isopropyl β-D-thiogalactopyranoside (IPTG) to induce Fab' production and a glycerol feed to provide energy and carbon post-induction. The objective was to determine the most suitable protocol to be used for the upstream case study in this thesis. The chosen process was then characterised in detail and the post-induction glycerol feed rate shown to be a critical process parameter.

Both of the protocols were characterised at 75 L pilot-scale. Analysis of the online and product production data shows the IPTG-induced process produced over 1 g/L Fab' in total, with less than 20% of this leaking to the extracellular medium. By contrast the lactose-induced process produced under half the total amount of Fab', with over 95% leakage to the extracellular medium and widespread cell death and lysis being observed. Therefore the IPTG-induced process was deemed most suitable for further study and its product formation and cell growth profiles and metabolic indicators were then characterised in detail through a set of 20 L pilot-scale trials. The impact of post-induction glycerol feed rate was studied in a series of 20 L scale fermentations and found to heavily influence biomass production and product yield and compartmentalisation. Results were used to determine the changes in Fab' production as feed rate varies. These results were used to predict that an optimal post-induction feed rate of 1.42 mL h^{-1} L^{-1} would generate the maximal Fab' yield of 1.11 g/L. Lower feed rates would not supply sufficient carbon and energy for maximal Fab' production, while higher feed rates result in widespread product leakage into the extracellular medium and cell death.

3.2 Introduction

The use of an industrial strain, plasmid and production strategy are critical to the relevance and usefulness of this work. As such, the A33 Fab' production *E. coli* used was kindly donated by UCB. This production system is *E. coli* strain W3110 (ATCC number 27325) transformed with the A33 expression vector pTTOD A33 IGS2. Strain W3110 is a prototrophic derivative of the wild-type K12: it has the same metabolic capabilities and nutritional requirements as wild-type. Therefore the molecular biology of the host strain has not been modified to facilitate either HCD culture (section 1.3.1.1) or recombinant protein production (section 1.3.1.2).

Production plasmid pTTOD A33 IGS2 encodes both the heavy and light chains of the A33 antibody fragment. The two antibody chains are expressed from a dicistronic operon to ensure the transcription of equal quantities of each chain. Furthermore, the light chain is situated upstream of the heavy chain so that it is translated first, to enhance both cell viability and the efficiency of antibody secretion (Tsumoto et al., 1994; Weir and Bailey, 1997). Expression is controlled by the synthetic *tac* promoter, therefore induction is induced chemically using either lactose or IPTG. Both chains are preceded by the ~ 4.8 kDa OmpA signal peptide in order to direct their secretion to the periplasmic space, which is cleaved upon secretion (Pugsley, 1993). The oxidizing environment and presence of a number of proteins important for folding and assembly of proteins such as protein disulphide isomerases (e.g. DsbA and DsbC), peptidyl prolyl isomerases (e.g. FkpA and RotA) and putative chaperone-like proteins (e.g. Skp and SurA) make the periplasmic space suitable for the correct folding of the Fab' protein (Arbabi-Ghahroudi et al., 2005). The plasmid can be selectively maintained by its conference of tetracycline resistance on the host, and maintains a medium copy number between 6 and 50. The A33 protein produced by the plasmid has been described previously (section 1.3.4). Further description of this plasmid is not possible here because of the nature of the IP agreement agreed with UCB to allow its use at UCL.

As well as supplying the strain used, UCB also supplied two fermentation protocols for the production of the A33 Fab' using the *E. coli* provided (section 2.2). Both of these have been used industrially to produce antibody fragments.

The two processes have many similarities. Both are standard industrial batch processes for the production of human therapeutic proteins. For example, fully-defined media free

from animal products is used in the production stage. They both operate in two phases. In the first phase (~ 32 h duration), *E. coli* cells are grown to high density (~ 50 g/L DCW) in a batch method. Glycerol, rather than glucose, is used as the carbon source, and the culture is kept constantly aerobic in order to halt acetate formation. Temperature is held at 30°C, lower than the optimum for *E. coli* growth, for plasmid maintenance without the necessity for antibiotic use and to reduce the oxygen demand of the culture. The pH is controlled by the addition of ammonia, which also serves to supply nitrogen. Towards the end of the growth phase the culture temperature is reduced to 25°C in preparation for Fab' production. This lower temperature both slows protein production giving more time for correct transport and assembly of the Fab' and also reduces outer membrane stress and therefore Fab' loss to the extracellular medium. A concentrated solution of divalent cations is added at the point of temperature reduction to increase the outer membrane stability and further reduce Fab' leakage to the medium. In the second phase, the induction phase, the cells so produced are exposed to a chemical inducer to stimulate Fab' production. In this phase growth is controlled by limiting nutrient concentration in order to help retain Fab' in the periplasm. In both processes this induction phase commences 36 h before harvest.

The main differences between the processes stem from the different inducer utilised. The first process uses lactose as the inducer while the second uses IPTG. The main advantages of lactose are that it is cheaper than IPTG and has no toxicity issues (Lim et al., 2004b). Lactose can be used as both the carbon source post-induction and the inducer. This is not without its problems however, as the need to maintain continually lactose concentration between 20-50 g/L to continue Fab' induction means restriction of carbon availability cannot be used to control post-induction growth. Therefore the lactose-induced fermentation is designed to be phosphate limited after induction, in order to control cell division during Fab' production and reduce Fab' leakage from the periplasm. IPTG has the advantage of being non-metabolised, facilitating easy control of cell growth post-induction in the IPTG-induced process via a glycerol feed. In this process phosphate concentration is kept non-limiting by multiple additions during the growth phase.

3.3 Results and discussion

3.3.1 Large pilot-scale process exploratory studies

Both the lactose- and IPTG-induced processes were run at large pilot-scale (75 L fermenter) at UCL in order to determine which process would be most suitable for use as the case study in this process.

3.3.1.1 Large pilot-scale process exploratory studies – the lactose-induced process

The lactose-induced process was run at 75 L pilot-scale with an initial working volume of 30L. Fig. 3-1 illustrates pertinent online data. The point of temperature reduction from 30°C to 25°C can be seen to occur in the last third of the growth phase. Although this temperature reduction reduced oxygen demand, it was still necessary to switch inlet air to 40:60 O_2:N_2 from ~ 26 h. A pH spike is visible at 35 h, this was accompanied by a DOT spike. This indicates that all glycerol had been consumed by 35 h, and this time point is taken for the onset of induction. This conclusion is supported by metabolite analysis of the culture supernatant (Fig. 3-2), which also did not detect acetate concentrations rising above 1 g/L during whole time-course of the fermentation. It should be noted from Fig. 3-2 that lactose addition occurred ~ 6 h prior to glycerol depletion and induction. This ensures sufficient lactose is available to the cells at induction, as time is required for the synthesis of lactose membrane transporters by the cell to allow the intake of sufficient lactose to induce Fab' production. This has been proved necessary to counter the slow initial rate of lactose uptake (Menzella et al., 2003). Note also that lactose concentration was held between 20-50 g/L by five batch additions from a 50% (w/v) solution, held at 70°C for solubility reasons. Lactose utilization rate was determined to be constant throughout the fermentation at 3.07 g L^{-1} h^{-1} (R^2 = 0.9945).

Three different growth rates were observed during the fermentation. Initially the culture grew with a constant growth rate (μ) of 0.17 h^{-1} (growth rates assessed from OD_{600} measurements). Upon temperature reduction to 25°C the growth rate reduced to μ = 0.06 h^{-1} for the remainder of the growth phase. After induction no growth occurred, indeed from 55 h cell death was observed, indicated by a drop in OD_{600} and increased demand for antifoam.

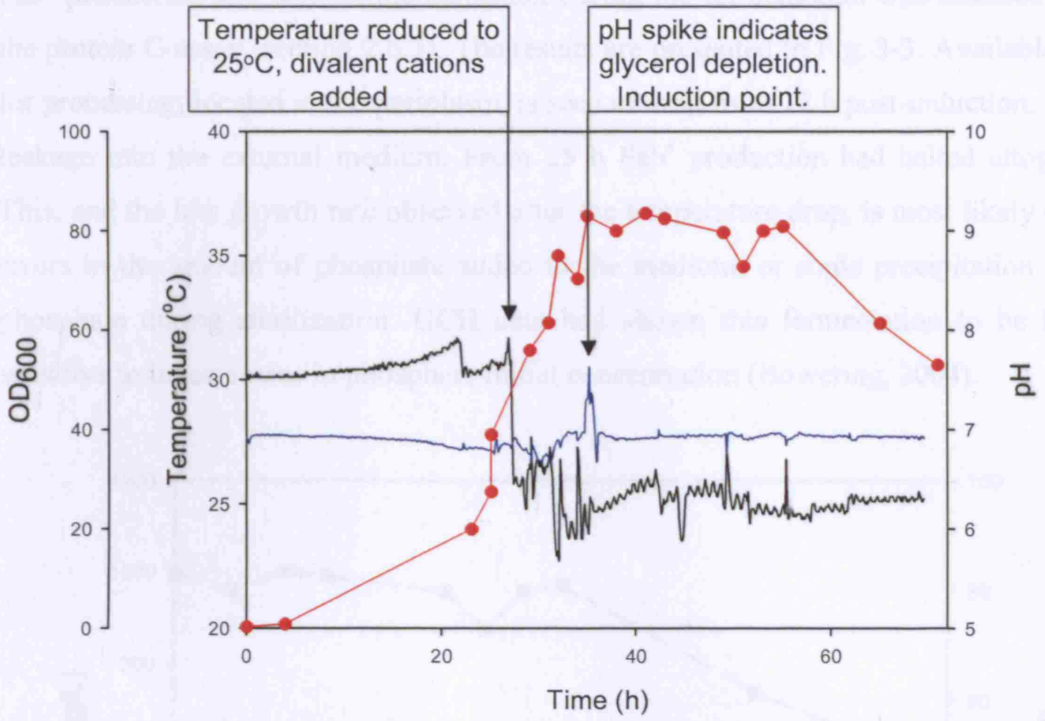

Fig. 3-1: Data from 75 L pilot-scale run of the lactose-induced fermentation. Online measurements of pH (—) and temperature (—) are plotted alongside OD_{600} cell density measurements (•). OD_{600} measurements were measured in triplicate and the average recorded, while pH and temperature readings are derived from online measurements.

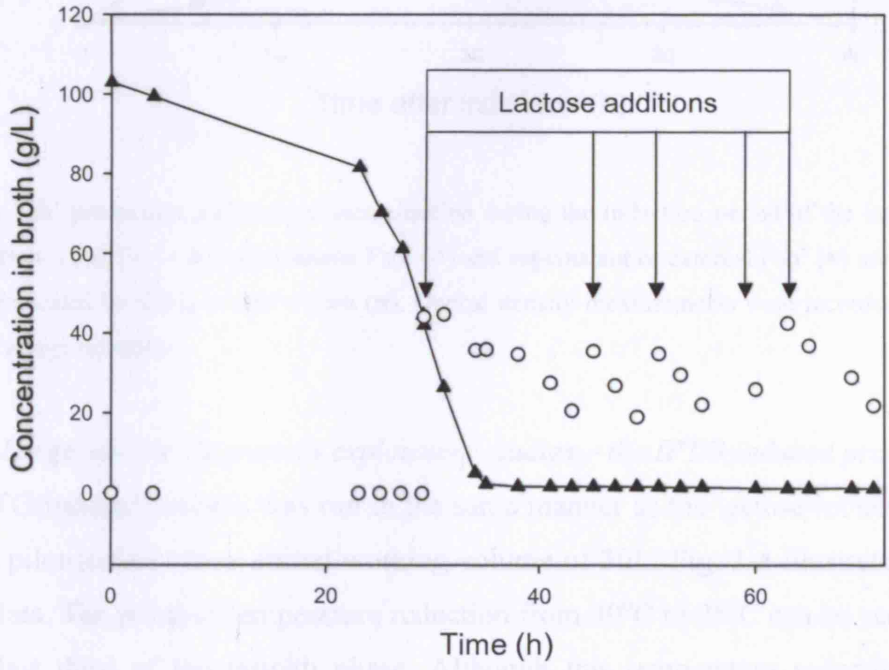

Fig. 3-2: Metabolite levels in the external medium during the time course of the lactose-induced fermentation. Glycerol (▲) and lactose (○) were measured from duplicate samples and the mean level is plotted.

Fab' production and compartmentalisation during the fermentation was assessed using the protein G assay (section 2.6.3). The results are presented in Fig. 3-3. Available Fab' for processing, located in the periplasm, is seen to drop from 12 h post-induction, due to leakage into the external medium. From 25 h Fab' production had halted altogether. This, and the low growth rate observed after the temperature drop, is most likely due to errors in the amount of phosphate added to the medium, or some precipitation of the phosphate during sterilization. UCB data had shown this fermentation to be highly sensitive to inaccuracies in phosphate initial concentration (Bowering, 2004).

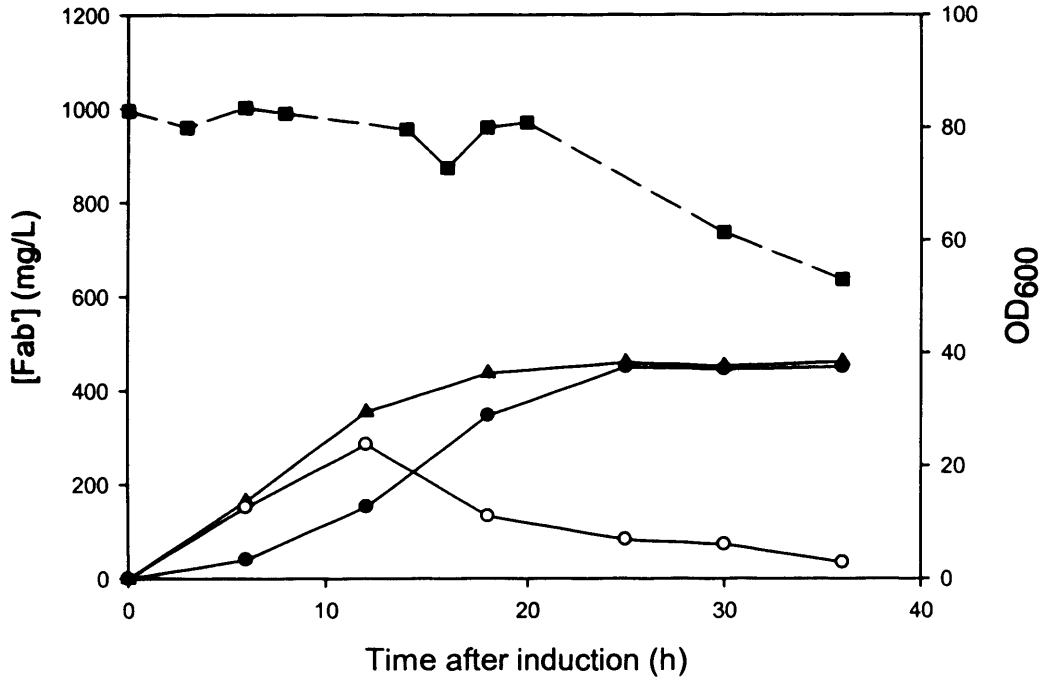

Fig. 3-3: Fab' production and compartmentalisation during the induction period of the lactose-induced fermentation. Total Fab' (▲), periplasmic Fab' (○) and supernatant or external Fab' (●) are plotted. Cell density, indicated by OD_{600} is also shown (■). Optical density measurements were recorded in triplicate and the average recorded.

3.3.1.2 Large pilot-scale process exploratory studies – the IPTG-induced process

The IPTG-induced process was run in the same manner as the lactose-induced process: at 75 L pilot-scale with an initial working volume of 30L. Fig. 3-4 illustrates pertinent online data. The point of temperature reduction from 30°C to 25°C can be seen to occur in the last third of the growth phase. Although this temperature reduction reduced oxygen demand, it was still necessary to switch inlet air to 40:60 O_2:N_2 from ~ 24.3 h. A pH spike is visible at 28.7 h, this was accompanied by a DOT spike, indicating that all glycerol had been consumed by 28.7 h, therefore at this point IPTG was added to induce

Fab' production and the glycerol feed was started at a constant rate of 1.65 mL h^{-1} L^{-1}. Metabolite analysis confirmed that acetate is not produced at concentrations higher than 1 g/L during the whole time-course of the fermentation.

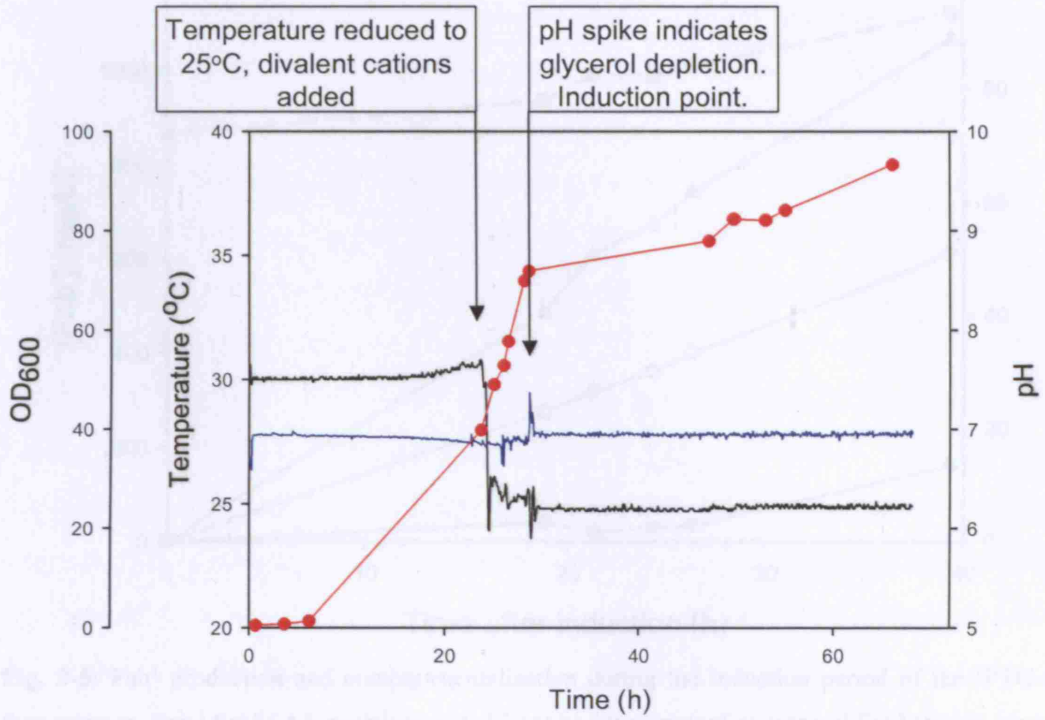

Fig. 3-4: Data from 75 L pilot-scale run of the IPTG-induced fermentation. Online measurements of pH (—) and temperature (—) are plotted alongside OD_{600} cell density measurements (•). OD_{600} measurements were measured in triplicate and the average recorded, while pH and temperature readings are derived from online measurements.

Three different growth rates were observed during the fermentation. Initially the culture grew with a constant growth rate (μ) of 0.19 h^{-1}, approximately equal to that found with the lactose-induced fermentation (growth rates assessed from OD_{600} measurements). Upon temperature reduction to 25°C the growth rate slowed to $\mu = 0.12$ h^{-1} for the remainder of the growth phase, significantly higher than during the lactose-induced process, perhaps due to increased phosphate availability. After induction the growth rate was constant at $\mu \sim 0.0058$ h^{-1} with little foaming and no OD reduction throughout the induction period. This was indicative of much lower levels of cell death/lysis than with the lactose-induced fermentation.

Fab' production and compartmentalisation during the fermentation was assessed by the protein G assay. The results are illustrated by Fig. 3-5. Significantly greater quantities

of Fab' were produced in total in the IPTG-induced process than in the lactose-induced process, and the majority of the total Fab' was located in the periplasm.

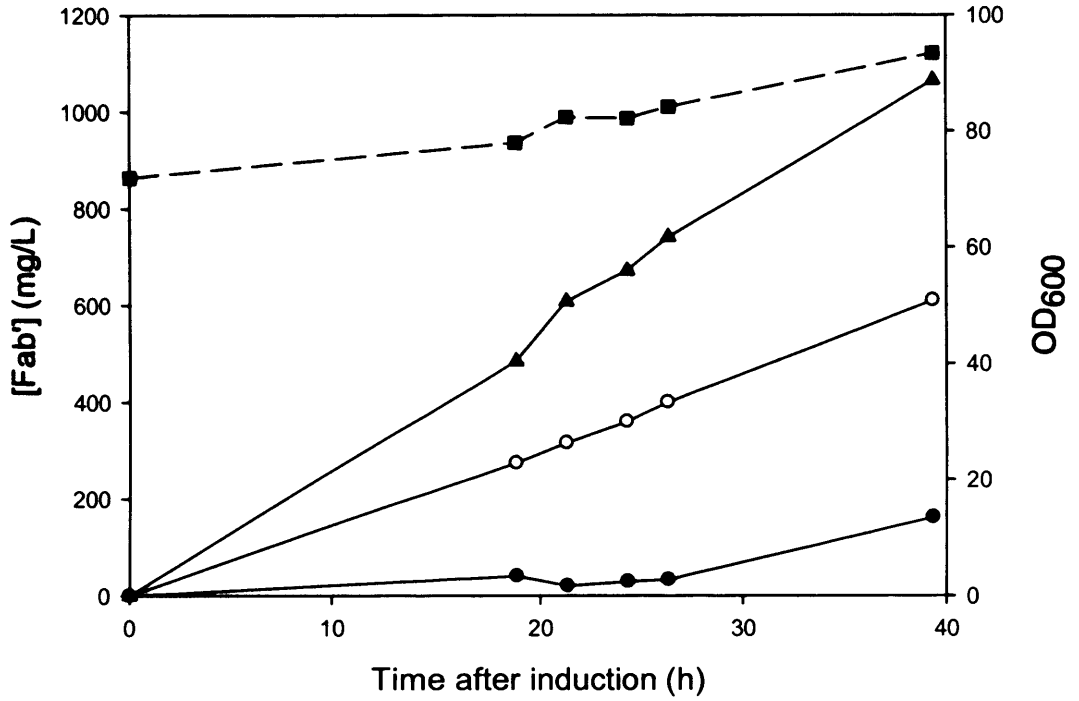

Fig. 3-5: Fab' production and compartmentalisation during the induction period of the IPTG-induced fermentation. Total Fab' (▲), periplasmic Fab' (○) and supernatant or external Fab' (●) are plotted. Cell density, indicated by OD_{600} is also shown (■). Optical density measurements were recorded in triplicate and the average recorded.

3.3.1.3 Discussion of 75 L fermentations and choice of upstream process

Both the IPTG-induced and the lactose-induced process explored at 75 L scale have many similarities. The initial growth phase at 30°C is basically identical between both processes. For example, both have specific growth rates in the region of 0.18 h^{-1}. However, differences in the process output variables arose after the temperature reduction to 25°C. In the IPTG-process the cell density increased up to induction at a much faster rate than that in the lactose-induced process. After induction, the IPTG-process culture remained healthy, with some growth occurring, albeit at a very slow rate due to the metabolism switch to recombinant protein production. In contrast the lactose-induced culture reduced in biomass after induction, indicative of cell death and lysis. This was reflected in the Fab' production profiles of the two strains: the IPTG-induced process produced over 1 g/L Fab' in total with less than 20% of this leaking to the supernatant, whereas the lactose-induced process produced under half the total amount of Fab' with over 95% being lost to the external medium by the end of the fermentation.

The IPTG-process was chosen for the upstream case study for this work as the results presented here showed that the IPTG-induced process ran satisfactorily while the lactose-induced process would need optimisation in order to run in an industrially relevant manner at UCL. The IPTG-process is also a more desirable process generally. The main quoted advantage given for the lactose-induced process over the IPTG system is the lack of need for IPTG, which is of high cost and may contain toxic contaminants which require clearance validation. However, recently the price of lactose for use in the production of therapeutics has increased due to the necessity to source material from certified prion-free herds. Also, with a production process for a high-value end-product such as a therapeutic antibody fragment, cost of IPTG will be less of a factor, and its toxicity will be less problematic due the comprehensive downstream process that is needed for protein purification. Therefore, as lactose is not a significantly more desirable inducer than IPTG the sacrifices that must be made for its use are less tolerable. For example, there is a loss of process control and reproducibility caused by the necessity to use phosphate rather than carbon-limitation to control growth post-induction. Also, the lactose process is practically difficult. Lactose concentration must be monitored every few hours during induction and lactose additions given approximately every 3-4 hours throughout the induction period. This problem is exacerbated in an academic environment where the researcher will also be running the DSP immediately afterwards. In addition, the frequent bulk additions of lactose needed throughout the induction period increase the total fermenter volume and therefore lower the maximum starting volume that can be used in a particular fermenter, thereby reducing the total amount of product that can be obtained in a set fermenter.

Recently, UCB have also decided to focus upon the IPTG-induced process for antibody fragment production in *E. coli*, in preference to the lactose-induced process. This decision was taken mainly because of the greater control allowed over Fab' compartmentalisation by use of the IPTG-induced process (Bowering, 2006).

3.3.2 IPTG-induced process characterisation at 20 L scale

A 20 L fermenter with an initial working volume of 10 L was chosen for routine use as this is the smallest size that will allow use of pilot-scale DSP equipment, for the verification of the USD mimics that will be developed and utilised as part of this study.

Therefore the IPTG-induced process was run using standard conditions at 20 L scale to fully characterise the process at the scale at which it will be operated.

Fig. 3-6 illustrates pertinent online data for a 20 L IPTG-induced fermentation with a post-induction linear glycerol feed rate of 1.58 mL h^{-1} L^{-1}. Dissolved oxygen tension (DOT) has been plotted in order to illustrate the DOT peak that occurs alongside a small pH rise at the point of induction. Carbon dioxide evolution (CER) and oxygen uptake (OUR) rates for this fermentation are plotted in Fig. 3-7.

Both OD_{600} and DCW were used as biomass indicators for this fermentation, and the relationship between them investigated. While DCW gives a more accurate measurement of biomass, OD_{600} is less labour-intensive, more facile and gives an instant reading as opposed to the need to wait for sample drying as during DCW assessment. Fig. 3-8 illustrates that there is a strong ($R^2 = 0.9954$) linear relationship between DCW and OD_{600} during the growth phase of this fermentation. However, during the induction phase of the fermentation, the correlation between OD_{600} and DCW is much weaker (Fig. 3-9). This is most likely due to shape changes in the bacteria occurring as more and more protein is transported into the periplasmic space. These shape changes will alter their light scattering properties and reduce the correlation between turbidity and cell number. Therefore, in this and all subsequent fermentations, OD_{600} will be used to assess cell number and growth rates prior to induction, whilst DCW will be used as the indicator post-induction.

As with the 75 L scale fermentation, three different growth rates were observed during the fermentation. Initially the culture grew with a constant growth rate (μ) of 0.18 h^{-1} ($\approx$ 75 L value of 0.19 h^{-1}). Upon temperature reduction to 25°C the growth rate was reduced to $\mu = 0.13$ h^{-1} ($\approx$ 75 L value of 0.12 h^{-1}) for the remainder of the growth phase. After induction the growth rate was constant at $\mu \sim 0.0043$ h^{-1}. Although this value is lower than that found at 75 L scale (0.0058 h^{-1}), this may be indicative of a high level of sensitivity of the fermentation to the exact post-induction feed rate used, as the 20 L fermentation used a rate of 1.58 mL h^{-1} L^{-1} whereas the 75 L fermentation used a rate of 1.65 mL h^{-1} L^{-1}. The fact that the value for the 75 L fermentation was determined from OD_{600} measurements rather than DCW may also be partly responsible for the difference.

Fab' production and compartmentalisation during the fermentation are illustrated by Fig. 3-10. Comparable levels of Fab' were produced at large (75 L) and small (20 L) pilot-scale fermentations. For example, both had produced 1.1 g/L of Fab' 36 h from the point of induction, with approximately 15% of this leaking into the extracellular medium (0.16 g/L for 75 L scale, 0.19 for 20 L scale). This indicates equivalence between the two runs, when error is taken into account. Periplasmic Fab', as determined experimentally using a test tube extraction method on frozen samples, showed the greater difference between the two samples: 0.80 g/L (20 L) compared to 0.61 g/L (75 L). This is likely to be due to the increased sample error in this determination. For example, the periplasmic samples must be frozen for storage before Fab' extraction, which weakens their cell integrity depending upon the rate of freezing, composition of extracellular medium, growth phase and metabolic state. Therefore in all future measurements total periplasmic Fab' were estimated as the internal Fab' concentration, determined by the difference between total Fab' and supernatant Fab'.

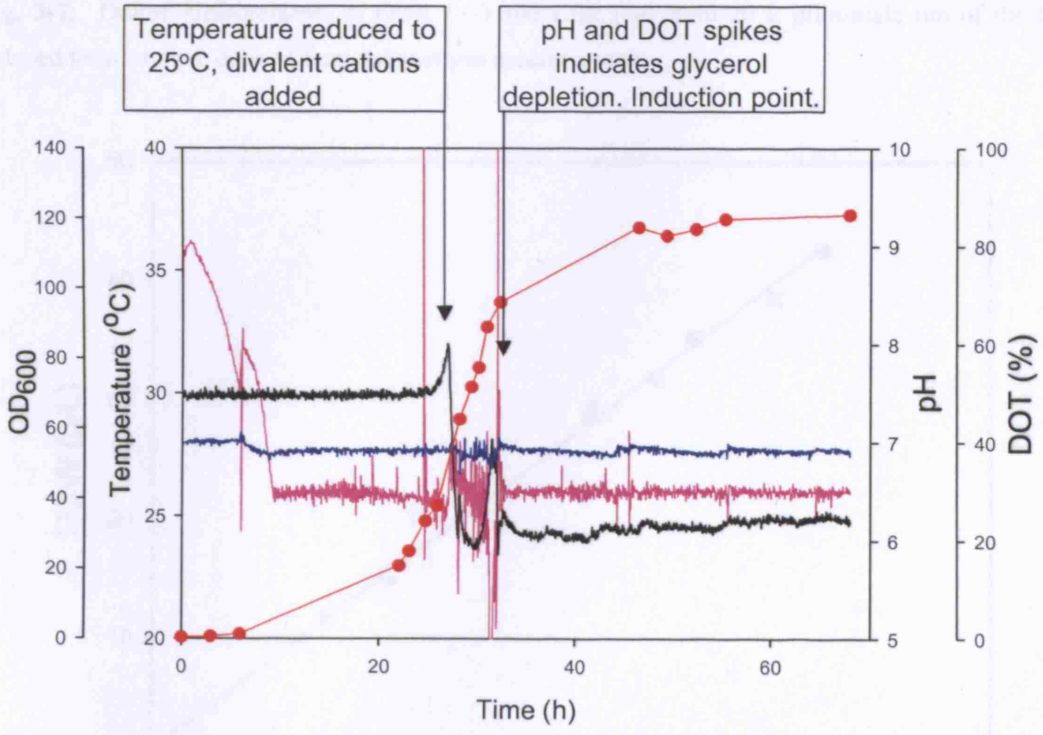

Fig. 3-6: Data from 20 L pilot-scale run of the IPTG-induced fermentation. Online measurements of pH (—), temperature (—) and DOT (—) are plotted alongside OD_{600} cell density measurements (•). OD_{600} measurements were measured in triplicate and the average recorded, while pH and temperature readings are derived from online measurements.

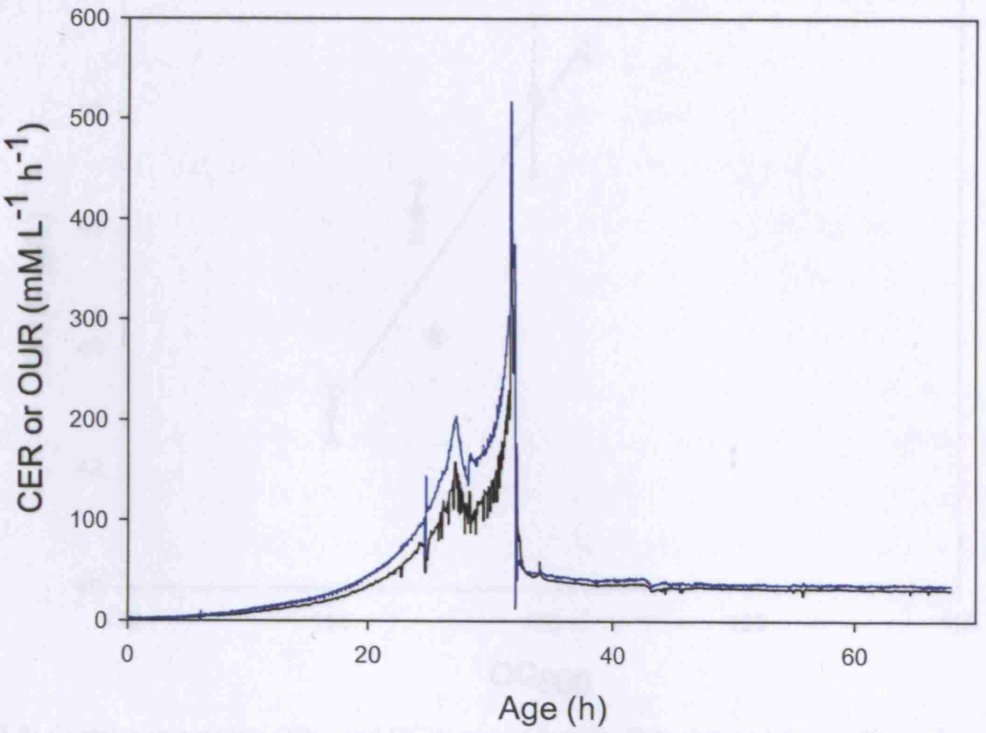

Fig. 3-7: Online measurements of OUR (—) and CER (—) from 20 L pilot-scale run of the IPTG-induced fermentation, derived from exhaust gas measurements.

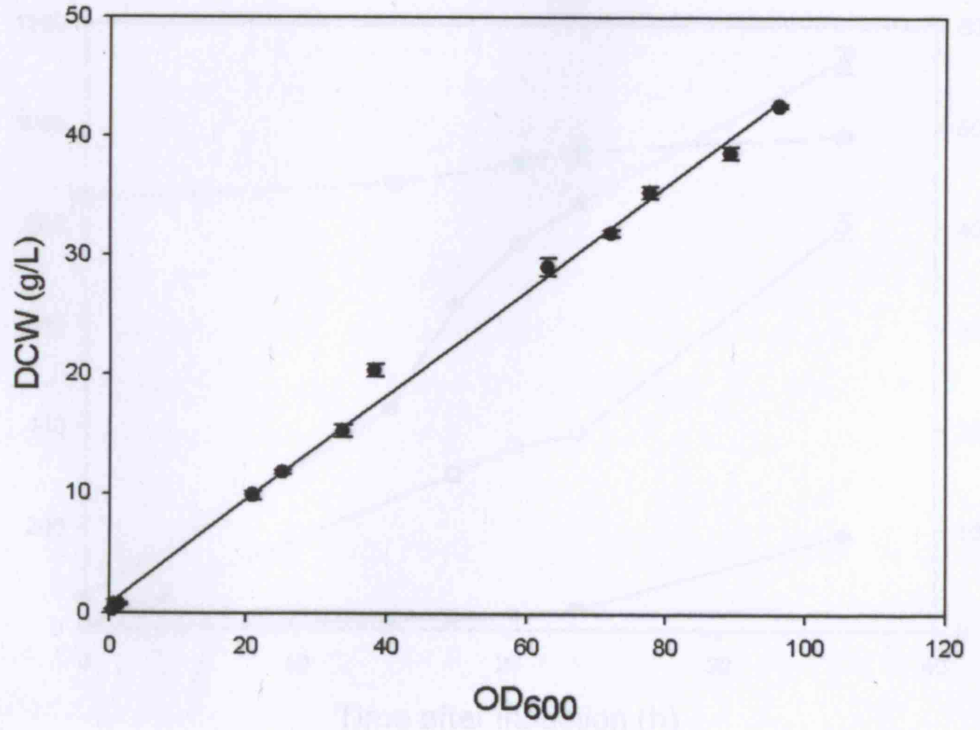

Fig. 3-8: Correlation between OD_{600} and DCW prior to induction. Data obtained during 20 L pilot-scale run of the IPTG-induced fermentation and error bars computed from the standard deviation of four DCW sample repeats.

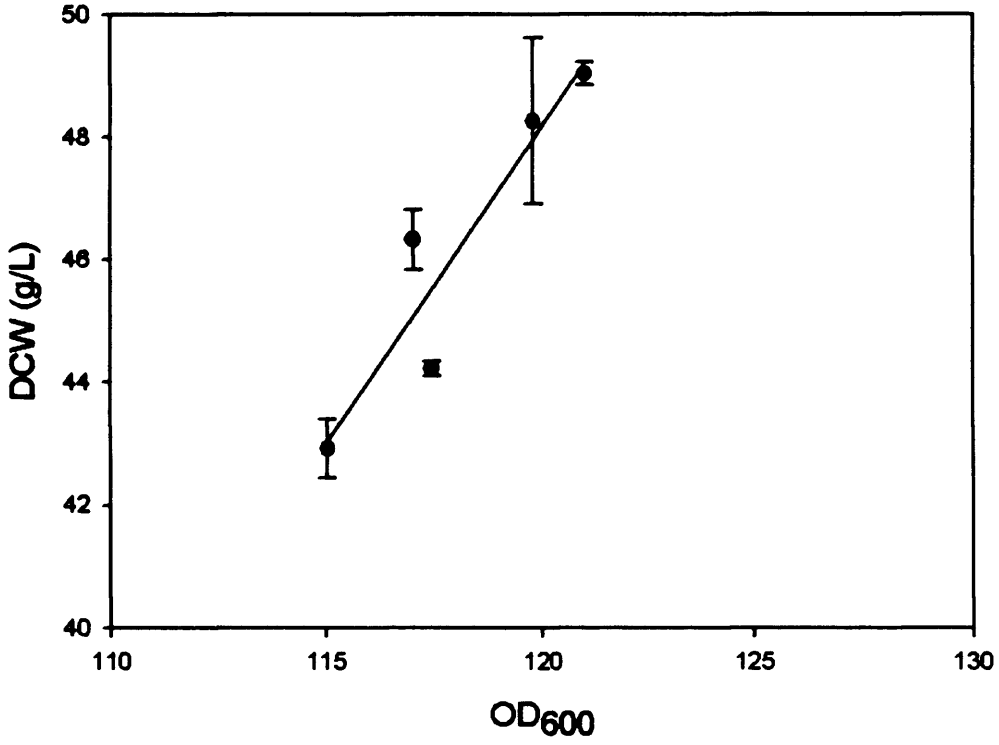

Fig. 3-9: Correlation between OD_{600} and DCW post-induction. Data obtained during 20 L pilot-scale run of the IPTG-induced fermentation and error bars computed from the standard deviation of four DCW sample repeats.

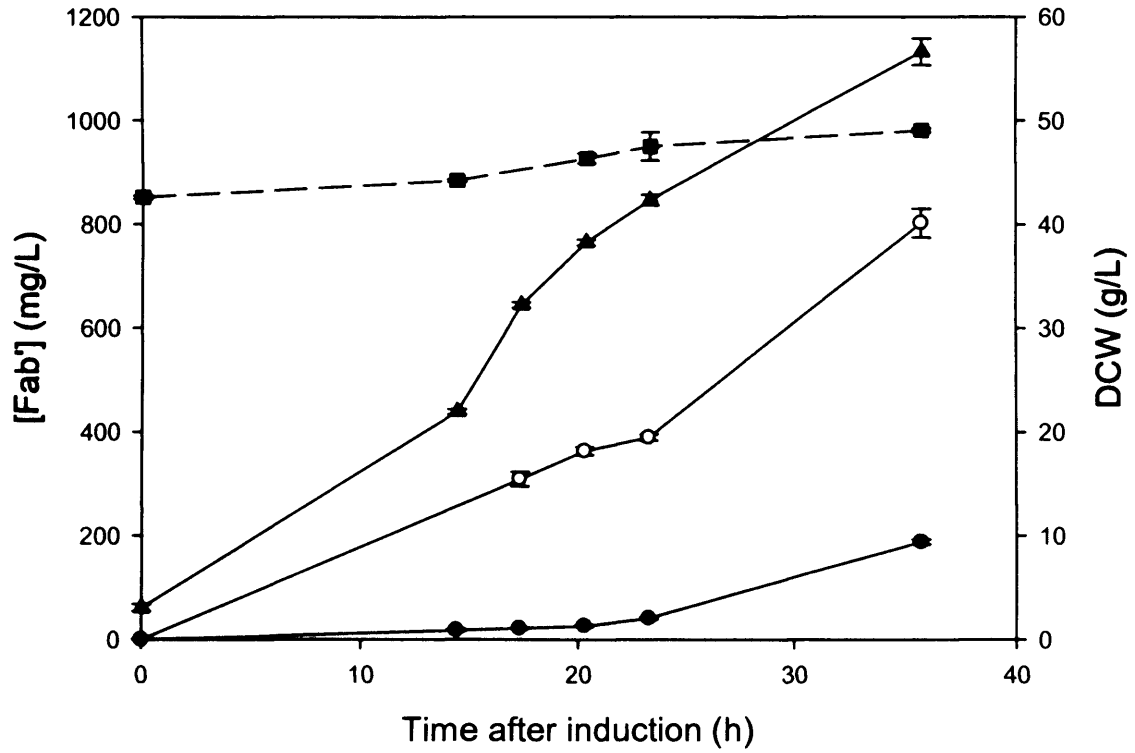

Fig. 3-10: Fab' production and compartmentalisation during the induction period of the 20 L IPTG-induced fermentation. Total Fab' (▲), periplasmic Fab' (○) and supernatant or external Fab' (●) are plotted. Cell density, indicated by DCW is also shown (■). Errors were computed from the standard deviation of four sample repeats (DCW) or triplicate sample measurements (Fab').

3.3.3 Investigation of upstream critical process parameter: post-induction carbon feed rate

Heuristic process knowledge obtained by UCB indicated that the post-induction carbon-feed rate was a highly sensitive key process parameter for the IPTG-induced fermentation. Therefore five 20 L scale (10 L starting volume) IPTG-induced fermentations were carried out using a variety of post-induction glycerol flow rates: 1.04, 1.40, 1.58, 1.65, and 1.80 mL h^{-1} L^{-1}. These rates were chosen as the protocol supplied by UCB suggested an optimum post-induction flow rate of 1.60 mL h^{-1} L^{-1}. The growth rates of all five fermentations varied post-induction, despite being within error of each other for the growth phase. These are shown in Table 3-1. All the growth rates were effectively constant throughout the induction phase, except for the 1.80 mL h^{-1} L^{-1} fermentation. In this case cell density decreased from ~ 20 h after induction, indicative of cell death and lysis caused by Fab' production at an unsustainable rate.

Table 3-1: Post-induction growth rates of the five 20 L fermentations undertaken to investigate the effect of post-induction carbon feed rate.

Post-induction carbon feed rate (mL h^{-1} L^{-1})	**Post-induction constant growth rate (h^{-1} x10^{-3})**
1.04	2.6
1.40	3.7
1.58	4.3
1.65	4.4
1.80	6.1 (initial)

Total Fab' production over the induction period for each fermentation is plotted in Fig. 3-11. It can be seen that glycerol feed rates between 1.40-1.65 mL h^{-1} L^{-1} produce similar levels of Fab', in a linear fashion. The lower glycerol feed rate (1.04 mL h^{-1} L^{-1}) produced approximately half the amount of total Fab', presumably due to the lower glycerol feed rate resulting in a lack of energy and carbon for Fab' synthesis. The highest glycerol feed rate initially produced equivalent levels of Fab' to the median three feed rates, in the same linear fashion. However, approximately 20 h after induction the rate of Fab' production slowed greatly, mirroring the drop in biomass found from this point in the fermentation.

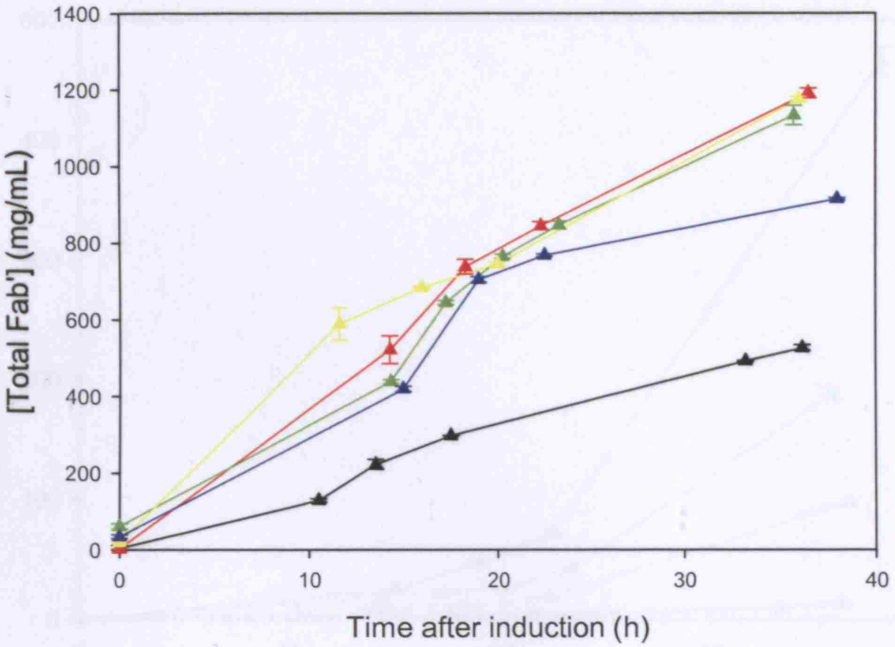

Fig. 3-11: Total Fab' production during the induction period of five 20 L IPTG-induced fermentations, with post-induction glycerol flow rates of 1.04 (▲), 1.40 (▲), 1.58 (▲), 1.65 (▲), and 1.80 (▲) mL h^{-1} L^{-1}. Errors were computed from the standard deviation of triplicate sample measurements.

Fig. 3-12 gives further insight into the effect of carbon feed rate post-induction by illustrating the level of Fab' lost to the extracellular medium during the induction phase of the five fermentations. This Fab' will be lost during the first centrifugation step in the DSP and therefore will not be available for purification. It can be seen that Fab' is lost to the supernatant over time in an exponential fashion. The higher the post-induction carbon feed the faster Fab' is lost to the extracellular medium. The functional consequences of this loss can be seen in Fig. 3-13. Here 'periplasmic' Fab', that is Fab' inside the cells available for processing, is calculated using Equation 3-1.

$$[Fab'_{periplasmic}] = [Fab'_{total}] - [Fab'_{supernatant}] \qquad [3\text{-}1]$$

Fig. 3-13 clearly shows that the amount of Fab' lost to the supernatant compromises the Fab' production in the standard protocol glycerol flow rate of 1.60 mL h^{-1} L^{-1} and therefore 1.40 mL h^{-1} L^{-1} is the optimum rate of carbon feed of the five used. The optimum post-induction carbon feed rate for maximising periplasmic Fab' production with a 36 h induction period was estimated by fitting periplasmic Fab' concentration to a 2nd order polynomial (Fig. 3-14). It can be seen from this graph that a maximum periplasmic Fab' concentration 36 h from induction of 1.11 g/L can be obtained using a post-induction glycerol feed rate of 1.42 mL h^{-1} L^{-1}.

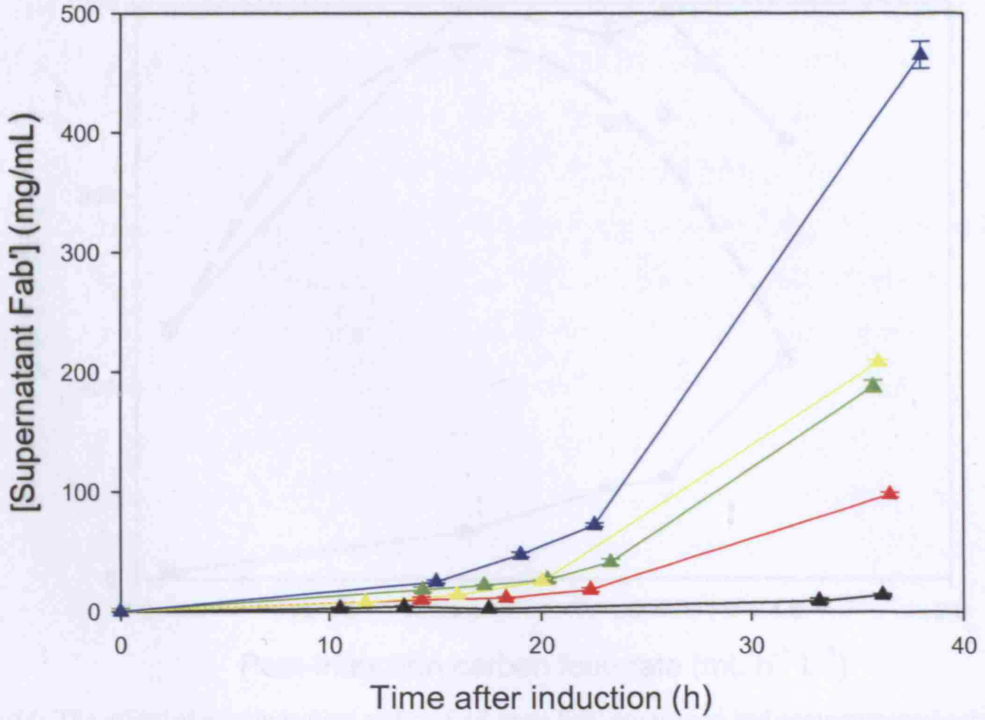

Fig. 3-12: Supernatant Fab' production during the induction period of five 20 L IPTG-induced fermentations, with post-induction glycerol flow rates of 1.04 (▲), 1.40 (▲), 1.58 (▲), 1.65 (▲), and 1.80 (▲) mL h^{-1} L^{-1}. Errors were computed from the standard deviation of triplicate sample measurements.

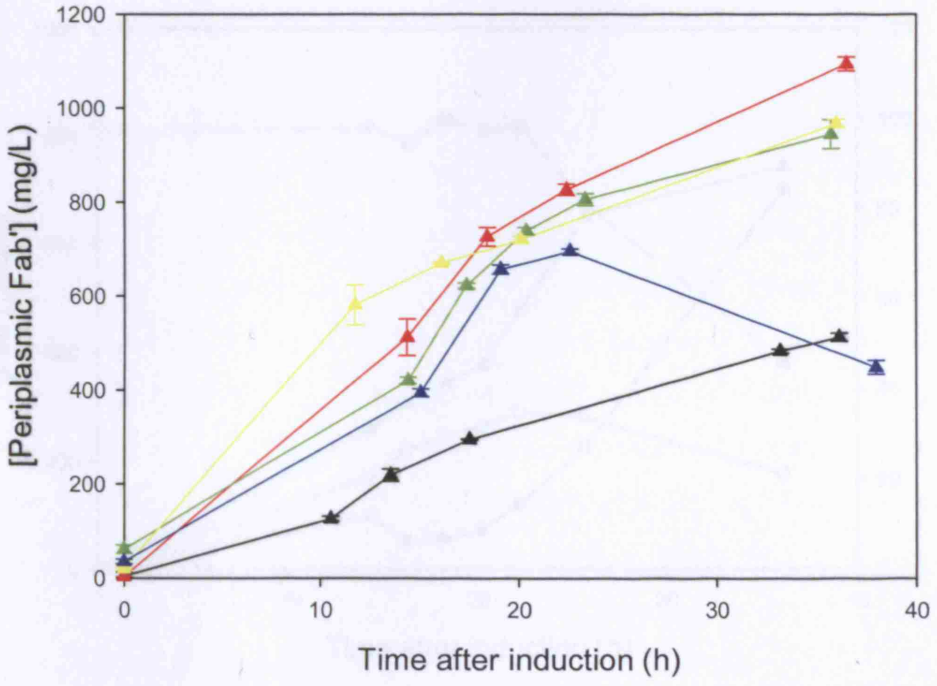

Fig. 3-13: Periplasmic (internal) Fab' concentrations during the induction period of five 20 L IPTG-induced fermentations, with post-induction glycerol flow rates of 1.04 (▲), 1.40 (▲), 1.58 (▲), 1.65 (▲), and 1.80 (▲) mL h^{-1} L^{-1}. Errors were computed from the standard deviation of triplicate sample measurements.

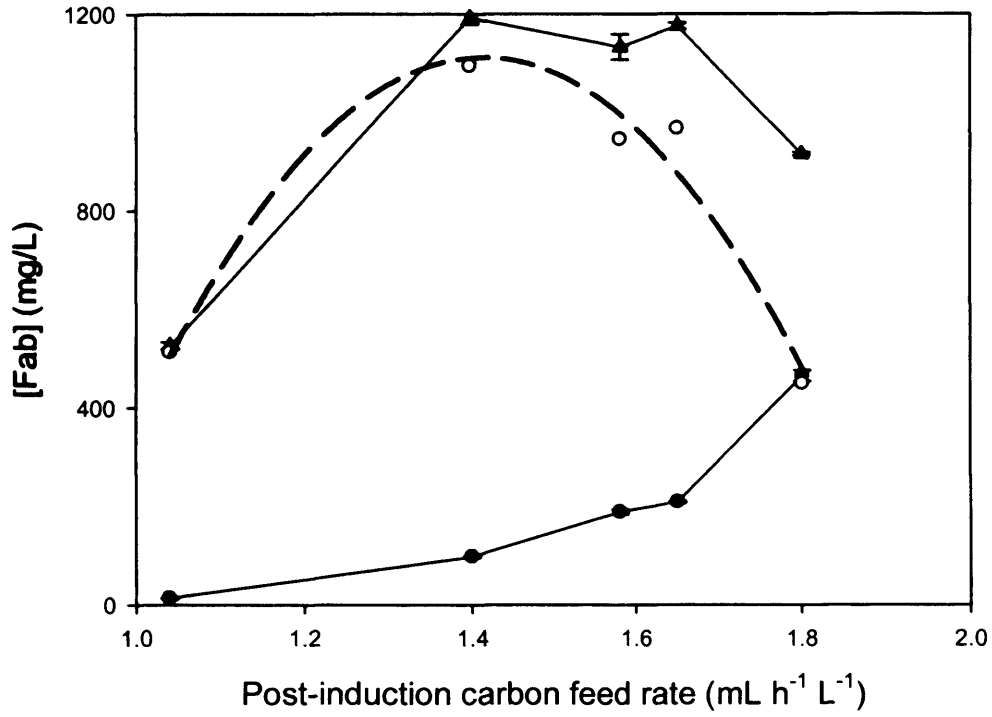

Fig. 3-14: The effect of post-induction carbon feed upon Fab' production and compartmentalisation 36 h after induction. Total Fab' (▲) and supernatant or external Fab' (●) are plotted, with periplasmic Fab' (○) derived from the difference between the two. Periplasmic Fab' production has been fitted to a quadratic function and the curve of the resultant equation plotted (— —). Errors were computed from the standard deviation of triplicate sample measurements.

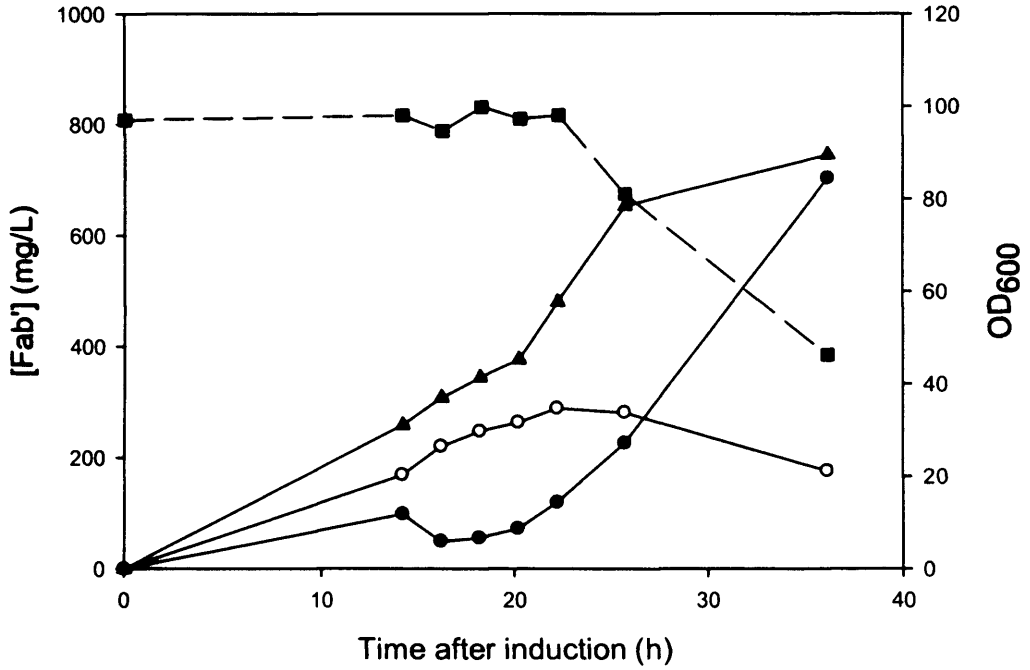

Fig. 3-15: Fab' production and compartmentalisation during the induction period of a 20 L IPTG-induced fermentation with a post-induction glycerol feed rate of 2.00 mL h^{-1} L^{-1}. Total Fab' (▲), periplasmic Fab' (○) and supernatant or external Fab' (●) are plotted. Cell density, indicated by OD_{600} is also shown (■). Samples were measured in triplicate and the average measurement plotted.

It is clear that using a post-induction glycerol feed rate lower than the optimum of 1.42 mL h^{-1} L^{-1} will produce a lesser amount of periplasmic Fab', due to a shortage of both carbon and energy available to the cells for Fab' production. However, it is not the case that merely increasing the feed rate continually will yield greater levels of periplasmic Fab'. It has been shown that increases in the feed rate increase the rate at which Fab' is lost to the extracellular medium, and rates above ~ 1.80 mL h^{-1} L^{-1} cause a drop in cell growth rate, and loss in cell density due to cell lysis. This loss in cell density decreases the rate of total Fab' accumulation, and eventually leads to a halt in Fab' production. Fig. 3-15 shows the Fab' accumulation and cell density profiles for a high post-induction glycerol feed rate of 2.00 mL h^{-1} L^{-1}. It can be clearly seen that from ~ 20 h post-induction, supernatant Fab' concentration increases while cell density and periplasmic Fab' concentration decreases.

There are multiple reasons why continually increasing the post-induction carbon feed rate is not beneficial for Fab' production. Considering Fig. 3-11, it is clear that while increasing the glycerol feed rate from 1.04 to 1.40 mL h^{-1} L^{-1} increases the rate at which Fab' is produced, further increases in the feed rate do not increase the rate of Fab' production even when no cell lysis occurs. This is the case even when increases in feed rate do result in a higher growth rate, for example between 1.40-1.65 mL h^{-1} L^{-1}. This suggests that above 1.40 mL h^{-1} L^{-1} carbon and energy availability is no longer the rate limiting factor for Fab' production. The fact that cell growth continues to increase at rates above 1.40 mL h^{-1} L^{-1} suggests that some other nutrient has not become rate limiting. Instead the limiting step may be the rate of Fab' folding in the periplasm. Although folding assistance is provided in the periplasm by protein disulphide isomerases (e.g. DsbA and DsbC), peptidyl prolyl isomerases (e.g. FkpA and RotA) and putative chaperone-like proteins (e.g. Skp and SurA), and the quantity of these folding assistance proteins will be upregulated upon the detection of unfolded protein in the periplasm by the Cpx and σ^E systems (see Missiakas and Raina, 1997a; Missiakas and Raina, 1997b; Raivio and Silhavy, 2004 for reviews), there will be a rate of Fab' creation that will be greater than these systems can compensate for. This will result in an accumulation of misfolded Fab' in the periplasm. Alternatively, the rate of Fab' transport into the periplasm via the Sec pathway (Manting and Driessen, 2000; Mergulhao et al., 2005) may have become the bottleneck for Fab' production, which would result in Fab' accumulation in the cytoplasm. However, it seems more likely that Fab' production is being constrained by the periplasmic folding rate, as this would

result in the presence of aggregated Fab' in the periplasm. This may activate a recently discovered envelope stress response secretion pathway which increases the formation and release of outer membrane vesicles in response to accumulation of misfolded periplasmic and membrane proteins (McBroom and Kuehn, 2007), thus resulting in the loss of periplasmic material, and with it correctly folded Fab', to the medium. This would explain why, as the post induction glycerol feed rate is increased above 1.40 mL h^{-1} L^{-1}, a greater level of Fab' leakage into the extracellular medium was observed (Fig. 3-12).

In may be possible to increase the maximal rate of Fab' accumulation observed in this study (observed at post-induction feed rates greater than or equal to 1.40 mL h^{-1} L^{-1}) by the use of a modified *E. coli* strain capable of greater rates of periplasmic folding. For example, a recent study showed that a combination of coexpression of the protein disulphide isomerase Dsb proteins DsbA, DsbB, DsbC and DsbD and an addition of sorbitol enhanced soluble expression of scFv in *E coli* (Sandee et al., 2005). Another study showed that coexpression of DsbC dramatically increased the formation of active correctly folded human tissue-type plasminogen activator (tPA) (Qiu et al., 1998). However, such work is beyond the scope of this thesis.

3.4 Conclusions

The characterisation of two fermentation protocols for the production of Fab' antibody fragments in *E. coli* has led to the selection of an IPTG-induced upstream process as the basis of subsequent DSP studies. This process has been found to generate industrially relevant quantities of Fab' (~1 g/L in total), and is capable of retaining the majority in the periplasmic space of the *E. coli* cells. The process has been shown to perform approximately equivalently under two pilot-scale protocols. A 20 L fermenter with an initial volume of 10 L has been chosen as the standard system for investigation.

The effect of variations in the post-induction carbon feed rate, a highly sensitive, key process parameter, have been determined. The effect of post-induction feed rate upon periplasmic Fab' concentration has been examined and an optimum feed rate, estimated at 1.42 mL h^{-1} L^{-1}, has been identified. This insight will be used in a later element of this thesis (Chapter 8) where the effects of variations in this critical process parameter are further elucidated to include its affect upon the initial DSP.

The next four chapters investigate the initial downstream process used in the purification of Fab' from the upstream material produced as described here. Millilitre-scale process mimics are developed for the centrifugal cell harvest, Fab' periplasmic extraction and centrifugal spheroplast removal process operations. Chapter 4 begins by investigating cell damage caused by the centrifugal unit operations.

4. Evaluation of centrifugation-induced cell damage

4.1 Abstract

The ability to recover intact cells from a fermentation broth can be an important factor in the determination of the overall performance of a biopharmaceutical process. Cell damage can result in either an increase in contaminant load or a loss in yield depending upon product location. Possible sources for cell and spheroplast damage during the DSP of the antibody production process studied are discussed for their relevance to process performance.

E. coli **cell damage occurring in the high-shear entry zone of industrial centrifuges is assessed. Use of a rotating disc shear device to apply maximum energy dissipation rates of up to $1.6x10^6$ W/kg to the fermentation harvest material resulted in negligible release of cellular protein or Fab'. Pilot-scale centrifugation of the same material in a disc-stack centrifuge, shown by CFD to have a maximum energy dissipation in its entry zone of $2.0x10^5$ W/kg, corroborated this result. Negligible additional Fab' or cellular protein was shown to be present in the supernatant as compared to that released by centrifugation in a low shear laboratory centrifuge.**

The extent of cell damage expected during ejection from the disc-stack machine used to separate the ***E. coli*** **cells from the extracellular medium prior to Fab' extraction was assessed. IPTG-induced fermentation harvest material generated using three different post-induction carbon feed rates was treated in a capillary device to generate jets with exit velocities ranging from 0-85 m/s, mimicking the jet effect experienced by the cells during exit from a disc-stack centrifuge. The performance of the subsequent Fab' extraction process step was found to be unrelated to this parameter, suggesting that cell damage occurring during disc-stack discharge will not affect process performance, for exit speeds of up to 85 m/s.**

These USD studies lead to the conclusion that centrifugation-induced cell damage will not be a major concern during the optimisation of the IPTG-induced process for antibody fragment production in ***E. coli.***

4.2 Introduction

4.2.1 Performance indicators of centrifugal unit operations

The initial downstream process studied (illustrated in Fig. 1-7) contains two centrifugation steps. The first uses a disc-stack machine to separate the Fab'-containing cells from the extracellular medium after the fermentation, while the second uses an advanced tubular bowl-type centrifuge to separate the Fab'-devoid spheroplasts from the extraction buffer. The choice of centrifuge type is based on the fact that the disc-stack centrifuge usually achieves rapid clarification but relatively poor dewatering compared with solids-bowl centrifuges such as the tubular bowl or multichamber bowl. Analysis of the performance of each of the two centrifugation steps can be separated into four performance parameters. These are damage to the cells/spheroplasts during separation, clarification efficiency; dewatering efficiency, and damage to the cells during exit from the centrifuge. Pilot-scale centrifugation has the advantage that it can simulate industrial-scale performance of all these parameters simultaneously. However, USD techniques are so far only capable of investigating these parameters individually, requiring a separate analysis for each. As there were no suitable USD methods for mimicking centrifugal dewatering and clarification in high cell-density cultures in the literature, the following two chapters detail two mimics developed during the course of the EngD to study their affects. In the following chapter, Chapter 5, a USD method for predicting centrifugal clarification efficiency (Hutchinson et al., 2006) is adapted for use with high cell-density cultures. Chapter 6 details a novel USD methodology for predicting centrifugal dewatering efficiency. Millilitre-scale methods for predicting cell damage during centrifugal separation and exit are avaliable in the literature, and this chapter uses these to investigate the extent of cell damage that can be expected during the application of centrifugation unit operations in the antibody fragment production process.

This chapter only investigates the shear sensitivity of the cells and spheroplasts. Damage to the Fab' protein itself has not been considered as it has previously been shown to be highly shear resistant. For example, Bowering (2000) demonstrated that 4D5 Fab' was shear stable at shear rates up to $1.1 \times 10^6\ s^{-1}$.

4.2.2 Centrifugation-induced cell damage

During the production of therapeutic proteins it is often critical to be able to process the cells with minimal disruption so as to avoid contamination of extracellular product or

undue loss of an intracellular product. Examples of contaminants that may be released upon unwanted cell lysis or leached from damaged cells include DNA, endotoxins, lipids, and proteases or other host-cell proteins. During the production of antibody fragments in *E. coli*, cell damage will lead to product loss if damage is to the whole cells at harvest or contaminant release if spheroplast rupture occurs.

4.2.2.1 Cell damage during separation

Maximum flow intensity has been shown to occur in the feed zone of continuous centrifuges (Boychyn et al., 2000; 2001). Computational fluid dynamic (CFD) modelling techniques have been used to determine the energy dissipation map of the entrance regions of both the pilot-scale disc-stack and pilot-scale advanced tubular bowl type centrifuge used in this thesis (Boychyn et al., 2004). In all cases, the zones of greatest power dissipation are located around a critical structure, in these instances where the feed first contacts the rotating part of the centrifuge. This is unsurprising as it will be in these zones that the greatest acceleration of the feed occurs. These data suggest that the majority of damage during separation occurs in the entry zone of continuous centrifuges.

As such, a device was designed to allow the small-scale creation of similar levels of shear as produced in centrifuge entry zones. A rotating shear device was first used to determine the effects of shear on plasmid DNA in solution (Levy et al., 1999b; 1999a). It has also been used to determine the effect of shear forces similar to those produced in multiple centrifuge entry zones upon protein precipitate solutions and yeast homogenate (Boychyn et al., 2000; 2001; 2004); and mammalian cell suspensions (Hutchinson et al., 2006). Only 20 mL of material is necessary to run the device, compared to the litres of material that would be necessary to obtain the same measurement at pilot-scale. The device, described in detail in Hutchinson et al. (2006), basically consists of a single flat aluminium disc, 40 mm diameter and 1 mm width, mounted in a stainless steel chamber of diameter 50 mm and 10 mm width in which liquid can be held and withdrawn. Rotation of the disc at specific speeds can then be used to apply a controllable level of shear to a sample. Fig. 4-1a illustrates the disc and chamber of the device, which is photographed in Fig. 4-1b. Computational fluid dynamics have been used to determine shear and energy dissipation rates of the device when operated at different spin speeds and times, and relate them to typical values found in large scale centrifuges (Levy et al., 1999a; Levy et al., 1999b).

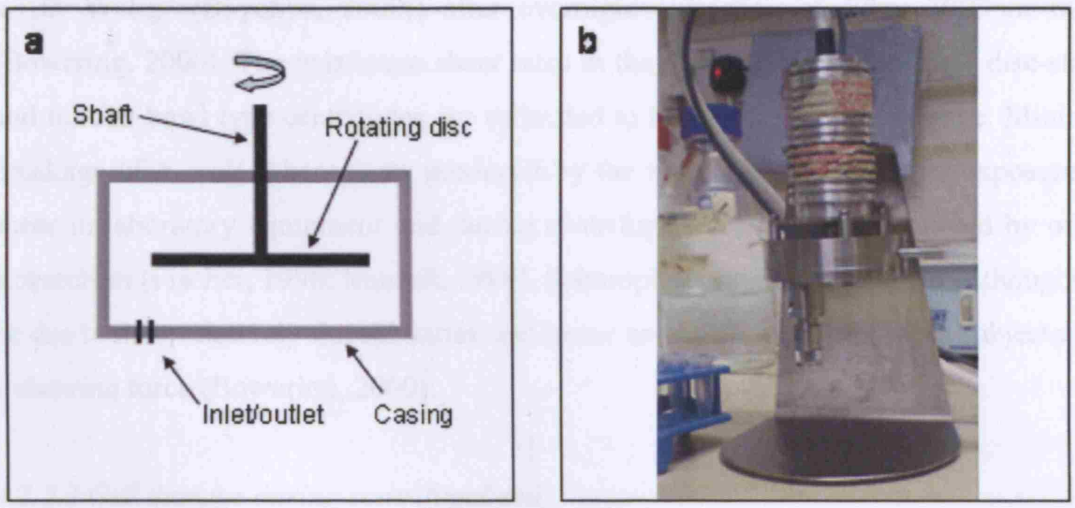

Fig. 4-1: Rotating disc shear device used to mimic centrifugal entry shear in the thesis. A schematic diagram is shown in Fig. 4-1a, and a photographic reproduction of the actual device as used can be seen in Fig. 4-1b.

Any damage occurring upon centrifugal entry that alters the particle size distribution (PSD) or density of sedimenting species, or solution viscosity, will alter subsequent clarification efficiency and possibly, to a lesser extent, dewatering efficiency. Therefore entry damage is mimicked in the clarification and dewatering mimics described in the proceeding two chapters. Moreover, any damage to the feed will also have additional affects depending on the location of the product in the process stream. During the first centrifugation unit operation in the process for antibody production using *E. coli*, the Fab' is located inside the periplasmic space and therefore it is the solids phase that goes forward in the processing chain. Hence any damage to the cells upon entry to the centrifuge could result in a drop in process yield as Fab' is liberated through a damaged outer membrane and lost with the broth supernatant. This was investigated in this chapter. During the second centrifugal unit operation, the Fab' is now in solution as it has been liberated from the cells during the periplasmic extraction. Hence any cell damage that occurs upon centrifugal entry will not alter yield, but will increase the contaminant load for the subsequent purification unit operation, as protein (including possible proteases), lipid, nucleic acids and endotoxins are liberated into solution. Cell entry damage during the second centrifugation unit operation is not investigated in this thesis as the spheroplasts created by the periplasmic extraction method of Weir and Bailey (1997) have been shown previously to be resistant to higher shear forces than found in centrifuge entry zones. They have been shown to be unaffected by shear rates

up to $1.1x10^6$ s^{-1} (approximately equivalent to a maximum energy dissipation rate of 1.2 x 10^6 W kg^{-1} (Boychyn, 2000)) after overnight extraction at either 30°C or 60°C (Bowering, 2000). The maximum shear rates in the feed zones of pilot-scale disc-stack and tubular bowl type centrifuges are estimated to be in the 10^5-10^6 s^{-1} range. Minimal breakage of *E. coli* spheroplasts produced by the extraction process after exposure to shear in laboratory equipment and during centrifugation has also been noted by other researchers (Fischer, 1996; Murrell, 1998). Spheroplasts resistance to shear is thought to be due to their relatively flaccid nature and hence an ability to deform when subjected to a shearing force (Bowering, 2000).

4.2.2.2 Cell damage during centrifugal exit

The disc-stack centrifuge used to separate cells from the extracellular medium and collect them for periplasmic extraction ejects solids from the spinning bowl at speed. The shear and impact forces that result have the potential to damage the ejected solids. Solids are ejected through the uncovering of a series of nozzles on the bowl sides and accelerated out into a wall that collects the solids. Previous studies on cell damage upon discharge from disc-stack centrifuges have shown approximately 10% disruption of *E. coli* cells grown in complex media, which can increase to 20% when cells are grown in defined media (Gray et al., 1972). Cell damage occurring during cell ejection is the result of a different engineering environment to that found in the entry zone and therefore a different device is needed to replicate this damage at millilitre-scale. Typically it is estimated that the sediment discharges from a disc-stack centrifuge at velocities approaching 100 m/s (Chan et al., 2006). Therefore impact effects must be considered in addition to shear as the paste passes through the exit nozzles. The small-scale capillary-based device used, shown in Fig. 4-2, is capable of subjecting cells to levels of shear and impact comparable to those found in industrial machines (Chan et al., 2006).

Any damage to the harvested cells upon centrifuge exit during the first centrifugation unit operation will not result in a decrease in yield as the next operation, periplasmic extraction, aims to permeabilise the outer membrane of the cells to release periplasmically-located Fab'. Yield may even be increased by some level of damage, as the cells are weakened and made more amenable to periplasmic permeablisation. However, damage to the cytoplasmic membrane during centrifuge exit will result in increased contaminant load as material is released from the cellular cytoplasm. The

effect of cell damage during exit is investigated in this chapter. As damage during exit will tend to alter the performance of the periplasmic extraction, damage levels are assessed after periplasmic extraction.

Ejection damage to spheroplasts during the second centrifugal unit operation has not been investigated in this work for two reasons. Firstly, the second centrifuge is an advanced tubular bowl-type, a Carr Powerfuge P6, which performs automated solids discharge at a very low spin speed (~ 40 rpm) using an internal vibrating knife to scrape the cell paste from the bowl. As such the cell paste is not exposed to high levels of shear or to jet effects during discharge. Secondly, the sedimented spheroplasts are not part of the process stream: they are discarded after centrifugation. Therefore any damage to them is immaterial.

4.2.3 Quantifying cell damage

The technique used to quantify cell damage will determine the type of damage that is assessed. Many of these techniques involve determining the levels of cell components in solution before and after cell damage. For example, total protein quantification can indicate generic cell damage while nucleic acid leakage or leakage of the cytoplasmic enzyme glucose-6-phosphate dehydrogenase indicates rupture of both inner and outer membranes. The leakage of a periplasmic enzyme such as alkaline phosphatase (Malamy and Horecker, 1961) or cyclic phosphodiesterase (Neu and Heppel, 1965) may be assayed to determine the extent of damage to the outer membrane. As well as measurement of such cell components, the state of the whole cell may be analysed. For example, measurement of the number of colony forming units before and after damage via dilution plating will allow assessment of any reduction in cell replicative viability. Recent advances in flow cytometry have allowed its application to bacterial cells (Steen, 2000). In this chapter only total protein and Fab' release have been assessed as the main concern is yield reduction and contaminant load increase. Total protein in solution will be released by damage resulting in a reduction in cell integrity, and can be used to indicate an increase in contaminant levels (especially since proteins represent a major contaminant). Fab' will be released into solution when the integrity of the outer membrane is compromised, and therefore can be used to indicate periplasmic damage as well as to assess a drop in yield. High-pressure homogenisation was used to generate a benchmark for 100% cell damage.

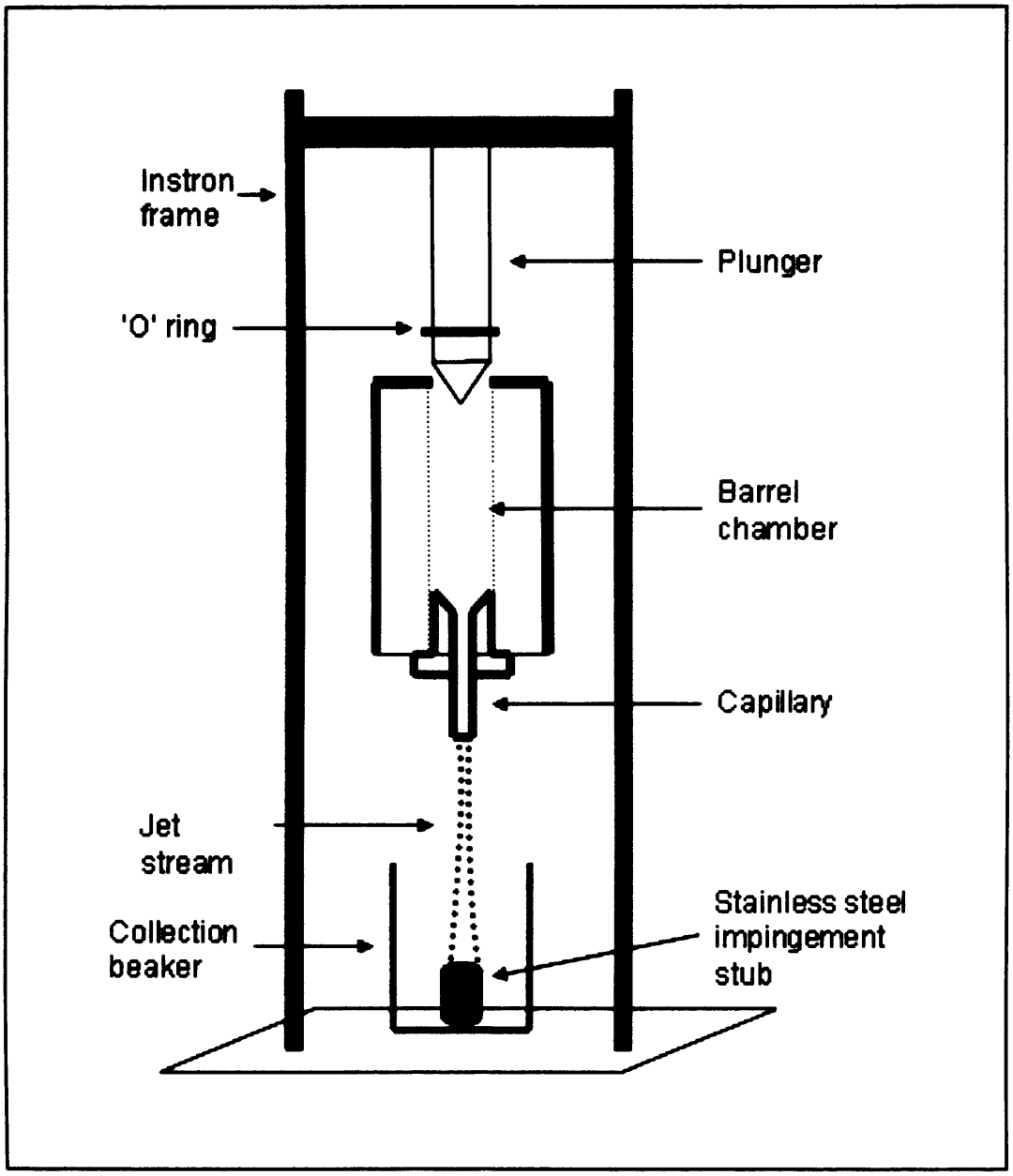

Fig. 4-2: Schematic diagram of the capillary device used to mimic centrifugal exit shear in the thesis, as described by Chan et al. (2006).

4.3 Theoretical considerations

4.3.1 Consideration of centrifugal entry damage

4.3.1.1 Maximum energy dissipations in industrial centrifuges

Industrial centrifuges typically apply maximal energy dissipation rates in the region 10^5-10^7 W kg^{-1} (Yim and Shamlou, 2000). However, the exact definition of an average or maximum energy dissipation rate is notoriously difficult in the case of centrifuges and other bioprocess equipment such as homogenisers, pumps and microfiltration rigs. This is due to the complex spatial distribution of energy dissipation across the flow field.

However, CFD can be used to help understand this problem by theoretically mapping the field flow within the piece of equipment under study. For example, the Carr P6 advanced tubular bowl type centrifuge used for the second centrifugation unit operation in the pilot-scale production of antibody fragments in this thesis has been shown to have a maximum energy dissipation rate (ε_{max}) of 1.4 x 10^6 W kg^{-1} when operating at its maximum speed of 15,300 rpm. This drops to 2.5 x 10^5 W kg^{-1} at its median operating speed of 10,000 rpm, and the lowest ε_{max} that can occur in the Carr is 5.0 x 10^4 W kg^{-1}, which occurs when it is operating at its lowest spin speed of 5,000 rpm (Boychyn et al., 2004). A pilot multichamber bowl centrifuge was shown to have a ε_{max} of 6.0 x 10^5 W kg^{-1} when flooded, increasing to 1.2 x 10^6 W kg^{-1} when air was present in the feed zone (non-flooded) (Boychyn et al., 2001). Pilot-scale disc-stack centrifuges, used for the separation of Fab'-containing *E. coli* cells in our process, have been shown by CFD to have slightly lower maximum energy dissipation rates. For example, a Westfalia SAOOH 1L pilot-scale model was modelled using CFD and found to have a ε_{max} of 2.0 x 10^5 W kg^{-1} when operated at its maximum spin speed of 9,800 rpm (Boychyn et al., 2004).

4.3.1.2 Maximum energy dissipations in USD rotating disc device

Energy dissipation rates found in industrial centrifuges can be replicated in the small-scale rotating disc shear device described above. The flow over a rotating disc has been theoretically described (Schlichting, 1979) and applied to the rotating shear device by Boychyn (2000). Standard analytical solutions of the equations of motion for flow over the rotating disc showed that the maximum shear stresses occurred in the laminar flow boundary layer δ (m), given by Equation 4-1.

$$\delta = 5\sqrt{\frac{\mu X}{\rho v_\infty}} \qquad [4\text{-}1]$$

Where X (m) is the distance from the edge of the disc, μ the viscosity (Pa s), ρ is the density of the suspension (kg m^{-3}) and v_∞ is the tangential tip velocity (m/s). The corresponding maximum shear stress, τ_{max} (Pa), at position X is determined by Equation 4-2.

$$\tau_{max} = 0.322\mu v_\infty \sqrt{\left(\frac{\rho v_\infty}{\mu X}\right)} \qquad [4\text{-}2]$$

Integration of Equation 4-2 over the diameter of the disc gives the applied torque T (kg m^2 s^{-2}), thus T can be calculated using Equation 4-3.

$$T = 0.664\pi\mu\nu_\infty\left(\frac{\rho\nu_\infty}{\mu}\right)^{1/2}\left(\frac{16R^{5/2}}{15}\right) \qquad [4\text{-}3]$$

Where R is the disc radius (m). The power input, P, (W) can then be determined using Equation 4-4.

$$P = 2\pi NT \qquad [4\text{-}4]$$

Where N is the rotational speed (rps). This allows calculation of the maximum energy dissipation rate, ε_{max}, (W kg^{-1}) using Equation 4-5.

$$\varepsilon_{max} = \frac{P}{\rho V_{bl}} \qquad [4\text{-}5]$$

Where V_{bl} is the volume of the boundary layer (m^3), which can be obtained by integrating the expression for the boundary layer thickness across the entire disc to give Equation 4-6.

$$V_{bl} = 2\times 2\pi\int_0^R (R-x)\delta dx = \frac{16\pi}{3}\sqrt{\frac{\mu}{\rho\nu_\infty}}R^{5/2} \qquad [4\text{-}6]$$

The theoretical values determined using these equations were tested by CFD. Further supporting evidence for the scaling of damage conditions from the rotating disc device to pilot/industrial-scale centrifuges using energy dissipation rates stems from the ability of the combined use of the rotating disc device and laboratory centrifuges to predict successfully the separating characteristics of industrial-scale disc-stack centrifuges, when the industrial-scale clarification of the shear sensitive material could not be predicted by use of laboratory centrifuge alone (Hutchinson et al., 2006).

4.3.1.2 Residence time

Previous work found increasing the residence time of samples in the rotating shear device from 5-30 s did not affect subsequent clarification (Hutchinson et al., 2006). Therefore a 20 s residence time was used in the shear cell device to avoid errors due to the acceleration/deceleration of the disc and incomplete mixing, thus ensuring sufficient time for exposure of all the sample to the highest shear region at the tip of the disc.

4.3.2 Consideration of centrifugal exit damage

The method of Chan (2006) was used to determine the vulnerability of the *E. coli* cells to damage during centrifuge exit. The theoretical basis of the method is briefly detailed below. A major assumption of the published technique is that the jet profiles produced at pilot and USD scale are identical. Although this is unlikely to be the case due to the larger nozzle size and rotational motion at pilot-scale, the mimic was still found to predict accurately pilot-scale cell damage with the Westfalia CSA-1 disc-stack machine used in this thesis (Chan et al., 2006).

4.3.2.1Exit damage in pilot-scale disc-stack centrifuge

Chan et al (2006) identified two possible sources of cell damage arising during ejection from a disc-stack centrifuge. Firstly, cell impact damage upon jet collision with the centrifuge collection bowl correlated with observed levels of damage to *E. coli* cells. The impact velocity can be determined for a disc-stack machine as detailed below.

The discharge pressure, P_d (Pa), can be calculated using Equation 4-7 (Ruthven, 1997).

$$P_d = \frac{\rho}{2}\omega^2(r_1 - r_I) \qquad [4\text{-}7]$$

Where ρ is the density (kg/m^3), ω angular velocity (rads/s), r_I the bowl inner radius (m) and r_I the radius of the inner liquid ring, e.g. the centripetal pump radius (m). P can then be used in Equation 4-8 to calculate the discharge viscosity for a fully opened nozzle centrifuge, v (m/s) (Ruthven, 1997).

$$v = \sqrt{\frac{2.P_d}{\rho}} \qquad [4\text{-}8]$$

The discharge velocity of the CSA-1 disc-stack used in this thesis has thus been calculated at a range of spin speeds (Table 4-1) using measured centrifuge dimensions (Table 4-2).

Table 4-1: Discharge velocities at shear rates of CSA-1 disc-stack centrifuge at a range of spin speeds

Centrifuge speed at discharge (rpm)	**Centrifuge discharge velocity ($m\ s^{-1}$)**	**Residence time ($x\ 10^{-4}$ s)**
9800	82	1.3
8000	67	1.6
7000	59	1.9
6100	51	2.2

Table 4-2: Features of the CSA-1 disc-stack centrifuge.

Feature	**Specifications**	**Units**
Bowl	Rotational speed (operating range) (rpm)	6100-9800
	Bowl volume (L)	0.6
	Approximate solids capacity (g)	250
	Radius of the outer bowl (r_0) (m)	0.0995
	Bowl inner radius (r_1) (m)	0.084
	Radius of the inner liquid ring (r_2) (m)	0.025
Nozzle	Height (m)	0.004
	Depth (m)	0.011
	Length (m)	0.043
Collection bowl	Gap size (m)	0.090

A second possible source of exit-induced damage was found to be shear stress when passing through the ejection nozzle of the disc-stack machine. It was found that negligible damage to freeze/thawed (i.e. highly weakened, see Chapter 9) *E. coli* cells could be detected at shear rates of up to ~ $6.5x10^5\ s^{-1}$ if the residence time, RT, (s) was < 0.004 s (Chan et al., 2006). Residence time in a nozzle can be calculated as in Equation 4-9.

$$RT = D_{noz}/v \qquad [4\text{-}9]$$

Where D_{noz} is the nozzle depth (m). Table 4-1 shows the RT for all a range of spin speeds in the CSA-1 disc-stack machine. All calculated residence times in the exit nozzles of the disc-stack pilot-scale machine used in this study were at least an order of magnitude lower than 0.004 s, even when run at minimum spin speed. Therefore no cell damage to the process feed was expected to be attributable to shear stresses inside the nozzle.

4.3.2.2 Forces generated in mimic

The capillary shear device shown in Fig. 4-2 allows fluid to be passed down a capillary of known length and diameter at a constant speed. The velocity of material, v (m/s) emerging from the capillary tip can be determined from Equation 4-10.

$$v = \frac{Q_c}{\pi . R_c^2} \qquad [4\text{-}10]$$

Where R_c is the capillary radius (m) and Q_c is the flowrate through the capillary (m^3/s) determined from Equation 4-11.

$$Q_c = X_i \frac{\pi (2.R_c)^2}{4} \qquad [4\text{-}11]$$

Where X_i is the operator set drive speed of the plunger (m/s).

The residence time of the fluid within the capillary can be calculated using Equation 4-12 to ensure it never exceeds 0.004 s and therefore shear effects within the tube can be ignored (Chan et al., 2006).

$$RT = {}^{L_c}\!/_{v} \qquad [4\text{-}12]$$

Where L_c is the capillary length. Table 4-3 details the ejection speeds and corresponding residence time in the capillary used in these studies. The specific capillary used had a length of 20mm and a 0.25mm diameter.

Table 4-3: Exit velocities and residence times used in capillary device

Exit speed (m/s)	Residence time (x 10^{-4} s)
11	18.0
21	9.5
42	4.8
53	3.8
85	2.4

4.3.2.3 Impact effects

A schematic representation of a typical fluid stream exiting from a capillary nozzle is shown in Fig. 4-3. The jet formed by such an exiting fluid stream is usually divided into three regions: the continuous flow region, the droplet flow region and the diffused flow region (Yanaida and Ohasi, 1978). The region immediately in front of the nozzle is known as the core zone (X_c). In this zone the velocity profile, stagnation pressure and density are uniform. In the continuous flow region, extending from the core, there is relatively little change in jet structure with the majority of the fluid moving in a coherent central stream, where it can be assumed the velocity remains approximately constant (Davies et al., 1980). Between the core zone (X_c) and the break-up point (X_b) fine droplets begin to develop as a result of the shear effect from the adjacent stationary air. On reaching the break-up point aerodynamic forces dominate over the flowing fluid stream and hence a decrease in velocity of the stream is observed (Chan, 2006; Chan et al., 2006).

The interface of the continuous flow region and the droplet flow region (X_b in Fig. 4-3) has been identified as the optimum point at which maximum energy dissipation occurs (Yanaida and Ohasi, 1978). Jet impact with a solid surface at this distance from the jet origin has also been shown to result in the highest levels of cell breakage if all other factors are constant (Chan et al., 2006). In these USD studies, the length from the capillary orifice to the flat steel slug impaction surface was maintained at a constant distance equal to the gap between the ejection nozzles and the collection bowl (90mm). This served to minimise any alterations in the jet structure at impact, assuming the jet profiles produced by the disc-stack machine and the capillary device are identical.

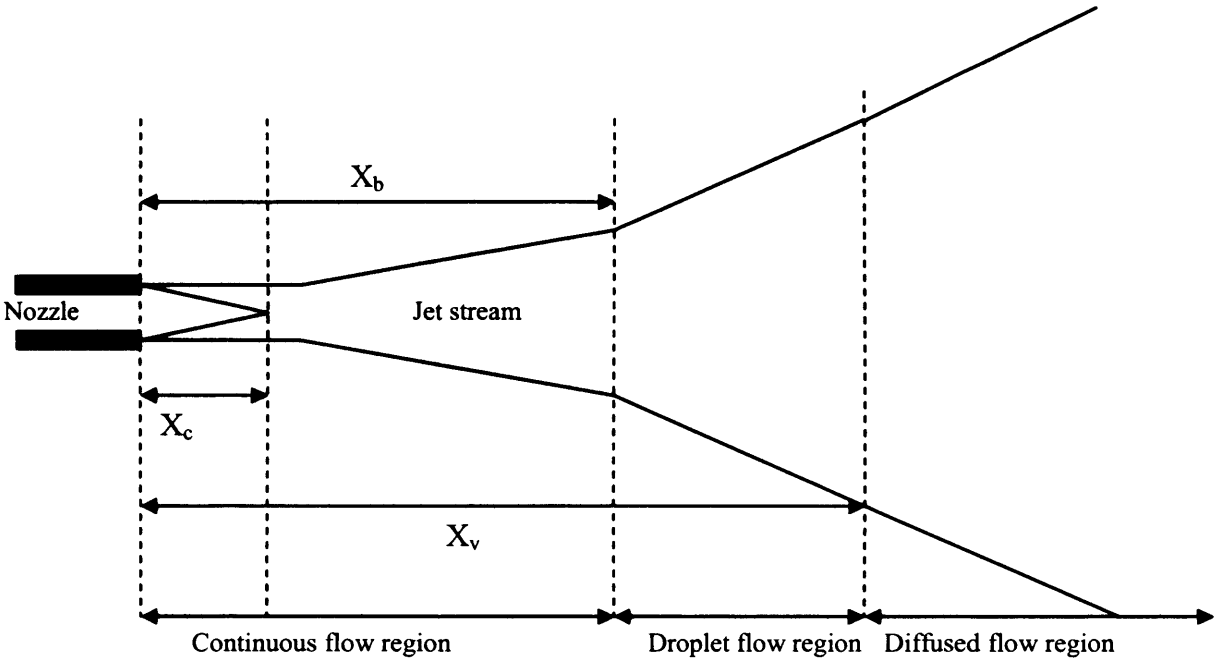

Fig. 4-3: Schematic representation of a typical fluid stream exiting from a capillary nozzle where X_c is the potential core, X_b is the break-up length and X_v the droplet flow length. Diagram taken from Chan et al. (2006).

4.3.3 Assessment of cell damage

Cell damage was assessed by measurement of protein release (total cell damage) and Fab' release (outer membrane damage). Both are presented as a percentage of the total available for release (Equation 4-13 and 4-14), determined by high pressure homogenisation under extreme conditions so as to ensure the release of all the cell contents.

$$\frac{[\mathrm{Pr}\,otein']_{RELEASED}}{[\mathrm{Pr}\,otein']_{TOTAL}} \times 100 = \%\ Protein\ release \qquad [4\text{-}13]$$

$$\frac{[Fab']_{RELEASED}}{[Fab']_{TOTAL}} \times 100 = \%Fab'release \qquad [4\text{-}14]$$

4.4 Results and discussion

4.4.1 Consideration of centrifugal entry damage

4.4.1.1 CFD of rotating disc shear device

Equation 4-5 was used to relate rotational speed of the rotating disc shear device to maximum energy dissipation (ε_{max}) in order to allow comparison to industrial machines. To provide confidence in the use of this equation, maximum energy dissipation rates were also computed using CFD simulations of three different rotational speeds. These were performed separately to this thesis by Ioannis Papantoniou, Department of Biochemical Engineering, UCL. The method used, also supplied by Ioannis Papantoniou, is detailed in section 2.7.1. Predictions of ε_{max} using Equation 4-5 are compared to the CFD results in Fig. 4-4, over the energy dissipation range predicted to occur in industrial centrifuges (Yim and Shamlou, 2000). The two methods of prediction are found to be considerably different. Therefore a curve fit to the CFD values was used to predict the ε_{max} in the shear device, as matching CFD derived ε_{max} has previously been shown to allow accurate clarification prediction with shear sensitive material (Boychyn et al., 2001; 2004).

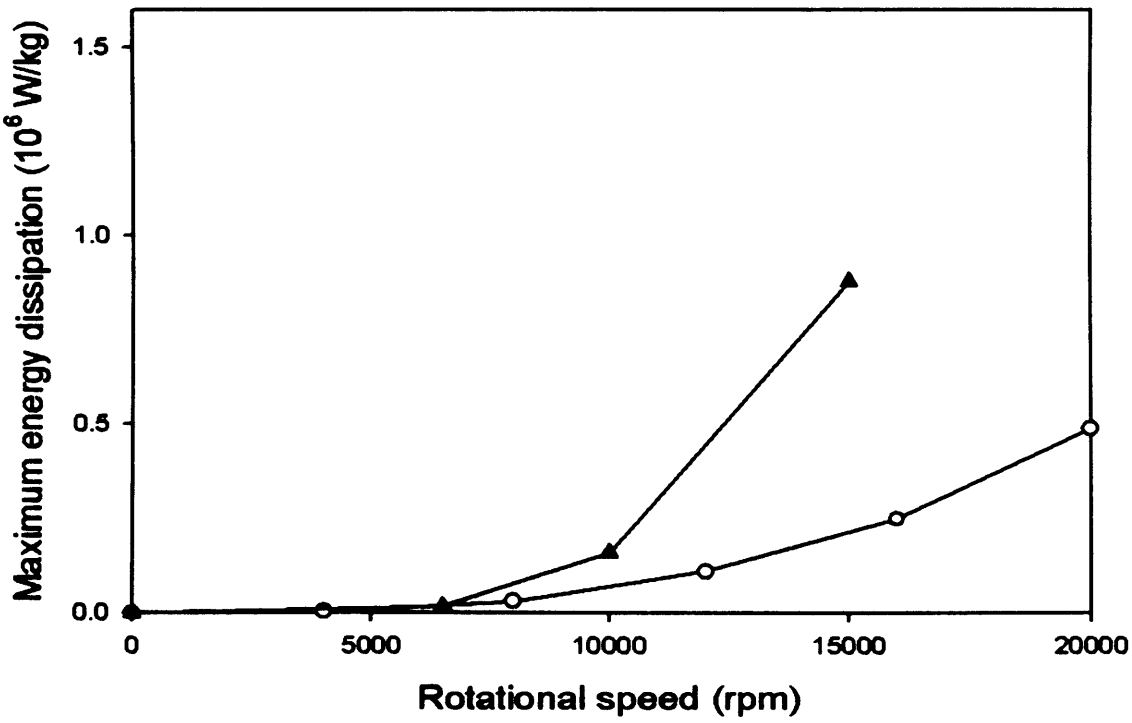

Fig. 4-4: Comparison of maximum energy dissipations found in the rotating disc shear device at a variety of rotational speeds predicted using CFD (▲) and Equation 4-5 (○). Water at 298K was used as the test liquid.

4.4.1.2 Assessing the shear sensitivity of pre-extraction E. coli cells

The rotating shear cell device was used to subject pre-extraction *E. coli* cells to different maximum energy dissipation rates and thereby determine the effect the shear forces prevailing in an industrial centrifuge entry zone might have upon the Fab' production process. Cells were obtained from a 20 L scale (10L working volume) IPTG-induced fermentation with a post-induction feed rate of 1.46 mL h^{-1} L^{-1}, harvested 36h after induction. Total cell damage was assessed by % protein release (Fig. 4-5). Shearing for 20 s in the device at maximum energy dissipations up to $1.6x10^6$ W kg^{-1} had no effect upon the level of protein found in the extracellular medium. As the pilot-scale disc-stack machine used in this study had been shown by CFD simulations to produce a maximum energy dissipation rate of $2.0x10^5$ W kg^{-1} at its highest spin speed (9800 rpm), it is expected that shear damage upon centrifuge entry will not significantly alter cell integrity. Furthermore, the level of protein release found in the supernatant from the disc-stack machine operated at a flow rate of 25 L/h was found to have an identical total protein concentration as that found when using a bench-top centrifuge (zero shear control). It may be concluded that the USD mimic gave a good agreement with pilot-scale experiments (Fig. 4-5).

Periplasmic damage was assessed by % Fab' release (Fig. 4-6). Again, only a tiny (~ 1%) increase in the concentration of Fab' in the supernatant after shearing was measured, therefore it is expected that shear damage upon centrifuge entry will not significantly alter the amount of Fab' lost to the supernatant during pre-extraction cell harvest. Furthermore, the level of Fab' release found in the supernatant from the disc-stack machine operated at a flow rate of 25 L/h within one standard deviation of that obtained when using a bench-top centrifuge. By this assessment it may be concluded that the USD mimic gave a good agreement with pilot-scale experiments (Fig. 4-6).

From these results it was concluded that shear damage to the pre-extraction cells upon disc-stack centrifuge entry would not result in significant damage to cell or loss of periplasmic integrity.

4.4.2 Consideration of centrifugal exit damage

The USD exit damage mimic of Chan (2006) was used in order to determine how any damage inflicted on the cells by centrifuge exit during disc-stack broth centrifugation might affect the process. Variations of post-induction carbon feed rate were used to give

three high cell density *E. coli* fermentations with differences in extracellular components, cell structural stability and cell viability. 20 L pilot-scale fermentations were performed using the IPTG-induced process. Immediately after sample processing in the capillary device the cells underwent periplasmic extraction at small-scale, in order to examine how any damage might affect the downstream process.

Fig. 4-7 shows the extent of protein release after periplasmic extraction of cells that have been ejected from the capillary device at a variety of speeds for the *E. coli* fermentation with the lowest carbon feed rate after induction of 1.4 mL h^{-1} L^{-1} (post-induction constant growth rate of 0.0037 h^{-1}, endpoint wet solids content of 16.1% (w/v)). This fermentation produced cells with the highest structural stability, indicated by the low level of Fab' leakage to the extracellular medium (~ 10% of total Fab' present located in supernatant at harvest). It can be seen that the ejection speed from the capillary device had no significant correlation with the level of protein found in the supernatant after periplasmic extraction. Fig. 4-8 indicates that the level of Fab' found in the supernatant after periplasmic extraction is also not a function of ejection speed.

Fig. 4-9 shows the extent of protein release after periplasmic extraction of cells that had been ejected from the capillary device at a variety of speeds for the *E. coli* fermentation with the median carbon feed rate after induction of 1.6 mL h^{-1} L^{-1} (post-induction constant growth rate of 0.0044 h^{-1}, endpoint wet solids content of 15.8% (w/v)). The cells produced from this fermentation were less structurally stable than those produced in the previous fermentation, as indicated by a greater level of Fab' leakage to the extracellular medium (~ 20% leakage observed). Again, no increase in protein release after periplasmic extraction with ejection speed can be observed. Fig. 4-10 indicates that the level of Fab' found in the supernatant after periplasmic extraction is also not a function of ejection speed.

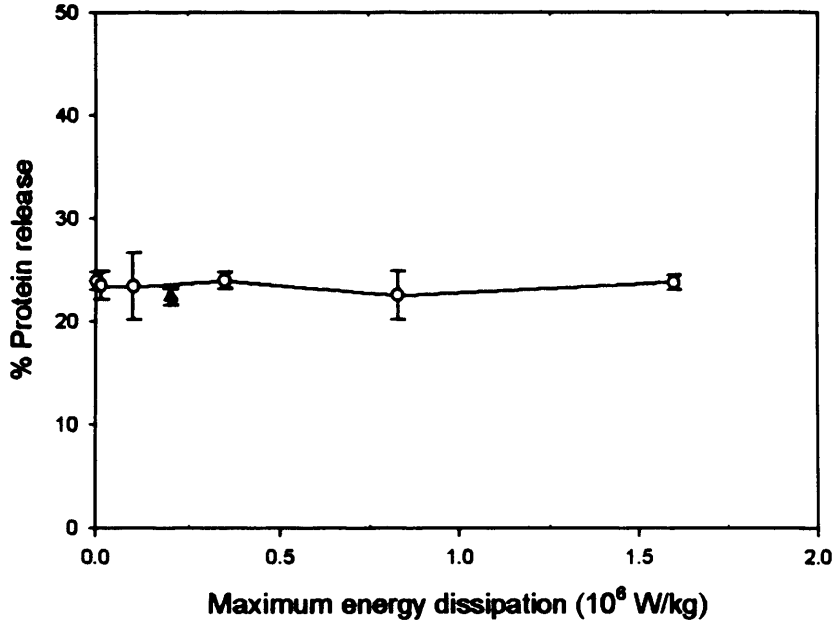

Fig. 4-5: The effect of similar energy dissipation rates to that found in the entry zone of industrial centrifuges upon cell integrity, generated by the USD rotating disc device (○) and the CSA-1 disc-stack centrifuge (▲) and assessed by total protein released into the supernatant after application of the shear force. *E. coli* cells were obtained from an IPTG-induced fermentation with a post-induction glycerol feed rate of 1.46 mL h^{-1} L^{-1}. The pilot-scale disc-stack was run at an inlet flowrate of 25 L/h.

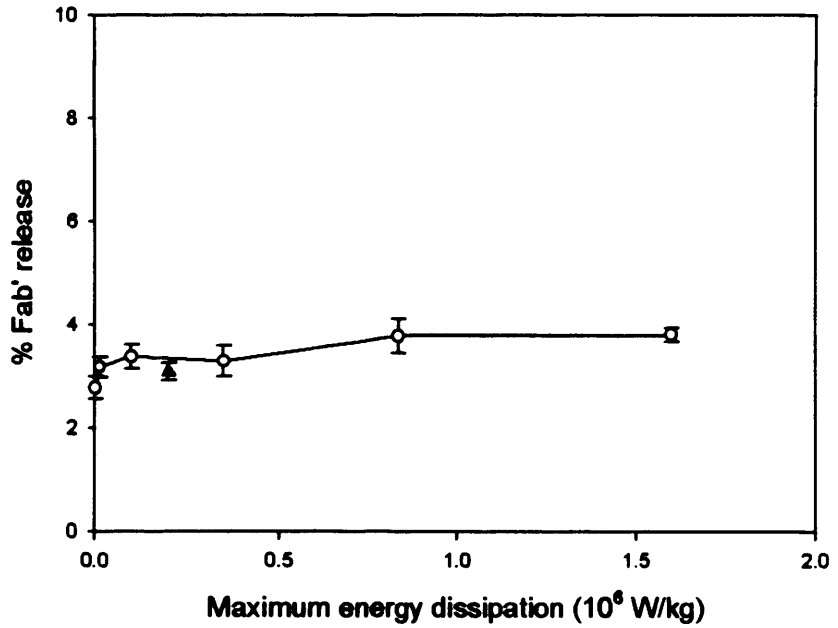

Fig. 4-6: The effect of similar energy dissipation rates to that found in the entry zone of industrial centrifuges upon periplasmic integrity, generated by the USD rotating disc device (○) and the CSA-1 disc-stack centrifuge (▲) and assessed by Fab' release into the supernatant after application of the shear force. *E. coli* cells were obtained from an IPTG-induced fermentation with a post-induction glycerol feed rate of 1.46 mL h^{-1} L^{-1}. The pilot-scale disc-stack was run at an inlet flowrate of 25 L/h.

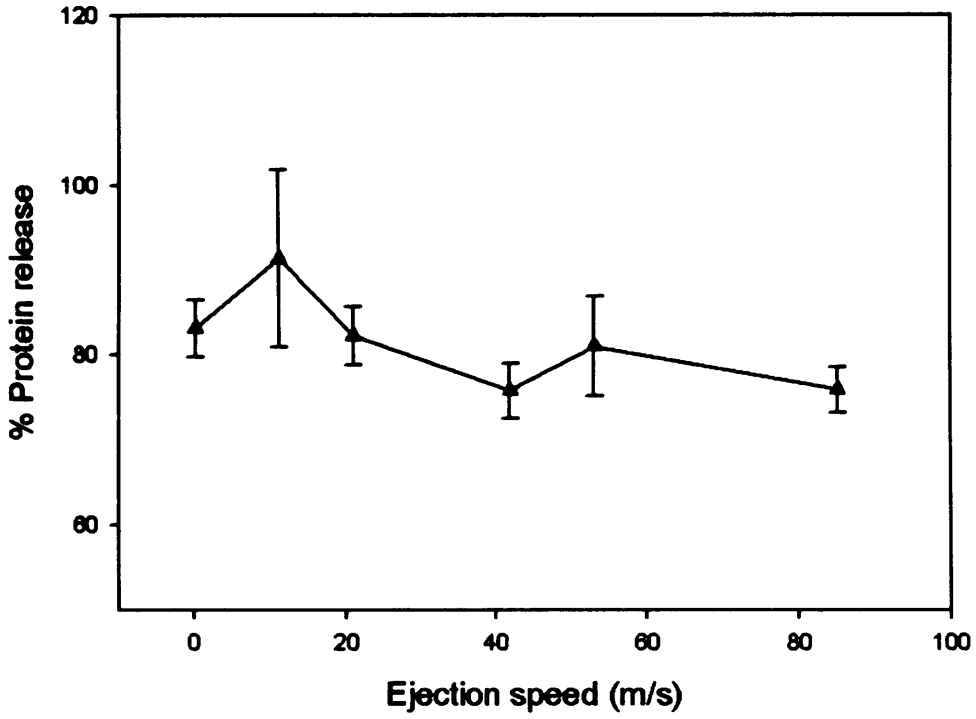

Fig. 4-7: The effect of ejection speed from the small-scale capillary device upon the % of total protein lost to the extracellular medium after small-scale periplasmic extraction (▲). *E. coli* cells were obtained from an IPTG-induced fermentation with a post-induction carbon feed rate of 1.4 mL h^{-1} L^{-1}.

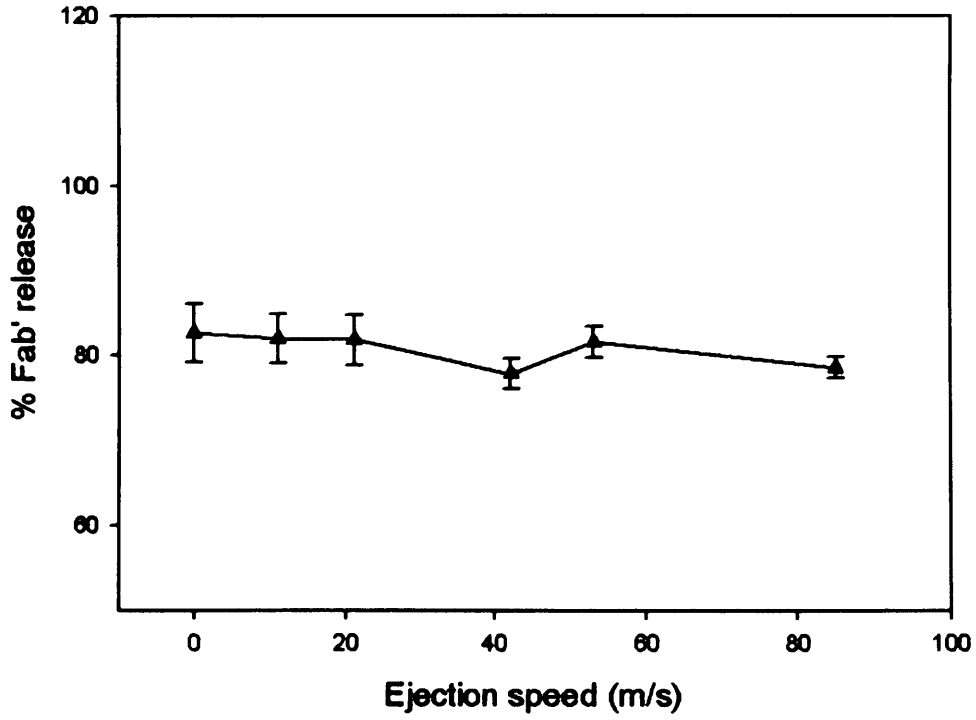

Fig. 4-8: The effect of ejection speed from the small-scale capillary device upon the % of total Fab' present in the extracellular medium after small-scale periplasmic extraction (▲). *E. coli* cells were obtained from an IPTG-induced fermentation with a post-induction carbon feed rate of 1.4 mL h^{-1} L^{-1}.

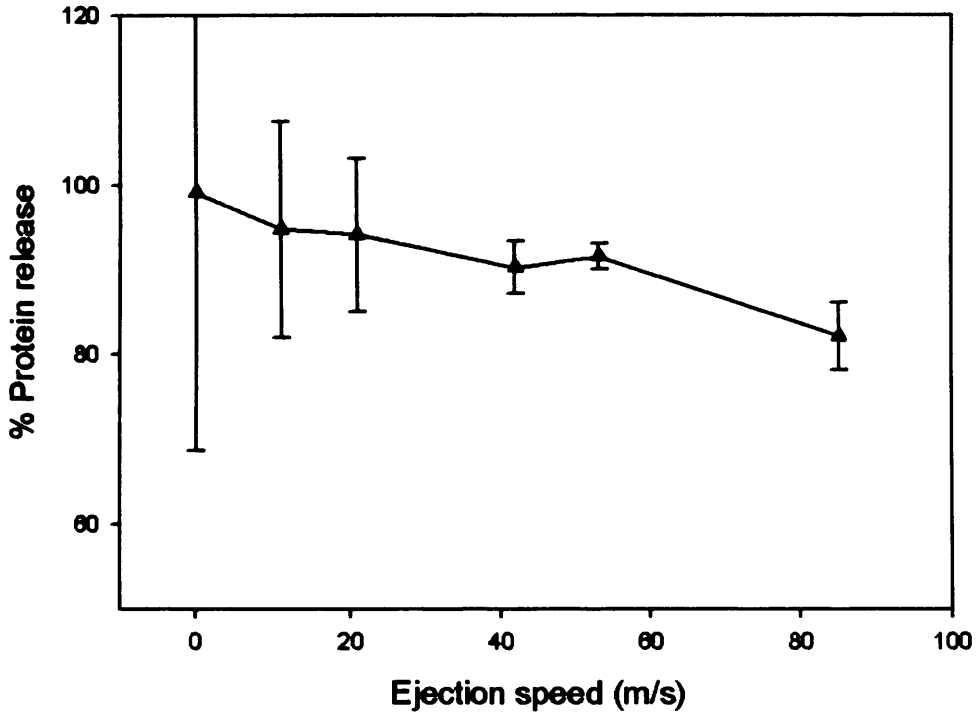

Fig. 4-9: The effect of ejection speed from the small-scale capillary device upon the % of total protein lost to the extracellular medium after small-scale periplasmic extraction (▲). *E. coli* cells were obtained from an IPTG-induced fermentation with a post-induction carbon feed rate of 1.65 mL h^{-1} L^{-1}.

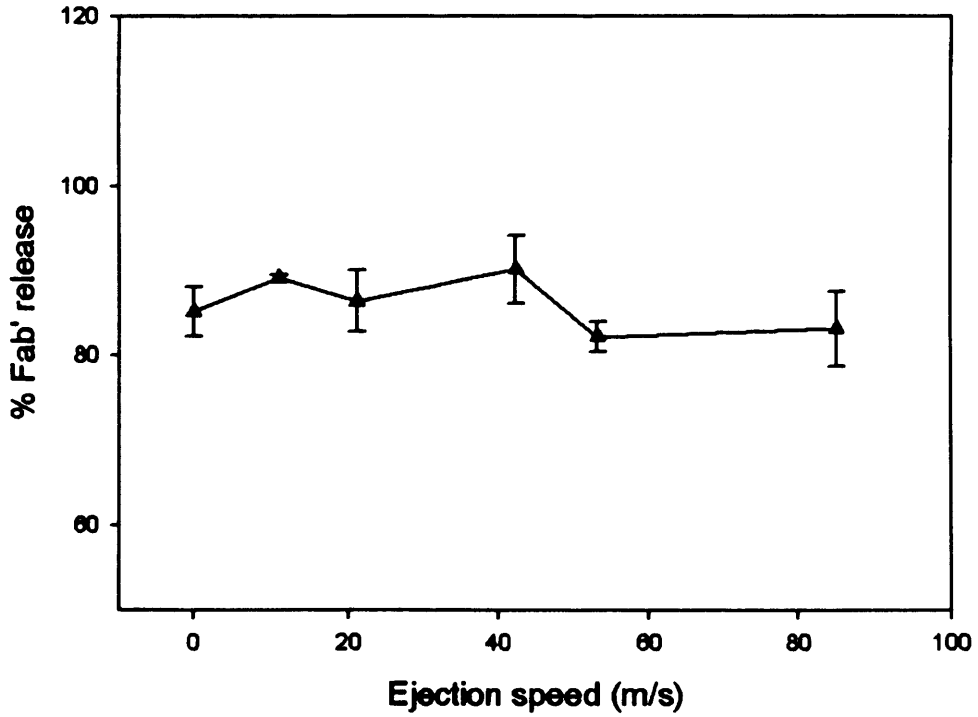

Fig. 4-10: The effect of ejection speed from the small-scale capillary device upon the % of total Fab' present in the extracellular medium after small-scale periplasmic extraction (▲). *E. coli* cells were obtained from an IPTG-induced fermentation with a post-induction carbon feed rate of 1.65 mL h^{-1} L^{-1}.

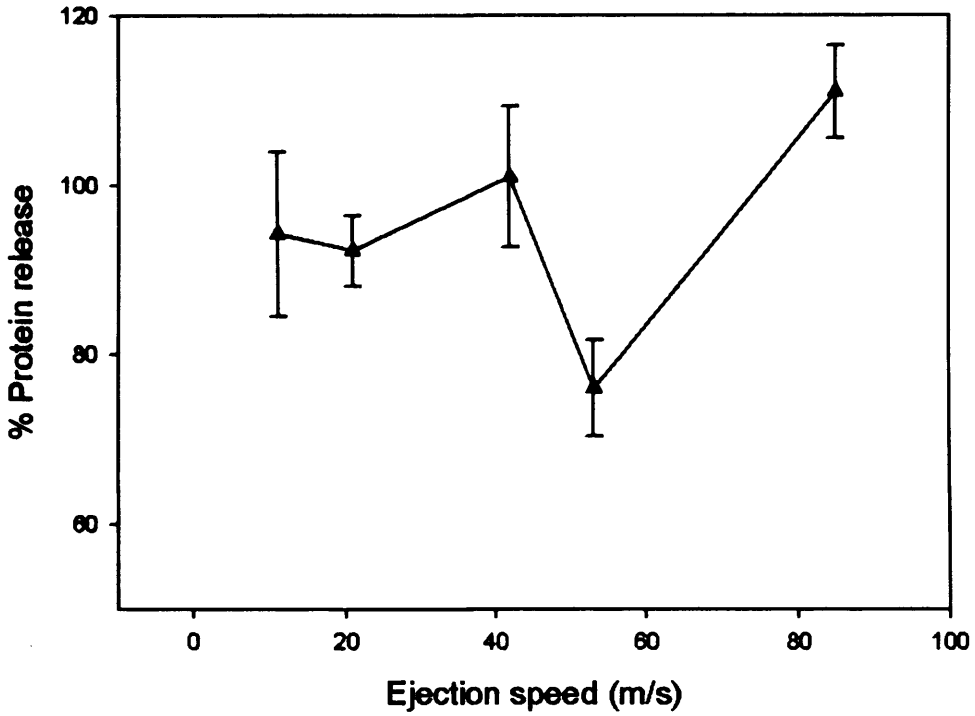

Fig. 4-11: The effect of ejection speed from the small-scale capillary device upon the % of total protein lost to the extracellular medium after small-scale periplasmic extraction (▲). *E. coli* cells were obtained from an IPTG-induced fermentation with a post-induction carbon feed rate of 1.8 mL h^{-1} L^{-1}.

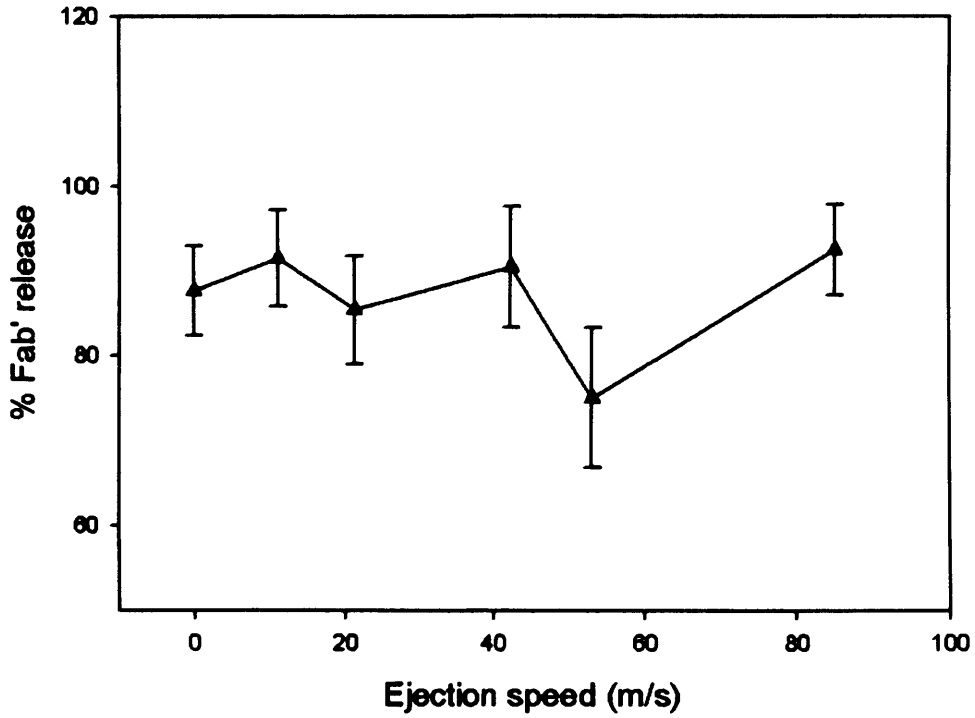

Fig. 4-12: The effect of ejection speed from the small-scale capillary device upon the % of total Fab' present in the extracellular medium after small-scale periplasmic extraction (▲). *E. coli* cells were obtained from an IPTG-induced fermentation with a post-induction carbon feed rate of 1.8 mL h^{-1} L^{-1}.

Fig. 4-11 shows the extent of protein release after periplasmic extraction of cells that had been ejected from the capillary device at a variety of speeds for the *E. coli* fermentation with the highest carbon feed rate after induction of 1.8 mL h^{-1} L^{-1}. This feed rate gave the highest post-induction growth rate of 0.0061 h^{-1} immediately after induction, but by harvest time the cells had entered death phase, giving an endpoint wet solids content of only 13.3% (w/v) due to cell lysis. This broth therefore had a liquid phase with much cell debris (indicated by the highest well spun supernatant $OD_{600\ nm}$ of 1.2) with the lowest level of structurally intact *E. coli* cells (~ 30% of Fab' lost to the extracellular medium). However, even using these cells, the weakest cell population that could be expected from a functional IPTG-induced Fab' fermentation, no increase in protein release after periplasmic extraction with ejection speed was observed. Furthermore, Fig. 4-12 indicates that the level of Fab' found in the supernatant after periplasmic extraction is also not a function of ejection speed.

Figures 4-7 to 4-12 suggest that any damage induced upon centrifuge ejection is not significantly extensive as to alter the performance of the periplasmic extraction step either in terms of Fab' or protein release. One hypothesis to explain this could be that the performance of the periplasmic extraction is independent of the cell structural stability and integrity. However, this hypothesis can be discounted because both protein and Fab' release appear to be dependant upon the post-induction glycerol flow rate. For example, a dependant t-test matching protein release measurements at the same ejection speed indicates that it can be stated with greater than 99.75% certainty that there is a statistically significant increase in protein release as the fermentation post-induction glycerol feed rate increases from 14-16.5 mL h^{-1} L^{-1}. Likewise, it can be stated with greater than 97.5% certainty that there is a statistically significant increase in Fab' release as the fermentation post-induction glycerol flow rate increases from 14-16.5 mL h^{-1} L^{-1}. A more likely explanation is that the freezing protocol used in the studies described in Chan et al (2006) adversely affected the *E. coli* cells structural integrity. The implications of using freeze/thawed cells for DSP studies are discussed in more detail in Chapter 9.

Both the maximum and minimum bowl spin speeds available using the pilot-scale disc-stack centrifuge used in this EngD will result in cell ejection velocities within the 0-85 m/s region studied by the USD device (Table 4-1). Exit damage has been measured within this range using the USD device for three IPTG-induced fermentations with

varying glycerol flow rates, including a high glycerol flow rate that generates weaker cells, and in all cases insufficient damage was caused to the cells to alter DSP performance. Therefore cellular damage during centrifugal exit has been regarded as insignificant to the process studied and not considered further.

4.5 Conclusions

The engineering forces applied to the process stream during centrifuge entry and exit were investigated using two established USD techniques. The exposure to shear during centrifuge entry was mimicked using the USD device of Boychyn et al. (2004). It was demonstrated that the application of energy dissipation levels in the range of those found in the entry zones of disc-stack centrifuges to pre-extraction cells yielded inconsequential levels of cell damage. As *E. coli* spheroplasts have also been shown to be highly resistance to the levels of shear experienced in disc-stack entry zones (Bowering, 2000; Fischer, 1996; Murrell, 1998), it was concluded that centrifuge entry damage will not be a key processing parameter in the process under investigation.

The damage to *E. coli* cells produced by the IPTG-induced upstream process was mimicked using a capillary device (Chan, 2006; Chan et al., 2006). Damage to the cells was assessed at a variety of ejection velocities from 0-85 m/s using this device. At all velocities tested no alteration in performance of a subsequent periplasmic extraction unit operation was observed. Therefore, as the maximum exit velocity during cell ejection produced by the disc-stack centrifuge used in this EngD is 82 m/s, it was concluded that centrifuge exit damage will also not be a key processing parameter in the process under investigation.

In the next chapter a USD method is developed to model another centrifugation process parameter: clarification efficiency.

5. Ultra scale-down methodology for predicting the centrifugal separation behaviour of high cell density cultures

5.1 Abstract

This chapter describes an ultra scale-down methodology for predicting centrifugal clarification performance in the case of high cell density fermentation broths (> 10% solids). Existing USD approaches generated for dilute systems lead to a 5- to 10-fold over-prediction of clarification performance when applied to such high cell density feeds. This is due to increased interparticle forces, leading to effects such as aggregation, flocculation, or even blanket sedimentation, occurring in the low shear environment of a laboratory centrifuge, which will not be apparent in the settling region of a continuous-flow industrial centrifuge. A USD methodology was created based upon the dilution of high solids feed material to ~ 2% wet weight/volume prior to the application of the clarification test. At this level of dilution cell-cell interactions are minimal. Since dilution alters the level of hindered settling in the feed suspensions mathematical corrections are applied to the resultant clarification curves in order to mimic the separation of the original high cell density feed accurately.

The methodology was successfully verified: corrected USD curves accurately predicted pilot-scale clarification performance of high cell density broths of *Saccharomyces cerevisiae* and *Escherichia coli* cells. The USD method allows for the rapid prediction of large-scale clarification of high solids density material using millilitre quantities of feed. The advantages of this method to the biochemical engineer, such as enabling rapid process design and scale-up, are discussed.

5.2 Introduction

This chapter progresses the current 'state of the art' USD methodologies to allow the prediction of the centrifugal clarification of high solids density feeds, such as those of the *E. coli* industrial fermentation that forms the case study upon which this project is based.

Current trends in bioprocessing, particularly in recombinant bacterial and yeast cultures, are leading to higher cell densities as manufacturers strive for greater levels of product

expression using recombinant systems. Solids concentrations of up to 30% (w/v) are readily achievable (Persson and Lester, 2004). The handling of process streams with significant solids loads presents a unique challenge to the downstream processing engineer, specifically in the selecting of appropriate operating conditions for high-speed centrifuges, needed to harvest the cells from the fermentation liquors.

Centrifugation is a key process step in the recovery of many biological materials (Belter et al., 1988). Although the application of centrifugation is widespread, prediction of the performance of the unit operation can be difficult because of the fragile nature of most biological materials. Until recently it has been difficult to quantify the impact of flow stress in centrifuges on their performance. Work with a protein precipitate system (Mannweiler and Hoare, 1992) concluded that the majority of breakage occurred in the feed zone of disc-stack centrifuges. Similar results were observed in a multi-chamber bowl machine (Boychyn et al., 2000). Such breakage of feed material in a centrifuge causes an increase in fines resulting in a reduction of clarification performance. The difficulties in characterising complex fluid flow patterns within centrifuges have been overcome, to some extent, by advances in computational fluid dynamics (CFD) software and have been well reported (Boychyn et al., 2000; 2001; 2004; Levy et al., 1999b). These advances have enabled the feed zone of an industrial centrifuge to be mapped in terms of shear forces, and these forces reproduced in a small rotating disc device (Boychyn et al., 2001; 2004). Coupled with the use of Sigma theory (Ambler, 1961; Maybury et al., 1998), this has allowed a USD centrifugation mimic to be developed and verified. The use of this approach for the prediction of industrial-scale centrifugal clarification of dilute feeds has been published (Hutchinson et al., 2006; Maybury et al., 2000).

The work above has focussed on mammalian cell culture and protein precipitate systems, which are characterised by fairly low solids density (< 2% wet weight/volume) and high shear sensitivities. In recent studies investigating the validity of the developed USD technologies applied to high cell density feeds it was found that the laboratory-scale mimic resulted in a substantial over-prediction of separation efficiency, and that this effect was accentuated at higher flowrates. Current USD approaches are therefore incapable of predicting the clarification of high cell density cultures, and this provided the motivation for this study. This chapter progresses the current USD centrifugation methodology by applying a novel approach to predict accurately the large-scale

clarification behaviour of cellular feeds with wet solids contents in excess of 10% (w/v). Two cellular feed materials are examined to verify the approach. The first is the recombinant bacteria *Escherichia coli*, expressing a Fab' antibody fragment to the periplasm, obtained using a high cell density batch/fed-batch industrial fermentation. The second is the eukaryote *Saccharomyces cerevisiae,* or Baker's Yeast, suspended from a packed form as used by the baking industry. The methodology aims to achieve an industrially feasible and generic method for the prediction of clarification performance of such cells and to verify the approach by comparison with pilot-scale data.

5.3 Theoretical considerations

5.3.1 USD centrifugation theory

Centrifugation of biological material is traditionally scaled on the basis of Sigma theory, a concept used to describe the solid-liquid separation performance of a centrifuge. The Sigma area, also called equivalent settling area, is defined as the surface area of a gravity settling tank with equivalent separation performance. The derivation of the Sigma concept is described elsewhere (Ambler, 1961).

Unique expressions for the Sigma area exist for each centrifuge design. Of interest to this research are the expressions used to calculate the Sigma values of a disc-stack centrifuge and of a swing-out laboratory centrifuge.

For a disc-stack centrifuge

$$\Sigma = \frac{2\pi n_d \omega^2 (r_2^3 - r_1^3)}{3g \tan\theta} f_1 \qquad (5\text{-}1)$$

where n is the number of active discs, $\omega = 2\pi N$, N is the rotational speed (rps), r_1 and r_2 are the inner and outer disc radius (m), g is acceleration due to gravity (ms^{-2}), θ is the half disc angle, f_1 is the correction factor for spacer caulks, determined using Equation (5-2):

$$f_1 = 1 - \left(\frac{3Z_L B_L}{4\pi r_2}\right)\left(\frac{1-\left(r_1/r_2\right)^2}{1-\left(r_1/r_2\right)^3}\right) \qquad (5\text{-}2)$$

where Z_L is the number of caulks on a disc, and B_L is the caulk width.

For the laboratory centrifuge:

$$\Sigma = \frac{V\omega^2(3-2x-2y)}{6g\ln(\frac{2R_o}{R_o+R_i})} \qquad (5\text{-}3)$$

where V is the volume of process material in laboratory tube (m^3), R_i is the inner radius (m) (the distance between the centre of rotation and the top of the liquid), R_o is the outer radius (m) (the distance between the centre of rotation and the bottom of the tube), and x and y are the fractional times required for acceleration and deceleration, respectively (Maybury et al., 1998).

The solid-liquid separation ability of a particular centrifuge is given by the ratio of the volumetric flow rate, Q, to the equivalent settling area, Σ, of the centrifuge. Comparison between different centrifuges, such as between an industrial-scale centrifuge (IS) and a laboratory centrifuge (USD), can be performed using Equation 5-4:

$$\frac{Q_{IS}}{\Sigma_{IS} c_{IS}} = \frac{V_{USD}}{c_{USD} t_{USD} \Sigma_{USD}} \qquad (5\text{-}4)$$

where Q_{IS} is flow rate through the industrial centrifuge ($m^3 s^{-1}$), t_{USD} is the residence time in the laboratory centrifuge (s), and c_{USD} and c_{IS} are correction factors to account for non ideal fluid flow patterns the values of which depends on centrifuge design. The laboratory centrifuge is usually considered the reference and hence $c_{USD} = 1.0$. As in this study the industrial centrifuge used is a disc-stack design, the disc-stack correction factor $c_{IS} = 0.4$ is applied (Boychyn et al., 2004).

5.3.2 Compensation for entry zone shear forces

Shear levels seen within the internal volume (particularly in the feed zone) of an industrial centrifuge can alter the properties of the feed prior to sedimentation. For example, particle attrition caused by shear can reduce the mean particle size. Also, the viscosity of the suspending fluid can be altered by the shear forces either causing leakage of cell contents into solution or by the destruction of dissolved macromolecular components, such as long strand DNA.

Laboratory centrifuges tend to be of a discrete, bottle design and hence expose the feed stream to no (or at least minimal) shear forces. Therefore one of the central concepts of the conventional USD centrifugation mimic is compensation for these shear forces via incorporation of a shear step using a high-speed rotating disc device prior to laboratory centrifugation. The theory and method of mimicking shear upon feed entry into an industrial centrifuge has been thoroughly described in the literature (Boychyn et al., 2000; 2001; 2004).

5.3.3 Settling of high cell density cultures

Initial trials using the previously developed USD methodology for predicting clarification levels (Boychyn et al., 2001) resulted in significant over-prediction of process-scale clarification of high solids density feed-streams. This implies that the high solids density material settles more quickly in the laboratory-scale centrifuge than it does in industrial-scale machines. The most likely explanation for this is that the consequences of interparticle forces are greater in the laboratory-scale centrifuge relative to industrial centrifuges. In the gentle environment of a laboratory centrifuge even weak aggregation of particles will lead to entrapment of liquid and a variation in the apparent volume fraction of the settling particles. In this case the level of entrained liquid will affect the settling behaviour drastically: low levels of entrainment will lead to aggregation and more rapid settling, higher levels will result in slow-settling flocs forming and at very high levels "blanket" sedimentation will occur where the settling blanket sweeps up and removes fine particles. The resultant effect will be an over-prediction of the clarification performance compared to the actual performance achieved in a continuous-flow centrifuge. All three of these effects may occur in a low-shear environment but are unlikely to prevail in an industrial centrifuge, where the high shear environment would most likely break up any such aggregate structures. In the case of the conventional USD method, a shear device is used to subject the test materials to

representative levels of shear and in the case of high solids feeds this will break the aggregates in the same manner as the entry zone of an industrial machine. However, there is a relatively long time period between application of shear and the subsequent clarification test. In the low-shear environment of a laboratory centrifuge tube this is likely to allow aggregates to reform. This effectively results in higher clarification levels for the laboratory-scale centrifuge than for the large-scale machine of equivalent separation conditions, and is a fundamental issue requiring resolution before a USD method applicable to high cell density feeds can be utilised.

The USD procedure detailed pre-dilutes high solids feeds in their original supernatant to a solids content of approximately 2% (w/v). At this concentration the conventional USD mimic has been shown to work successfully (Hutchinson et al., 2006). This approach will maintain the same liquid viscosity but prevent hindered settling and aggregation effects from occurring during USD clarification. Mathematical correction of the settling data based upon changed hindered settling relationships (Richardson and Zaki, 1954) can then be used to yield a prediction of sedimentation behaviour of the high solids load feeds in industrial machines.

5.3.4 Correcting sedimentation rate for the effect of suspended particle concentration

Richardson and Zaki (1954) determined an empirical method of correlating the concentration of suspended particles with the rate of settling (Equation 5-5):

$$U = U_t \varepsilon^n \qquad (5\text{-}5)$$

where U is the settling velocity of the suspension, ε is the voidage, U_t is settling velocity at ε=1, and n is the slope obtained from a plot of log U versus log ε. In order to determine n, it is necessary to determine the Particle Reynolds number (Re_p) with respect to the particle (Equation 5-6):

$$Re_p = \frac{d_p U \rho_f}{\mu} \qquad (5\text{-}6)$$

where d_p is the size of the particle, μ the fluid viscosity and ρ_f the fluid density. As $Re_p <$ 0.2 for cellular material, in both the laboratory-scale and industrial centrifuge particles

will settle in a viscous flow regime. For settling under these conditions, the parameter n has been found to be 4.8 for identical spheres (Gibilaro, 2001), assuming that the ratio of the diameter of the particle to pipe is negligible, as will be the case for the cells used in this study with diameters in the μm range.

It has been assumed that the density of biological cells is approximately that of water. This assumption is supported by the fact that small (± 5%) differences in density would alter the correction factor by < ± 2%. This allows determination of ε from the cellular solids fraction, φ.

$$\varepsilon = (1 - \varphi) \tag{5-7}$$

As U is proportional to $Q/c\Sigma$, we can substitute Equation (5-7) into a modified form of Equation (5-5) and write:

$$\left(Q/c\Sigma\right)_{IS} = U_t\left(1 - \varphi_{IS}\right)^{4.8} \tag{5-8}$$

and

$$\left(Q/c\Sigma\right)_{USD} = U_t\left(1 - \varphi_{USD}\right)^{4.8} \tag{5-9}$$

where IS and USD refer to the undiluted industrial-scale feed and the diluted USD feed respectively. Substituting Equation (5-8) into Equation (5-9) gives us our correction factor:

$$\frac{\left(Q/c\Sigma\right)_{IS}}{\left(Q/c\Sigma\right)_{USD}} = \frac{\left(1 - \varphi_{IS}\right)^{4.8}}{\left(1 - \varphi_{USD}\right)^{4.8}} \tag{5-10}$$

This derivation does assume that all cells are uniform and spherical. This is a fair assumption as the dilution will have the effect of minimizing interparticle forces and shape factors are therefore unlikely to be a key concern. Temperature must be maintained from industrial-scale to mimic to ensure a constant liquid viscosity.

5.3.5 Proposed generic USD methodology

The conventional USD method detailed in the literature subjects the feed material to an equivalent shear force to that found in the industrial centrifuge under consideration using a high-speed rotating disc device before determining clarification levels at a range of V/ctΣ values in a laboratory centrifuge. This can then be used to predict performance of an industrial centrifuge using Equation 5-4. This conventional method has been modified to allow prediction of the centrifugal clarification efficiency of high solids density feeds using pre-dilution. Feed material is sheared in the high-speed rotating disc device, and the liquid portion is isolated via centrifugation. This liquid, representative of the suspending liquid after entrance into the industrial centrifuge, is then used to dilute a portion of the original feed to a solids concentration too low to allow re-aggregation of solids particles after shearing, a wet solids concentration of ~ 2% (w/v). The diluted feed is then analysed as per the conventional USD method: it is sheared in the high-speed rotating disc device before determining clarification levels at a range of V/ctΣ values in a laboratory centrifuge. However, the V/ctΣ values must be corrected using Equation 5-10 to account for the reduced level of hindered settling that would occur in an industrial machine.

Dilution of the feed to ~ 2% (w/v) solids concentration was chosen as it was necessary to choose a dilution of the original to feed where solids re-interaction/aggregation after shearing would be effectively removed. The original USD method has been shown to be accurate with mammalian cells even in the late decline phase of growth when the cell viability was below 10%: prime conditions for interaction and aggregation (Hutchinson et al., 2006). However, this work did not observe an aggregation problem and therefore it was assumed here that the solids density used in these experiments would be 'safe' to halt rapid cell interactions from forming between shearing in the USD device, and the clarification test. This 'rule of thumb' was shown to be successful in our studies.

5.4 Results and discussion

5.4.1 Method verification using high cell density *E. coli* fermentations

Variations of the post-induction carbon feed rate were used to give three high cell density *E. coli* fermentations with differences in extracellular components, cell structural stability and cell viability. In all the *E. coli* broths used, and with the Baker's Yeast suspension, it was assumed that solids content (w/v) was equivalent to the void

fraction. This is justifiable as the densities of *E. coli* and Baker's Yeast cells are approximately that of water, the suspending liquid. However, this does mean that an accurate determination of solids content was crucial. To this end, all solids contents were calculated from the DCW and knowledge of the internal water content of the cells, as detailed in section 2.4.3.1. This approach was taken, as traditional methods that weigh well spun wet sediment include significant errors due to the presence of interstitial liquid in the wet sediment.

Fig. 5-1 compares the two USD methods with the pilot-scale disc-stack results for the *E. coli* fermentation with the lowest carbon feed rate after induction, (post-induction constant growth rate of 0.0026 h^{-1}, endpoint wet solids content of 14.1% (w/v)), which gave the broth with the cleanest liquid phase (indicated by OD_{600} value). Most *E. coli* cells obtained from this broth were structurally intact, indicated by a negligible level of Fab' lost to the extracellular medium. While the conventional USD method can be seen to significantly over-predict industrial-scale clarification, the USD dilution method gives good agreement with the pilot-scale data, despite the non-sphericity of the *E. coli* cells, suggesting the *n* value of 4.8 for the viscous flow regime (Equation 5-5) can be used without shape factors causing significant inaccuracies.

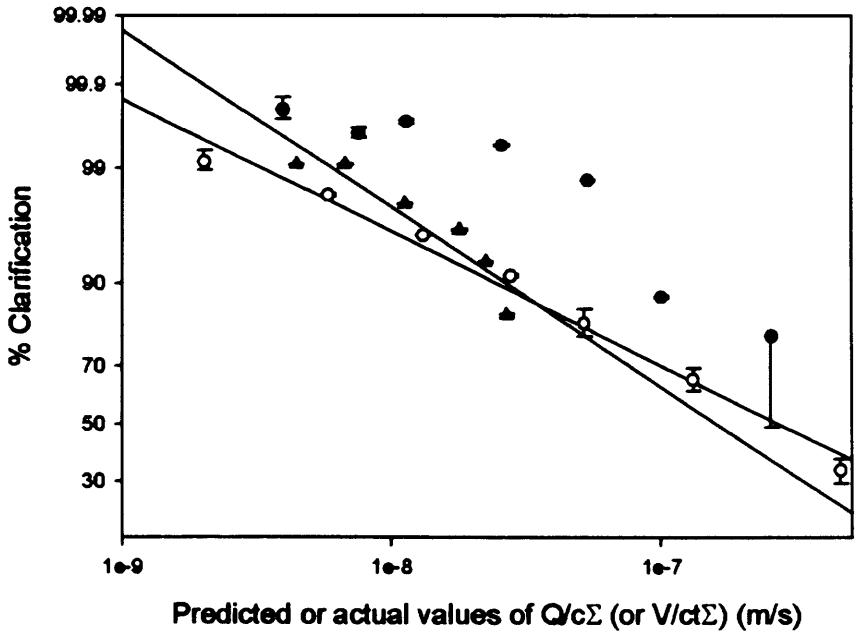

Fig. 5-1: Clarification plotted against equivalent flowrate/settling area for *E. coli* cells obtained with a specific growth rate of 0.0026 h^{-1} after induction, for pilot-scale disc-stack centrifugation (▲), conventional undiluted USD methodology (●), and the novel dilution USD methodology (○). The solids content of the feed was 14.1% (w/v). Error bars are calculated from the average standard deviation of triplicate data points.

The reason for the failure of the conventional USD method and the success of the USD dilution methodology was investigated by particle size analysis. Samples of broth produced from the above *E. coli* fermentation were prepared according to the conventional and dilution USD method, but instead of the clarification test, the particle size distribution was analysed. Samples were held at 4°C for 1h after shearing to replicate the typical time gap between shearing and the clarification test when using USD methodology. Fig. 5-2 shows that undiluted, sheared material has a similar level of cell aggregates to that found in the unsheared broth. Material prepared by the dilution USD method prevents the reformation of cell aggregates post-shearing and generates a realistic feed material for subsequent clarification studies.

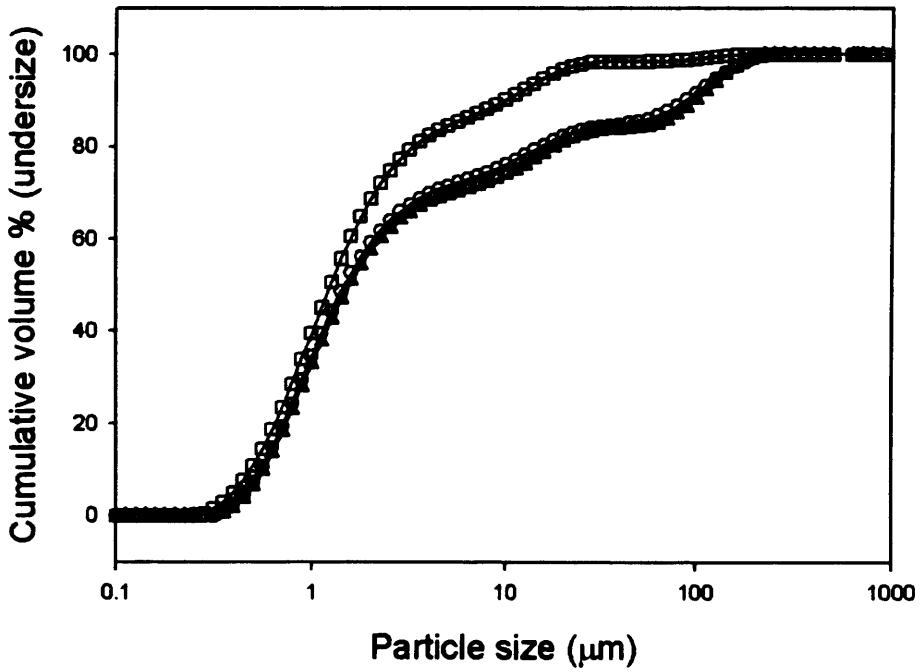

Fig. 5-2: Cumulative particle size distributions of *E. coli* cells obtained with a specific growth rate of 0.0026 h^{-1} after induction, either prepared according to the conventional USD methodology (Δ), the dilution USD methodology (|), or non-sheared (○).

Fig. 5-3 compares the two USD methods with the pilot-scale disc-stack results for the *E. coli* fermentation with the median carbon feed rate after induction, (post-induction constant growth rate of 0.0037 h^{-1}, endpoint wet solids content of 16.1% (w/v)), with a moderately clean liquid phase (indicated by $OD_{600\ nm}$ value) with a high level of structurally intact *E. coli* cells (only ~ 10% of Fab' lost to the extracellular medium). Again, the conventional USD method can be seen to significantly over-predict

industrial-scale clarification, whereas the USD dilution method gives good agreement with the pilot-scale data.

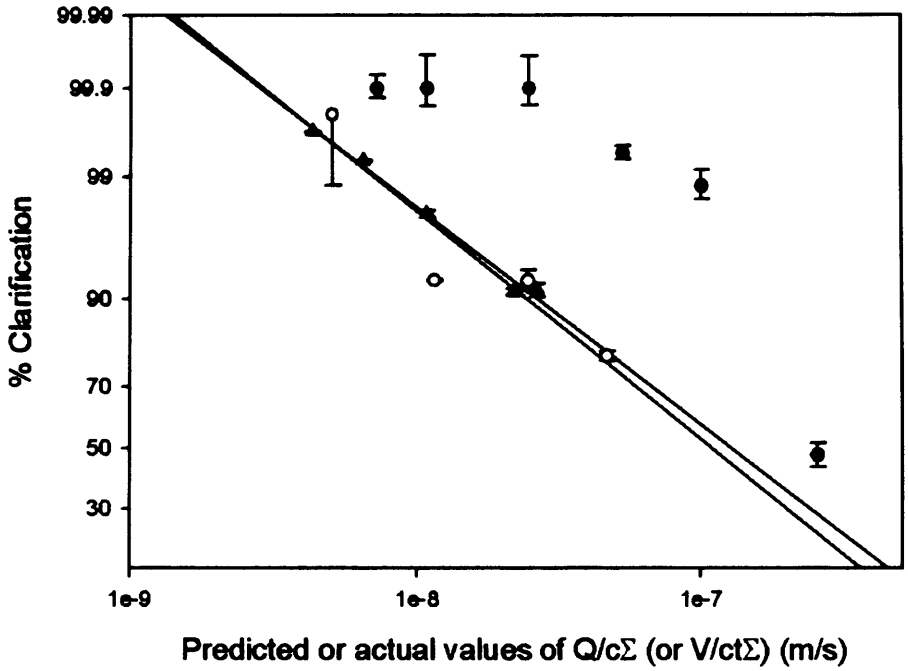

Fig. 5-3: Clarification plotted against equivalent flowrate/settling area for *E. coli* cells obtained with a specific growth rate of 0.0037 h^{-1} after induction, for pilot-scale disc-stack centrifugation (▲), conventional undiluted USD methodology (●), and the novel dilution USD methodology (○). The solids content of the feed was 16.1% (w/v). Error bars are calculated from the average standard deviation of triplicate data points.

Fig. 5-4 compares the two USD methods with the pilot-scale disc-stack results for the *E. coli* fermentation with the high carbon feed rate after induction. This feed rate gave the highest post-induction growth rate of 0.0044 h^{-1} immediately after induction, giving an endpoint wet solids content of 15.8% (w/v). The lower solids content of the broth at the end of the fermentation compared to the 0.0037 h^{-1} growth rate cells, despite the higher initial growth rate, is due to lysis of a significant minority of the cells. This is presumably caused by the higher carbon availability leading to too rapid Fab' accumulation inside the cells and therefore causing structural instability. Although the broth here had a small but significant level of cell debris and therefore some variety in particle size, the adapted USD method still accurately predicted the industrial-scale clarification performance.

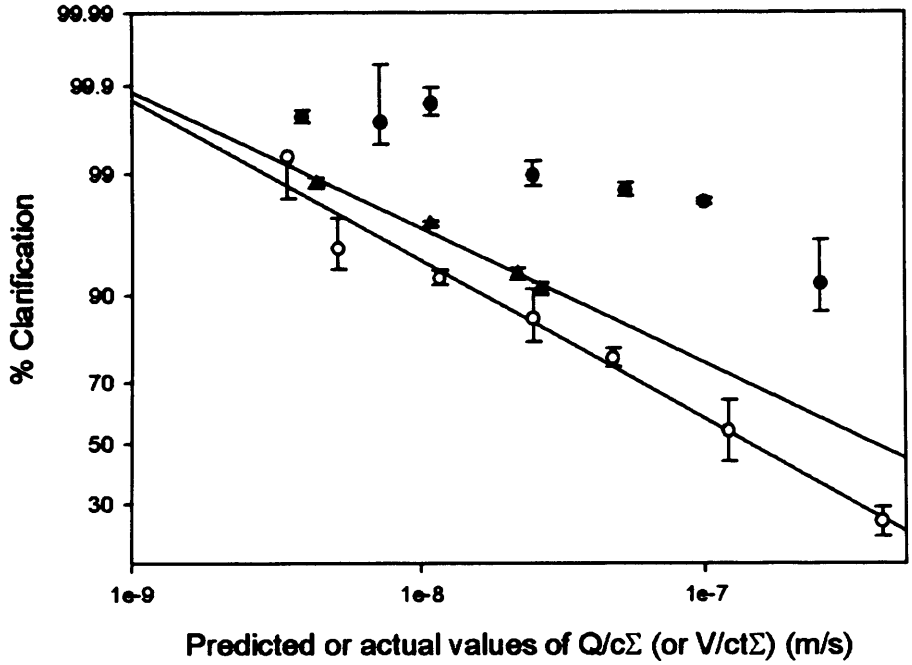

Fig. 5-4: Clarification plotted against equivalent flowrate/settling area for *E. coli* cells obtained with a specific growth rate of 0.0044 h^{-1} after induction, for pilot-scale disc-stack centrifugation (▲), conventional undiluted USD methodology (•), and the novel dilution USD methodology (○). The solids content of the feed was 15.8% (w/v). Error bars are calculated from the average standard deviation of triplicate data points.

5.4.2 Method verification using Baker's Yeast

Packed Baker's Yeast was resuspended to 15% packed wet w/v. This gave an actual wet solids content of 11.5% (w/v) when determined as described in section 2.4.3.1. The clarification efficiency was assessed using pilot-scale disc-stack centrifugation, and with both USD methods. Fig. 5-5 shows that in this case both the conventional and dilution USD methods give good prediction of pilot-scale clarification performance and suggests that Baker's Yeast does not form aggregates or generate other cell-cell interactions under these conditions. Such artefacts would cause the conventional USD method to overpredict clarification efficiency. In order to investigate this hypothesis, samples of the resuspended Baker's Yeast were prepared according to the conventional and dilution USD method, but instead of the clarification test, the particle size distributions were analysed (Fig. 5-6). As with the *E. coli* samples analysed by PSD, these samples were held at 4°C for 1h after shearing. As predicted, the particle size distributions of the material produced using the conventional and dilution USD methodology were identical, whereas the resuspended unsheared sample contained significant aggregates. The initial aggregation found in the unsheared sample is likely due to incomplete resuspension of the cells. The lack of re-aggregation with the conventional method may stem from the absence of extracellular components in the liquid phase of the Baker's Yeast feed, and

the healthy state of the Baker's Yeast cells. Moreover, the fact that the dilution method predicts pilot-scale performance as closely as the conventional USD method provides good evidence that the dilution method is not subject to significantly greater experimental sources of error than the standard approach.

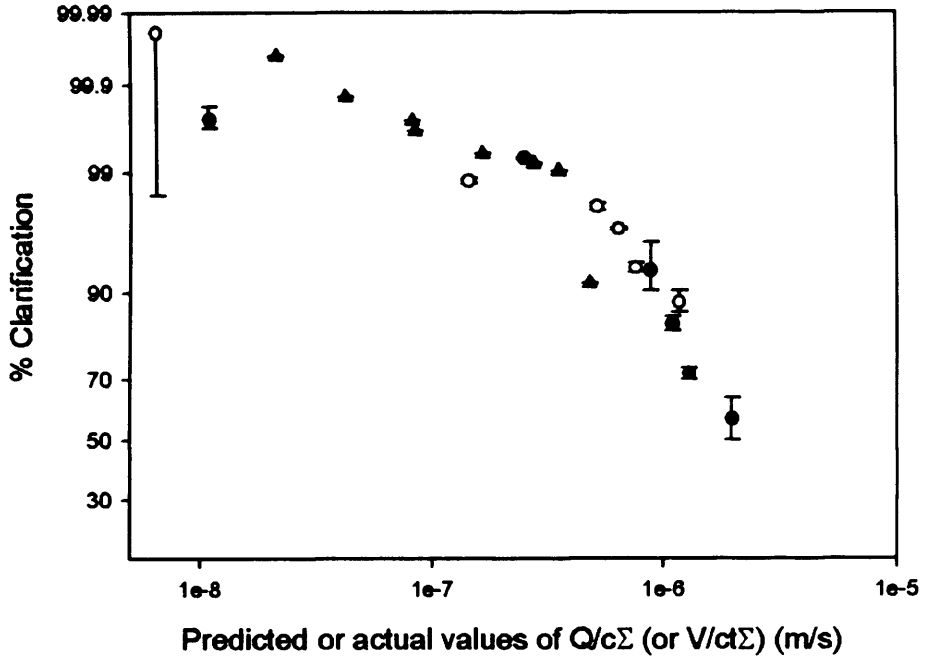

Fig. 5-5: Clarification plotted against equivalent flowrate/settling area for Baker's Yeast cells resuspended to a solids content of 11.5% (w/v) for pilot-scale disc-stack centrifugation (▲), conventional undiluted USD methodology (•), and the novel dilution USD methodology (○). Error bars are calculated from the average standard deviation of triplicate data points

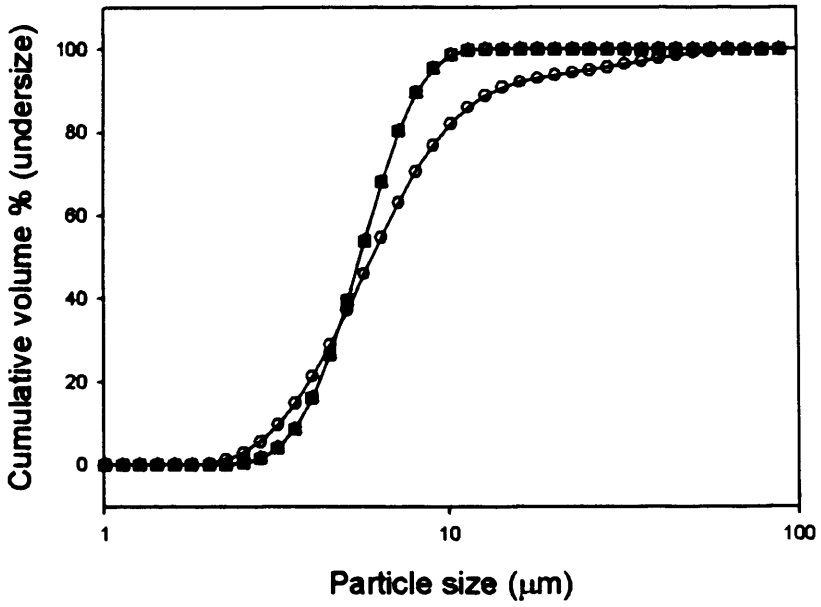

Fig. 5-6: Cumulative particle size distributions of resuspended Baker's Yeast cells, either prepared according to the conventional USD methodology (Δ), the dilution USD methodology (□), or non-sheared (○).

It should be noted that although it was necessary to use a higher range of $Q/c\Sigma$ values when investigating the Baker's Yeast system, the ranges used reflect the settling ability of the species only. The $Q/c\Sigma$ range will not alter the applicability of the methodology.

5.5 Conclusions

The dilution USD methodology presented here provides a centrifugal clarification mimic to allow prediction of the sedimentation performance in cases where the solids density is sufficiently high (greater than ~ 10% wet cell weight) as to create significant hindered settling and aggregation effects.

The USD methodology provides an inexpensive and effective way of determining centrifugation conditions that maximise centrifugal clarification during the processing of high cell density cultures. Used in combination with other USD methods, this mimic will allow faster process development and targeting of pilot-scale process development to key variables, while only requiring millilitre quantities of material.

The utility of this USD clarification method for process development and understanding is exemplified in Chapter 8 by its application, along with other USD unit operation mimics, to the initial DSP for the production of antibody fragments in HCD *E. coli* culture.

6. Ultra scale-down approach for predicting the dewatering of cellular sediments in industrial centrifuges

6.1 Abstract

If, during centrifugal separation, the product is in the liquid phase, poor dewatering will result in a drop in yield. This chapter proposes an ultra scale-down method for mimicking the centrifugal dewatering of biological cell pastes. Such a methodology could be used to aid the selection of an appropriate type of centrifuge and operating conditions to minimise losses.

The novel procedure, based on the use of a laboratory centrifuge, is described, and verified against pilot-scale results using an advanced tubular bowl centrifuge. Dewatering performance was determined for three feed materials: *E. coli* cells (obtained from the IPTG-induced fermentation detailed in Chapter 3) before and after a heat/chemical periplasmic extraction procedure, and *Saccharomyces cerevisiae* cells, used to provide a eukaryotic example for method verification purposes.

The laboratory-based technique was able to predict the dewatering levels obtained at pilot-scale to within ± 8% under all conditions studied. The accuracy of prediction increased to within ± 1% as pastes reach the maximum dewatered level possible under standard centrifugation conditions. This maximal level is shown to correlate with the theoretical maximal packing density of the cells studied.

The scale-down studies allow process development to progress with only the need for millilitre quantities of material, and are a valuable tool alongside other, similar methodologies already developed to mimic key bioprocessing steps.

6.2 Introduction

Previous chapters have discussed the need to generate predictive small-scale models of individual unit operations in order to maximise the information that can be gained from limited quantities of material. It has been shown how entry shear, exit shear and clarification efficiency can be modelled using USD methods to investigate the outputs of a centrifugation unit operation in a bioprocess. However, although the level of

dewatering achieved during centrifugation is important in many applications, to date little work in the bioprocessing sector has been carried out to generate predictive models. Dewatering levels are particularly important when an expensive product is in the liquid phase. For example, if a high value biopharmaceutical is secreted to the medium during fermentation, such as in mammalian cell antibody production processes.

The majority of published work has focussed on the dewatering of waste-water sludge and mineral slurries. The former is more applicable here due to the biological nature of the material. In these studies, ease of cake compaction, choice of spin speed, and spin time were found to be the most significant factors in determining the levels of dewatering (Chu and Lee, 2001; Lee et al., 2003). However, these investigations used low solids concentrations and mostly involved flocculated material. Furthermore in such cases filtering rather than sedimenting centrifuges were commonly used. This chapter attempts to develop a dewatering mimic applicable to bioprocess applications using sedimenting centrifuges.

Three different cellular feed materials are examined in order to establish the generality of the approach. The first is the eukaryote *Saccharomyces cerevisiae,* or Baker's Yeast, suspended from a packed form as used by the baking industry. *E. coli* cells produced by the IPTG-induced fermentation discussed in Chapter 3 provide the second and third examples. This organism exhibits some key differences to *Saccharomyces cerevisae* that may affect its dewatering properties. It is an order of magnitude smaller in size (~ 1 micron compared to 5-10 microns), and is a spherocylinder as compared to a sphere or ovoid, which will impact the packing density that may be achieved.

As discussed in Chapter 1, the Fab' protein product in the *E. coli* system is expressed to the periplasm and hence processing involves two centrifugation steps. Briefly, the first separates the broth from the cells containing the Fab' to allow resuspension in a chemical extraction buffer. Incubation at 60°C overnight in this buffer permeablises the periplasmic membrane releasing the Fab' into solution, while leaving the cell membrane intact (Weir and Bailey, 1997). The second centrifugation step then removes the post-extraction cells. Dewatering of the cell paste is of most relevance in the centrifugation of the extracted cells as any liquid present in the cell paste will contain Fab' which will be lost. Inefficient dewatering in the first centrifugation step will however lead to carry over of broth contaminants into the next process step. Both pre- and post-extraction

cells have been studied here for the purpose of elucidating the key parameters determining the extent of dewatering, and verifying the proposed mimic.

The USD mimic is verified against pilot-scale data generated in a Carr Powerfuge P6, an advanced version of a tubular bowl centrifuge capable of solids ejection without dismantling. Consideration will be given as to how the mimic may be extended to the case of disc-stack centrifuges which are widely used in bioprocessing for similar process duties, but where more modest levels of dewatering are realised. Finally, attempts will be made to relate the experimental findings to proposed models of solids packing in order to elucidate further the likely packed structures of biological materials.

6.3 Theoretical considerations

6.3.1 Factors affecting centrifugal dewatering

Before a dewatering mimic can be suggested it is first necessary to define the factors that will determine the extent of dewatering of a biological cake.

6.3.1.1 Spin Time and Spin Speed

Both spin time and speed affect the dewatering achieved for a compactable cake. Higher spin times and speeds increase the level of dewatering achieved. However, at high relative centrifugal force (RCF) or time, the level of dewatering reaches a steady state where further increases in either factor have no affect upon the level of dewatering achieved (Leung, 1998). Further dewatering can then only be achieved by use of a physical press to compress the solids mechanically and express liquid from the voids.

In order to mimic the residence time between industrial-scale centrifuges, where feed is continually pumped through the separating device, and bench-top centrifuges (where there is no flow), it will be necessary to differentiate between the time a particle spends in suspension (clarification time) and in the formed paste (compaction time).

Sigma theory, detailed in Chapter 5, could be used to determine the clarification time for any centrifuge or particular set of conditions if sufficient previous experiments have been undertaken to allow plotting of % clarification against $Q/c\Sigma$ for the feed used. Once the clarification time has been determined it can be used, with the total spin time, to calculate the compaction time in a laboratory (non-flow) centrifuge. For industrial centrifuges, this can be defined more simply as shown in Equation (6-1):

$$t_{comp.} = \frac{V_S}{2F\phi Q} + t_{delay} \qquad [6\text{-}1]$$

where t_{comp} is the time for compaction, F is the fractional recovery of solids, V_s is the solids holding capacity of the bowl, ϕ is the volumetric solids fraction entering the bowl, and t_{delay} is the time the centrifuge is spun with a full bowl prior to solids ejection.

6.3.1.2 Sediment height

The compressive force experienced at any position in the sediment cake is dependent upon the height and mass of sediment above that position. This determines the dewatering of sediment throughout the cake (Chu and Lee, 2001; Lee et al., 2003; Munro and Van Til, 1988). Here the compressive stress profile between centrifuges is mimicked using the sediment height.

Sediment height is approximated as the area of a cross-section of the solids collection zone, divided by the width. Note that we ignore curvature, or 3D effects, on the sediment height to simplify calculations. The sediment height parameter can be measured in industrial or pilot-scale centrifuges and then mimicked in a variety of test tubes of different geometry (Fig. 6-1a-e). Fig. 6-1a-b illustrates how sediment height was calculated for industrial machines. For the tubular bowl Carr Powerfuge™ P6 sediment height is constant for full bowls: the height of the sediment being parallel to the centrifugal axis (Fig. 6-1a). The complicated shape of the solids collection area in the CSA-1 disc-stack centrifuge (Westfalia Separator, AG, Oelde, Germany) required detailed calculations of the cross-sectional area to determine average sediment height: (Fig. 6-1b). Fig. 6-1c-e show how this parameter is calculated for centrifuge tubes of varying geometry. In the simplest case of a flat bottomed tube (Fig. 6-1c) sediment height is defined as for tubular bowl centrifuges. For round bottomed tubes (Fig. 6-1d), the height of the sediment for the simple horizontal portion of the tube is added to the 'average sediment height' in the bottom portion. Fig. 6-1e illustrates how sediment height has been defined for the more complicated geometry of a conical-bottomed tube.

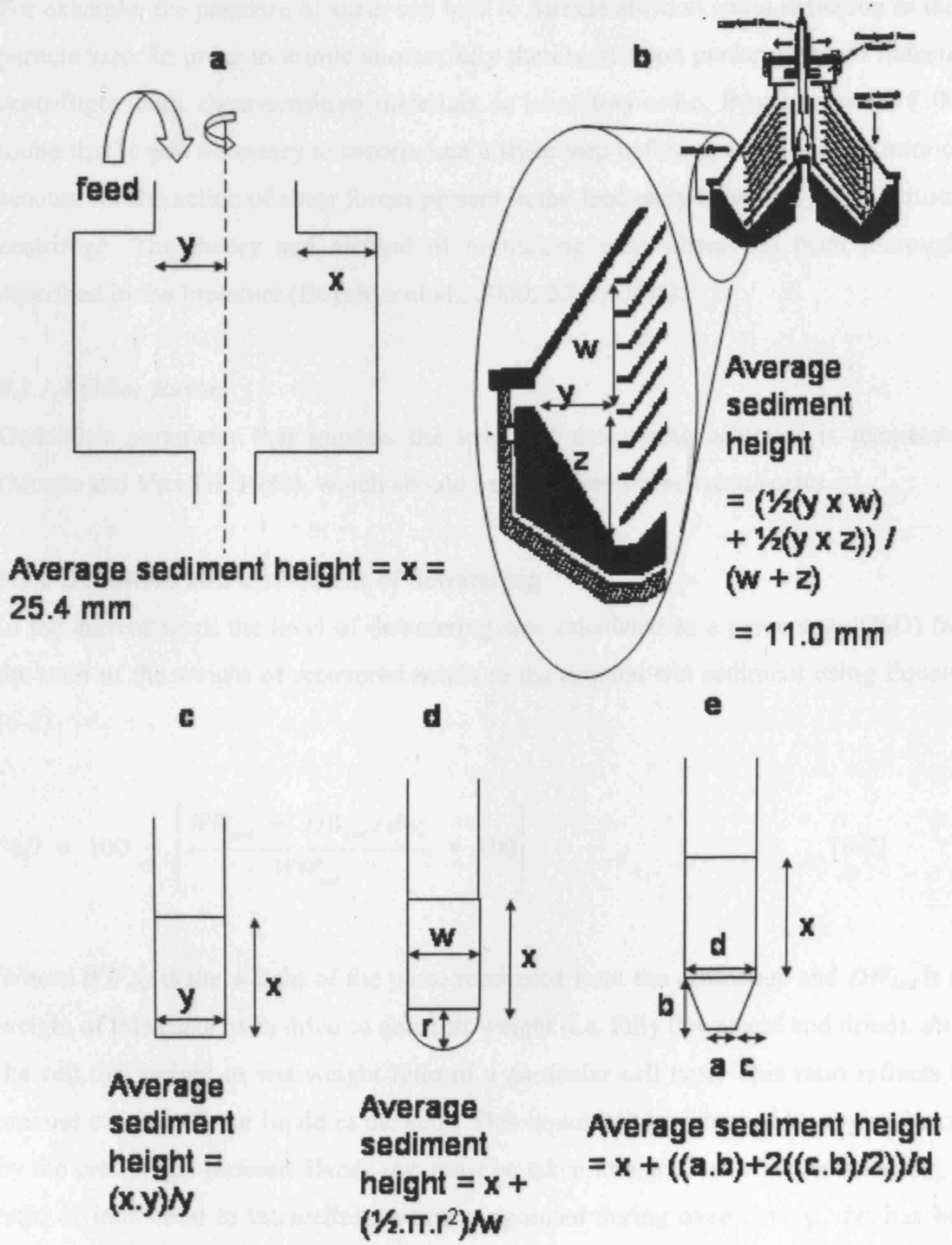

Fig. 6-1: Examples of calculations of sediment height for a variety of industrial and laboratory centrifuges. (a) and (b) show sediment height calculated for a tubular bowl and a disk-stack machine respectively. Actual values are given for The Carr Powerfuge P6 (a), and the CSA-1 disk stack centrifuge (b) in millimetres. (c) - (e) show how sediment height is calculated for different geometries of laboratory centrifuge tube.

6.3.1.3 Feed properties and the effects of shear

Properties of the feed, such as solution viscosity and the size and shape of particles, will also affect dewatering. These properties can be altered by the engineering environment.

For example, the presence of shear can lead to particle attrition and a reduction in mean particle size. In order to mimic successfully the clarification performance of industrial centrifuges with shear-sensitive materials at laboratory-scale, Boychyn et al. (2003) found that it was necessary to incorporate a shear step before the clarification mimic to account for the action of shear forces present in the feed entry zone of a given industrial centrifuge. The theory and method of mimicking entry shear has been thoroughly described in the literature (Boychyn et al., 2000; 2001; 2004).

6.3.1.4 Other factors

One other parameter that impacts the levels of dewatering achieved is temperature (Munro and Van Til, 1988), which should be kept constant between scales.

6.3.2 Definition and assessment of dewatering

In the current work the level of dewatering was calculated as a percentage (%D) from the ratio of the weight of recovered solids to the original wet sediment using Equation (6-2).

$$\%D = 100 - \left[\frac{WW_{sed} - DW_{sed} / dw_r}{WW_{sed}} * 100 \right] \qquad [6\text{-}2]$$

Where WW_{sed} is the weight of the paste recovered from the centrifuge and DW_{sed} is the weight of this paste oven dried to constant weight (i.e. fully dewatered and dried). dw_r is the cell dry weight to wet weight ratio of a particular cell type. This ratio reflects the amount of intracellular liquid in the cells. This liquid will be removed by drying but not by the centrifugal process. Hence dw_r must be taken into account when considering the ratio of interstitial to intracellular water evaporated during oven drying. dw_r has been found to be 0.30 for *E. coli* (Watson, 1965) and 0.35 for *Saccharomyces cerevisae* (Zierold, 1988).

6.3.3 The effect of shape on maximal levels of dewatering

The maximal levels of dewatering that may be realised can be predicted from theoretical maximum packing densities, which are unique functions of the cell shape. In applying such a theoretical approach it is assumed that the compressive forces prevailing during centrifugation are insufficient to cause deformation of the cells, and hence cell shape is

a constant. It is also assumed, for all practical purposes, that the cells are of a uniform size and shape although in reality a heterogeneous population will exist.

For any particular shape there exists a maximal ordered packing density, and a maximal non-ordered packing density. Ordered packing patterns are also known as lattices. They consist of one packing pattern repeating many times. This is the type of packing that would occur in a crystalline structure. By contrast non-ordered packing occurs when there is no pattern of packing and results in 'random close packing' or, more accurately, 'maximally random jammed' (Molecular Physics Correspondent, 1972). Centrifugal separation will at first result in a 'maximally random jammed' state as the particles sediment from solution. After initial disordered packing, the sedimentation of more particles will cause compaction pressure and therefore the formation of higher density ordered conformations. Theoretically, if more pressure was exerted on the paste, by for example a mechanical press, the particles would deform and then rupture. As the solids pass through these stages of sedimentation, compaction, and compression, more water is excluded and the formed paste will become increasingly dewatered. The implication is that there may be a dewatering level associated with the sedimentation stage before increases in sediment height or spin speed generate sufficient force for compaction to occur, leading to structural re-arrangements and to a further increase in dewatering.

Knowledge of cell shape and the theoretical maximum packing densities provides an estimate as to the upper bound of dewatering that can be achieved by application of centrifugal force alone.

6.4 Results: method development

6.4.1 Preparation of feed material

For all Baker's Yeast studies, packed cells were suspended to 50% (packed wet weight/volume). This stock concentrate was then diluted in PBS pH 7.0 to the appropriate concentrations for study.

For method development studies on *E. coli*, frozen cell paste, stored at -80°C, from a 75 L IPTG fermentation (section 2.2.3.2) with a post-induction glycerol flow rate of 1.65 mL h^{-1} L^{-1} was suspended in PBS pH 7.0 to make a 50% (packed wet weight/volume) suspension of pre-extraction cells. *E. coli* post-extraction samples were created by suspending frozen cells from this fermentation to form a 50% (packed wet

weight/volume) suspension in 100mM Tris, 10mM EDTA at pH 7.4. 200 mL of this suspension was heated at 60°C for 16 h in a 2L shake flask (agitation rate 200 rpm). It was subsequently cooled to 20°C and then diluted to the appropriate concentration for study.

6.4.2 Determination of dry mass content of cells

The dry cell weight to wet weight ratios for Baker's Yeast and *E. coli* were obtained from literature (Watson, 1965; Zierold, 1988): 0.35 and 0.30 respectively. The 0.30 value for intact *E. coli* could not be used for post-extraction *E. coli* as their water content will have been significantly altered by the thermal and chemical treatment they have undergone. Instead water content was quantified experimentally. A variety of methods exist for this (Terryn et al., 2000). In this study the post-extraction cell suspension was filtered to remove the majority of the interstitial water. The resulting filter cake was dried at 100°C until constant mass was achieved and the ratio of dry weight to wet weight was calculated. The dry weight to wet weight ratio for post-extraction *E. coli* by this method was 0.28.

6.4.3 Baker's Yeast studies

The literature suggests that, for a given feed, the key variables determining centrifugal dewatering are spin time, RCF, and sediment height. The effect of these variables upon dewatering was first evaluated using Baker's Yeast. The effect of spin time is shown in Fig. 6-2. A relatively low RCF of 3000 g was selected so as to exaggerate the effect of time.

The results show that dewatering occurs at a similar rate to clarification under these conditions. As the minimum recommended time between discharges for a disc-stack machine is typically 120 seconds and the Carr Powerfuge takes ~ 300 seconds to slow down to allow discharge, these data suggest that in industrial-scale operations Baker's Yeast cell suspensions reach their steady-state dewatering level with regard to time before discharge.

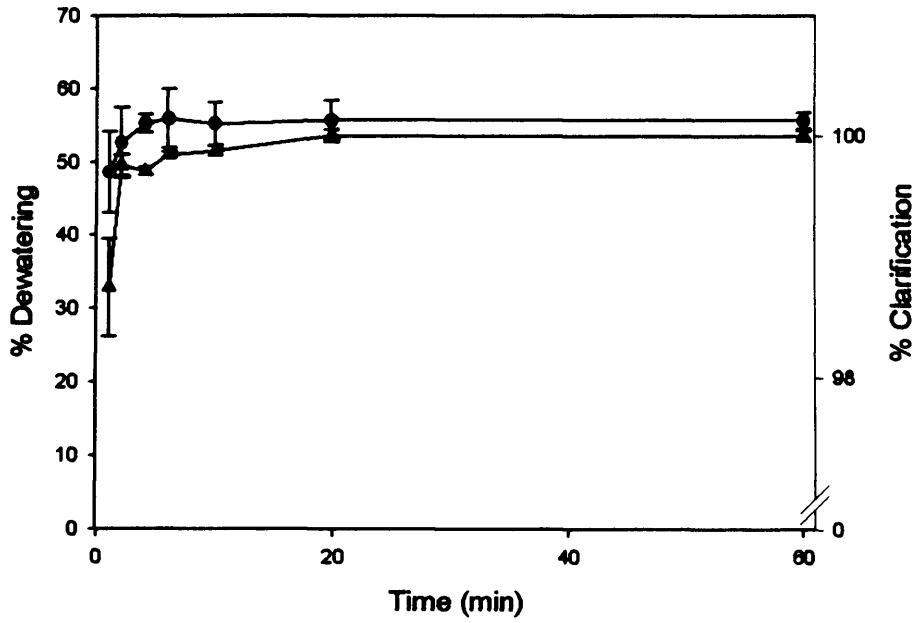

Fig. 6-2: The effect of spin time upon % dewatering (▲) and % clarification (●) for Baker's Yeast. 2.2 mL microfuge tubes containing 2 mL of a 10% solution (packed wet weight/volume) Baker's Yeast were spun at an RCF_{max} (i.e. the RCF experienced in the bottom of the tube) of 3000 g in an Eppendorf 5810R centrifuge.

Fig. 6-3 illustrates the effect that spin speed has upon the dewatering of Baker's Yeast. RCFs of 2000–16,000 g were used: approximately the range of RCFs available in industrial centrifuges. In line with earlier results samples were spun for 30 min to ensure that a steady-state level of dewatering with regard to time was achieved. A 50% (packed wet weight/volume) Baker's Yeast suspension was used to give a significant sediment height. Above an RCF of 2000 g the final level of dewatering for Baker's Yeast was constant at ~ 66%. This result indicates that any mimic of the dewatering achieved during the separation of Baker's Yeast by centrifugation need only use an RCF_{max} of 2000 g and a spin time of less than 30 min to be effective.

To mimic the compressive stress profile formed within the sediment the effect of varying sediment height upon the total level of dewatering was explored using both 5 mL flat- and 50 mL conical- bottomed tubes. Sediment heights up to 60 mm were obtained by using different concentrations and amounts of Baker's Yeast solution carefully chosen so as to ensure the volume of liquid above the sediment at a steady-state level of dewatering was constant throughout. Dewatering of the Baker's yeast suspension increased with sediment height (Fig. 6-4). It is therefore vital to ensure that sediment height is a constant in any mimic. Furthermore, % dewatering is well

correlated with sediment height and is not related to the geometry of the tube used to generate such data.

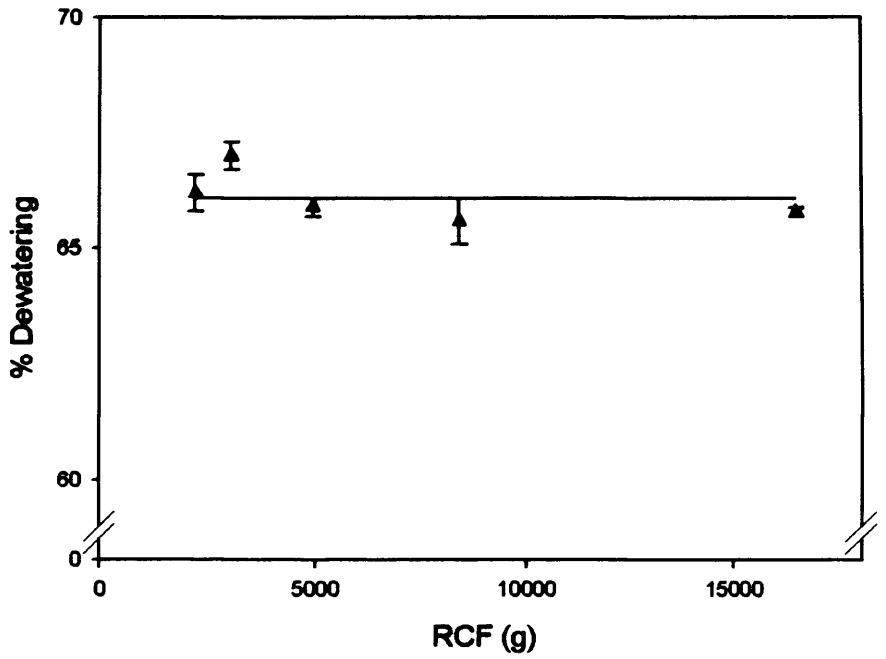

Fig. 6-3: The effect of RCF upon % dewatering (▲) for Baker's Yeast. 2.2 mL microfuge tubes containing 2 mL of a 50% solution (packed wet weight/volume) of Baker's Yeast were spun for 30 min at 2000-16000 g in an Eppendorf 5810R centrifuge.

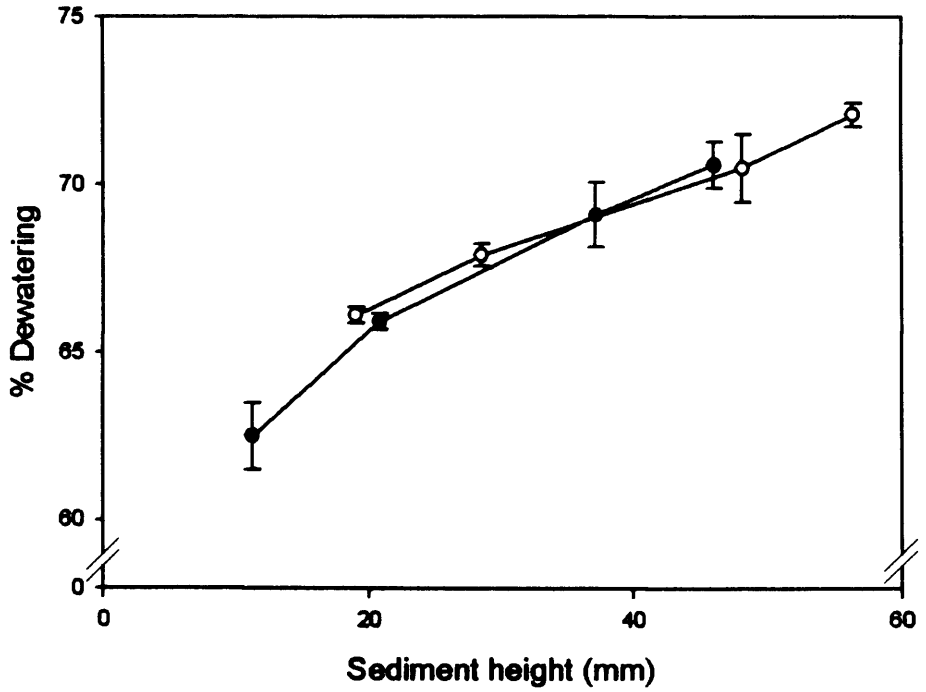

Fig. 6-4: The effect of sediment height upon % dewatering for Baker's Yeast. 50 mL conical-bottomed tubes (○) and 5 mL round-bottomed tubes (●) were filled with varied concentrations and amounts of cell suspension to vary sediment height while keeping solution height constant. Tubes were spun for 30 min at 3100 g in an Eppendorf 5810R centrifuge.

It is likely that changes in sediment height alter the level of dewatering by alteration in the compressive force profile in the sediment. However, increases in sediment height do increase the overall dewatering of the paste, even when increases in spin speed do not. This can be explained by an additive effect caused by re-expansion of the paste after centrifuge slowdown. The dewatered paste will comprise of bulk dewatered material and a layer immediately adjacent to the supernatant, that will expand upon centrifuge slowdown, take up liquid, and hence be poorly dewatered. The depth of the wetted layer will be approximately constant irrespective of the sedimentation conditions used. However, the relative depth of this top layer as a proportion of the total sediment will decrease as total sediment height increases. Hence the overall % dewatering of deep sediments will appear to rise as the net contribution of the wetter layer falls.

The height of liquid above the sediment was not found to be statistically significant in determining % dewatering for Baker's Yeast.

6.4.4 *E. coli* pre- and post-extraction studies

The key centrifugation variables controlling the level of dewatering for *E. coli* before and after the periplasmic extraction procedure were examined. It is likely that the process of heat/chemical extraction will significantly alter the size distribution and shape of the sedimented species, which will change the dewatering properties. Therefore the size distribution of *E. coli* cells pre- and post-extraction was examined using a laser diffraction particle size analyser.

Fig. 6-5 illustrates the differences in particle size distribution (PSD). Whilst the majority of cells in both samples remain as single cells in suspension, in both cases cell aggregation was seen. The post-extraction sample contains a much higher proportion of small particles. These are likely to be membrane-blebbed vesicles and lysed cell matter, the presence of which will affect the clarification and dewatering characteristics of the feed. It should be noted that as both pre- and post-extraction cells used in these method development studies are derived from frozen cell paste their size distributions will differ from that obtained with non-frozen cells in section 5.4.1.

Baker's Yeast cell suspensions reached a steady state level of dewatering with respect to time in less than 4 min at 3000 g. In the case of *E. coli,* 2 mL of a 20% (packed wet

weight/volume) suspension of *E. coli* pre- and post-extraction was spun at 1341 g (lower end of the range in common usage) for a variety of times and the dewatering and clarification was calculated. Fig. 6-6 shows that both pre- and post-extraction *E. coli* cells require much longer spin times to reach their dewatering asymptote than Baker's Yeast cells. There is a delay of several minutes between the attainment of complete clarification and maximal dewatering. This can be related to the respective shapes and sizes of the cells. Spherical Baker's Yeast cells are both larger and of a different shape to spherocylindrical *E. coli* cells. The difference in shape might be expected to influence the speed of compaction as the particles rearrange themselves.

Fig. 6-6 also indicates that while pre-extraction *E. coli* cell paste dewaters more rapidly than post-extraction *E. coli* paste, the latter achieves a higher steady-state level of dewatering. This fits in well with the size distribution data. The large numbers of small particles in the post-extraction material will cause slower clarification and initial compaction, but given enough time these small particles will be able to occupy the voids formed between the larger whole cells, resulting in a more highly dewatered paste.

The impact of spin speed on the level of dewatering achieved is examined in Fig. 6-7. This shows that alterations in RCF in the range commonly used in industrial centrifugation have a significant effect upon subsequent dewatering of the cell paste, even at a long spin time. Hence spin speed and time must both be incorporated into any USD mimic. Again, the steady-state levels of dewatering are higher for post-extracted cells than pre-extracted, for the same reasons as for the spin-time experiments.

With Baker's Yeast sediment height was found to be the only relevant variable factor that altered the level of dewatering. For *E. coli* cell sediments, tubes were filled with varying amounts and concentrations of cell suspension, so as to vary sediment height while keeping the height of liquid above the steady-state sediment constant. Fig. 6-8 shows that sediment height appears to have much less of an effect upon dewatering. Indeed, increasing sediment height appears to reduce dewatering slightly. It is suggested this could be due to *E. coli* cells having less propensity to re-expand after centrifuge slowdown, therefore reducing the additive effect caused by the top-layer of the sediment being poorly dewatered. Hence while sediment height must be considered in a generic dewatering mimic, it may not be a major contributing factor to dewatering levels observed in the *E. coli* cell sediments studied here.

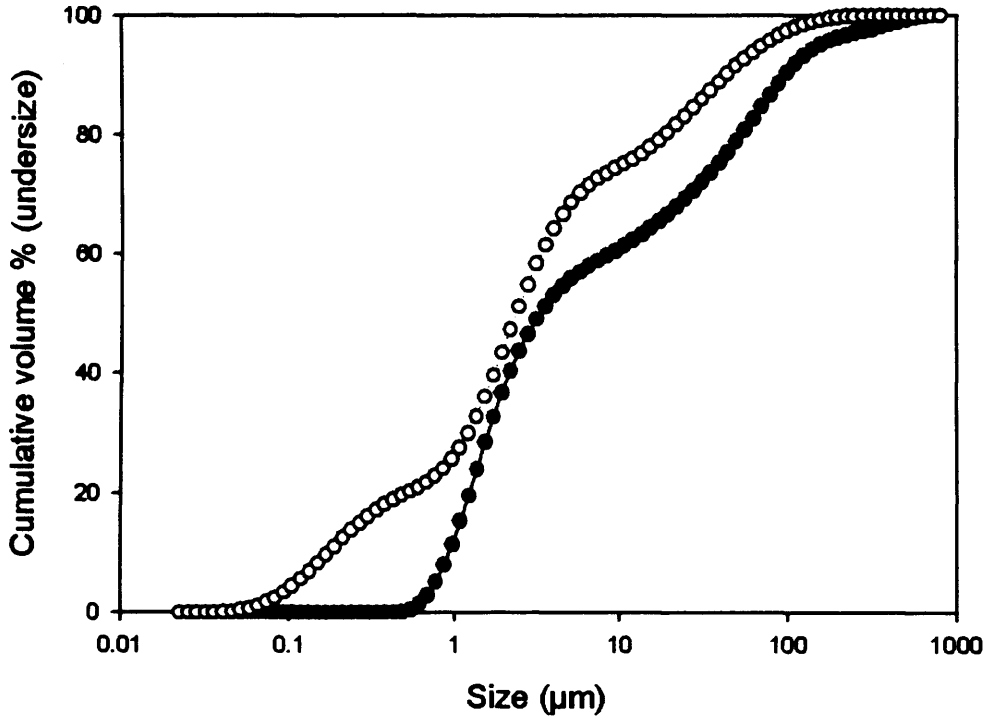

Fig. 6-5: The cumulative size distribution on volume basis of *E. coli* (•) and post-extraction *E. coli* (○), obtained by laser diffraction.

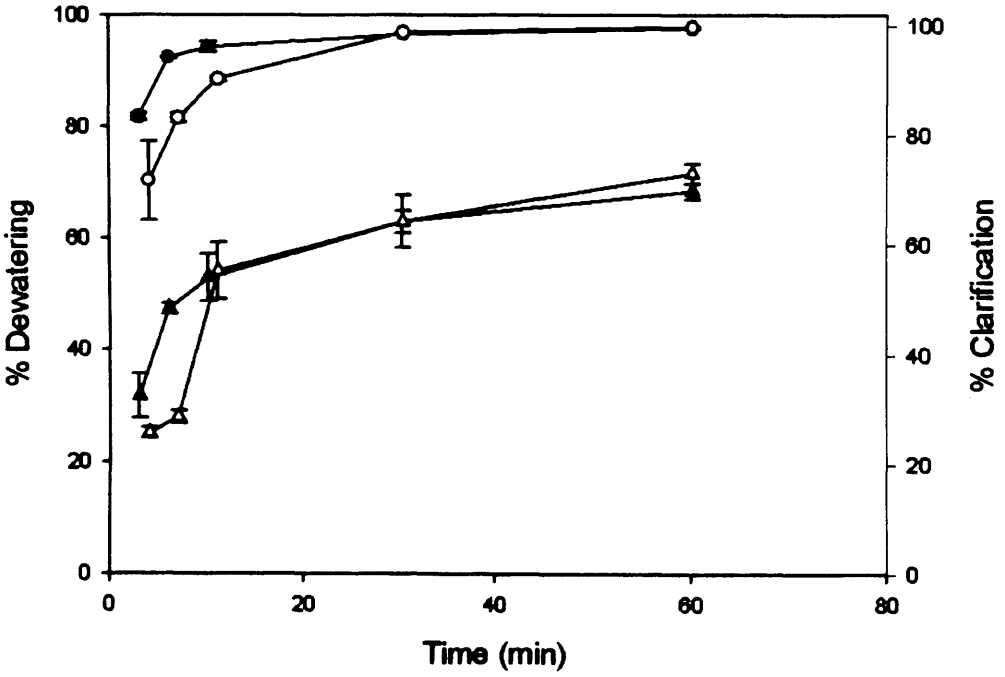

Fig. 6-6: The effect of spin time upon % dewatering (▲) and % clarification (•) for *E. coli* cells (solid symbols) and the same cells post-extraction (hollow symbols). 2.2 mL microfuge tubes containing 2 mL of a 20% solution (packed wet weight/volume) of the cells was spun at an RCF_{max} (i.e. the RCF experienced in the bottom of the tube) of 1340 g in an Eppendorf 5810R centrifuge.

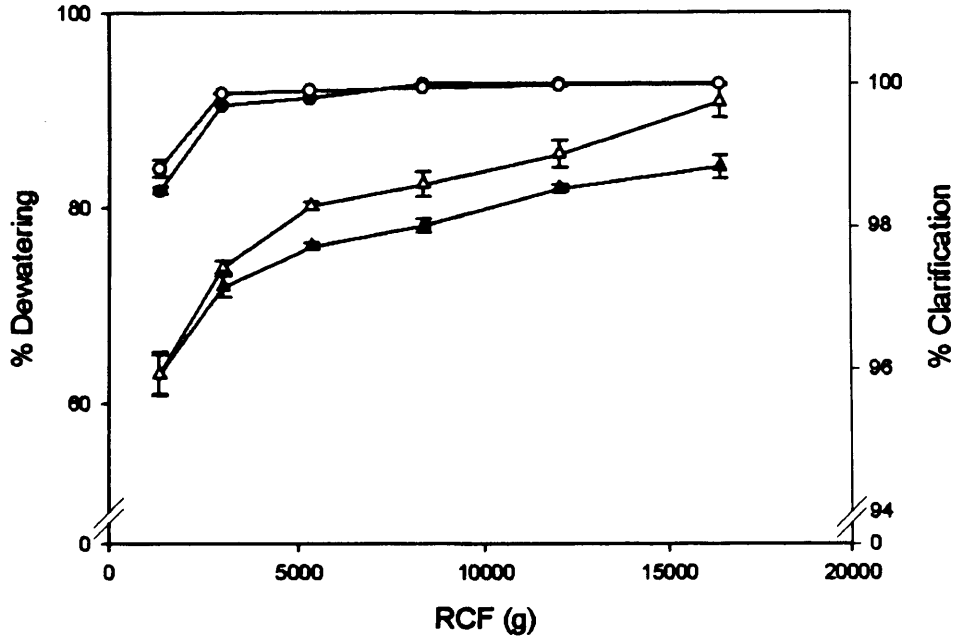

Fig. 6-7: The effect of RCF upon % dewatering (▲) and % clarification (●) for pre- (solids symbols) and post-extraction (hollow symbols) *E. coli* cells. 2.2 mL microfuge tubes containing 2 mL of a 20% solution (packed wet weight/volume) of the cells were spun for 30 min at a variety of RCFs, using an Eppendorf 5810R centrifuge.

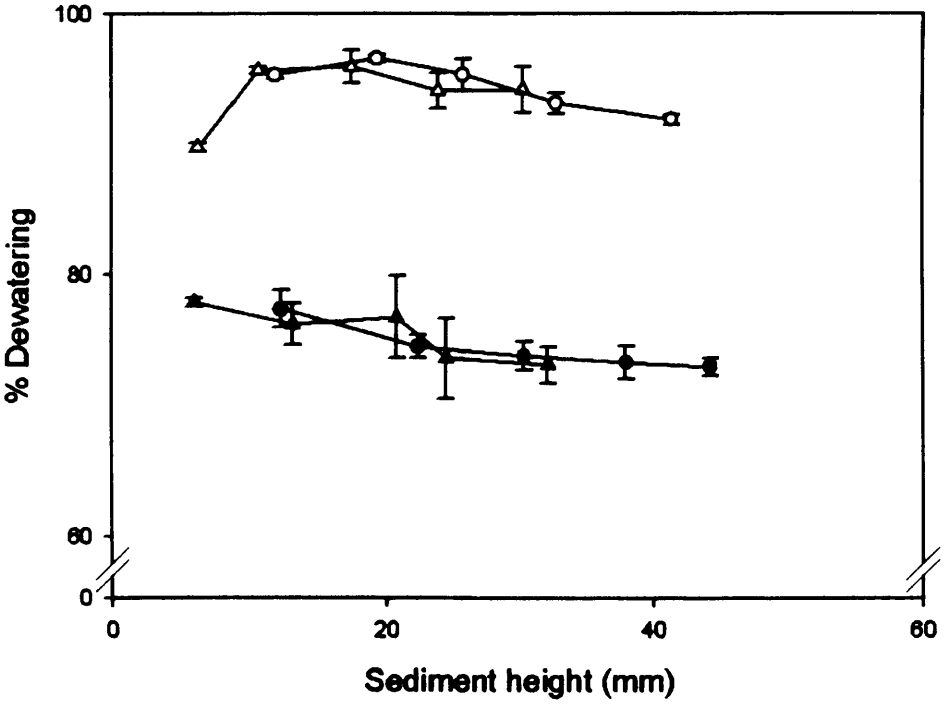

Fig. 6-8: The effect of sediment height upon % dewatering for pre- (solid symbols) and post-extraction (hollow) *E. coli* cells. 5 mL round-bottomed tubes (▲) and 50 mL conical-bottomed tubes (●) were filled with varied concentrations and amounts of cell suspension to vary sediment height while keeping solution height constant. Tubes were spun for 90 min at 3100 g in an Eppendorf 5810R centrifuge.

The height of the liquid above the steady-state sediment was found not to alter dewatering levels with either pre- or post-extraction *E. coli*. This is in agreement with work on casein curd carried out by Munro & Van Til (1988), and earlier results using Baker's Yeast. Therefore this factor need not be incorporated in a generic USD mimic.

6.5 Generic USD method

From consideration of the factors found to be crucial in determining the extent of dewatering during centrifugation, the following method is proposed to mimic dewatering levels of biological feeds in industrial or pilot-scale centrifuges. This generic method is summarised for clarity in Fig. 6-9. The first step in mimicking the dewatering performance of a particular centrifuge and feed is to determine the values of the parameters of the industrial centrifuge to be mimicked. These parameters are: spin speed, sediment height, spin time and the temperature of the feed during compaction. Spin speed will be equal to the RCF_{max} of the centrifuge at the speed used. Sediment height will be equal to the length of a cross section of the solids collection area/width, as shown in Fig. 6-1. Spin time will be equal to the average amount of time a particle spends sedimented in the bowl being compacted, as defined in Equation 6-3. Finally, the temperature can be estimated depending on the particular centrifuge's cooling system.

Once the industrial parameters have been defined, the USD method can be tailored to mimic the particular centrifuge. There is a certain order in which these parameters must be set. Firstly the sediment height is approximated to that found at industrial-scale by spinning five different amounts of solids in suspension to steady state clarification and measuring the resulting sediment height (Fig. 6-1). By plotting sediment height against amount of solids, the mass of solids that gives the same sediment height in the spin tubes as in the industrial centrifuge can be determined. A volume of supernatant in which to suspend this mass so as to give a solids concentration as close as possible to that of the feed is then selected. Secondly, the spin speed should be chosen so that the RCF_{max} is the same as in the industrial machine. This will subject the sediment to approximately the same force profile as at industrial-scale. Thirdly, the approximate time an average particle spends at bottom of the tube being compacted, $t_{compUSD}$, should be set equal to t_{comp} at large scale. $t_{compUSD}$ can be estimated using Equation (6-3):

$$t_{compUSD.} = \frac{t_{95\%}}{2} + (t_{total} - t_{95\%}) \qquad [6\text{-}3]$$

Where t_{total} is the total laboratory centrifuge set time and $t_{95\%}$ the time for 95% clarification to be obtained in the centrifuge (i.e. most particles sedimented).

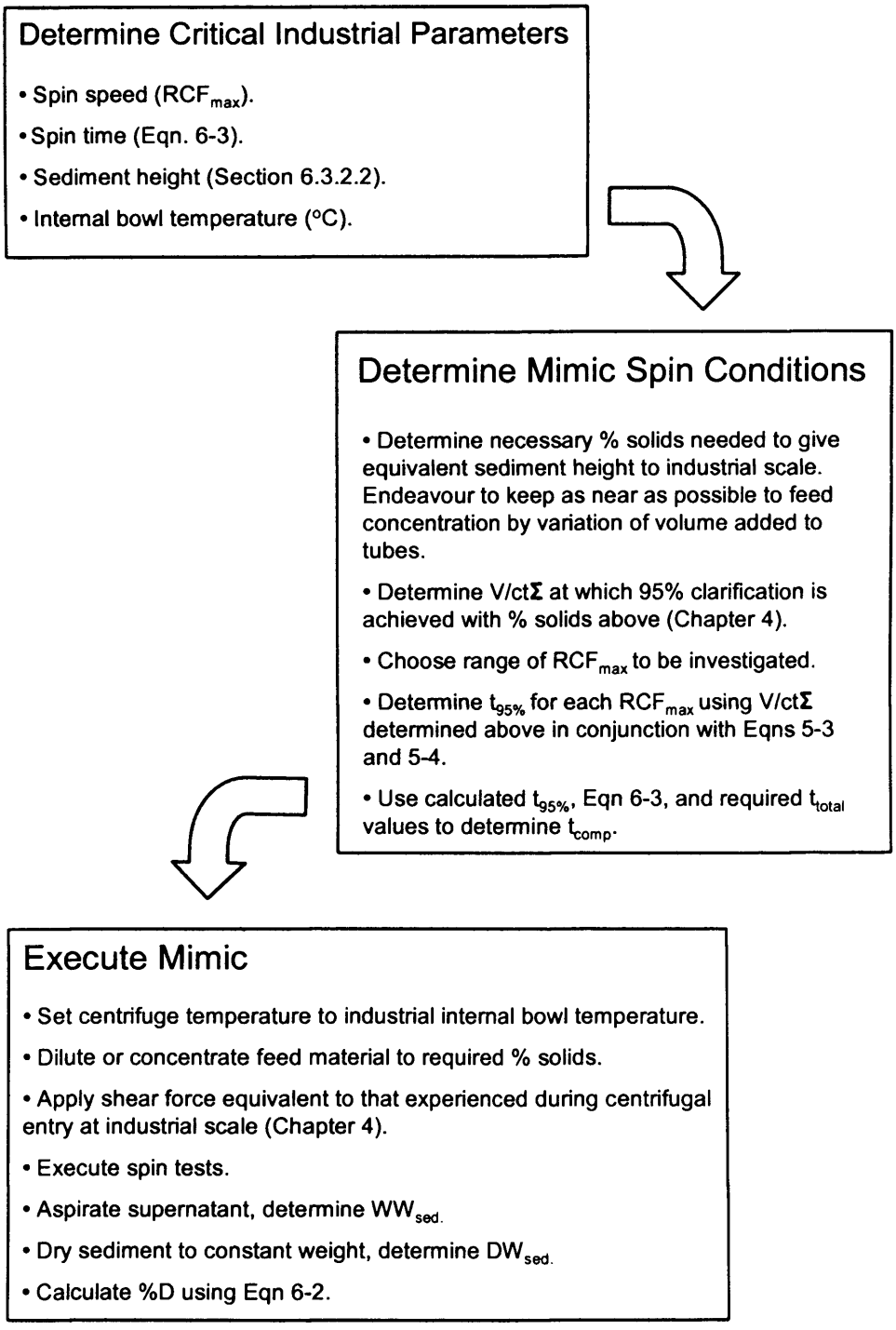

Fig. 6-9: Proposed generic USD methodology for predicting industrial-scale dewatering.

The value of $t_{95\%}$ can be determined using Sigma theory. The feed material is spun in the laboratory centrifuge at the concentration determined above at a variety of V/(ctΣ) to give a range of clarification performances. This is then plotted on a probability log axis to provide a linear data set and from this V/(CtΣ) for 95% clarification determined. Hence $t_{95\%}$ can be calculated for each spin speed to be used. Finally, the temperature found at industrial-scale should be maintained.

A key requirement is for a cooled laboratory centrifuge capable of achieving the RCF generated in the industrial centrifuge and able to accommodate spin tubes of sufficient length to produce an equivalent sediment height to that found in the industrial machine.

Previous studies have shown how shear within centrifuges can damage delicate biological materials and therefore alter the sedimentation properties (Boychyn et al., 2000). If the centrifuge being mimicked develops shear levels sufficient to alter the properties of the feed material, then the material must also be subjected to that shear prior to conducting the dewatering test.

6.6 Results: method verification

6.6.1 Preparation of feed material

Pilot-scale feed material for verification studies was prepared as follows. Baker's Yeast cells were resuspended from packed form to 10% packed wet weight/volume. Pre-extraction *E. coli* cells were used directly from a 75 L IPTG fermentation with a post-induction glycerol flow rate of 1.65 mL h^{-1} L^{-1}. Pre-extraction cell paste obtained from these pilot-scale experiments was used to create the post-extraction cells by pilot-scale periplasmic extraction in a 75 L LH high category vessel fermenter

For USD experiments, where cell concentration needed to be increased to alter sediment height, Baker's Yeast and *E. coli* cell paste was taken from the Carr Powerfuge P6 after pilot-scale experiments and resuspended in supernatant to 40% (packed wet weight/volume) to provide a stock suspension for these investigations: this by-passed the need to mimic centrifuge entry shear. In Chapter 8, as material is limited, the shear cell device described in Hutchinson et al. (2006) is used to mimic the effects of entry shear on the feed material.

6.6.2 Performance of USD mimic for the Baker's Yeast cells

The Baker's Yeast suspension was separated in the Carr P6 at a variety of RCFs and the level of dewatering obtained assessed. USD prediction was carried out using 42.5 mL of a 35% (w/v) Baker's Yeast suspension in an Eppendorf 5810R centrifuge, rotor T-60-11 (N = 2000-14000 rpm) with 50 mL conical bottomed tubes to give an equal sediment height at USD to that found in the Carr P6. The level of dewatering attained at pilot-scale was successfully mimicked by the USD data at a variety of spin speeds (Fig. 6-10). The mimic accurately predicted the dewatering performance of the Carr P6 to within ± 0.5%. As predicted from the method development studies, spin speed increases had no effect upon the level of dewatering obtained for the RCF range used in this study.

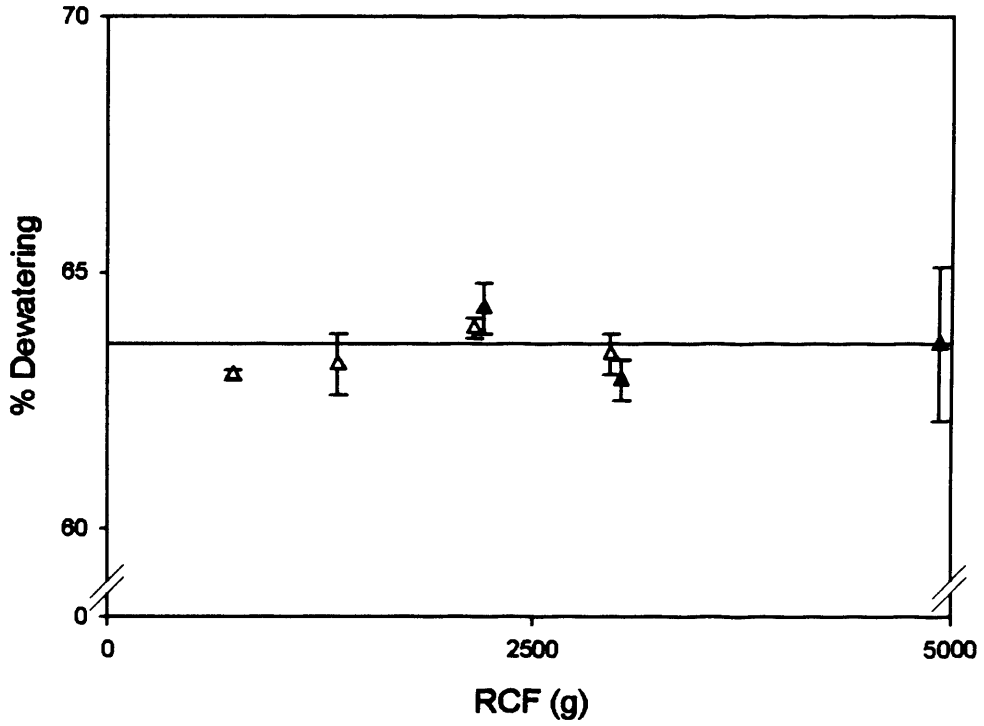

Fig. 6-10: Successful prediction of the dewatering performance of the Carr Powerfuge P6 with Baker's Yeast at a variety of RCFs. Spin time was constant at 30 min in both pilot-scale (▲) and USD (Δ) experiments.

6.6.3 Performance of USD mimic for pre-extraction *E. coli* cells

Prediction of the dewatering of *E. coli* suspensions in industrial machines was expected to be more complicated as dewatering has been shown to be sensitive to changes in both spin time and speed, across the range of conditions studied.

Pilot-scale results were obtained using four runs of the Carr Powerfuge P6. All conditions were run to breakthrough and dewatering of the resulting cell paste assessed.

Spin time for each run was calculated using Equation 6-1 (t_{delay} = 2 min, V_s = 1000 g, F~1, ϕ = 0.2). The temperature inside the bowl was estimated at 10°C. An Avanti JE Centrifuge System JS-13.1 swing-bucket rotor (N = 300-13000 rpm, RCF_{max} = 26750 g) with 15 mL tube adaptors was used for the USD experiments.

The amount of pre-extraction *E. coli* cells necessary to give a sediment height of 25.4 mm was determined to be 2.0 g by spinning five 5 mL round-bottomed tubes to steady-state clarification with varying concentrations and volumes of cell suspension in the Avanti JE Centrifuge System with the JS-13.1 swing bucket rotor, at 19200 g for 30 min. Accordingly 5 mL of a 40% (packed wet weight/volume) cell suspension was used in all subsequent *E. coli* USD experiments. The cell suspension was also used to yield $V/ct\Sigma$ so that $t_{95\%}$ and therefore $t_{compUSD}$ could be calculated (Equation 6-3). The runs completed are summarised in Table 6-1.

Fig. 6-11 shows that the level of dewatering was successfully mimicked at a variety of RCFs and spin times to within ± 5% (approximately ± 1 σ of pilot plant replicates). However, the USD mimic consistently slightly underpredicts the level of pilot-scale dewatering. This could be due to the much longer deceleration time of the Carr Powerfuge (~ 3 min) to the lab centrifuge (30 s), and drain-off of some of the less dewatered top sediment through the residual valve in the Carr P6, which drains the centre of the bowl of any unclarified supernatant before solids ejection. Also, the greater error for the *E. coli* system relative to the packed Baker's Yeast studies is probably because the bacterial feed material does not reach a steady state level of dewatering under the industrial conditions studied. Therefore small inaccuracies in the approximations of sediment height, spin time and RCF have an exaggerated affect upon the dewatering levels predicted by the small-scale experiments.

Table 6-1: Successful prediction of the dewatering performance of the Carr Powerfuge P6 with pre- and post-extraction *E. coli* at a variety of RCFs. Pilot-scale error is standard deviation of five separate measurements of a single batch, USD error is standard deviation of three repeat batches.

Centrifuge conditions		**% D**	
RCF_{max} (g)	**t_{comp} or $t_{compUSD}$ (min)**	**Pre-Extraction *E. coli***	
		Pilot-scale (± 4.5 %)	**USD (± 0.5 %)**
14400	17	80.1	76.4
19200	17	82.8	78.9
19200	8	76.7	74.2
19200	5	76.3	71.7
RCF_{max} (g)	t_{comp} or $t_{compUSD}$ (min)	Post-Extraction *E. coli*	
		Pilot-scale (± 3.3 %)	USD (± 0.4 %)
14400	26	74.6	75.2
19200	26	85.8	79.0
19200	11	75.8	71.1

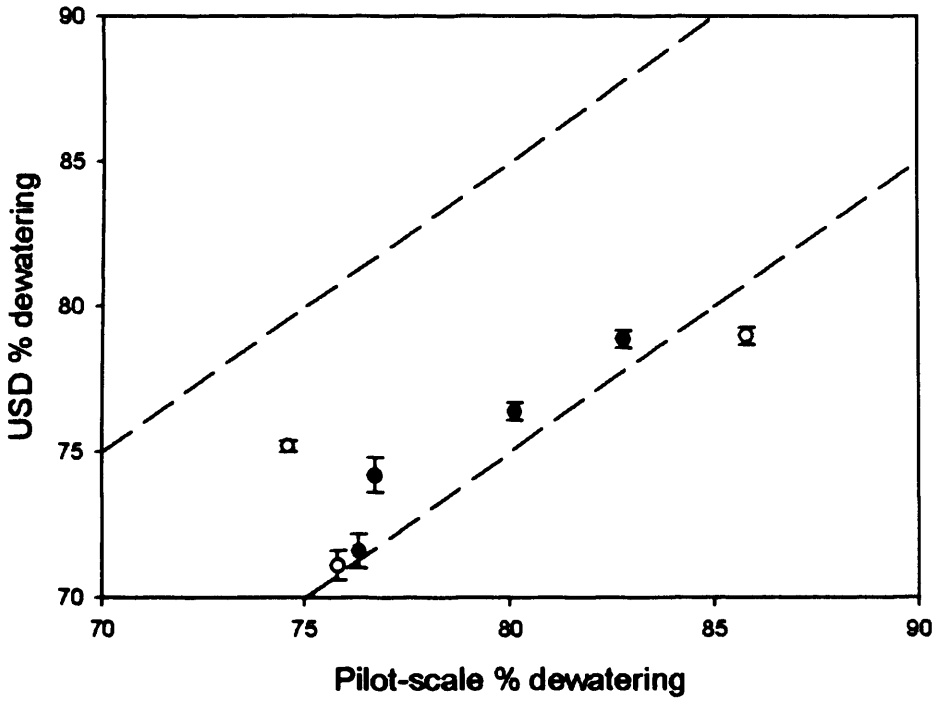

Fig. 6-11: Parity plot comparing USD dewatering performance with that of the Carr Powerfuge™ P6 with pre- (●) and post-extraction (○) *E. coli* at a variety of RCFs, as detailed in Table I. Dotted line 'gates' indicate ± 5 % pilot-scale dewatering (approximately ± 1σ of replicate pilot-scale experiments).

6.6.4 Performance of USD mimic for post-extraction *E. coli* cells

The USD dewatering method was also applied to post-extraction *E. coli* cells, except that a 50 L/h flow rate into the Carr Powerfuge P6 was not tested as this gave poor clarification with this feed. Table 6-1 summarises the experimental runs completed, while Fig. 6-11 illustrates that the method accurately mimicked pilot-scale data, although with a slightly greater error of up to ± 8% than for pre-extraction *E. coli* cells. This is probably because the post-extraction material is further from its steady-state level of dewatering than the pre-extraction material, therefore the errors. as discussed for pre-extraction cells, are magnified.

6.7 Discussion

6.7.1 Wider application of the proposed USD method

The mimic described in this thesis has been verified for an advanced tubular-bowl type centrifuge capable of giving high levels of dewatering of biological solids. Fig. 6-1 gives an example of the determination of sediment height of an industrial disc-stack centrifuge. However, application of the mimic to disc-stack machines is likely to require further studies. In such a case there are two additional sources of error. Firstly, it is practically difficult to operate a pilot-scale disc-stack so as to eject only the solids cake and none of the supernatant inside the bowl. This error may cause an overprediction of dewatering by the mimic. Secondly, disc-stack machines eject solids at speed; therefore there is no possibility of cake re-expansion accompanying centrifuge slowdown prior to solids ejection, unlike in tubular bowl and bench-top centrifuges. This error may cause an underprediction of dewatering by the mimic. The predictive accuracy of the mimic towards disc-stack centrifuges will depend on the relative contribution of these two competing factors.

6.7.2 Relating the experimental levels of dewatering obtained to theoretical maximum packing densities

For the purposes of estimating packing densities Baker's Yeast cells can be modelled as spheres. Random close packing of spheres has been shown by a variety of experiments and algorithms to give a packing density of 64% (Jaeger and Nagel, 1992). This approximates the maximal % dewatering found in the experiments in this paper (Fig. 6-10) using a relatively small sediment height. However, as sediment height increases, dewatering increased to 72% (Fig. 6-4) and extrapolation of the curve suggests a maximal level of dewatering of ~73%. This corresponds well with the density of a

close-packed lattice. Hence it seems Baker's Yeast pack in a dense lattice structure prior to re-expansion of a portion of the paste upon centrifuge slowdown. Cubic close-packing and hexagonal close-packing both have packing densities of 74% (Steinhaus, 1987; Wells, 1986; Wells, 1991). The theoretical maximum packing density of spheres has been shown to be slightly higher at 78% (Hales, 1992), although this has never been achieved physically. The experimental values of dewatering correlate closely to those predicted from theory considering the sources of error: the Baker's Yeast suspensions will contain some ellipsoid cells, budding cells, and cells of different sizes. Furthermore it has been assumed that Baker's Yeast cells will not deform from their spherical shape under the compressive forces applied during compaction, and that the level of interstitial water content will be constant from batch to batch.

E. coli cells can be modelled as spherocylinders with an average aspect ratio of ~ 2. Spherocylinders exhibit a very different packing behaviour to that of spheres. The maximally random jammed state has been modelled for spherocylinders using Monte Carlo techniques (Abreu et al., 2003) and mechanical contraction simulations (Williams and Philipse, 2003). The density of this state is highly variable with aspect ratio. For an aspect ratio of 1 the density is approximately 66%, decreasing as aspect ratio increases, e.g. 62 % for an aspect ratio of 2.

By contrast, as aspect ratio increases the maximal lattice packing density will approach 91% (Donev et al., 2004). For spherocylinders with an aspect ratio of 2, such as *E. coli,* the maximal lattice packing will be 82%. Here spherocylinders are stacked lengthways in a hexagonal pattern, and is therefore the combination of the maximal packing densities of circles (91%) and spheres (74%) as shown below:

$$\frac{91}{2}+\frac{74}{2}=82\%$$

With *E. coli* cells % dewatering increases gradually until the dewatering maxima, which is in good agreement with the theoretical maximum lattice packing density. Pre-extraction *E. coli* cells achieved highest packing density at very high RCFs of ~ 84%, in good agreement with the theoretical value of 82%. This is despite the influence of batch variations in cell water content, possible deformation of the cells under the compressive stress applied during the compaction, and cells being of different sizes at different

stages in their growth cycle, which will also alter their aspect ratio. Post-extraction *E. coli* cells achieved a somewhat higher experimental maximal level of dewatering (~ 95%) than both pre-extraction *E. coli* cells and the theoretical maximum. However, given the limitations above, the values achieved are still in good agreement with theory. Furthermore, Fig. 6-5 shows that a large volume fraction of the solids content consists of particles an approximate order of magnitude smaller than a typical *E. coli* cell. These lysed cells/vesicles are likely able to fill the voids between the lattice structure of the cells, increasing the dewatering further. This filled lattice structure model is supported by the fact that the maximum theoretical lattice packing for spheroids with an aspect ratio of two, with lattice packed spheres in the free space, is 95%. This is the same level of dewatering as found experimentally with post-extraction *E. coli*. Another possible contributing factor to the higher dewatering found in post-extraction *E. coli* cells is that the extraction process weakens the cells, allowing for a greater level of compression and shape distortion and therefore an increased level of dewatering.

Table 6-2 summarises these results by comparison of the theoretical maximal lattice and maximal random jammed packing densities for shapes of the cells used in this study with the maximal % dewatering obtained in our experiments.

6.8 Conclusions

The results presented here indicate that a number of factors influence centrifugal dewatering in tubular bowl type centrifuges including spin speed, spin time, and sediment height. A USD mimic has been designed to use this knowledge to predict pilot or industrial-scale dewatering using only millilitres of material. The mimic has been found to accurately mimic dewatering to at least within ± 8% of pilot-scale data with all feeds used. The nearer the feed is to reaching its centrifugal dewatering maxima, the more accurate the mimic. The observed maximum levels of dewatering obtained with the biological feeds match the theoretical maximum lattice packing density of the shape of the cells used.

The utility of this USD centrifugal dewatering methodology for process development and understanding is exemplified in Chapter 8 by its application, along with other USD unit operation mimics, to the initial DSP for the production of antibody fragments in high cell-density *E. coli* culture.

Table 6-2: Comparison of the maximal lattice and maximal random jammed (MRJ) packing densities for shapes of the cells used in this study with the maximal % dewatering obtained experimentally.

Shape	**Cell Type**	**Theoretical maximum Packing Density (%)**		**Maximum Dewatering obtained experimentally (%)**
		MRJ	**Lattice**	
Sphere	Baker's Yeast	64	74 (highest known)	~ 72
Spheroid (aspect ratio 2)	Larger *E. coli*	~ 62	82	~ 84 pre-extraction
Spheroid (aspect ratio 1)	Smaller *E. coli*	~ 66	80	~ 95 post-extraction
Mixture of Spheroid (aspect ratio 2) and spheres	Post-Extraction *E. coli*	86	95	~ 95 post-extraction

7. Periplasmic extraction characterisation and scale-down

7.1 Abstract

This chapter describes and verifies an ultra scale-down (USD) methodology for predicting the performance of the periplasmic extraction unit operation in the process for antibody fragment production in *E. coli*. This unit operation releases Fab' into solution by selective heat and chemical permeabilisation of the outer membrane of the *E. coli* cells. The USD methodology is performed using standard laboratory equipment and requires only one millilitre of feed material. The performance of the USD mimic is compared to pilot-scale extraction in a jacket-heated vessel using three feeds with different cellular integrities, provided by adjustment of the fermentation post-induction glycerol feed rate. In all tested cases the mimic is shown to predict yield and contaminant carry-over (assessed by total protein) to at least ± 6% of pilot-scale results. The methodology is then used to identify cell integrity and extraction temperature as key parameters in the periplasmic extraction procedure, using a 2-factor statistical design of experiments sensitivity analysis.

7.2 Introduction

In the antibody fragment production process studied, the Fab' protein produced is targeted to the periplasm of the *E. coli* cells. The periplasm is the 12-15 nm space found between the inner (cytoplasmic) and outer (periplasmic) membrane of gram-negative bacteria. The outer membrane is characterised by several well-studied structural proteins, a limited number of minor proteins, and the presence of lipopolysaccharide (LPS) (Osborn and Wu, 1980). While the inner leaflet of the outer membrane is mainly composed of the common cell membrane constituent phosphatidylethanolamine (PE), LPS is unique to the outer leaflet of the bacterial outer membrane (Muhlradt and Golecki, 1975). It can be divided into three distinct elements (Fig. 7-1): lipid A, which anchors the molecule in the outer membrane (Luderitz et al., 1982; Rietschel et al., 1982); the sugar core unit; and the O-antigen chain, which protrudes into the surroundings of the bacterium (Luderitz et al., 1982; Muhlradt and Golecki, 1975). The polysaccharide element of LPS requires associated cations to stabilise the outer membrane through formation of salt bridges and neutralization of the repulsive forces of neighbouring LPS chains. This leads to a tight cross-linking of the LPS layer (Ferris and

Beveridge, 1986; Van Alphen et al., 1978). The outer membrane is also characterised by the presence of a unique class of proteins, the porins. These highly β-sheet proteins form channels for the entrance and exit of hydrophilic low molecular weight substances. The membrane contains both specific and non-specific porins, meaning that the outer membrane is relatively permeable to both hydrophilic (through the porins) and hydrophobic (through the lipid bilayer) small molecules. In fact, one of the major functions of the outer membrane is to stop certain macromolecules, such as those responsible for nutrient sequestration, from diffusing away from the bacterial cell. The periplasm itself has a gel-like consistency, with a 100-fold lower diffusion coefficient than the cytoplasm. The periplasm plays a key role in solute transport, protein translocation, lipid biosynthesis, motility, attachment, cell division and oxidative phosphorylation. It is also the site of the peptidoglycan bacterial cell wall (Madigan et al., 2000).

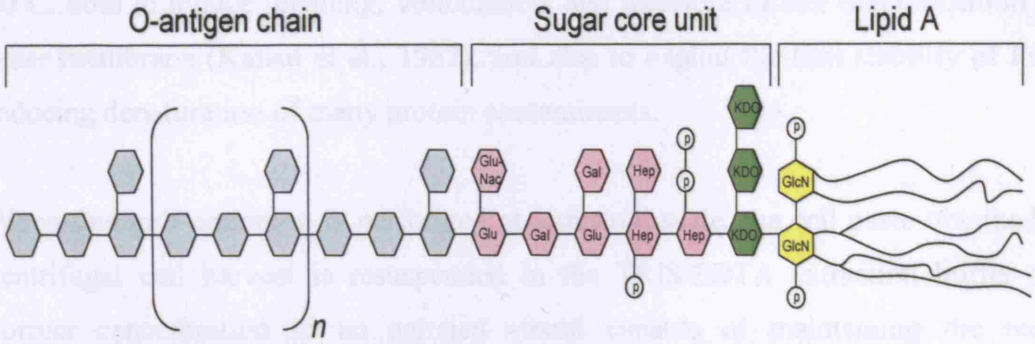

Fig. 7-1: Structure of a generic lipopolysaccharide of gram-negative bacteria. Although the precise chemistry of lipid A and the polysaccharide components varies, the sequence of major components is generally uniform. The common chemical subunits are shown. These are ketodeoxyoctonate (KDO), heptose (Hep), glucose (Glu), galactose (Gal), N-acetylglucosamine (GluNac), glucosamine (GlcN) and phosphate (P). Figure adapted from Madigan et al. (2000).

Bacterial proteins are marked for export to the periplasm by signal peptide sequences encorporated onto their primary sequence (Mergulhao et al., 2005). This is exploited in the Fab' production process by the grafting of the N-terminal signal peptide from the outer membrane porin OmpA onto the Fab' coding sequence. This facilitates Fab' translocation across the inner membrane via a type II secretion mechanism mediated by the *E. coli* translocase (Saier, 2006), although there may be some overlap with the TAT secretory system especially during the high-level expression of recombinant proteins (Mergulhao and Monteiro, 2004). This system transports unfolded proteins via an ATP-dependant mechanism (reviewed in de Keyzer et al., 2003; Manting and Driessen, 2000).

The OmpA signal peptide is cleaved from the Fab' protein during the process of translocation by the membrane bound protease, signal peptidase (Von Heijne, 1998).

The aim of the extraction unit operation is to release selectively periplasmic material whilst maintaining cell integrity so that the process stream does not become contaminated with intracellular material such as proteases, DNA, or lipids that may degrade the product or cause problems in subsequent purification process steps. During the extraction step, high concentrations of EDTA and TRIS rapidly permeablise the outer membrane. EDTA destabilises the outer membrane structure by chelating the stabilizing divalent cations from the LPS (Marvin et al., 1989), whilst the polycation TRIS molecules intercalculate between LPS molecules, further disrupting the outer membrane structure (Irvin et al., 1981). The chemical extraction is greatly facilitated by the removal of the broth supernatant before TRIS/EDTA addition to prevent EDTA sequestration by broth components (Bowering, 2000). The extraction is performed at 60°C, both to induce blebbing, vesiculation, and therefore further destabilisation of the outer membrane (Katsui et al., 1982); and also to exploit the heat stability of Fab' by inducing denaturation of many protein contaminants.

When this unit operation is performed at industrial-scale, the cell paste obtained from centrifugal cell harvest is resuspended in the TRIS/EDTA extraction buffer to the correct concentration in an agitated vessel capable of maintaining the required temperature over the duration of the extraction. The agitation rate must be sufficiently low so as to not cause damage to the spheroplasts whilst high enough to prevent sedimentation and allow efficient heat transfer. Due to the high shear resistance of the spheroplasts (Chapter 4), the agitation rate can be varied across a wide range within these constraints and is therefore not an important process parameter. However, vessel temperature control must be sufficiently accurate to prevent the maximum temperature reached in the vessel exceeding the extraction temperature by more than a few degrees centigrade. This would result in Fab' denaturation and a drop in yield, as the temperature is kept as near to the Fab' denaturation temperature as possible in order to denature the maximum number of contaminant proteins.

Three different measures are used to assess the performance of the extraction step in this chapter. The quantity of Fab' released is assessed by Protein G affinity chromatography. The level of contaminant release is indicated by a total protein measurement. Product

quality is a complex and time consuming factor to quantify as there are so many ways in which the protein can reduce in quality: by deamination, oxidation, aggregation, loss of affinity to antigen, loss of *in vivo* stability and efficacy. Therefore multiple analytical techniques are needed to fully quantify product quality. In this study quality assessment is confined to gel electrophoresis. Future work could expand quality assessment through the use of multiple complementary techniques.

7.3 Results and discussion

7.3.1 Creation of USD mimic of extraction unit operation

The periplasmic extraction step was carried out at pilot-scale by adding the cell paste, resuspended in extraction buffer, from the primary centrifugation step into a vessel capable of maintaining the desired extraction temperature. As discussed in Chapter 4, the whole *E. coli* cells and spheroplasts have been found to be highly resistant to shear levels applied during centrifugation. As low levels of mixing with a Rushton turbine (< 400 rpm) only produce energy dissipations of 10^0-10^2 W/kg compared to the 10^5-10^7 produced during centrifugation (Yim and Shamlou, 2000), a small-scale mimic of this aspect of the engineering environment is assumed not to be necessary. However, despite the increased simplicity, the millilitre-scale mimic of periplasmic extraction described is still referred to as an USD mimic for the purposes of clarity.

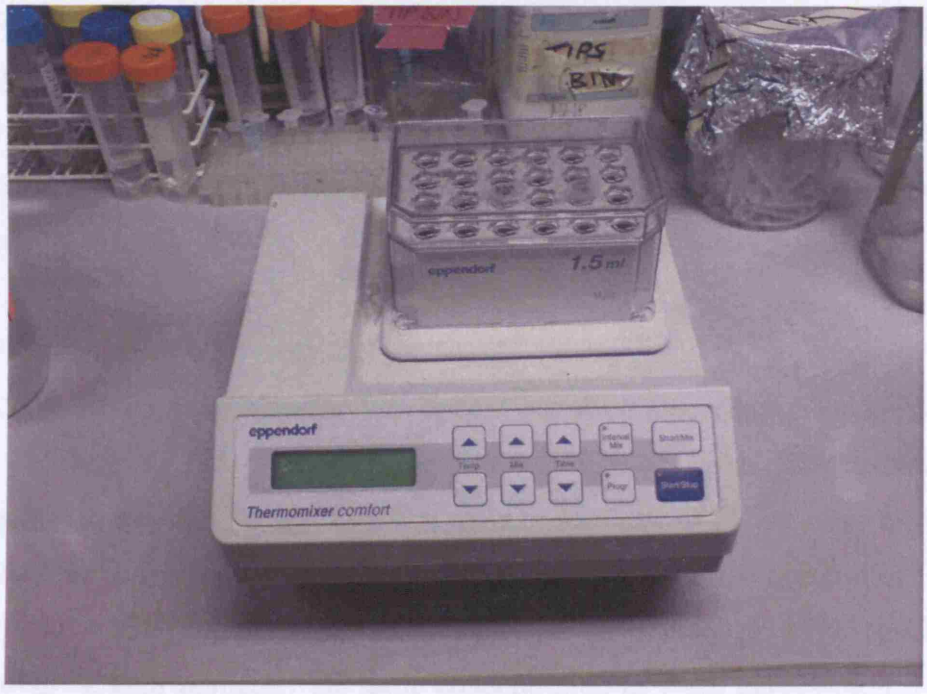

Fig. 7-2: Photographic reproduction of the Eppendorf Thermomixer R used in the USD mimic of the periplasmic extraction.

7.3.1.1 Calibration of USD equipment

An Eppendorf Thermomixer R was used at small-scale to provide heat and agitation to microfuge tubes containing the extraction mixture for the same duration as at pilot/industrial-scale. The device is capable of simultaneously incubating up to 24 x 1.5 mL tubes, as can be seen in Fig. 7-2. As Eppendorf Ltd. only specify heating accuracy to within ± 2°C below 20°C and above 45°C (± 0.5°C from 20-45°C), the Squirrel SQ1600 data logger (Amber Instruments, Chesterfield, UK) was used to investigate operating water temperature of individual tubes whilst in the thermomixer. After allowing a 20 min equilibration period at 1000 rpm, a K-type wire thermocouple attached to the SQ1600 was used to assess the water temperature through a ~ 3 mm diameter aperture created in the microfuge tube lid using a surgical needle. A 1 mL water volume was used, identical to the volume at which the extraction was subsequently performed. The data presented in Fig. 7-3 shows that the thermomixer is capable of maintaining the set temperature across a large range of values. The consistency in temperature across all block positions is indicated by the small error bars, which represent the total range of readings not standard deviation. As the extraction was carried out at 60°C, Fig. 7-4 illustrates the accuracy of the thermomixer for set-points between 55-65°C. The thermomixer is shown to be highly precise in this range, as the small error bars represent total range not standard deviation, across the 24 incubation points. Thus the thermomixer is capable of maintaining the critical process parameter incubation temperature equally accurately no matter which of the incubation holes the microfuge is placed into. However, in this range there is a constant +1°C offset between set-point and the temperature achieved. Therefore in all future experiments, the thermomixer was set to 1°C above the quoted temperature to ensure the correct accuracy is attained.

7.3.1.2 Verification of USD methodology

A 75 L IPTG-induced fermentation was carried out using a post-induction glycerol feed rate of 1.65 mL h^{-1} L^{-1}. The cell paste was harvested 28 h after induction, by centrifugation in the Carr Powerfuge P6 at an inlet feed rate of 25 L/h prior to storage at -80°C. A portion of this stored cell paste was resuspended in extraction buffer (100 mM TRIS, 10 mM EDTA, pH 7.4) to a final concentration of 15% (packed wet weight/volume), approximately the same concentration as when harvested. 1.5 L of the suspension was added to a 3 L LH 500 series fermenter (the 3 L vessel) and incubated at 60°C for 20 h, agitator speed 300 rpm. Concurrently, 1 mL of suspension was added to

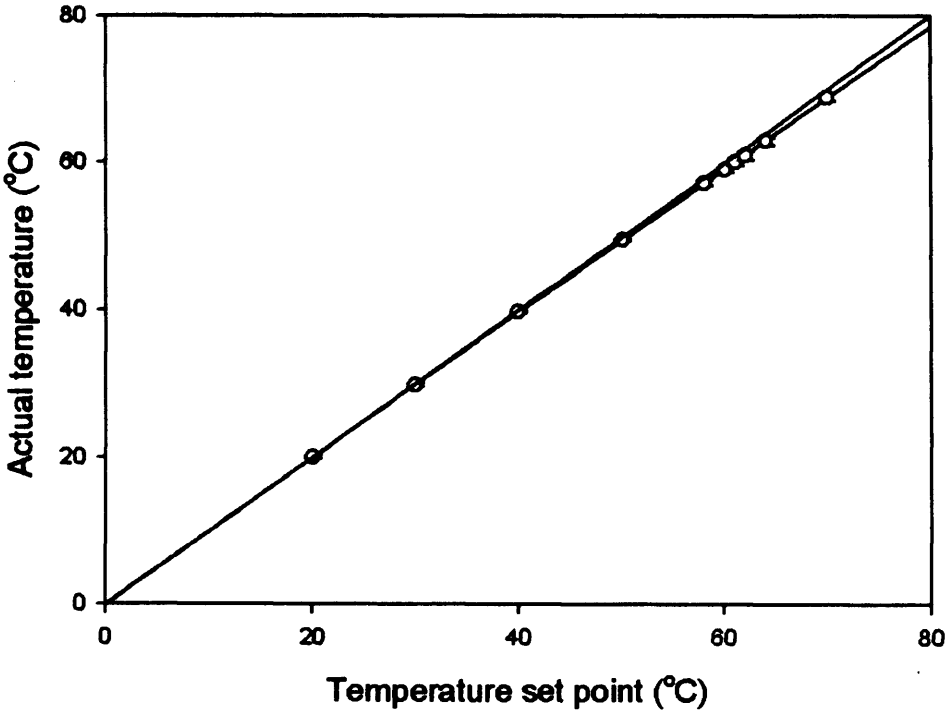

Fig. 7-3: Parity plot illustrating the equivalence of the actual temperature in microfuge tubes incubated in the Eppendorf Thermomixer R with the set-point, at a broad range of temperatures. Error bars represent the total range of measurements across the 24 microfuge tube incubation points.

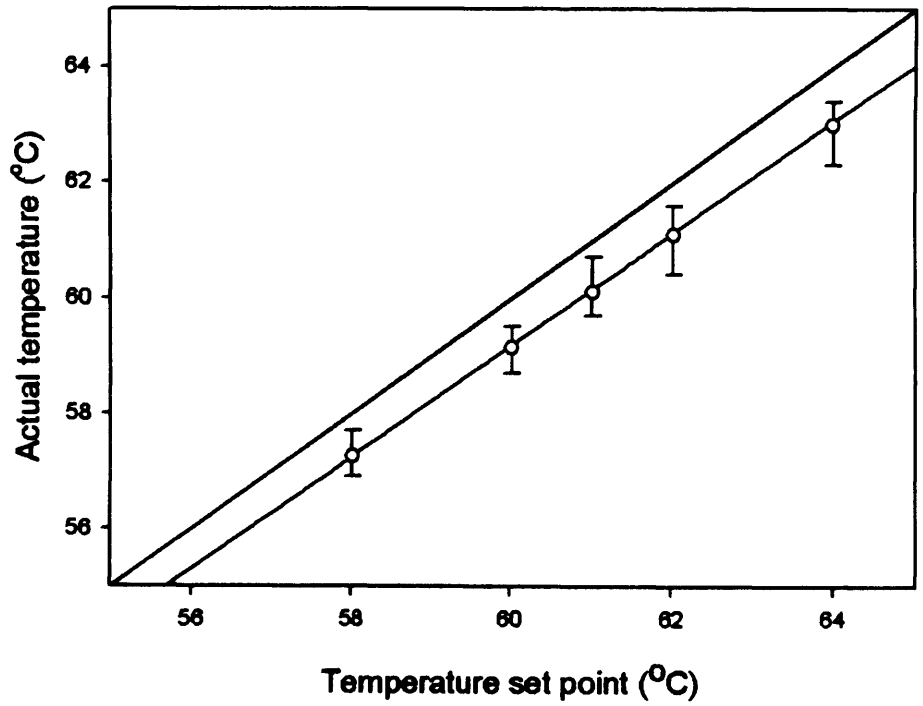

Fig. 7-4: Parity plot illustrating the equivalence of the actual temperature in microfuge tubes incubated in the Eppendorf Thermomixer R with the set-point, at around the standard temperature at which the extraction is performed (60°C). Error bars represent the total range of measurements across the 24 microfuge tube incubation points.

each of 24 microfuge tubes, which were then incubated at 60°C for 20 h, agitation speed 1000 rpm, in the Eppendorf thermomixer. 1000 rpm was used as the agitation speed as it was observed to be capable of keeping the cells in suspension for the duration of the incubation period. The 0 h sample was taken at room temperature prior to heating, and the timer started when the suspensions reached 60°C. The rate of heating in the thermomixer is much faster than in the vessel, therefore the heating in the thermomixer was manually controlled to proceed at the same rate as the 3 L vessel. The release of total protein (Fig. 7-5) and Fab' (Fig. 7-6) into the extracellular medium was plotted over time.

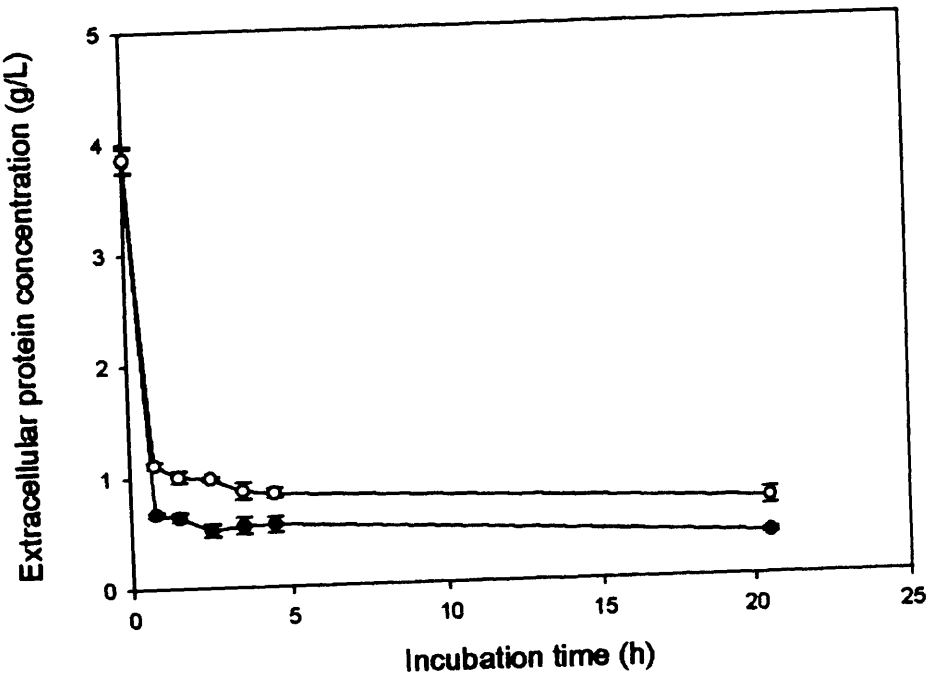

Fig. 7-5: Protein release over time for thawed resuspended *E. coli* cells incubated at 60°C in a 3 L vessel (●) and an Eppendorf Thermomixer R (○). Error bars are calculated from the standard deviation of triplicate samples (pilot-scale) or triplicate runs (USD).

These data reveal multiple insights into the extraction unit operation. Firstly, it can be observed that increased temperature does not increase Fab' release beyond that attained by chemical treatment alone. The function of the temperature increase is therefore to degrade contaminating proteins, malformed Fab' and single chain Fab' fragments. Secondly, the majority of Fab' is released, and contaminating protein degraded, within 45 min of temperature attainment. The long process hold at 60°C is to increase product quality by degradation of malfolded and single chain Fab' fragments (Bowering, 2004). Thirdly, the USD mimic greatly overestimates the level of Fab' release achieved in the 3 L vessel, while underestimating the amount of protein that can be cleared: after 20 h

the pilot-vessel:thermomixer ratio of total protein is 1:1.81, and for extracellular Fab' 1:1.62. The reason for this was evident upon inspection of the vessel's internal heating element, a metal cylinder of ~ 10 mm diameter and 80 mm length. The element was encrusted with denatured protein after the extraction. In order to maintain 60°C in the vessel the element must maintain a higher temperature. This results in the degradation of Fab' and other protein in close proximity to the heating element. These data therefore suggest that periplasmic extraction must be performed in a vessel with a either a heating system with high surface area to minimise the temperature differential between the heating system and the suspension temperature or better fluid mixing to prevent the formation of localised 'hot-spots'.

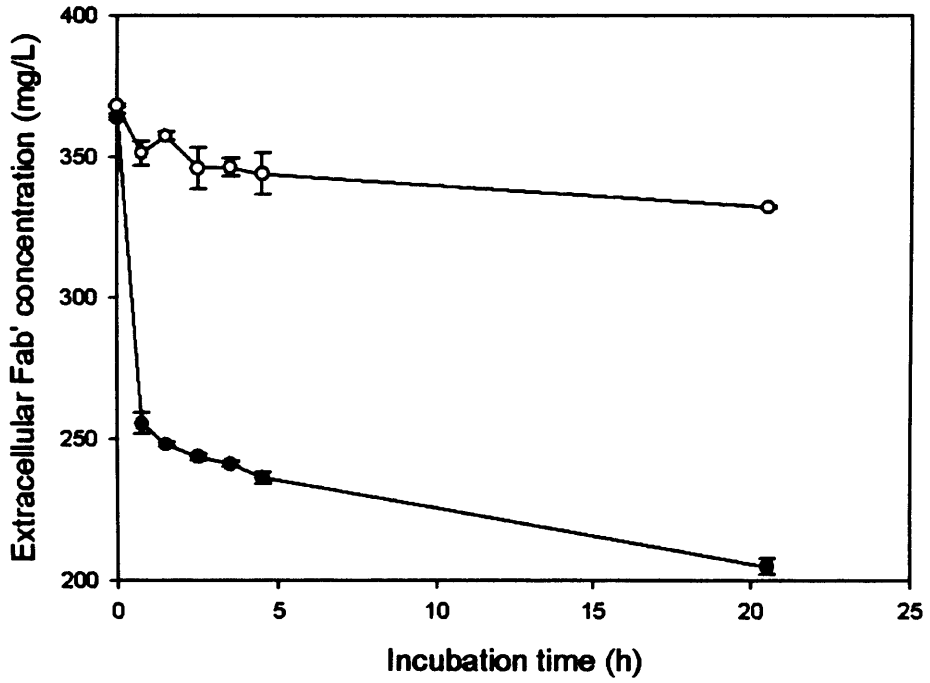

Fig. 7-6: Fab' release over time for thawed resuspended *E. coli* cells incubated at 60°C in a 3 L vessel (•) and an Eppendorf Thermomixer R (○). Error bars are calculated from the standard deviation of triplicate samples (pilot-scale) or triplicate runs (USD).

A second portion of cell paste was resuspended as detailed above and 10 L added to a jacket heated 20 L vessel (the Applikon Type-20 Bioreactor) and incubated at 60°C for 20 h, with an agitator speed of 300 rpm. The USD mimic was performed concurrently to the 20 L extraction in the same manner as it was performed concurrently with the 3 L extraction. The release of total protein (Fig. 7-7) and Fab' (Fig. 7-8) into the extracellular medium was plotted over time.

These data again show that Fab' and total protein release occurs rapidly (within 45 min) after re-suspension in extraction buffer. However, the USD mimic can be seen to much more accurately resemble extraction at 20 L scale than the 3 L scale vessel. After 20 h the ratio of total protein and Fab' between the 20 L scale data and the USD mimic is approximately 1:1. This is likely because at the larger scale the vessel supplies heat to the suspension though the whole area of the jacket rather than by using a relatively small internal heating element.

The data presented above suggested that periplasmic extraction in the thermomixer can provide a good mimic of pilot-scale extraction both in terms of total protein release and Fab' release. In order to provide more evidence for the equivalence of the extraction method, two IPTG-induced fermentations were undertaken at 20 L scale. Each was performed identically except for the key process parameter post-induction glycerol feed rate, shown in Chapter 4 to affect the performance of the periplasmic extraction procedure.

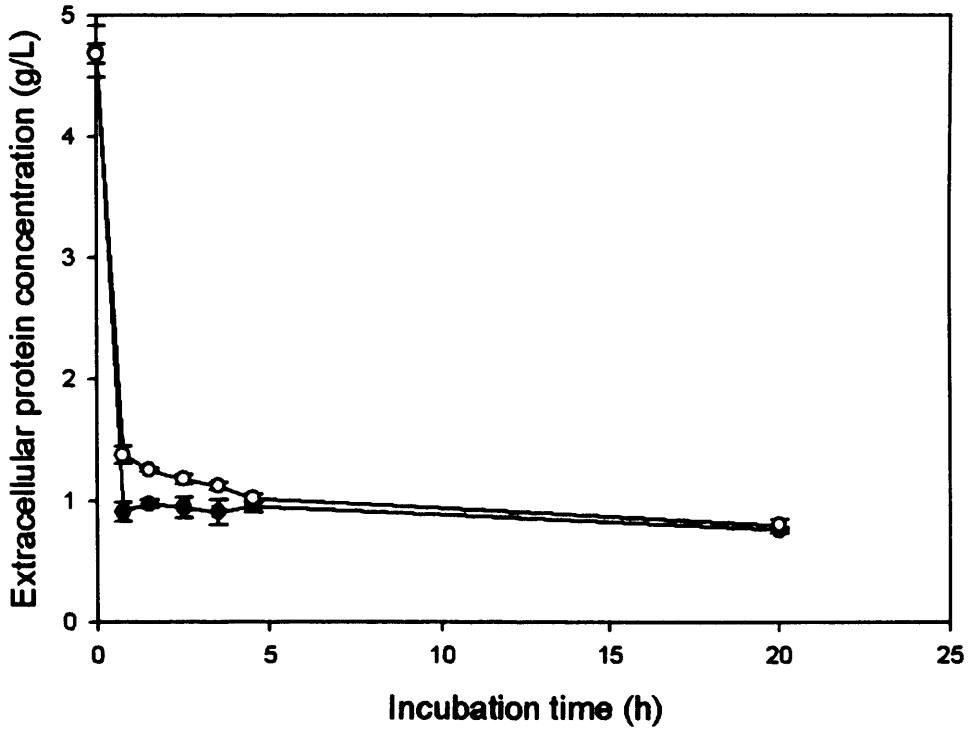

Fig. 7-7: Protein release over time for thawed resuspended *E. coli* cells incubated at 60°C in a 20 L vessel (•) and an Eppendorf Thermomixer R (○). Error bars are calculated from the standard deviation of triplicate samples (pilot-scale) or triplicate runs (USD).

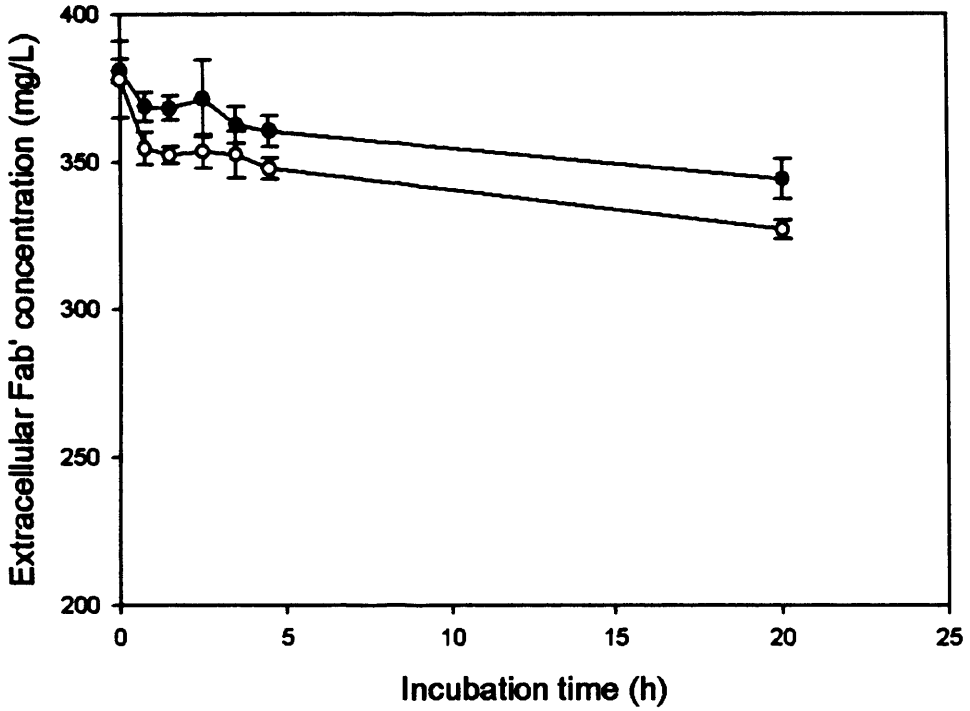

Fig. 7-8: Fab' release over time for thawed resuspended *E. coli* cells incubated at 60°C in a 20 L vessel (•) and an Eppendorf Thermomixer R (○). Error bars are calculated from the standard deviation of triplicate samples (pilot-scale) or triplicate runs (USD).

After each fermentation, cells were harvested in the CSA-1 disc-stack centrifuge at an inlet feed rate of 25 L/h and immediately resuspended in extraction buffer (100 mM TRIS, 10 mM EDTA, pH 7.4) to a total volume of 10 L, resulting in an approximate cell concentration of 15% (w/v) depending on the harvest cell density of the fermentation. 1 mL of suspension was added to each of three microfuge tubes, which were then incubated concurrently with the fermenter extraction as described above, except that incubation time was 16 h in both the 20 L vessel and the USD mimic. After incubation, the concentration of total protein and Fab' in the extracellular medium was assayed. Table 7-1 shows that for these fermentations, and for the previous results upon frozen cells, the USD methodology provided a good mimic of pilot-scale performance. A paired *t* test on these three samples found no significant difference between the performance of the USD mimic and the pilot-scale extraction, with minimal *t* scores of 0.068 (protein) and 0.30 (Fab') for the three tests. It is therefore concluded that the USD mimic accurately predicts Fab' and total protein release during periplasmic extraction.

7.3.1.3 Product quality variations between pilot and USD extractions

SDS-PAGE gel analysis was performed in order to obtain a gross measure of any product quality and contaminant profile variations between extractions performed in the

20 L vessel, the 3 L vessel, and using the USD mimic (Fig. 7-9). The Fab' protein runs as a large band on the gel at a molecular weight of approximately 47 kDa. Lanes 3-6 compare periplasmic extraction material from the different experiments using the freeze-stored cells obtained using the 1.65 mL h^{-1} L^{-1} fermentation. Extracts obtained using the 3 L vessel (lane 3) were compared to the concurrently run USD extract (lane 5). The protein profile is similar, but the faintness of the pilot material indicates a lower protein and Fab' content. In addition, the pilot material appeared to lack some contaminant bands, presumably these have degraded due to the local temperature maxima near to the heating element. Extracts obtained using the 20 L vessel (lane 4) are also compared to the concurrently run USD extract (lane 6). In contrast to the 3 L vessel extractant, here the USD and pilot-scale contaminant profiles appear similar. It was therefore concluded that USD mimic produces a comparable periplasmic extraction protein profile to that obtained using correctly functioning pilot-scale equipment.

7.3.2 Identification of critical process parameters in the periplasmic extraction unit operation

Having demonstrated the ability of the USD operation to mimic pilot-scale performance in section 7.3.1, the mimic was used as the basis of a statistical design of experiments (DoE) examination of the extraction procedure. The combination of DoE and USD is powerful as it allows much relevant process information to be gained rapidly and at low cost. A standard 2-factor design was used with 8 input variables chosen to cover all possible key process parameters. Percentage release of total protein and Fab' were chosen as response outputs. Input variables and high/low limits, given in Table 7-2, were based on consideration of the maximum error that could be made during industrial operations. These limits were chosen so as to investigate ranges of conditions around the fixed processing protocol to increase process knowledge by investigation the size of the design space for this unit operation (Rathore et al., 2007), and to identify important process parameters. The experiments were therefore not designed to aid process optimisation but to increase process knowledge and thereby increase regulatory flexibility. The power of the combined use of DoE and USD methodologies for this aim is further discussed in Chapter 11.

Table 7-1: Comparison of the performance of the USD mimic with pilot-scale extraction in the 20 L vessel with three different *E. coli* cell populations. Note that the two 1.65 mL h^{-1} L^{-1} fermentations do not have identical levels of Fab' and protein release because of differences in induction time and cell storage, and also because the cells were resuspended in extraction buffer to different concentrations. Standard deviation is the result of triplicate measurements (fermenter) or samples (USD). Error from standard deviation of triplicate samples (pilot-scale) or triplicate experiments (USD).

Fermentation Conditions		**Protein release (g/L)**					**Fab' released (mg/L)**				
Post-induction glycerol feed rate (mL h^{-1} L^{-1})	**Fresh/ Frozen**	**Applikon**	**Error**	**USD**	**Error**	**USD accuracy (% of pilot-scale)**	**Applikon**	**Error**	**USD**	**Error**	**USD accuracy (% of pilot-scale)**
1.65	Frozen	0.759	0.0268	0.804	0.0402	106	344	6.67	327	3.33	95.1
1.65	Fresh	1.34	0.146	1.34	0.317	100	368	11.5	379	8.84	103
1.80	Fresh	1.39	0.121	1.35	0.121	97.1	251	9.84	266	15.2	106

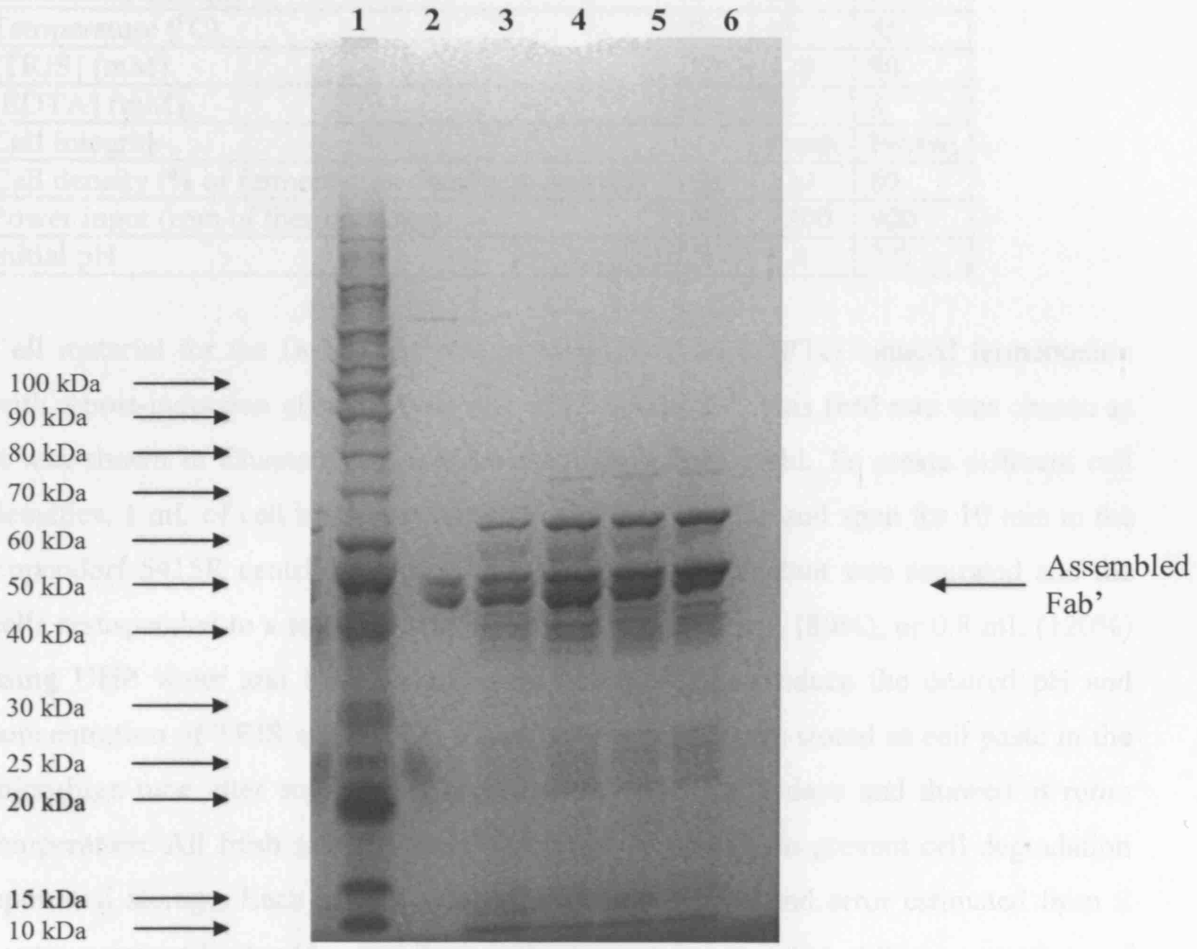

Fig. 7-9: Non-reducing 8-16 % SDS-PAGE gel showing protein profile of periplasmic extractions performed using a variety of pilot and USD equipment. The fact that Fab' appears as a double band is not representative of Fab' sub-populations: it is an artefact of this particular gel.

Lane 1: Molecular weight markers
Lane 2: Purified A33 Fab' standard
Lane 3: Pilot-scale extraction using 3L vessel (internal heating element)
Lane 4: Pilot-scale extraction using 20L vessel (jacket heated)
Lane 5: USD extraction (concurrently with 3L extraction)
Lane 6: USD extraction (concurrently with 20L extraction)

Table 7-2: Input variables and corresponding high/low limits used for 2-factor DoE study of periplasmic extraction process robustness. Note that cell integrity is a discrete variable and therefore lacks a midpoint value.

Input variable	0	+	−
Incubation time (h)	16	20	12
Temperature (°C)	60	65	55
[TRIS] (mM)	100	120	80
[EDTA] (mM)	10	12	8
Cell integrity	-	Fresh	Frozen
Cell density (% of fermentation density at harvest)	100	120	80
Power input (rpm of thermomixer)	1000	1200	800
Initial pH	7.4	7.8	7.0

Cell material for the DoE study was provided by a 20 L IPTG induced fermentation with a post-induction glycerol flow rate of 1.4 mL h^{-1} L^{-1}. This feed rate was chosen as it was shown in Chapter 3 to produce the highest Fab' yield. To create different cell densities, 1 mL of cell broth was added to a microfuge tube and spun for 10 min in the Eppendorf 5415R centrifuge, rotor F45-24-11. The supernatant was aspirated and the cells resuspended to a total volume of 1 mL (100%), 1.2 mL (80%), or 0.8 mL (120%) using UHP water and the relevant extraction buffer to produce the desired pH and concentration of TRIS and EDTA. Frozen cell samples were stored as cell paste in the microfuge tube after supernatant aspiration at -20°C for 3 days and thawed at room temperature. All fresh samples were performed in parallel, to prevent cell degradation upon cell storage. Each sample was only performed once and error estimated from 8 centre point replicates (4 using fresh cells, 4 using frozen cells). All concentrations of Fab' and total protein determined were normalised to 100% cell density in order to allow comparison between different cell density samples, which would have different starting Fab' and total protein concentrations.

The results of the study are displayed as half-normal plots. Fig. 7-10 illustrates which process parameters impact the total protein concentration after extraction. It can be seen that the major process parameter affecting contaminant carry-over is the temperature at which the extraction is performed. Predictably, the lower the temperature, the less total protein is degraded but contaminant carry-over is increased. A second important process parameter is initial pH. Again this is easily explained, as the nearer the pH is to neutral the more stable the majority of proteins, therefore fewer will be denatured during extraction. In addition to these two major effects, cell density, an interaction between

cell integrity and pH, and an interaction between temperature and cell density all show up as possibly having an affect upon the levels of total protein clearance achieved, although their standardised effects are very low and so this may just be a result of noise in the unreplicated readings. Interestingly, cell integrity had no discernable effect upon the level of protein release achieved.

The parameters controlling Fab' concentration after extraction are illustrated in Fig. 7-11. The major parameter indicated is cell integrity, as would be expected from Chapter 4. The freeze/thawed cells show much greater Fab' release than fresh cells, indicating that Fab' is more easily released from damaged cells. An interaction between temperature and cell integrity also appears to be a key process parameter. A third, but less important parameter is temperature itself; increased extraction temperature decreases Fab' yield. Other parameters with small effects identified by this study are time, pH, and an interaction between time and temperature. These all seem sensible as time of exposure, pH and temperature all alter protein stability.

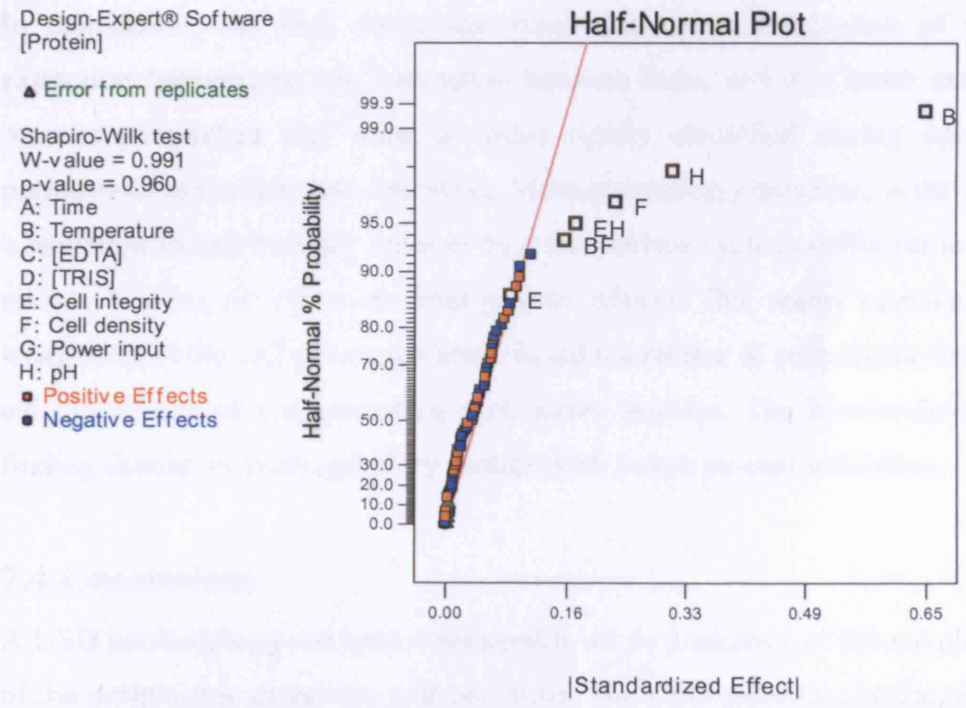

Fig. 7-10: Half-normal plot illustrating the critical process parameters affecting the level of total protein found in the extracellular medium after extraction.

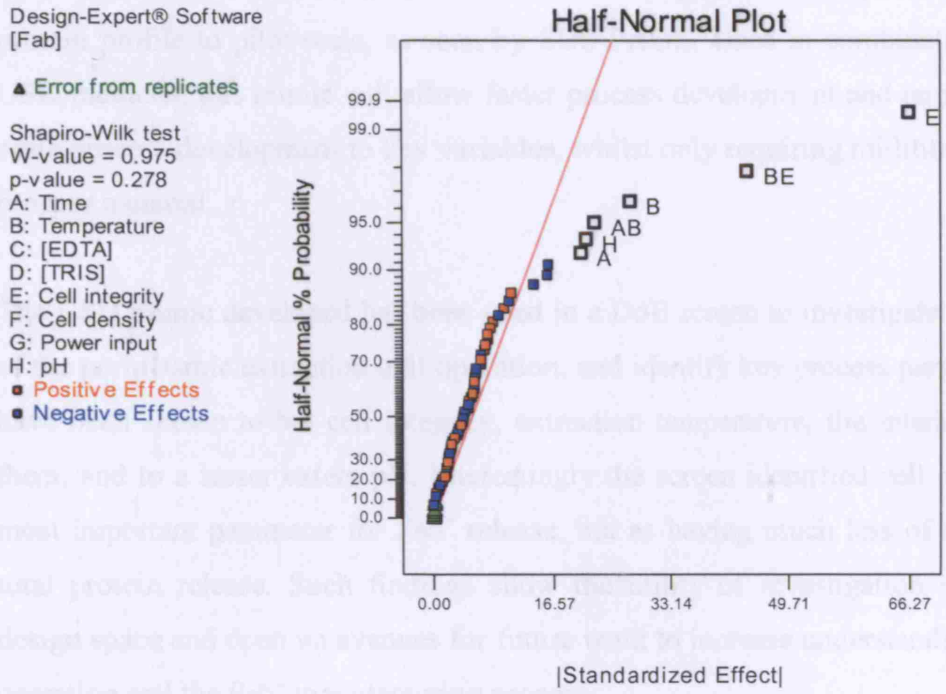

Fig. 7-11: Half-normal plot illustrating the critical process parameters affecting the amount of Fab' found in the extracellular medium after extraction.

In conclusion, the DoE study has resulted in the identification of cell integrity, extraction temperature, the interaction between them, and to a lesser extent pH as the process parameters that must be most rigidly controlled during operation of the periplasmic extraction unit operation. Most interestingly however, is the discovery that a reduction in cell integrity induced by a freeze/thaw cycle is sufficient to increase Fab' release but has no effect on total protein release. This seems counter-intuitive: any weakening of the cell outer membrane to aid the release of periplasmic Fab' should also aid the release of contaminating periplasmic proteins. The biochemical basis of this finding should be investigated by further work before process validation.

7.4 Conclusions

A USD methodology has been developed to allow prediction of pilot-scale performance of the periplasmic extraction unit operation. The USD procedure is simple, inexpensive and only requires standard laboratory equipment. Comparison of periplasmic extraction performance using three feed streams of different cellular integrity showed the USD mimic to perform statistically identically to pilot-scale extraction in the 20 L vessel, in terms of Fab' and total protein released into the extracellular medium. In all cases the level of Fab' and total protein released at USD level was within ± 6% of pilot-scale

measurements. The mimic has also been shown to generate an equivalent supernatant protein profile to pilot-scale, as seen by SDS-PAGE. Used in combination with other USD methods, this mimic will allow faster process development and targeting of pilot-scale process development to key variables, whilst only requiring millilitre quantities of process material.

The USD mimic developed has been used in a DoE screen to investigate the robustness of the periplasmic extraction unit operation, and identify key process parameters. These have been shown to be: cell integrity, extraction temperature, the interaction between them, and to a lesser extent pH. Interestingly the screen identified cell integrity as the most important parameter for Fab' release, but as having much less of an effect upon total protein release. Such findings show the utility of investigation of the process design space and open up avenues for future work to increase understanding of this unit operation and the Fab' manufacturing process.

The utility of this USD method for process development and understanding is exemplified in Chapter 8 by its use, along with centrifugal USD methods, to investigate the effect of changes in the upstream process upon the initial DSP for the production of antibody fragments in *E. coli*, in terms of process yield.

8. Case study of the use of USD methods to gain whole process information: The effect of post-induction carbon feed rate on yield after initial DSP in the antibody fragment production process

8.1 Abstract

The utility of the USD methods developed have been demonstrated by their use to determine interactions between post-induction carbon feed rate, a key upstream process parameter, and Fab' yield during the initial DSP. Five fermentation harvests generated using post-induction carbon feed rates between 1.0 and 1.8 mL h^{-1} L^{-1} are assessed using the USD clarification method, the USD periplasmic extraction method, and the USD dewatering method. The initial DSP was also assessed at pilot-scale. The data generated was used to quantify interactions between the upstream parameter and Fab' yield during: cell harvest via centrifugation, periplasmic extraction and centrifugal spheroplast removal. A process model demonstrating the affect of post-induction carbon feed rate upon Fab' yield after initial downstream processing was then generated using the relationships determined above. Crucially, the USD and pilot-scale model outputs are practically identical. Both USD and pilot-scale data indicate that a 0.5 mL h^{-1} L^{-1} increase in the operating range of the post-induction carbon feed rate would increase Fab' yield after the initial DSP by ~ 5%. It is concluded that the USD methodology developed in this thesis can provide useful process information with an approximate thousand-fold reduction in the amount of upstream material required. The benefits of this reduction in the requirement for process material are discussed.

8.2 Introduction

USD methodology has been developed as a tool to enable process development activity with only millilitres of material. One advantage of this ability to gain process information with such small amounts of material is enabling process design work to commence earlier in the drug development pathway when there is typically only a small amount of material available, and this is often highly coveted for other work, such as animal studies (Titchener-Hooker et al., 2001). The earlier commencement of process

development work in the drug development pathway is highly desirable in order to achieve rapid market penetration and so maximise the benefits accorded by patent exclusivity. Up to US$1M of income may be lost for every day the product is not on the market (Lim et al., 2004a).

Another example of the usefulness of laboratory-scale process development is that the number of studies that can be performed on a given amount of material is vastly increased. Coupled with the use of statistical design of experiments theory to maximise the process insights that can be gained from a given data set, these laboratory-scale studies can therefore greatly decrease the cost of extensive process studies. This accumulation of process knowledge at lower financial cost is due to the reduction in the need for upstream process material and pilot-scale facility utilisation. The increased process knowledge gained can aid process validation through the FDA's Quality by Design (QbD) initiative (Yu, 2006) and also facilitate process analytical technology (PAT) by increased knowledge of process limitations and interactions between unit operations (Low et al., 2007). An example of the use of USD methods has been given by the application of an USD approach for the prediction of full-scale recovery of ovine polyclonal immunoglobulins used in the manufacture of snake venom-specific Fab fragments (Neal et al., 2003). Here USD experiments were used to evaluate process interactions. For example, results showed that the protein precipitate size distribution was critically influenced by a first-stage centrifugation step in addition to the precipitation conditions.

In this chapter the use of USD methodology to advance knowledge of a defined process is exemplified by the use of the USD techniques developed in previous chapters to determine the interaction between post-induction carbon feed rate, a key process parameter in the upstream process, and process yield after initial downstream processing. The accuracy of the USD approach is compared with more traditional pilot-scale studies, and the reduction in material required by an USD approach calculated.

8.3 Results and discussion

8.3.1 Overview of pilot and USD process flowsheets

The process flowsheet studied in this chapter is detailed in Fig. 8-1. The pilot-scale unit operations are given along with the standard operating conditions supplied by UCB at the onset of this project. Each centrifugation step has been split into four output

variables: entry, damage, exit damage, clarification, and dewatering. The USD methodologies that can be used to determine these outputs are detailed in Chapters 4, 5 and 6 respectively. USD methodology not applied in this chapter is marked in red. Exit and entry damage has not been assessed for either the first or second centrifugation step, as it was shown in Chapter 4 that any damage induced on the *E. coli* cells or spheroplasts by the pilot-scale centrifuges used does not alter the process performance. Also, dewatering has not been assessed for the first centrifugation step and clarification for the second, as this chapter focuses on Fab' yield rather than contaminant clearance. Product quality is also not assessed.

Process material used for both pilot and USD studies is obtained from a series of pilot-scale 20 L IPTG-induced fermentations. For this exploratory study, pilot plant produced upstream material was used for both the pilot and USD experiments in order to allow the comparison of USD methods for predicting the performance of initial DSP unit operations with pilot-scale data. However, if USD methods need be undertaken before pilot-scale upstream process material becomes available, a miniature bioreactor system could be used. These have been recently comprehensively reviewed (Betts and Baganz, 2006). Process material for later USD unit operations can be supplied either by a previous USD method (black arrows, Fig. 8-1) or from the pilot-scale process chain (blue arrows, Fig. 8-1). It is recommended that if pilot-scale experiments are to be run concurrently with a USD experiment, then the pilot-scale material should be used for the USD experiments to reduce error due to any inaccuracy in the previous USD mimic. However, the USD methods proposed should be sufficiently accurate to allow experimental material produced in one unit operation to be used as the source of material for the subsequent one. This will be explored in this chapter.

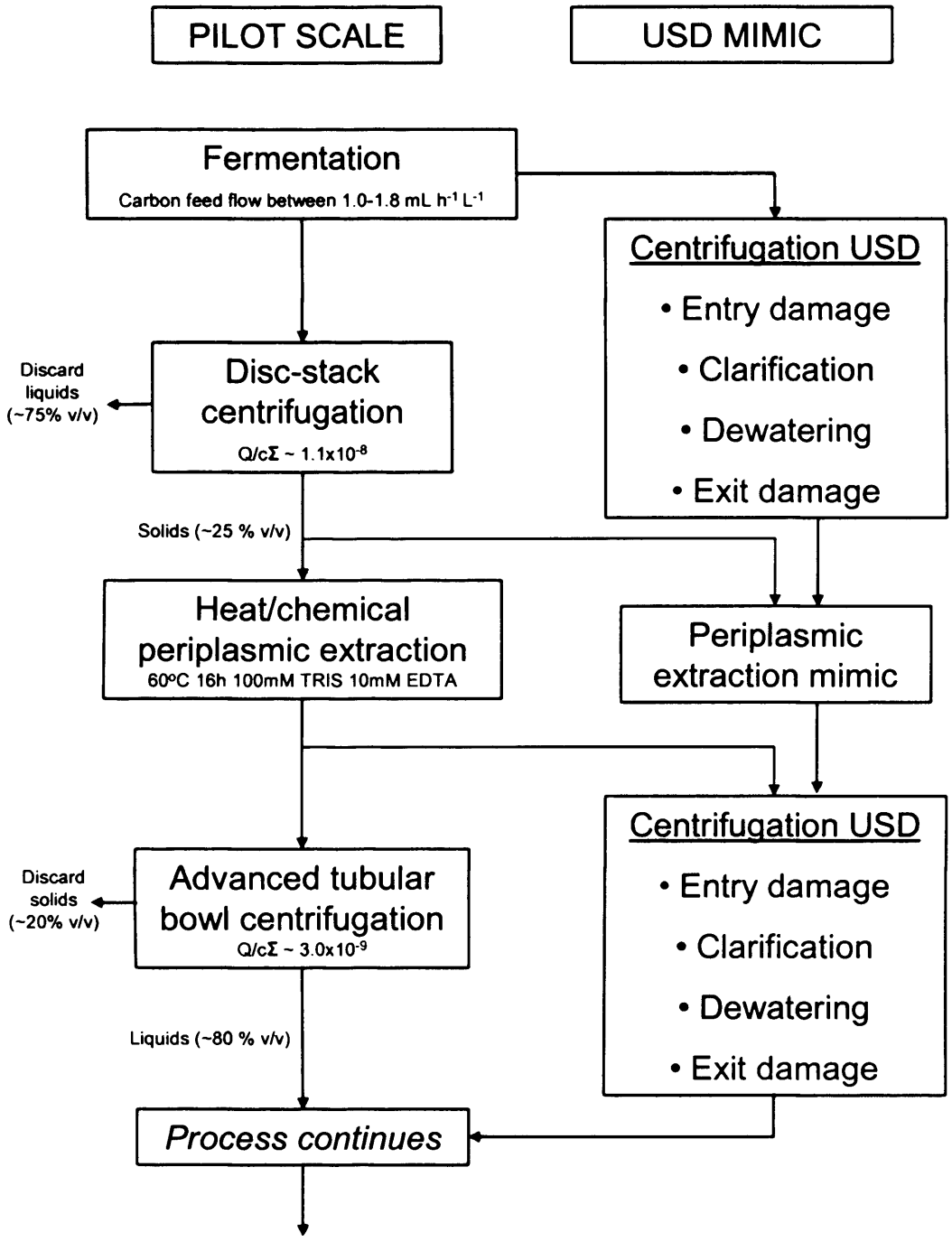

Fig. 8-1: Process flowsheet for initial DSP of antibody fragment production in *E. coli*. Optional USD methods not used are marked in red. Blue arrows indicate where pilot-scale experiments could supply material for USD experiments in order to reduce experimental time, if the pilot-scale process is run concurrently to the USD process. Note that all material used in these studies is descended from 20 L pilot-scale IPTG-induced fermentations.

8.3.2 Fermentation unit operation

The IPTG-induced upstream process for the production of antibody fragments in *E. coli* was used in this study, as detailed in Chapter 3. All process parameters were identically maintained in the upstream process except for the post-induction glycerol flow rate. Five variations in this process parameter were used. These were 1.04, 1.40, 1.58, 1.65 and 1.80 mL h^{-1} L^{-1}. Fab' concentration in the extracellular medium and after complete mechanical homogenisation of the cell harvest was assessed by Protein G HPLC and used to determine the concentration of internal Fab' at each carbon feed rate. Internal Fab' can be considered the yield of the unit operation, as the supernatant is discarded after harvesting. This was fitted to a quadratic with the x term representing the post-induction carbon feed rate. A quadratic was chosen as it was the lowest order polynomial that was capable of fitting to the data sufficiently well to yield an R^2 value < 0.85. This was plotted in Fig. 8-2. The reasons for the bell-shape of the dependency of Fab' yield upon glycerol feed rate have already been discussed in Chapter 3. Briefly, if the feed rate is too low the energy and carbon supply will be insufficient for maximal Fab' production. If the feed rate is too high Fab' leakage and eventually cell lysis will result.

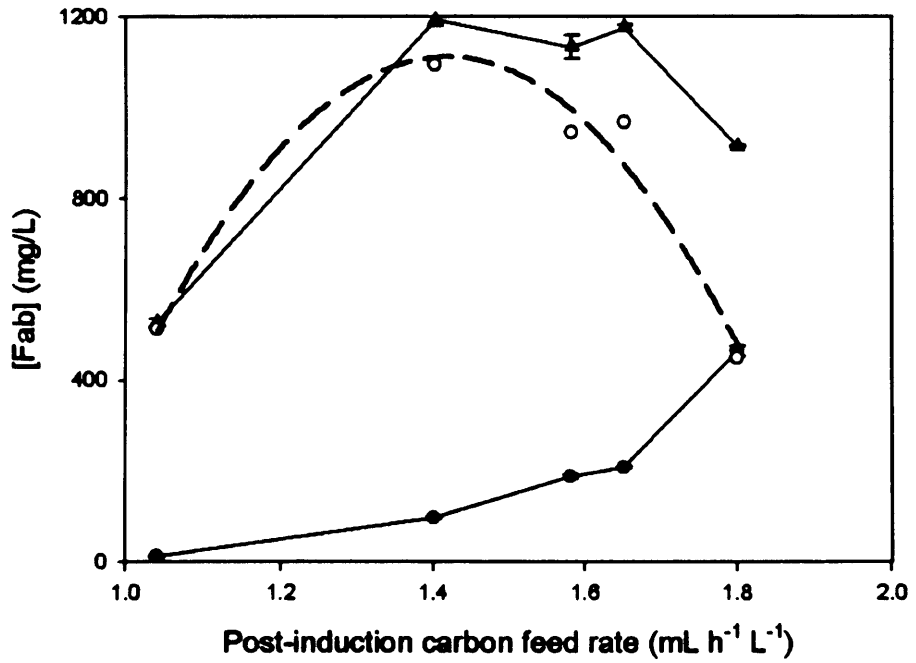

Fig. 8-2: The effect of post-induction carbon feed upon Fab' production and compartmentalisation 36 h after induction. Total Fab' (▲) and supernatant or external Fab' (●) are plotted, with periplasmic Fab' (○) derived from the difference between the two. Periplasmic Fab' production has been fit to a quadratic and the curve of the resultant equation plotted (— —). Errors were computed from the standard deviation of triplicate sample measurements.

Consideration of the fermentation stage in isolation would lead to a glycerol feed rate of 1.42 mL h^{-1} L^{-1} being chosen as the optimum in terms of Fab' yield. In the rest of this chapter this assumption is tested by determination of the interactions between fermentation glycerol feed rate and the performance of subsequent initial DSP unit operations.

8.3.3 Centrifugal cell harvest

8.3.3.1 Pilot-scale prediction of clarification efficiency

Cells from the fermentations with post-induction glycerol feed rates of 1.04, 1.40, 1.65 and 1.80 mL h^{-1} L^{-1} were harvested in the disc-stack centrifuge at 9800 rpm at a variety of feed flow rates to generate a range of Q/cΣ values from 4.36×10^{-9} to 2.62×10^{-8} m/s and the clarification efficiency calculated using optical density measurements (Equation 2-1). Results for each different harvest were plotted on a probability/log chart and the % clarification for the standard Q/cΣ value of the process of 1.1×10^{-8} m/s determined from the regression line (Fig. 8-3).

8.3.3.2 USD prediction of clarification efficiency

Cells from all five fermentations were analysed using the USD clarification mimic adapted for HCD cultures. Cell harvest was analysed at a variety of spin speeds and times to generate a range of predicted equivalent settling areas (V/ctΣ) from 1.8×10^{-9} to 4.7×10^{-7} m/s and the clarification efficiency calculated using optical density measurements (Equation 2-1). Results for each different harvest were plotted on a probability/log chart and the % clarification for the standard V/ctΣ (equivalent to Q/cΣ) value of the process of 1.1×10^{-8} m/s determined from the regression line (Fig. 8-4).

8.3.3.3 Interaction between USP and yield during cell harvest

The predicted % clarification at a Q/cΣ value of 1.1×10^{-8} determined in Figures 8-3 and 8-4 is plotted against post-induction glycerol flowrate to elucidate the relationship between this upstream parameter and yield during cell harvest, under standard centrifugation conditions (Fig. 8-5). The peak in clarification at around the point of maximal Fab' production seems logical. Above this point increased leakage of Fab' and periplasmic material will tend to reduce cell size, and there will be an increased quantity of cell debris generated by the increasing incidence of lysed cells. Below the optimum, cells will be carbon limited, and as a result produce less Fab' and may also be slightly reduced in size.

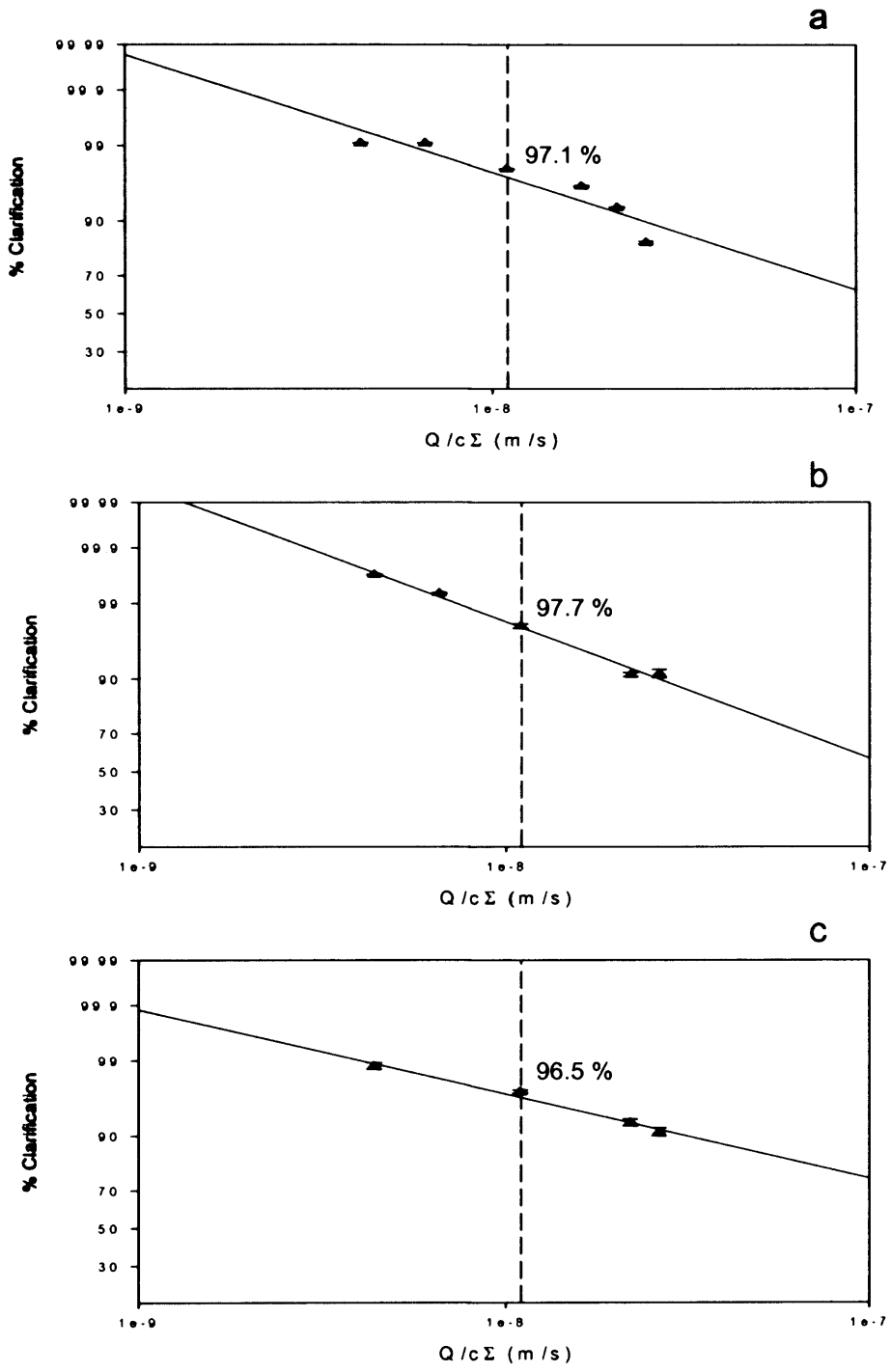
a
99 99
99 9
99
90
70
50
30
% Clarification
97.1 %
1e-9
1e-8
1e-7
Q /cΣ (m /s)
b
99 99
99 9
99
90
70
50
30
% Clarification
97.7 %
1e-9
1e-8
1e-7
Q /cΣ (m /s)
c
99 99
99 9
99
90
70
50
30
% Clarification
96.5 %
1e-9
1e-8
1e-7
Q /cΣ (m /s)

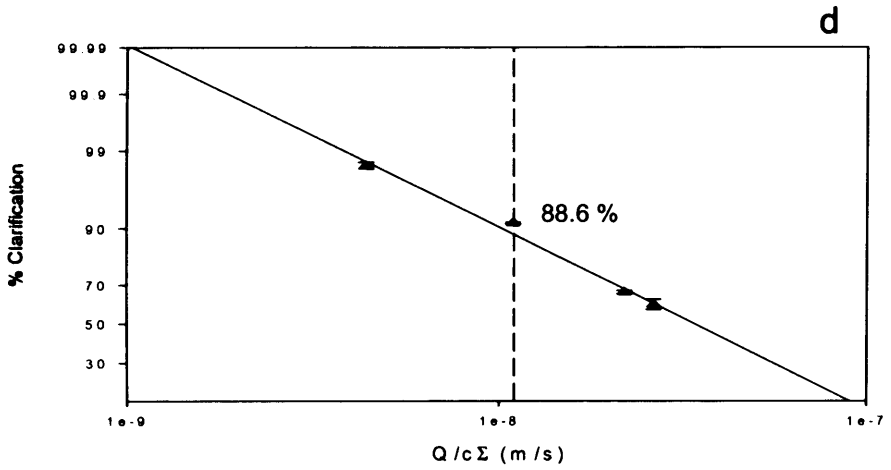

Fig. 8-3: Clarification plotted against equivalent settling area for *E. coli* cells harvested in the disc-stack centrifuge after fermentations using a post-induction glycerol feed rate of 1.04 (a), 1.40 (b), 1.65 (c) and 1.80 (d) mL h^{-1} L^{-1}. The % clarification predicted from the regression line at a $Q/c\Sigma$ value of 1.1×10^{-8} m/s is shown on each graph. Due to scarcity of material error bars are calculated from the standard deviation of triplicate repeat samples of a single run.

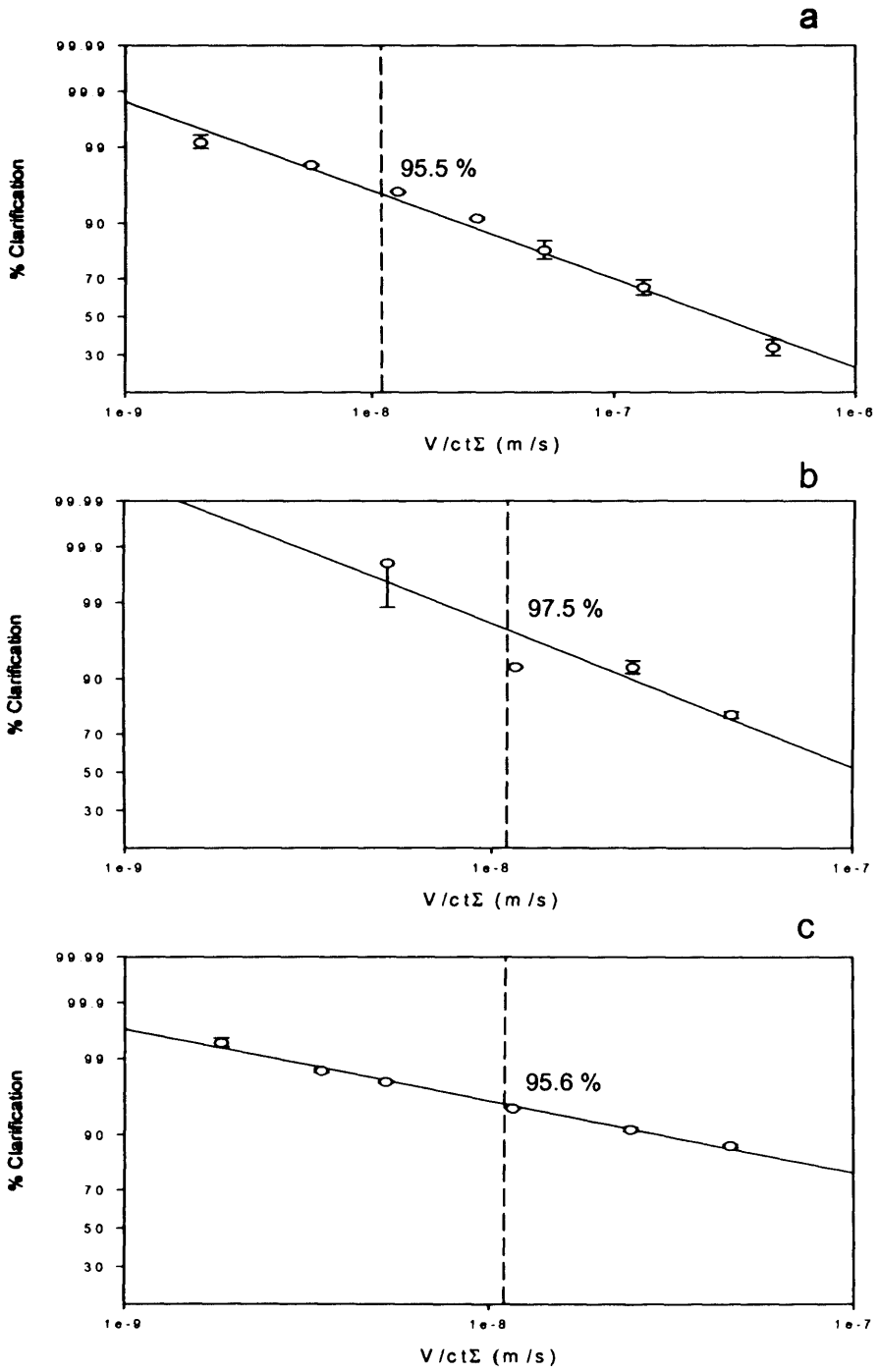
a
99.99
99.9
99
90
70
50
30
% Clarification
95.5 %
1e-9
1e-8
1e-7
1e-6
V/ctΣ (m/s)
b
99.99
99.9
99
90
70
50
30
% Clarification
97.5 %
1e-9
1e-8
1e-7
V/ctΣ (m/s)
c
99.99
99.9
99
90
70
50
30
% Clarification
95.6 %
1e-9
1e-8
1e-7
V/ctΣ (m/s)

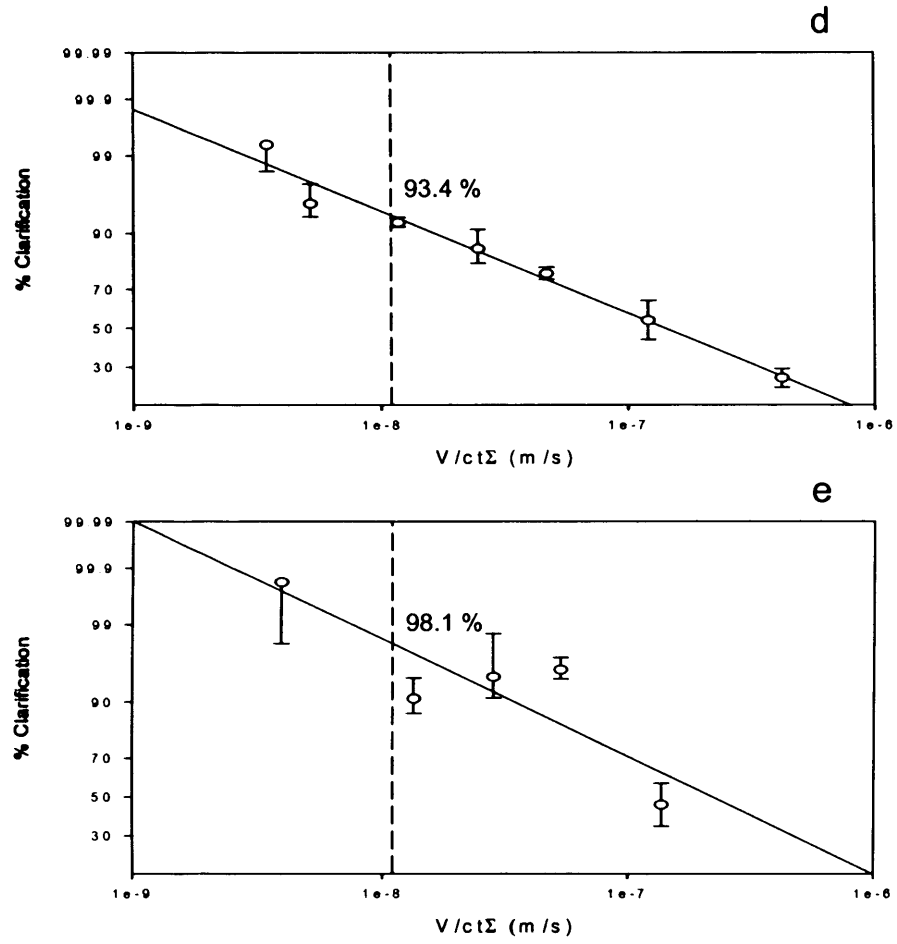

Fig. 8-4: Clarification plotted against predicted equivalent settling area for *E. coli* cells analysed by the adapted USD clarification method after fermentations using a post-induction glycerol feed rate of 1.04 (a), 1.40 (b), 1.58 (c), 1.65 (d) and 1.80 mL h^{-1} L^{-1} (e). The % clarification predicted from the regression line at a V/ctΣ value of $1.1x10^{-8}$ m/s is shown on each graph. Error bars are calculated from the standard deviation of triplicate experiments.

Second order polynomials used to fit the pilot and USD data as they were the lowest order polynomial that was capable of fitting to the data sufficiently well to yield an R^2 value < 0.85. These are plotted in Fig. 8-5. Assuming that a drop in clarification is linearly related to a drop in yield, these equations can be easily modified to determine the dependency of yield of the harvest clarification unit operation upon post-induction carbon feed rate (Equation 8-1).

$$Yield = \frac{(\%clarification)}{100} \qquad [8\text{-}1]$$

Although it would be possible to use the harvest data generated to determine a Q/cΣ value necessary to maintain a % clarification above a certain level, and then study the effects on the process productivity, it was decided to focus upon the effect post-induction glycerol flow rate has upon process yield if standard conditions were adhered to.

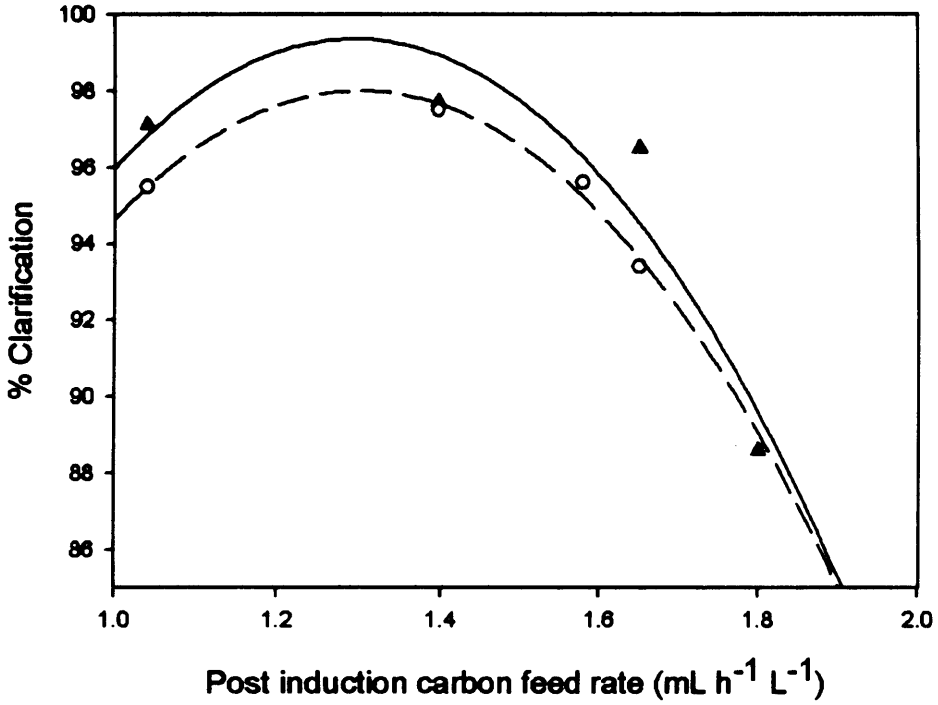

Fig. 8-5: Clarification levels during cell harvest at a fixed equivalent settling area of $1.1x10^{-8}$ m/s after fermentations performed at different post-induction glycerol flowrates, as determined at pilot-scale (▲) and by use of the USD clarification method adapted for HCD feeds (○). % Clarification has been fit to a quadratic and the curve of the resultant equation plotted for the pilot-scale (——) and USD (— —) data.

8.3.4 Periplasmic extraction

8.3.4.1 Pilot-scale prediction of extraction efficiency

Total solids obtained using the disc-stack centrifuge from the fermentations with post-induction glycerol feed rates of 1.40, 1.65 and 1.80 mL h^{-1} L^{-1} were resuspended to a total volume of 10 L in extraction buffer. Periplasmic extraction was undertaken in the Applikon Type-20 Bioreactor at 60°C, agitation rate 300 rpm. After 16 h the cell extractant was cooled to 15°C and percentage extraction calculated via comparison of the concentration of Fab' in the extracellular medium and the total Fab' present, as determined by complete sample homogenisation.

8.3.4.2 USD prediction of extraction efficiency

The USD method was undertaken entirely independently of pilot-scale centrifugation or extraction equipment. Cell harvest from fermentations with post-induction glycerol feed rates of 1.04, 1.40, 1.58, 1.65 and 1.80 mL h^{-1} L^{-1} was sheared in the shear cell device described in Hutchinson et al. (2006) for 20 sec at 13,000 rpm in order to mimic the impact of high-shear regions in the disc-stack centrifuge entry zone leading to potential cell damage and disruption. Centrifugal exit shear was not applied to the samples as this has been previously shown not to alter the performance of the periplasmic extraction unit operation (Chapter 4). Periplasmic extraction was then performed at millilitre-scale. Percentage extraction was calculated via comparison of the concentration of Fab' in the extracellular medium and the total Fab' present, as determined by complete sample sonication.

8.3.4.3 Interaction between USP and yield during periplasmic extraction

The variation in performance of the periplasmic extraction unit operation with changes in the upstream parameter, post-induction glycerol feed rate, is shown in Fig. 8-6. Both pilot-scale and USD data indicate that there is an interaction between the efficiency of the periplasmic extraction unit operation and the post-induction glycerol flow rate. This relationship was also suggested by data in Chapter 4. The most likely physiological reason for this relationship is a weakening in periplasmic membrane integrity at higher carbon feed rates, as also indicated by increased Fab' leakage and eventually cell lysis with progressive increases in feed rate (Fig. 8-2).

Good agreement can be seen between USD and pilot-scale data. All pilot-scale measurements are within one standard deviation of the corresponding USD point. A simple linear equation was fitted to the more limited pilot-scale data, while the five USD points have been curve fitted to a quadratic, as this was the lowest order polynomial that yielded and R^2 value > 0.85.

Assuming that the amount of Fab' degraded during the extraction procedure is constant at different post-induction glycerol feed rates, these equations can be modified to determine the dependency of yield of the harvest clarification unit operation upon post-induction carbon feed rate as shown below.

$$Yield = \frac{(\%Extraction)}{100} \qquad [8\text{-}2]$$

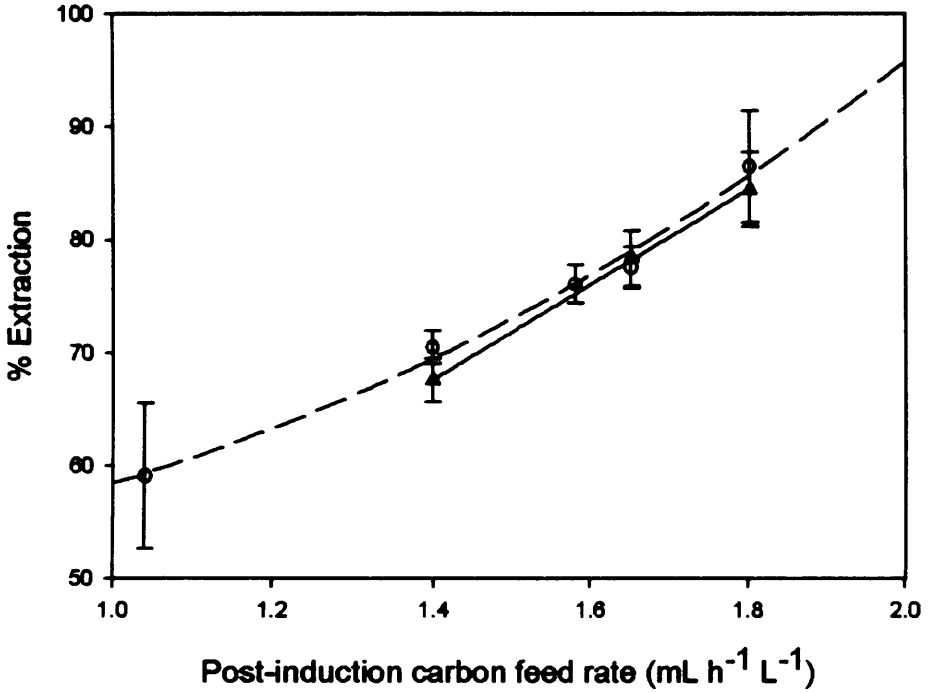

Fig. 8-6: Efficiency of periplasmic extraction unit operation in terms of % total Fab' released into the cellular media after extraction, after fermentations performed at different post-induction glycerol flowrates, as determined at pilot-scale (▲) and by use of the USD periplasmic extraction mimic (○). Error at pilot-scale was calculated from the standard deviation of triplicate repeat samples of a single run due to scarcity of material. At USD error bars are derived from the standard deviations of triplicate experiments. % extraction has been curve fit and the resultant equation plotted for the pilot-scale (——) and USD (— —) data.

8.3.5 Centrifugal spheroplast removal

8.3.5.1 Pilot-scale prediction of centrifugal dewatering efficiency

E. coli spheroplast suspensions were obtained after the pilot-scale lysis described above from the fermentations with post-induction glycerol feed rates of 1.40, 1.65 and 1.80 mL h^{-1} L^{-1}. Each suspension was separated in an advanced tubular bowl centrifuge, the Carr P6, using an inlet feed rate of 170 mL/h, giving a spin time (t_{comp}) of approximately 22-25 min with the solids concentrations used. This was extended to a standard time of 26 min by manual introduction of a delay of the required time before solids ejection. Spin speed was maintained at 15,000 rpm, giving a RCF of ~19,200 g. As the bowl volume of the centrifuge was 1 L, there were only sufficient solids for one experimental run for each upstream batch.

8.3.5.2 USD prediction of centrifugal dewatering efficiency

E. coli spheroplast suspensions were obtained after the pilot-scale lysis described above from the fermentations with post-induction glycerol feed rates of 1.40, 1.65 and 1.80 mL h^{-1} L^{-1}. The suspension was sheared in the shear cell device described in Hutchinson et al. (2006) for 20 sec at 13,000 rpm in order to mimic the impact of high-shear regions in the centrifuge entry zone leading to potential cell damage and disruption. Subsequently the USD dewatering mimic was used as described in section 2.4.4, with RCF, sediment height and temperature of 19,200 g, 25.4 mm and 10°C respectively, set to match the pilot-scale Carr P6. Spin time, in terms of $t_{compUSD}$, was varied between 6-56 min in order to determine the effects that different inlet flow rates have on dewatering performance (Fig. 8-7). To allow dewatering performance comparison with the pilot-scale data, log curves were fitted to the data points and the predicted dewatering performance at a compaction time of 26 min determined.

E. coli spheroplast suspensions from the fermentations with post-induction glycerol feed rates of 1.04 and 1.58 mL h^{-1} L^{-1} were obtained from the USD periplasmic extraction mimic in order to demonstrate that the USD methods used can provide valid process information when operated entirely independently of initial pilot-scale DSP. The material so obtained was treated identically to the pilot-scale material in all regards, except that there was only enough cell suspension to allow generation of one data point (with four repeats to assess error). Therefore a $t_{compUSD}$ of 26 min was used to allow comparison with the pilot-scale data.

8.3.3.3 Interaction between USP and yield during spheroplast removal

The % dewatering obtained at different post-induction carbon flow rates is compared at both USD and pilot-scale using the standard pilot-scale conditions described above (Fig. 8-8). A linear decrease in dewatering can be observed as the upstream carbon feed rate is increased. This is presumably due to a change in the particle shape and size distribution with post-induction carbon feed rate. The effect of % dewatering upon product yield can be determined using Equation 8-3.

$$Yield = \frac{T_l - \left(\frac{Ts}{\%D/100} - T_s \right)}{T_l} \qquad [8\text{-}3]$$

Where T_l and T_s are the total liquid and solid proportions in the feed respectively (Equations 8-4 and 8-5).

$$T_s = \frac{DCW}{dw_r} \qquad [8\text{-}4]$$

Where DCW is the dry cell weight of the feed (kg/L), dw_r is the cell dry weight to wet weight ratio of a particular cell type (in this case *E. coli* spheroplasts). Assuming the density of the spheroplasts is approximately that of water.

$$T_l = 1 - T_s \qquad [8\text{-}5]$$

Equations 8-3 to 8-5 have been used to convert Fig. 8-8 into Fig. 8-9, which illustrates the effect post-induction carbon feed rate has upon the dewatering yield of the centrifugal spheroplast separation, and therefore the overall yield of the second centrifugal unit operation. A linear equation was used to fit the USD data as this was the lowest order polynomial that gave an R^2 value of > 0.85. A linear equation was also used to fit the more limited pilot-scale data set. It should be noted that, as would be expected from the data presented in Chapter 6, the USD dewatering mimic underpredicts the dewatering level that can be obtained at pilot-scale, and therefore slightly underestimates the yield that can be obtained under standard centrifugation conditions.

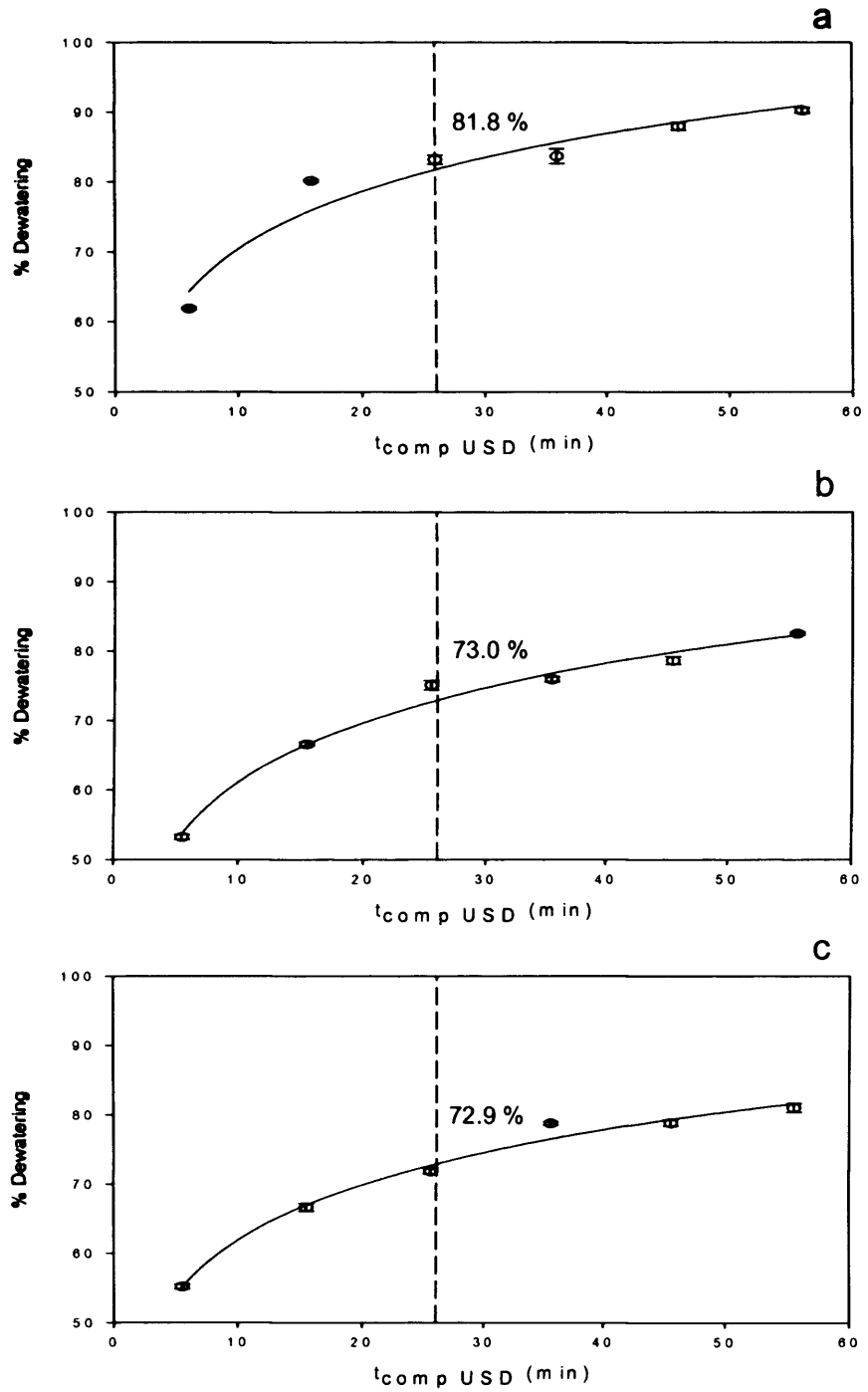

Fig. 8-7: % Dewatering plotted against compaction time for *E. coli* spheroplasts, produced by a pilot-scale extraction, analysed by the USD dewatering method after fermentations using post-induction glycerol feed rates of 1.40 (a), 1.65 (b) and 1.80 mL h^{-1} L^{-1} (c). The % dewatering predicted at a compaction time of 26 min from the log curve fitted to the data is shown on each graph. Error bars are calculated from the standard deviation of four repeat experiments.

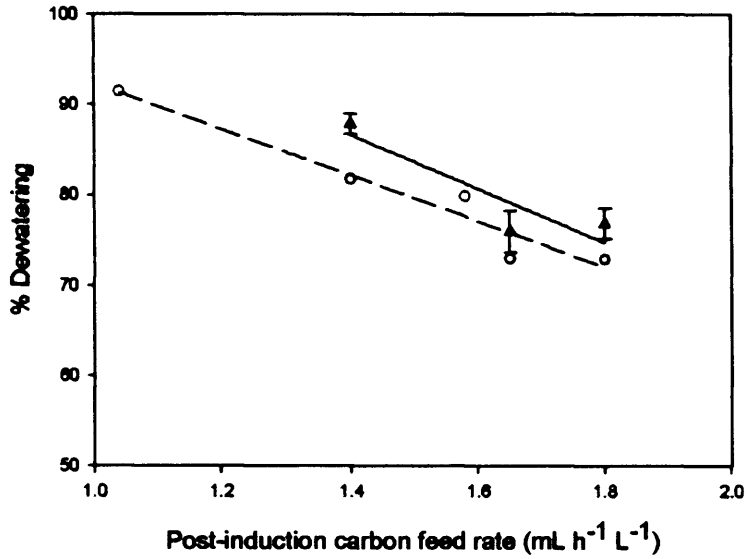

Fig. 8-8: % Dewatering during centrifugal spheroplast removal at constant compaction time, sediment height and RCF of 26 min, 25.4 mm and 19,200 g respectively, using upstream cell material obtained at varying post-induction carbon feed rates. Dewatering data was determined at pilot-scale (▲) and at USD (spheroplasts produced at pilot-scale ○, spheroplasts produced using USD periplasmic extraction ○). % dewatering has been fit to a linear equation and this plotted for the pilot-scale (——) and USD (— —) data. For pilot-scale data, error is estimated by the standard deviation of five measurements of the cell paste obtained during a single experimental run.

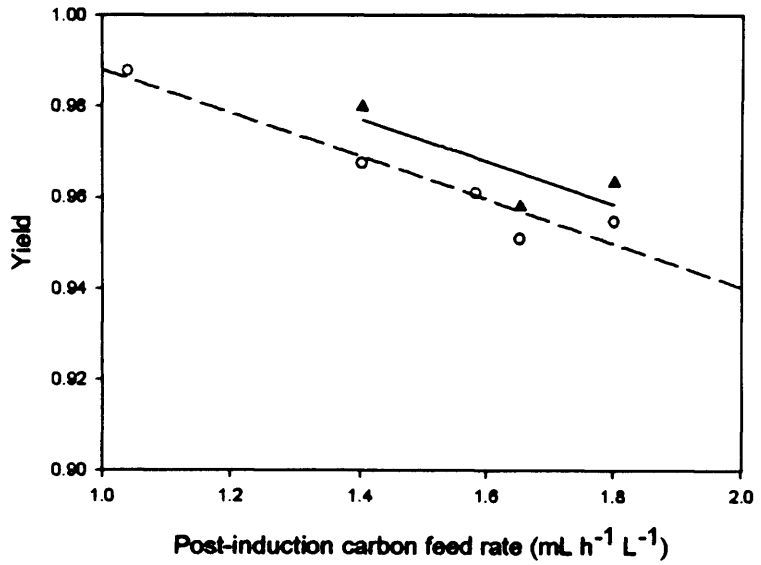

Fig. 8-9: Yield during centrifugal spheroplast removal at constant compaction time, sediment height and RCF of 26 min, 25.4 mm and 19,200 g respectively, using upstream cell material obtained at varying post-induction carbon feed rates. Data was determined at pilot-scale (▲) and at USD (spheroplasts produced at pilot-scale ○, spheroplasts produced using USD periplasmic extraction ○). Yield has been fit to a linear equation and this plotted for the pilot-scale (——) and USD (— —) data.

8.3.6 Interaction between post-induction carbon feed rate and product yield after initial DSP

The yield equations derived earlier were used to create a process model predicting the effect of post-induction carbon feed rate upon yield after initial down stream processing, i.e. after centrifugal spheroplast removal. MATLAB 7.1 was used to calculate process yield for values of x (post-induction glycerol feed rate) between 1 and 2 mL h^{-1} L^{-1}, with yield calculated at 0.01 intervals. The model output is plotted in Fig. 8-10, alongside the yield of the upstream process before DSP initiation, derived from Fig. 8-2.

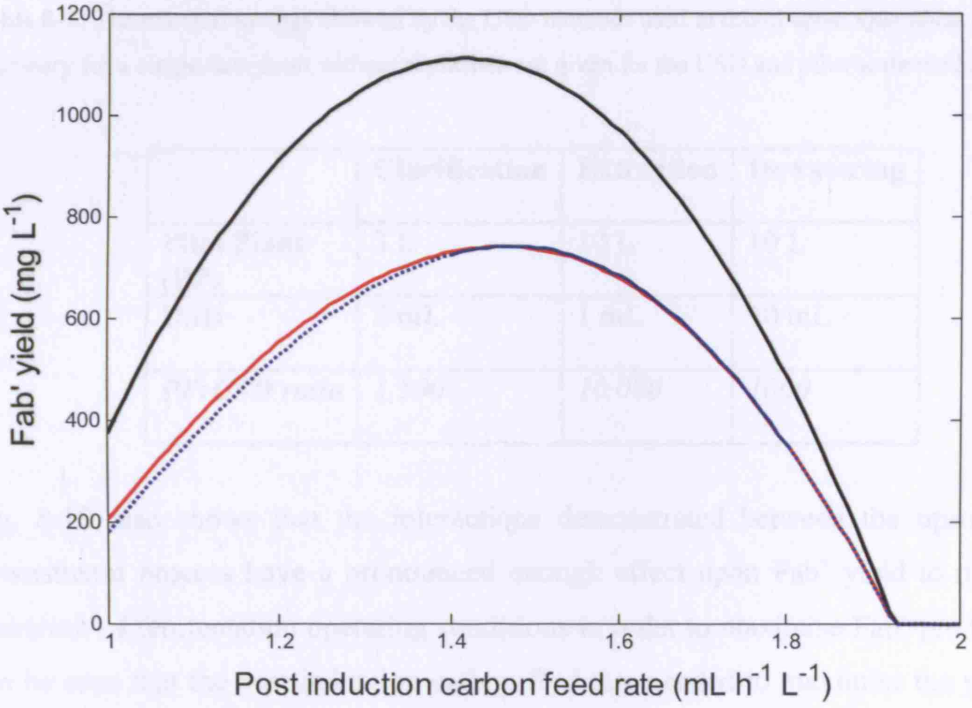

Fig. 8-10: The variation in Fab' yield at different post-induction carbon feed rates at harvest (—) and after initial downstream processing, as indicated by pilot-scale (—) and USD (—) data. As a full pilot-scale set was only available between 1.4-1.8 mL h^{-1} L^{-1}, it was necessary to extrapolate the pilot-scale data (---).

Crucially, Fig. 8-10 shows an extreme similarity between the yields after initial DSP as predicted by USD and pilot-scale data. The USD prediction not only illustrates the same general trends as the pilot-scale data, it is virtually identical. The only section of the curve where any variation exists between the two data sets is for post-induction carbon feed rates from 1.0-1.4 mL h^{-1} L^{-1}: the extrapolated section of the pilot-scale curve. In contrast, the 1.4-1.8 mL h^{-1} L^{-1} region, where both USD and pilot-scale methods have a full data set, the curves are identical. This therefore is likely only due to a lack of pilot-scale data and serves as a warning of the dangers of extrapolation in process

development. Consideration of the reduction in amount of upstream material required for USD studies demonstrates the motivation for using the USD techniques. Table 8-1 compares the amount of upstream material necessary to generate one experimental point at USD and pilot-scale. Application of USD methodology to the process for antibody fragment production in *E. coli* allows the generation of approximately three orders of magnitude more data than pilot-scale experimentation, in addition to the benefit of the increased availability of pilot plant facilities for other work. The increased experimentation allowed facilitates both an increased number of experimental conditions to be evaluated and an increased number of replicates at each condition.

Table 8-1: The material savings allowed by the USD methods used in this chapter. Quantities of material necessary for a single data point without replicates are given for the USD and pilot-scale methods used.

	Clarification	**Extraction**	**Dewatering**
Pilot Plant (PP)	3 L	10 L	10 L
USD	2 mL	1 mL	10 mL
PP:USD ratio	*1,500*	*10,000*	*1000*

Fig. 8-10 also shows that the interactions demonstrated between the upstream and downstream process have a pronounced enough effect upon Fab' yield to necessitate alteration of fermentation operating conditions in order to maximise Fab' production. It can be seen that the post-induction carbon feed rate needed to maximise the yield after the initial downstream process steps is higher than that predicted by consideration of the upstream process alone. A shift in the glycerol feed rate operating range of approximately + 0.5 mL h^{-1} L^{-1} would increase the yield after initial DSP by ~ 5%. The most significant process interaction demonstrated is therefore that between the upstream process and the periplasmic extraction procedure, as both the first and second centrifugation steps were found to have an inversely proportional relationship between Fab' yield and post-induction carbon feed rate. This illustrates the necessity to consider all unit operations when considering intra-process interactions. For example, if only the interaction between fermentation and centrifugation were considered, it may have appeared that post-induction process feed rate must be reduced in order to maximise yield. This suggests that further work should be undertaken to determine if the optimal feed rate is changed yet again as additional DSP operations are included in the analysis,

e.g. chromatographic separations. This may be the case for product quality and the contaminant profile, yet it seems unlikely that interactions between fermentations and chromatographic separation would impact process yield, as cellular material/debris is removed by this stage in the process.

8.4 Conclusions

Three interactions between the upstream process parameter, post-induction carbon feed rate, and the downstream process have been defined. At too low a feed rate insufficient energy and carbon supply for maximal Fab' production leads to a low Fab' yield while too high a feed rate leads to Fab' leakage and eventually cell lysis. Therefore an optimal feed rate exists and requires determination.

The first interaction defined was with the performance of cell harvest during centrifugation. Specifically, the post-induction feed rate was found to alter clarification efficiency: the clarification efficiency was shown to peak at approximately the point of maximal Fab' production. Above this point the increased leakage of Fab' and periplasmic material will tend to reduce cell size, and there will be an increased presence of cell debris from the increasing incidence of lysed cells. Below the optimum, growth will be carbon limited, and as a result less Fab' is produced and the cells will possibly be slightly reduced in size.

A second interaction was defined between the upstream process parameter and the effectiveness of the periplasmic extraction unit operation. The periplasmic extraction protocol was seen to be more effective using cells produced at higher post-induction carbon feed rates. The most likely physiological reason for this relationship is a weakening in periplasmic membrane integrity at higher carbon feed rates, as also indicated by increased Fab' leakage and eventually cell lysis with progressive increases in feed rate.

The final interaction defined was between the upstream parameter and the centrifugal spheroplast removal unit operation. Here, dewatering efficiency was the only centrifugal parameter altered by the fermentation feed rate found to alter Fab' yield during the centrifugal unit operation. A small linear decrease in dewatering was observed as the upstream carbon feed rate increased. This was presumably due to a change in the particle shape and size distribution with post-induction carbon flow rate.

A process model was created, using the interactions defined, to determine the effect changes in the upstream parameter have upon Fab' yield after the initial DSP, to the point of cell removal, when standard processing conditions are used. This model indicated that the fermentation feed rate needed to maximise the yield after the initial downstream steps is higher than that predicted from consideration of the fermentation alone. The suggested shift in the operating range of the upstream parameter would increase the yield after initial DSP by ~ 5%. This demonstrated the necessity to consider process interactions during process development and optimisation. Furthermore, the high level of agreement between pilot-scale and USD data demonstrates the usefulness and potential of USD as a methodology to provide timely decision-making support, both early in the drug development pathway when process material is limited and in high demand, and also during later process development (Zhang et al., 2007). The USD methods used were able to provide a valid data set even in the absence of any pilot-scale material after the initial fermentation. Application of USD methodology during later process development can greatly increase the number of experiments that can be performed on a process without need for increased pilot plant utilisation to either perform the trials or to supply multiple batches of process material. The increased data set thus generated, especially if used in conjunction with intelligent use of statistical design of experiments techniques, can greatly facilitate PAT incorporation into a manufacturing process (Low et al., 2007), aid process validation in conjunction with the FDA QbD initiative (Yu, 2006), and allow the creation of a more effective process using the insights gained into interactions within the process flowsheet.

9. Discussion of cryopreservation as a mechanism of long-term storage of upstream cell material for later downstream process development

9.1 Abstract

In order to allow time for detailed USD analysis of DSP unit operations it would be convenient to store cells without damage for a prolonged period of time following harvest. As cryopreservation is capable of facilitating storage of cellular material for time periods of greater than ~ 48 hrs, a variety of freezing protocols were investigated to determine if freeze-storage was a viable option, or whether all DSP experiments must be performed on fresh material.

Multi-parametric flow cytometry is shown to be a powerful technique for rapidly obtaining *E. coli* physiological information. Dilution plating and flow cytometry were used to assess cellular freeze/thaw damage.

Freezing cell harvest from an IPTG-induced fermentation in a -80°C chest freezer was shown to result in widespread cell damage and death, even with the addition of 15% glycerol as a cryoprotectant. Subsequent freeze/thaw studies using *E. coli* grown in complex media showed widespread differences in cell survival dependant upon cooling rate and the presence of cryoprotectant. This indicated that the damage induced by cryopreservation is highly dependant upon the metabolic state of the cells. Also, no suitable method for obtaining > 95% cell survival was determined. It was concluded that the likely time and financial input for optimising a cryopreservation technique would outweigh the potential benefits. This line of study was not taken further.

9.2 Introduction

9.2.1 Motivation for assessment of cryopreservation as a mechanism of long-term storage of upstream cell material

The process for antibody fragment production studied is operated continuously. Cells are grown, harvested, permeablised and removed without temporal pause. This minimises concerns about damage to the cells or product during storage. Yet in order to allow time to carry out detailed USD analysis it would be convenient to store cells for a

prolonged period of time following harvest. This would allow both USD and pilot-scale tests to be carried out on cells from a single fermentation. In addition, long-term storage would allow secondary tests to be performed on the same material used in the primary tests, after data analysis and processing. However, all techniques presently available for the storage of cellular material will manifestly affect cell properties, invalidating tests on stored material to a greater or lesser degree. The least damaging techniques used for the long-term storage of living cells are cryopreservation and lyophilisation (freeze-drying). For the current study lyophilisation is undesirable as it introduces extra steps where damage will occur to a significant percentage of the cell population: drying and re-hydration. Therefore only cryopreservation has been investigated.

9.2.2 Mechanisms of cell damage during freezing

There are two main mechanisms by which freezing can damage cells, depending upon the rate of cooling. At low freezing rates cellular dehydration is the main cause of damage. Freezing is a probabilistic process and, in most cases, the extracellular solution has a higher volume than the intracellular solution. Also biological solutions *in vivo* can usually supercool a few degrees or more. For these reasons extracellular freezing occurs before intracellular freezing. This concentrates the extracellular solutes in a small quantity of unfrozen water, increasing the osmotic pressure of the medium and causing water to leave the cells (Wolfe and Bryant, 2001). Extensive water loss can kill cells in a variety of ways. Solutes can be concentrated to toxic levels. The changing ionic strength caused by dehydration can denature vital proteins. The lipid cellular membrane can be badly damaged during contraction. The large transient electric field associated with an advancing ice front in a weak electrolyte solution causes a potential difference across the cells, which is large enough to rupture membranes (Steponkus et al., 1985). The membrane can also be disrupted by a lack of water molecules available to hydrate the membrane, and therefore altering its physical state.

At high freezing rates, insufficient cellular dehydration occurs after extracellular freezing to prevent the formation of intra-cellular ice crystals. These can damage the cells by a variety of mechanisms. Ice is a poor solvent compared to liquid water; therefore the remaining intracellular water may have toxic levels of solutes. Furthermore, ice and water interact differently with hydrophilic surfaces. This is important because the surface tension of water is involved in maintaining the native

state of enzymes and lipid bilayers (Wolfe and Bryant, 2001). Ice crystals may also directly damage cell structure by volumetric expansion (Mazur, 1970).

Once the cell is frozen all processes of injury and metabolism are effectively halted provided the temperature is maintained below approximately -60°C (Mazur, 1966), although damage can occur during storage if the now brittle sample is subjected to mechanical shock.

9.2.3 Determinants of the extent of cell damage induced by a freeze-thaw cycle

As well as the freezing rate the main factors determining the extent of cell damage induced by a freeze-thaw cycle are: the type or species of the frozen cells; the cell state upon freezing (e.g. its growth phase); the composition of the surrounding medium; and the presence or absence of cryoprotective substances.

The ideal freezing regime would minimise cell damage by cooling a cell quickly enough to avoid excessive dehydration but sufficiently slowly that the cell contents become concentrated to a level where intracellular ice formation is avoided. This is easier in theory than practise because of the vast range of factors that determine this rate, and because some cells can not be dehydrated to an extent that would prevent internal freezing with significant dehydration damage. Mazur (1966) made an attempt to estimate a general plot of approximate survival of *E. coli* as a function of cooling velocity and determined an ideal freezing rate of 10-100°C min^{-1}.

It is also possible to freeze the cells so quickly (~ 10^{4}°C/min) that the intracellular water will either vitrify to a glassy state or the ice crystals will not have time to form to a sufficient size and stability to damage the cell. However, this method of avoiding intracellular ice formation requires storage below a critical temperature and fast thawing in order to avoid recrystallization and crystal growth and modification. The maximum temperature at which cells can be stored so as to avoid recrystallisation varies from species to species. In *E. coli* it can be prevented if the temperature remains above about -30°C (Heckly, 1985). For this reason fast cooled cells should be fast thawed, while for slow cooled cells the rate of thawing is immaterial to subsequent viability.

The size and surface area to volume ratio of the cell to be frozen is another key factor in determining the amount of cellular damage that occurs upon cell freezing. For example,

Saccharomyces cerevisiae exhibits intracellular ice formation at a cooling rate of around 10°C/min whereas *E. coli* becomes sufficiently dehydrated at this cooling rate to avoid ice damage (Mazur, 1970). Although there is great variation in susceptibility to ice damage it is possible to see a general trend in cell types and cell damage. Organisms that are reasonably tolerant to dehydration or to immersion in concentrated non-penetrating solutes at room temperature will survive best if cooled at around 1°C/min. Intracellular ice is unlikely to form at this cooling velocity in any but the largest of cells with their high surface area to volume ratio reducing the rate of water loss. Conversely, small or highly permeable cells that are highly sensitive to altered concentrations of external solutes should be cooled rapidly at 10°C/min or more. This higher cooling rate will lessen the exposure to solutes and might still be sufficiently slow as to preclude intracellular ice. Difficulties arise in avoiding injury during the freezing of cells that are both large and also sensitive to altered solute concentrations, such as mammalian cells.

The metabolic state of the cell is also a key factor in determining the extent of damage caused by freezing. In both *E. coli* and *Saccharomyces cerevisiae* growth phase has been shown to alter sensitivity. Early log phase cells are much more sensitive than stationary or lag phase cells (Hollander and Toyokawa, 1956; Park et al., 2005). Aerobically growing *E. coli* are less susceptible to ice damage than anaerobically growing cells (Nei et al., 1967). The resistance of yeast cells is lower during the fermentative growth phase than during the respiratory growth phase (Park et al., 2005). Generally, cells which are more resistant to oxygen damage survive freezing better. More specific evidence for this is given by experiments with alfalfa expressing a high level of superoxide dismutase (McKersie et al., 2005). More uncommon metabolic processes can also alter a cells susceptibility to damage. For example, the halotolerant alga *Dunaliella* stores glycerol intracellularly in high salt conditions, which acts as a cryopreservant during freezing (Levy and Zamir, 1994).

Cells reacting to environmental stress are commonly more resistant to freezing injury. Yeast cells which are adapted to osmotic shock are more tolerant to freezing (Park et al., 2005), and although cold shock does not increase tolerance to freezing in yeast, temperature shocked *E. coli* are more tolerant to freezing (Mazur, 1966).

The extracellular freezing medium can alter the extent of freeze/thaw damage. Usually this is simply due to the osmotic affect of dehydration of cells occurring faster in media

with a higher concentration of electrolytes. It has also been noted that higher cell concentrations tend to exhibit slightly less percentage damage than lower cell concentration (Packer et al., 1965).

The presence of certain chemicals, known as cryoprotectants, in sufficient concentrations can protect cells from freeze-thaw damage. There are two types of cryoprotectant defined by their ability to cross the cell membranes: penetrating (e.g. glycerol, dimethylsulphoxide (DMSO), and ethylene glycol) and non-penetrating (e.g. dextran, sucrose, and trehalose).

A typical penetrating cryoprotectant, such as DMSO, has little effect upon the damage caused by intracellular ice, as cell survival remains low if rapid cooling is done before the cells have had a chance to dehydrate. However, slow cooling injury can be greatly reduced. Penetrating cryoprotectants eliminate slow cooling injury by penetrating the membranes and acting to reduce the increase in salt concentration (McGann, 1978; McGann, 1979). Interestingly, the penetrative cryoprotective agent glycerol is also produced naturally in some organisms to alleviate osmotic stress (Levy and Zamir, 1994).

Non-penetrating cryoprotectants allow cooling at higher rates without the formation of lethal intracellular ice. They give no protection against slow cooling injury. Non-penetrating cryoprotectants are thought to act by dehydrating the cell at high sub-freezing temperatures, thereby allowing them to be rapidly cooled without the formation of intra-cellular ice. These compounds are generally polymers that form extensive hydrogen-bonds with water, reducing the water activity to a much greater extent than would be predicted by their molar concentration. Some of these compounds are used by organisms for this reason to protect against high osmotic strength in the growth medium. For example, *E. coli* synthesise trehalose intracellularly in high osmotic strength medium (Larsen et al., 1987).

9.2.4 Freeze-thaw issues specific to industrial process under consideration

There are three main issues specific to the use of cryopreservation to preserve upstream *E. coli* cellular material for later downstream analysis. Firstly, the use of cryopreservants is undesirable as their subsequent presence in later USD analysis may alter the performance of the mimic. Secondly, the fact that cell damage is dependent on

cell metabolic state complicates cryopreservation studies, as the freeze/thaw protocol must be shown to cause minimal cell damage in all metabolic states. Thirdly, there is some evidence that the periplasmic membrane of *E. coli* is especially susceptible to freezing damage, probably as it is exposed to extracellular ice. This will complicate the assessment of freeze-thawed material as the integrity of the outer membrane has been shown to be an important process parameter in the performance of the periplasmic extraction unit operation (Chapter 7). Freezing affects the LPS structure in such a way that the cells become sensitive to lysozyme, surface active agents, and antimycin D. They also fail to adsorb many phages (Kempler and Ray, 1978). Biochemical analysis indicates that heptose may be lost from the LPS. All this damage seems linked to dehydration of the membrane (LPS are normally highly hydrated) due to ice replacing liquid water. This damage has been seen to be greatly alleviated by the addition of 10% glycerol in the medium (Souza, 1980), perhaps by keeping enough water unfrozen around the cell surface to stabilise the LPS structure (Ray et al., 1975).

9.2.5. Flow cytometry as a method for assessing bacterial cell damage

In Chapter 4 the diversity of techniques that can be used to assess various forms of damage to bacterial cells was discussed. Flow cytometry is a powerful technique that can be used for the rapid characterisation of damage to cell populations at the single cell level.

During flow cytometry, cells pass individually through a laser beam and the resultant scattered light is collected in two planes. Forward angle light scatter (FS) is measured in the plane of the beam and gives relative information on cell size. Right or side angle light scatter (SS) is measured at 90° to the beam and can provide information on cell granularity, although for most microbial applications FS and SS are highly correlated. With the addition of specific fluorescent dyes, important information on cell viability and physiology can be obtained (Hewitt et al., 1998; 1999a; 1999b). For example, propidium iodide (PI) staining can be used to measure cell permeability. This dye binds to nucleic acids, but cannot cross an intact cytoplasmic membrane, therefore PI staining indicates a loss of cell membrane integrity. Fluorescent dyes can also detect metabolic state. For example, the lipophilic anionic dye Bis-(1,3-dibutylbarbituric acid)trimethine oxonol (BOX) accumulates inside cells providing the cytoplasmic membrane potential is reduced, and therefore can be used to indicate the lack of protonmotive force (Sundstrom et al., 2004). Emitted light from any fluorescent stains added to the sample

is measured at the 90° angle using detectors of specific wavelength. This information, coupled with the rapid throughput of thousands of individual cells per second, provides real-time, statistically reliable information on cell physiology and viability and therefore can give a rapid, detailed analysis of the damage caused by freeze/thaw (Hewitt and Nebe-von-Caron, 2004).

Despite its advantages, multi-parameter flow cytometry analysis of cell damage must be complemented by supplementary techniques as, compared with the analysis of mammalian cells, the use of flow cytometry for analysis of bacteria is much more difficult and less substantiated. This is because the application of flow cytometry to bacterial cells is complicated by their smaller size (Al-Rubeai and Emery, 1996).

9.3 Results and discussion

9.3.1 Flow cytometry controls

Multi-parameter flow cytometry has been used successfully to indicate *E. coli* physiological state in order to characterise, for example, multiple batch (Lewis et al., 2004) and fed-batch (Hewitt et al., 1999b) fermentations, inclusion body formation (Wallberg et al., 2005), antibiotic effects (Jepras et al., 1997), the impact of fluid mechanical stress (Hewitt et al., 1998), fermentation scale-up issues (Hewitt et al., 2000; Onyeaka et al., 2003) and the monitoring of active but non-cultural cells (Sachidanandham et al., 2005). However, in order to prove that the method was capable of providing meaningful results under the conditions used in this study, both positively and negatively stained control samples were prepared.

One vial of WCB was added to 200 mL of 2 x PY medium and incubated at 37°C. A growth phase sample was taken after 5 h of incubation and analysed in the flow cytometer both unstained (Fig. 9-1A) and stained with BOX and PI (Fig. 9-1B). After 24 h of incubation a stationary phase sample was stained and analysed in the same way (Fig. 9-1C). The stationary phase sample was also analysed after heat treatment (80°C for 15 min) in order to give a positively stained control (Fig. 9-1D).

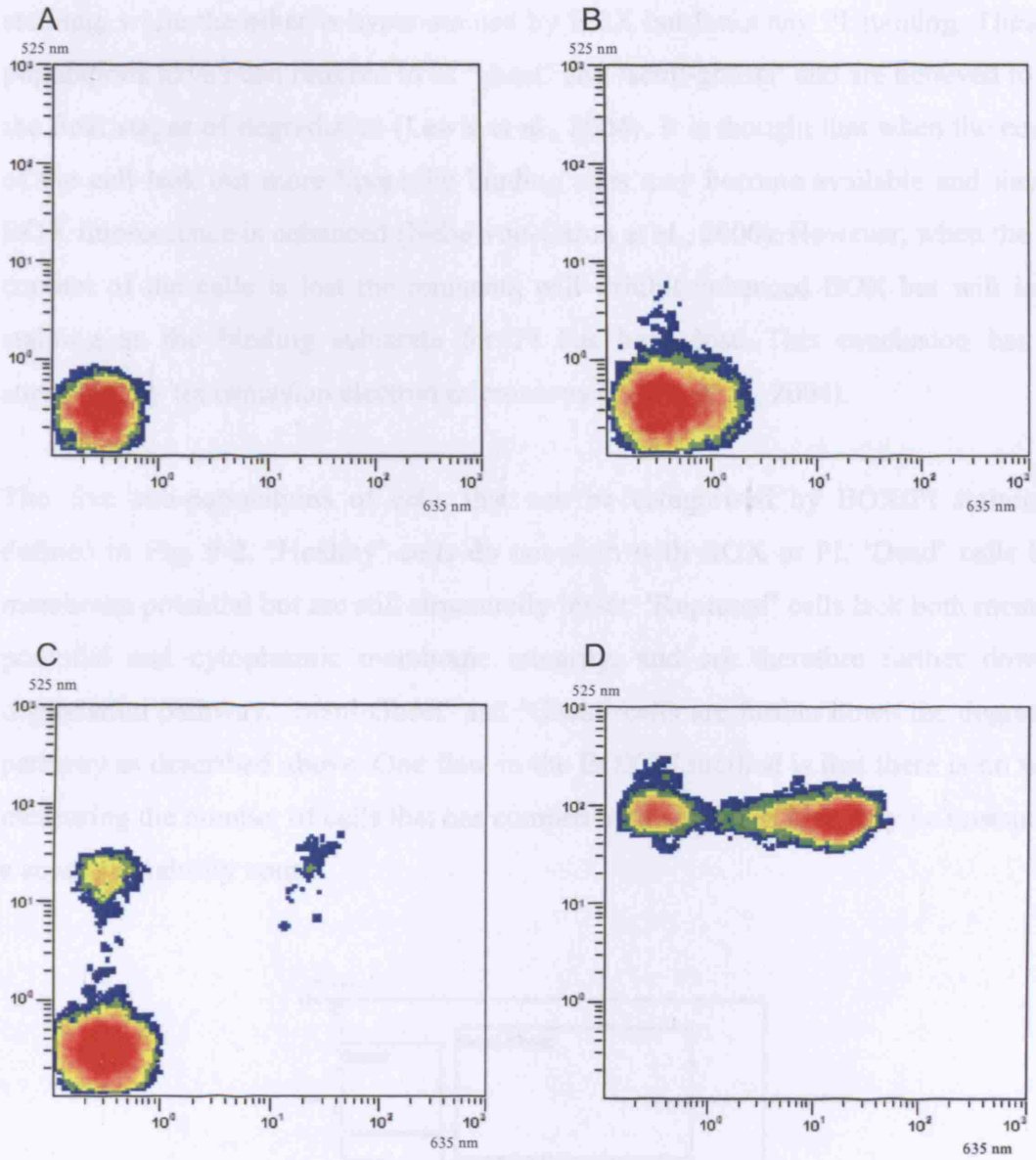

Fig. 9-1: Control samples illustrating functionality of flow cytometric method used. Four density plots are shown illustrating the extent of BOX or PI emitted fluorescence for each cell, at 525 nm or 635 nm respectively. A control unstained sample is shown (A), alongside healthy *E. coli* cells in mid growth phase (B), cells in the stationary phase (C) and heat treated cells (D) (80°C for 15 min).

These data show that in the growth phase the vast majority of cells appear healthy and stain with neither PI nor BOX: the spectrograph resembles an unstained sample. However, as the fermentation progresses into the stationary phase significant numbers of cells exhibit BOX fluorescence indicating the lack of membrane potential, therefore cell death. Some cells also exhibit PI fluorescence indicating a loss of cell membrane integrity in addition to the lack of membrane potential indicated by the BOX stain. Drastic heat treatment at 80°C for 15 min would be expected to damage severely *E. coli* cells and this can be observed with the emergence of two new sub-populations of stained cells. One group of cells are hyper-stained with BOX and also exhibit PI

staining, while the other is hyper-stained by BOX but lacks any PI staining. These cell populations have been referred to as 'ghost' and 'semi-ghosts' and are believed to be in the final stages of degradation (Lewis et al., 2004). It is thought that when the contents of the cell leak out more lipophilic binding sites may become available and therefore BOX fluorescence is enhanced (Nebe-von-Caron et al., 2000). However, when the DNA content of the cells is lost the remnants will exhibit enhanced BOX but will lack PI staining as the binding substrate for PI has been lost. This conclusion has been supported by transmission electron microscopy (Lewis et al., 2004).

The five sub-populations of cells that can be categorised by BOX/PI staining are defined in Fig. 9-2. 'Healthy' cells do not stain with BOX or PI. 'Dead' cells lack a membrane potential but are still structurally intact. 'Ruptured' cells lack both membrane potential and cytoplasmic membrane integrity, and are therefore further down the degradation pathway. 'Semi-Ghost' and 'Ghost' cells are further down the degradation pathway as described above. One flaw in the BOX/PI method is that there is no way of measuring the number of cells that has completely degraded. These may be measured by a separate viability count.

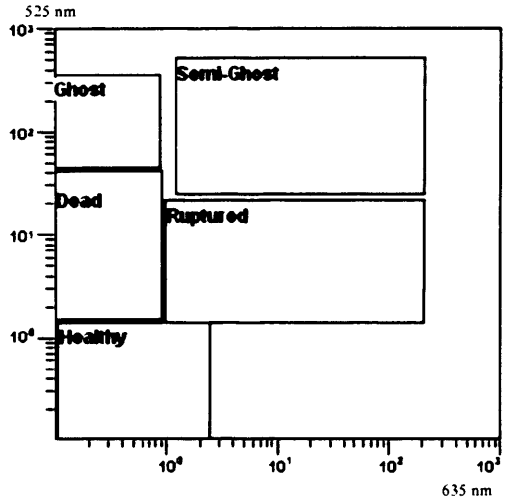

Fig. 9-2: Schematic of flow cytometry spectrograph showing the different categories of cell population that can be identified by PI and BOX.

9.3.2 Assessment of freeze/thaw protocol to IPTG-induced process

Flow cytometry was used to assess the extent of cell damage induced during cryopreservation of harvest from a 20 L IPTG-induced fermentation using a simple freeze/thaw procedure. The fermentation was performed using a post-induction glycerol feed rate of 1.7 mL h^{-1} L^{-1}, and harvested 36 h after the addition of IPTG (the point of

induction). This feed rate was chosen as it was the median point between the optimum flow rate for Fab' production (1.4 mL h^{-1} L^{-1}) and the highest possible (2.0 mL h^{-1} L^{-1}), above which all detectable Fab' is lost into the external medium at this harvest time. Therefore the cells produced were of median strength, in terms of cellular integrity. The penetrative cryoprotectant glycerol was added to a final concentration of 15% (w/v), in order to protect against slow cooling injury, before a 40 mL sample was frozen in an agar plate at -80°C using a chest freezer. This was found to give a cooling rate of approximately 2°C/min via separate measurement of the cooling rate of water under these conditions using a K-type wire thermocouple attached to the Squirrel SQ1600 data logger. The cells were subsequently stored for 2 days at -80°C prior to thawing at room temperature before analysis. The storage time is immaterial to the extent of cell damage as storage of cellular material below ~ -60°C has been shown to eliminate virtually all metabolic activity and therefore cells can remain viable for many years below this temperature (Mazur, 1966). Likewise the speed of thawing should have no impact upon cell survival due to the slow rate of cooling.

Cells were analysed by PI/BOX flow cytometry both immediately after harvest (Fig. 9-3A), and the freeze/thaw procedure (Fig. 9-3C). Table 9-1 details the % of total detected cells that fell in each of the five sub-populations, as defined in Fig. 9-3B and 9-3D. It can be seen that after the fermentation a majority of cells are healthy. In addition, the vast majority of non-healthy cells have only begun to degrade, and still retain intact membranes. The spectrograph obtained resembles that found with other W3110 *E. coli* fed-batch fermentations (Hewitt et al., 2000; Onyeaka et al., 2003). However, this cell population was dramatically changed by the freeze/thaw protocol. Here, despite the addition of glycerol as a cryoprotectant, less than 10% of cells are healthy, with the majority transitioning between the 'ruptured' and 'semi-ghost' state. These results indicate the freeze/thaw protocol must be vastly improved if cryopreservation is to be considered as a method for the long-term storage of upstream material in a state suitable for DSP studies.

9.3.3 Cryopreservation protocol optimisation studies

The major drawback to this study is that many of the parameters that can affect cell freeze/thaw survival also alter the cell properties; compromising subsequent experiments performed using the thawed material. For example, the major cryoprotectant used for mammalian cell work, DMSO, alters the permeability of the cell

membrane. Moreover, other key determinants of cell survival are properties of the cells themselves, such as size, growth phase, and metabolic state. Therefore the only two parameters varied were the presence of cryoprotectant and freezing time.

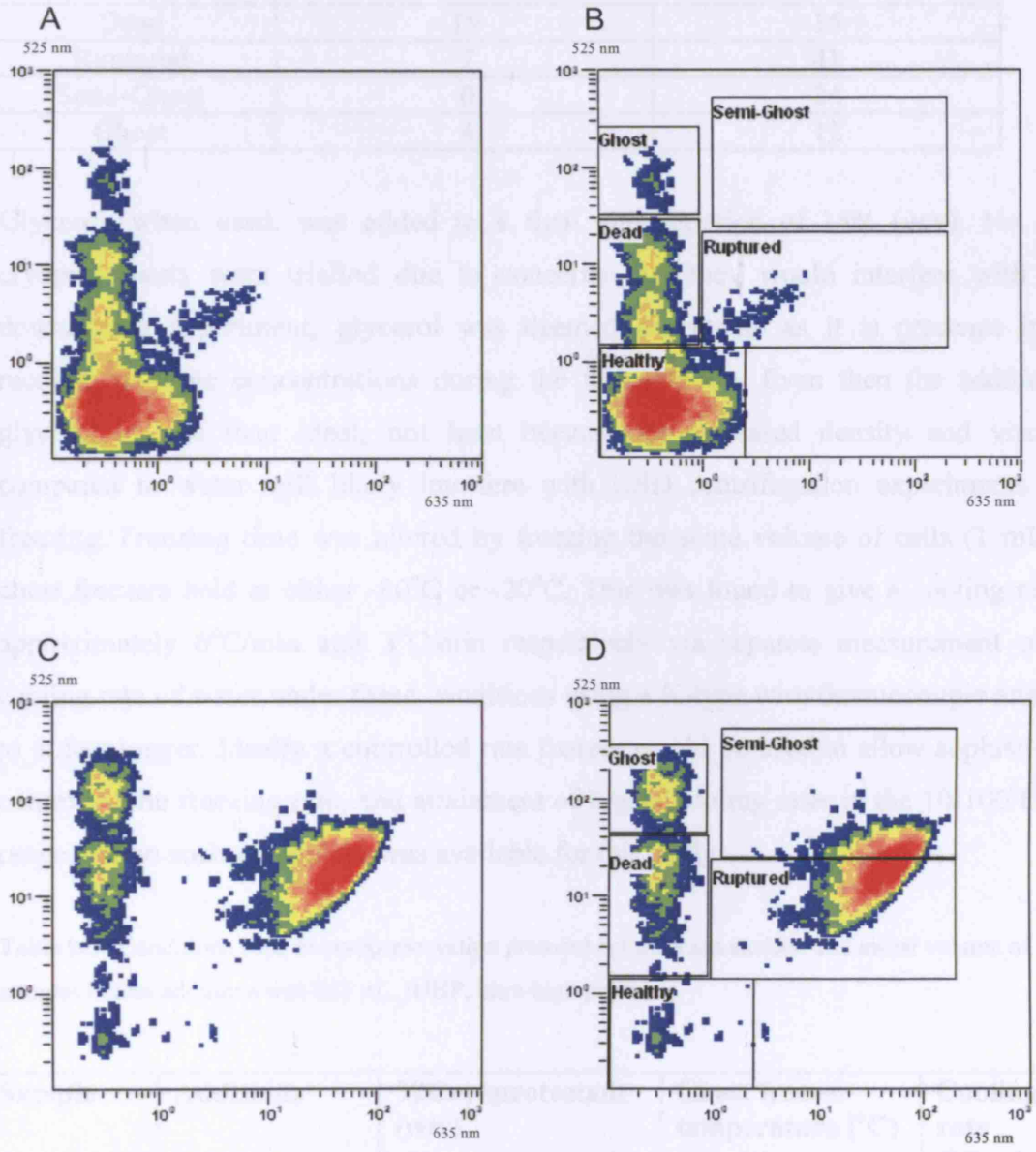

Fig. 9-3: PI/BOX stained flow cytometry spectrograph indicating physiological state of cells from the IPTG-induced process at harvest (A) and after a freeze/thaw cycle (C). The cells were sub-divided into five populations as indicated in (B) and (D) for the harvest and freeze thawed sample respectively.

Table 9-1: The percentages of total cells within each of the five cell sub-population boundaries defined in Fig. 9-2 for the fermentation endpoint and freeze/thawed samples.

Cell sub-population	Fermentation harvest (%)	Freeze-thaw sample (%)
Healthy	69	7
Dead	19	15
Ruptured	7	41
Semi-Ghost	0	24
Ghost	4	12

Glycerol, when used, was added to a final concentration of 15% (w/v). No other cryoprotectants were trialled due to concerns that they would interfere with later downstream experiment; glycerol was deemed acceptable as it is presence in the medium in large concentrations during the fermentation. Even then the addition of glycerol is less than ideal, not least because its increased density and viscosity compared to water will likely interfere with USD centrifugation experiments after freezing. Freezing time was altered by freezing the same volume of cells (1 mL), in chest freezers held at either -80°C or -20°C. This was found to give a cooling rate of approximately 6°C/min and 3°C/min respectively via separate measurement of the cooling rate of water under these conditions using a K-type wire thermocouple attached to a data logger. Ideally a controlled rate freezer would be used to allow sophisticated control of the freezing rate, and attainment of higher cooling rates in the 10-100°C/min range, but no such equipment was available for this study.

Table 9-2: Conditions used in cryopreservation protocol optimisation studies. The initial volume of all samples before additions was 813 µL. (UHP, ultra-high purity).

Sample	Additions	%Cryoprotectant (w/v)	Chest freezer temperature (°C)	Cooling rate (°C/min)
Control	187 µL UHP water	0	Not frozen	n/a
Fast cool	187 µL UHP water	0	-80	6
Glycerol fast cool	187 µL 80% (w/v) glycerol	15	-80	6
Slow cool	187 µL UHP water	0	-20	3
Glycerol slow cool	187 µL 80% (w/v) glycerol	15	-20	3

Cryopreservation optimisation studies were carried out using the first step in the seed train, cell resurrection in complex media, to minimise the experimental burden. One vial of WCB was added to 200 mL of 2 x PY medium and incubated at 37°C. 5 h post-inoculation a growth phase sample was prepared as shown in Table 9-2. 24 h post-inoculation a stationary phase sample was assessed using the same protocol. After thawing at room temperature cell survival was assessed by dilution plating, in terms of percentage viable cells compared to the control (Fig. 9-4), and PI/BOX stained multi-parameter flow cytometry, in terms of percentage of healthy cells compared to the control (Fig. 9-5). For both growth and stationary phase cells the presence of 15% (w/v) glycerol in the medium as a cryoprotectant increased cell survival for both rates of cooling. Dilution plating results indicated that the faster rate of cooling increased cell survival both with and without glycerol at both stationary and growth phase. Flow cytometry also indicated that fast cooling increased cell survival both with and without glycerol with growth phase cells, but the results for stationary phase cells were less conclusive. Both dilution plating and flow cytometry show a large interaction between cooling rate and presence of glycerol for growth phase cells, with both fast cooling and glycerol required to obtain more than 10% cell survival with growth phase cells. This is unsurprising as glycerol is a slow cooling penetrating cryoprotectant and therefore protects against dehydration injury, allowing reduced cooling rates.

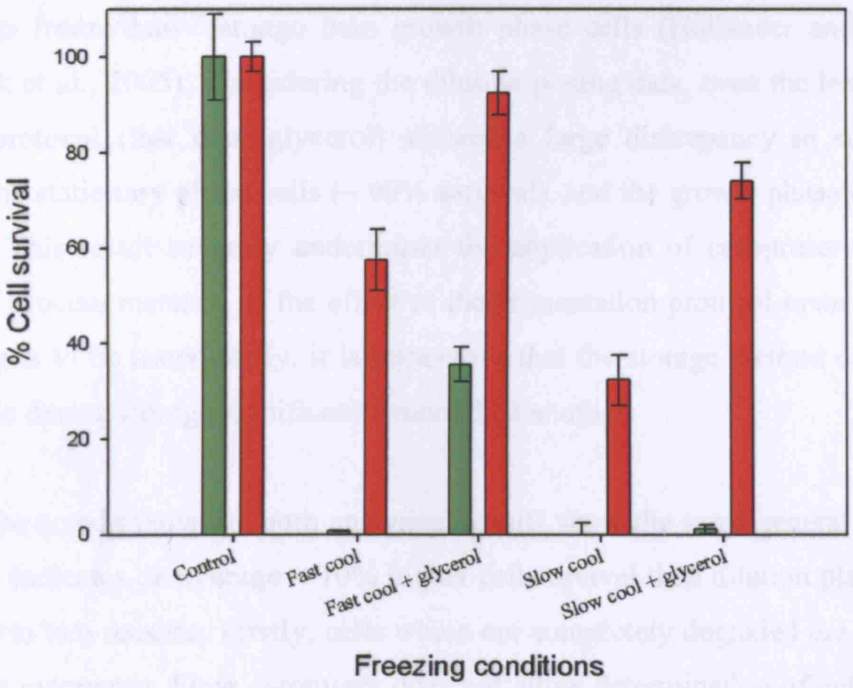

Fig. 9-4: Survival of cells frozen under a variety of conditions in mid-growth (■) and stationary (■) phase, determined by dilution plating. Error is estimated from the standard deviation of triplicate experimental runs.

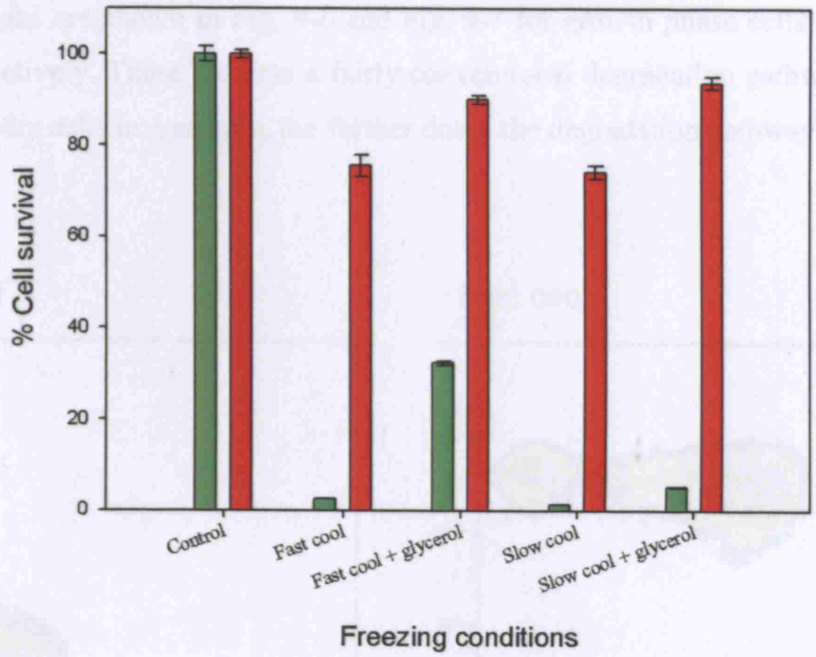

Fig. 9-5: Survival of cells frozen under a variety of conditions in mid-growth (■) and stationary (■) phase, determined by PI/BOX multi-parameter flow cytometry. Cells are judged to have survived freezing if they stain with neither PI nor BOX. To allow ease of comparison with the results from dilution plating results have been normalised so that the control sample represent 100 % cell survival. In actuality only 93 % and 90 % of cells remained unstained in the growth and stationary phase samples respectively. Error is estimated from the standard deviation of triplicate sample measurements.

As described in the literature, stationary phase cells were found to be much more resistant to freeze/thaw damage than growth phase cells (Hollander and Toyokawa, 1956; Park et al., 2005). Considering the dilution plating data, even the least damaging freezing protocol (fast cool glycerol) showed a large discrepancy in survival rates between the stationary phase cells (~ 90% survival), and the growth phase cells (~ 30% survival). This result severely undermines the application of cryopreservation to the storage of process material. If the effect of the fermentation protocol upon downstream processing is to be tested fairly, it is imperative that the storage method does not alter one sample during storage significantly more than another.

It should be noted that while both analytical results show the same general trends, flow cytometry indicates on average ~ 10% higher cell survival than dilution plating. This is likely due to two reasons. Firstly, cells which are completely degraded are not detected using flow cytometry. Flow cytometry does not allow determination of cell survival as such, only the quantity of healthy cells as a percentage of the total number in suspension. Therefore flow cytometry is only a semi-quantitative technique, and the spectrographs

produced must always be considered in addition to quantitative data. Representative spectrographs are shown in Fig. 9-6 and Fig. 9-7 for growth phase cells and stationary cells respectively. These indicate a fairly conventional degradation pathway, where the fewer healthy cells in a sample, the further down the degradation pathway the unhealthy cells are.

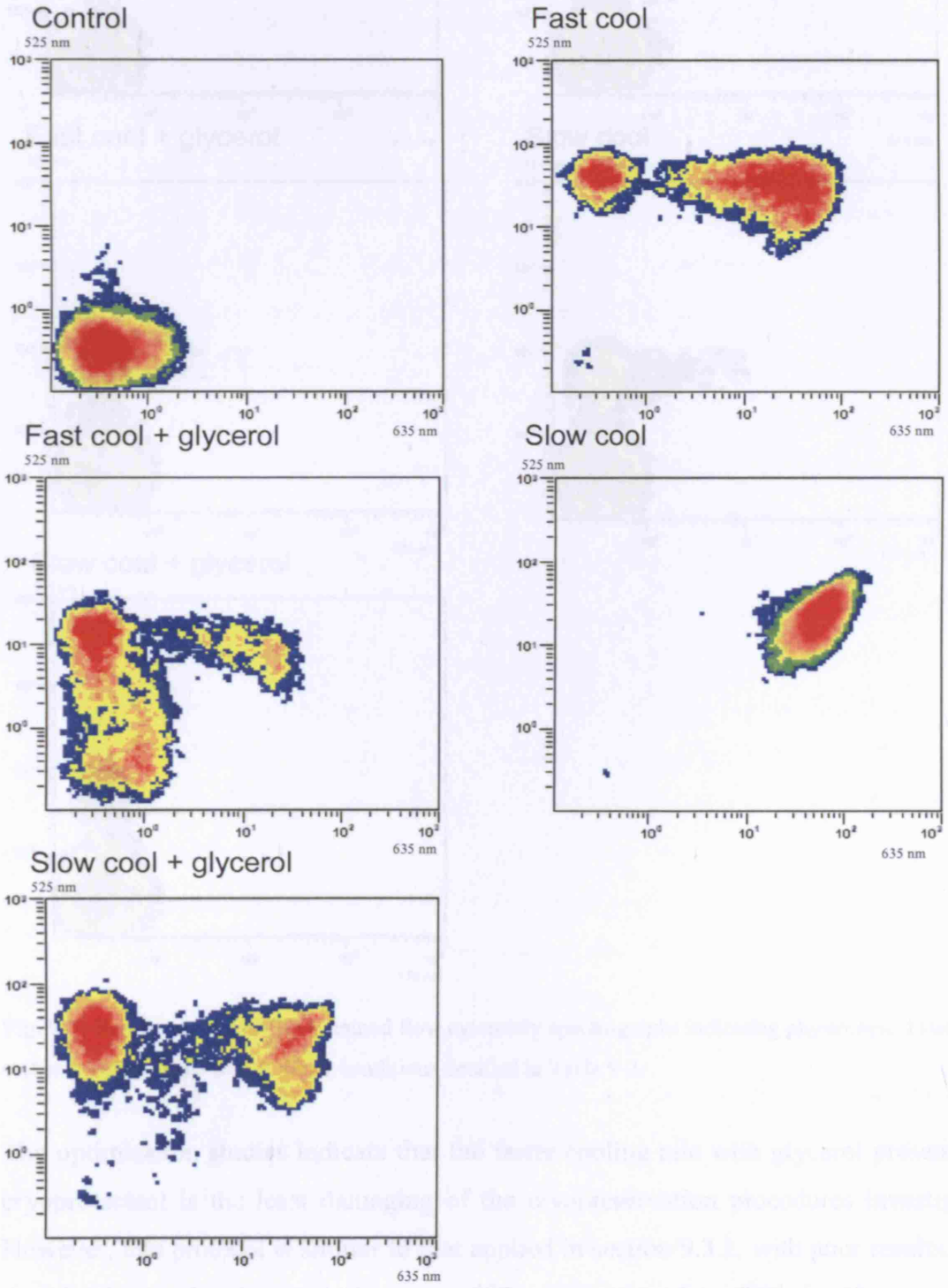

Fig. 9-6: Representative PI/BOX stained flow cytometry spectrographs indicating physiological state of mid-growth phase cells frozen under conditions detailed in Table 9-2.

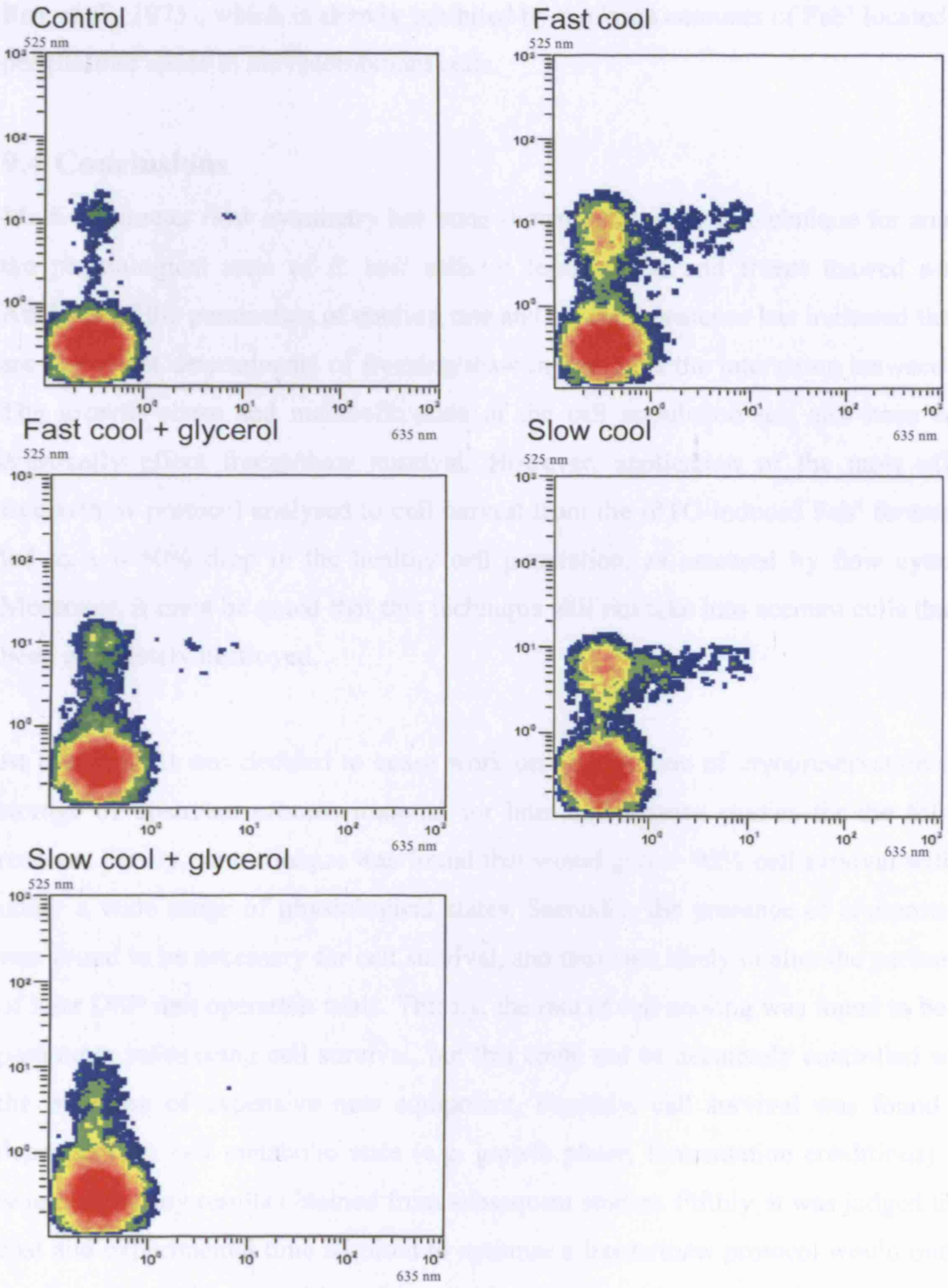

Fig. 9-7: Representative PI/BOX stained flow cytometry spectrographs indicating physiological state of stationary phase cells frozen under conditions detailed in Table 9-2.

The optimisation studies indicate that the faster cooling rate with glycerol present as a cryoprotectant is the least damaging of the cryopreservation procedures investigated. However, this protocol is similar to that applied in section 9.3.2, with poor results. This may be due to the slower cooling rate, 2°C/min compared to 6°C/min. However, it is likely that these cells will also have an increased freeze-susceptibility, as a major target of freeze/thaw damage in *E. coli* is the periplasmic membrane (Kempler and Ray, 1978;

Ray et al., 1975), which is already inhibited by the large amounts of Fab' located in the periplasmic space in the recombinant cells.

9.4 Conclusions

Multi-parameter flow cytometry has been shown to be a useful technique for analysing the physiological state of *E. coli* cells in fermentation and freeze thawed samples. Analysis of the parameters of cooling rate and glycerol presence has indicated that both are important determinants of freezing/thaw injury, as is the interaction between them. The growth phase and metabolic state of the cell population has also been seen to drastically effect freeze/thaw survival. However, application of the most effective freeze/thaw protocol analysed to cell harvest from the IPTG-induced Fab' fermentation led to a ~ 60% drop in the healthy cell population, as assessed by flow cytometry. Moreover, it must be noted that this technique will not take into account cells that have been completely destroyed.

At this stage it was decided to cease work on optimisation of cryopreservation for the storage of upstream process material for later downstream studies for the following reasons. Firstly, no technique was found that would give > 95% cell survival with cells under a wide range of physiological states. Secondly, the presence of cryoprotectants was found to be necessary for cell survival, and these are likely to alter the performance of later DSP unit operation trials. Thirdly, the rate of cell cooling was found to be a key parameter influencing cell survival, but this could not be accurately controlled without the purchase of expensive new equipment. Fourthly, cell survival was found to be dependent on cell metabolic state (e.g. growth phase, fermentation conditions) which would skew any results obtained from subsequent studies. Fifthly, it was judged that the cost and experimental time required to optimise a freeze/thaw protocol would outweigh the financial and temporal benefits gained: following cell removal from the extractant mixture, the supernatant can be stored for several hours at 4°C without loss of binding activity (Bowering, 2004; Ujam, 2007). Therefore only the initial DSP unit operations need be undertaken after the fermentation without temporal pause: the subsequent chromatographic separation techniques can be perfected with chilled material. However, perfection of *E. coli* cryopreservation techniques through future studies could have multiple other applications, for example the production of improved cell banks of reduced volume to facilitate easier storage.

10. Conclusions and future work

This chapter summarises the main conclusions and findings of this work. Firstly, the individual unit operations and the USD methodologies used to mimic them at millilitre-scale are discussed. Secondly, the process studied is considered holistically: the applicability of the USD methodologies to scale-down of the whole initial DSP is demonstrated and interactions between the upstream and downstream process elucidated. Finally, avenues for future study that have arisen as a result of this work are presented.

10.1 Conclusions

Comparison of IPTG- and lactose-induced processes for the production of antibody fragments in *E. coli* fed-batch fermentations at 75 L pilot-scale concluded that the IPTG-induced process was superior for both small-scale and industrial Fab' production. The IPTG-induced process was shown to be more robust and controllable, gave greater control over Fab' compartmentalisation, and allowed a greater initial working volume and therefore maximised fermenter capacity. Recent increases in the cost of lactose to the biopharmaceutical industry further favoured the IPTG-induced process. For these reasons the IPTG-process was chosen as the case study process for the thesis. This is corroborated by the recent decision by UCB to use this fermentation protocol for all future *E. coli* Fab' production, as it allows greater control of product compartmentalisation (Bowering, 2006).

Further characterisation of the IPTG-induced upstream process at 20 L pilot-scale led to the identification of post-induction glycerol feed rate as an important process parameter. An optimum feed rate of 1.42 mL h^{-1} L^{-1} was located, which produced the highest concentration of periplasmic Fab' (~ 1.1 g/L) at the chosen harvest time of 36 h from Fab' induction via IPTG addition.

The initial DSP of the process studied contained two centrifugation unit operations. Analysis of the performance of each of the centrifugation operations must be separated into four performance parameters for USD analysis, as current USD methods only allow the assessment of a single one of these parameters. These four performance parameters are: damage induced upon centrifugal entry and exit, clarification efficiency and dewatering efficiency.

Centrifugal entry damage was assessed using the pre-existing USD method of Boychyn et al. (2004). Firstly, rotational speeds needed in the shear device to obtain maximal energy dissipations in the desired range of $1x10^5$-$1x10^6$ W/kg were predicted by CFD. The subsequent application of energy dissipations similar to those found in the entry zones of disc-stack centrifuges (~ $2.0x10^5$ W/kg) to the *E. coli* cell harvest yielded inconsequential levels of cell damage. As *E. coli* spheroplasts have also been shown to be highly resistance to the levels of shear experienced in disc-stack entry zones (Bowering, 2000; Fischer, 1996; Murrell, 1998), it was concluded that centrifuge entry damage will not be a critical processing parameter in the process under investigation.

Centrifugal exit damage was assessed using the USD device described by Chan et al. (2006). The application of ejection velocities from 0-85 m/s to fermentation harvest material resulted in no discernable alteration in the subsequent performance of the periplasmic extraction procedure. Therefore it was concluded that centrifugal exit damage would not be a critical processing parameter.

The state-of-the-art USD methodology for determining clarification efficiency (Hutchinson et al., 2006) was found to be unable to predict the clarification efficiency of the HCD (> 10% wet weight per volume) harvest material under investigation due to significant hindered settling and aggregation effects. Therefore a new USD procedure utilised feed dilution to at least 2% wet weight per unit volume to reduce post-shear aggregation. A mathematical correction for hindered settling effects then allowed USD prediction of HCD feed material. This inexpensive and effective method was shown to accurately predict the pilot-scale clarification efficiency of packed yeast resuspended to ~ 15% wet weight per volume in addition to three IPTG-induced cell harvests produced using different post-induction glycerol feed rates. Use of this USD mimic to investigate interactions between the upstream post-induction glycerol flow rate and this parameter found that clarification efficiency of the cell harvest peaked around the point of maximal fermentative periplasmic Fab' production. Above this point the increased leakage of Fab' and periplasmic material will tend to reduce cell size, and there will be an increased presence of cell debris from the increasing incidence of cell lysis. Below the optimum, cells will be carbon limited, and as a result have produced less Fab' and will be possibly reduced in size.

Finally, as there were no suitable published USD methodologies for predicting the dewatering efficiency of large-scale centrifuges, a novel method was developed. Key dewatering parameters were determined to be spin time, spin speed, sediment height and temperature. These were maintained from millilitre to pilot-scale. This method was found to be capable of accurately mimicking pilot-scale dewatering levels to at least within ± 8% with all feeds studied. Interestingly, the observed maximum levels of dewatering obtained with the biological feeds matched the theoretical maximum lattice packing density of the particular cell shapes. Use of this USD mimic to investigate interactions between the upstream post-induction glycerol flow rate and this parameter found that the dewatering efficiency during centrifugal spheroplast removal was found to decrease as the upstream glycerol feed rate increased. This was presumably due to a change in the particle shape and size distribution with the post-induction glycerol feed rate.

The only non-centrifugation unit operation in the initial DSP was a heat/chemical extraction operation to release the periplasmically-located Fab' into the extracellular medium. It was determined that this unit operation could be mimicked at millilitre-scale to within ± 6% of 20 L pilot-scale performance, in terms of Fab' and protein released. No additional millilitre-scale mimic of the engineering environment was found to be necessary for this unit operation. The USD methodology so developed was used in a 2-factor DoE screen to expand knowledge of the design space of this key processing step. This identified cell integrity, extraction temperature, a temperature/integrity interaction, and too a lesser extent pH as important process parameters for this unit operation. Further use of this USD mimic to investigate interactions between the upstream post-induction glycerol flow rate and Fab' yield during this unit operation found that efficiency increased with increased post-induction glycerol feed rate. It was suggested that this was due to a weakening in periplasmic membrane integrity at higher glycerol feed rates.

The USD mimics developed were used to create a complete USD process chain for the initial DSP, which was run concurrently with the 20 L pilot-scale process for five fermentations performed with post-induction glycerol flow rates from 1-2 ml h^{-1} L^{-1}. The high correlation found between the USD and pilot-scale data demonstrated the usefulness and potential of USD as a methodology to provide timely decision-making support. Furthermore, it was predicted that the fermentative feed rate needed to

maximise Fab' yield when the initial DSP is considered is higher than that predicted from consideration of the fermentation alone. A 3.5% shift in the operating range of the upstream parameter would increase the yield after initial DSP by ~ 5%. This demonstrated the necessity to consider process interactions during process development and optimisation.

The USD methods discussed would be greatly facilitated by the capacity to store feed material. This would enable secondary tests to be performed on identical material to that used in primary investigations. Multi-parameter flow cytometry was found to be an excellent technique for assessment of cryopreservation procedures. However, within the scope of these studies no cryopreservation protocol suited for the long-term storage of material could be found. To do so would require significant optimisation requiring investment in facilities and operator time.

This work therefore provides an illustration of the ability of USD laboratory procedures, when combined with mimics of the process engineering environment, to predict accurately large scale-performance whilst requiring only millilitres of process material. The capacity to predict process performance in the laboratory rather than the pilot plant has two main applications. Firstly, it allows process development to begin earlier in the drug development pathway, when the investment needed for larger scale development work is too high to justify the risk of drug failure during clinical trials. This is highly desirable as an aid to reducing development time, allowing rapid market penetration and maximum patent exploitation. Secondly, the vast increase in the number of process data points that can be created from a given amount of material can significantly reduce the cost and pilot plant utilisation time of detailed process studies. In combination with intelligently planned statistical experimental design techniques, this will increase knowledge of the process 'design space' (Nail and Searles, 2008) and therefore facilitate process validation via the U.S. Food and Drug Administration's Quality by Design (QbD) initiative (Yu, 2006). The implementation of process analytical technology (PAT) will also be assisted by increased knowledge of process limitations and interactions between unit operations. This and other applications to the business and regulatory communities of the USD methodology developed and showcased will be discussed at greater length in Chapter 11.

10.2 Future work

The work here has opened up several avenues for future study, both for academic and industrial purposes.

10.2.1 Extend USD process coverage

This thesis has developed and applied USD methods for mimicking all aspects of the initial DSP for antibody fragment production in *E. coli*. USD methods have also been developed for mimicking the performance of depth filtration (Reynolds et al., 2003), pump operation (Zhang et al., 2007) and expanded bed absorption (Willoughby et al., 2005). Work upon small-scale mimics of chromatographic operations are also under development at UCL (Wenger et al., 2007) and elsewhere (Booth et al., 2008; Lacki et al., 2008). Future work could extend USD process coverage to chromatographic separations and beyond, increasing the size of the design space that can be studied and allowing determination of a larger range of intra-process interactions. The dewatering mimic developed could also be extended to allow dewatering performance prediction of disc-stack and multi-chamber bowl centrifuges in addition to tubular bowls.

10.2.2 Increase understanding of the periplasmic extraction unit operation

The 2-factor statistical design of experiments screen upon the periplasmic extraction detailed in Chapter 7 began to explore the design space around the operating range of this unit operation. A surprising finding was that a reduction in cell structural integrity induced by a freeze/thaw cycle resulted in a significant increase in % Fab' release but not in % total protein release. This insight into the process provides an opportunity for further study to increase process understanding by determination of the reasons behind this finding.

10.2.3 Further cryopreservation work

If the rate of cell freezing could be controlled via the use of a controlled rate freezer or similar a study could determine if there exists a freezing rate that can give minimal cell damage to the IPTG-induced harvest, therefore allowing cryopreservation of cell-containing process material. This study would use the methods developed in this thesis to quickly assess freeze/thaw damage.

10.2.4 Increase small-scale throughput

Now that the process steps of centrifugation and periplasmic extraction have been brought out of the pilot plant and into the laboratory it should be possible to reduce scale further from millilitre to the microlitre scale or even nanolitre (microfluidic) scale. This would allow the use of microwell systems, facilitating automation. Automation could allow further enhancement of experimental throughput, reduce human error during experimentation, and facilitate the parallel evaluation of competing process options (Micheletti and Lye, 2006).

11. EngD requirements: Bioprocess management and regulatory implications of USD technology

11.1 Introduction

An industrial biopharmaceutical process for the production of antibody fragments in *E. coli* has been studied and a complete laboratory-scale process mimic of the initial DSP generated. The effects of variations in an upstream critical process parameter upon the initial DSP have been assessed using this mimic and have been shown to match the conclusions generated from pilot-scale studies. In this chapter the positioning of USD technology and other small-scale process mimics within the overall scheme of biopharmaceutical drug development, and the regulatory implications of utilising this technology, are discussed. Firstly the traditional drug development model is described and the drivers for change in this model analysed. The possible aid USD methodology could give to the implementation of these changes is then suggested, including its role at the start of, and during later process development. Secondly, the regulatory issues during drug development are briefly explained. Both the role USD techniques can play during process validation, and the need to validate the USD techniques themselves are clarified.

11.2 Commercial and management relevance of USD methodology

11.2.1 Traditional pharmaceutical process development

As soon as a novel therapeutic is discovered and/or patented, companies must strive to develop it in as short a timeframe as is possible (Hausner, 1998; Levin and Papageorgiou, 2004) in order to achieve rapid market penetration, as up to US$1M of income may be lost for every day that a product is not on the market (Basu et al., 1998; Lim et al., 2004a). Rapid drug development maximises the benefits accorded by patent exclusivity. The historical success of this strategy was based on the ability of companies to command large premiums for the drugs that succeed in reaching market (Pisano and Wheelwright, 1995). This often more than compensated for high manufacturing costs generated by the high time pressures imposed upon process development, and the high drug failure rate: ~ 85% of products will fail during development, often after undergoing clinical trials (Petrides et al., 2002).

11.2.2 Current challenges in bioprocess development

The situation described above is unlikely to survive the changing financial pressures imposed by governments, regulators, and healthcare providers. Many more challenges are now encountered during product commercialisation (Shah, 2004). These include the growing complexity of potential new therapeutics such as genes or even whole cell-based therapies, the drive to apply Good Manufacturing Practise (GMP) earlier in product development, increasing candidate failure rates during clinical trials and the increasing R&D cost per drug. Consequently, new therapeutics may cost US$800M or more to develop and take up to 15 years to arrive in the marketplace (Bauer and Fischer, 2000; DiMasi et al., 2003). On reaching the market, drugs now face shorter effective patent lives, greater worldwide competition from the advent of biogenerics and therefore stronger reimbursement pressures than before. Only a third of novel biopharmaceuticals re-cover their full development costs and make a real profit. In this atmosphere the traditional development model of sacrificing process optimisation efforts in order to be first-to-market is now increasingly challenged.

11.2.3 The role of increased process optimisation

The factors detailed above can be addressed using a variety of different approaches. For example, strategies identified by Roger Perlmutter during his introduction to the Society for Biochemical Engineering's 2007 conference on Accelerating Biopharmaceutical Development included the following strategies to reduce R&D costs (Perlmutter, 2007).

- Drug development should focus upon grievous illness.
- Scientists should be prepared to exploit any treatment modality, from small molecules to cells.
- Human disease should be prioritised as preclinical animal models do not fully mirror the situation in humans.

In addition to these strategies for the optimisation of drug discovery research, increased understanding of manufacturing processes and more rapid process development is necessary in order to reduce cost of goods for biopharmaceutical manufacture and achieve top quality processes while keeping process development off the drug development critical path to market. This goal could be achieved using a range of methodologies. For example, computational techniques could be used to a greater extent for evaluating operating strategies that optimise financial and technical goals such as

maximising product yield, improving resource utilisation and reducing processing costs and time (Chhatre et al., 2007). However, this thesis is concerned with facilitating rapid process development and increased process understanding by use of laboratory-scale experimental process mimics. The place of mimics in the facilitation of these goals is discussed below.

11.2.4 Strategies for applying USD methodologies during bioprocess development

USD methodologies can complement traditional process development activity at two separate stages in the drug development pathway. Firstly, USD methodologies could be used to allow process development to begin earlier and to allow candidate screening activity to incorporate measurement of the 'processability' of strain/drug candidates. Secondly, USD methodology could be used towards the end of process development to investigate ranges of conditions around fixed processing protocols to evaluate robustness of operating conditions. In this way an increased knowledge of the design space could be obtained without large numbers of costly pilot-scale experiments requiring large amounts of process material.

11.2.4.1 USD methodology for pre-pilot plant studies

The start time of traditional biopharmaceutical process development is usually governed by two competing factors: the need to as far as possible keep process development off the critical path to market; and the need to reduce the cost investment in a drug candidate that may well fail during clinical trials. Also, during the initial stages of drug development scarce process material is at a premium and is frequently not available in sufficient quantities for pilot-scale process development trials (Titchener-Hooker et al., 2001). By allowing process trials to be undertaken with vastly reduced amounts of process material (c.f. Table 8-1) USD methodology can reduce the cost of early process development, therefore reducing financial investment while increasing process knowledge, and also not diverting excessive material away from early development (Fig. 11-1). This USD approach also greatly complements the use of computational decisional tools as a means for integrating business and process factors (Chhatre et al., 2007), as it allows the integration of real process data into early simulations.

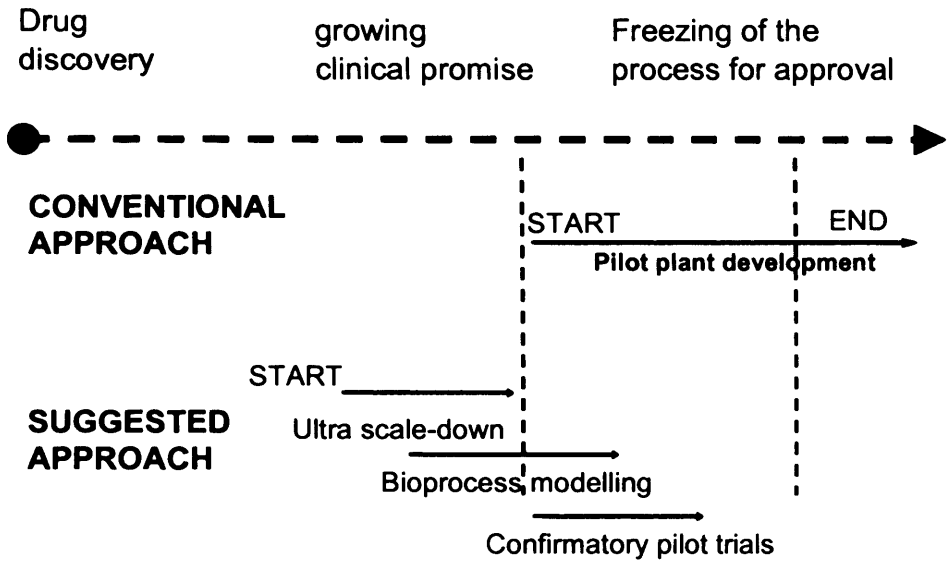

Fig. 11-1: USD allows bioprocess development to begin earlier in the discovery process and becomes especially powerful when combined with computational modelling techniques.

It is suggested that USD methodologies should be used in early process development for two main means. Firstly, USD methodologies could allow early strain screening to include data on the 'processability' of multiple strain candidates. For example, a possible question during early drug development could be which *E. coli* strain is best suited to the periplasmic operation unit operation? The USD methodology developed in Chapter 7 to allow prediction of the periplasmic extraction unit operation could be applied to multiple *E. coli* strains transformed with the Fab' encoding plasmid and thereby suitability for use with the extraction procedure could be easily determined. Secondly, USD methodology could examine preliminary route scouting and help target the pilot-scale development effort. For example, the USD periplasmic method above might indicate that all tested strains have an extremely low level of product release using this permeablisation procedure and therefore a different method of product release must be investigated.

11.2.4.2 USD methodology for increased process understanding

The second suggested industrial use for USD methodologies is towards the end of process development to investigate ranges of conditions around fixed processing protocols to evaluate process robustness. USD methods can allow the larger number of experiments necessary to investigate sufficient ranges of conditions to satisfactorily characterise not only the operating space of the process, but also the design space and beyond (Rathore et al., 2007). The concept of design space is elucidated in Fig. 11-2.

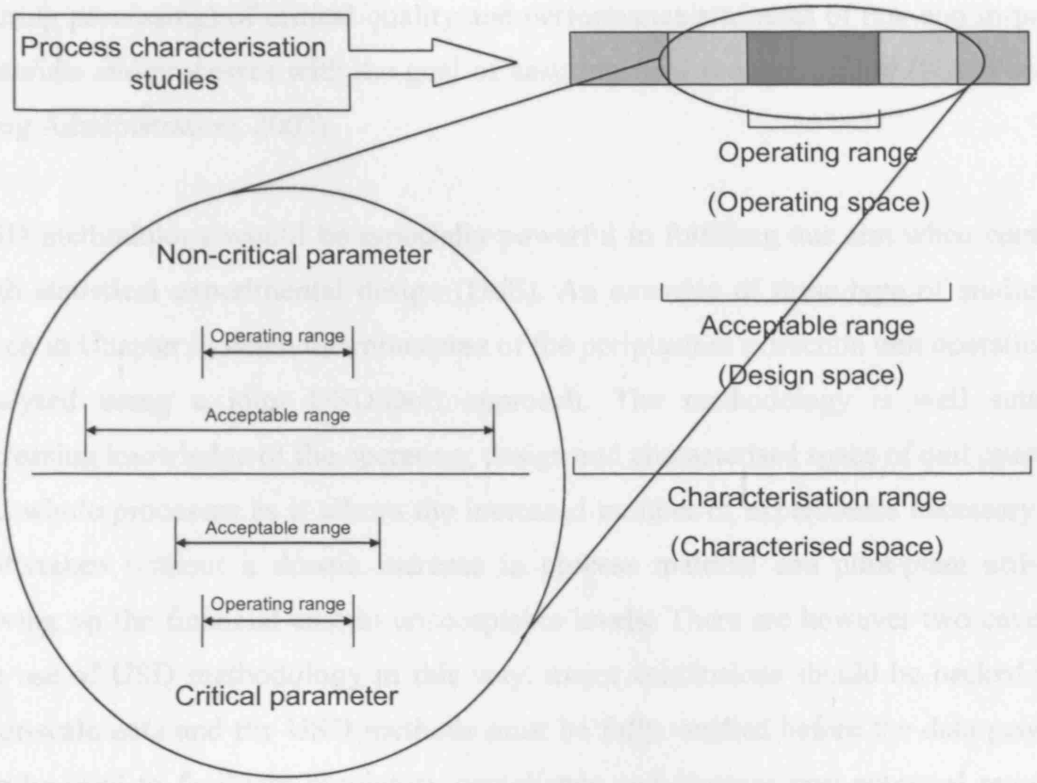

Fig. 11-2: Illustration of the creation of design space from process characterisation studies, the relationship between design space and the characterised and operating spaces, and the practical difference between critical and non-critical parameters.

Increased characterisation of the design space would allow critical and non-critical process parameters to be distinguished by determining the difference between their operating ranges and the ranges at which the process remains acceptable (Fig. 11-2). However, the primary benefit of an approved design space is regulatory flexibility. For example, the ICH Q8 guideline, which was finalised in November 2005 and went into effect in May 2006, recommends process submissions should include additional information in order to demonstrate a high degree of understanding of the manufacturing process. The design space is defined here as "the multidimensional combination and interaction of input variables (e.g. material attributes) and process parameters that have been demonstrated to provide assurance of quality" (U.S. Food and Drug Administration, 2006). The use of design space knowledge in allowing regulatory flexibility will be discussed further in Section 11.3. Increased knowledge of the design space is also necessary for satisfactory application of process analytical technology (PAT). Application of PAT can also lead to regulatory flexibility; PAT has been encouraged by the Centre for Drug Evaluation and Research (CDER) branch of the FDA in 2002 by creation of the PAT initiative. Here it is defined as a system for designing, analysing, and controlling manufacturing through timely measurements

(during processing) of critical quality and performance attributes of raw and in-process materials and processes with the goal of ensuring final product quality (U.S. Food and Drug Administration, 2002).

USD methodology would be especially powerful in fulfilling this aim when combined with statistical experimental design (DoE). An example of these type of studies was given in Chapter 7, when the robustness of the periplasmic extraction unit operation was analysed using a joint USD/DoE approach. The methodology is well suited to increasing knowledge of the operating, design and characterised space of unit operations and whole processes as it allows the increased number of experiments necessary to be undertaken without a drastic increase in process material and pilot-plant utilisation driving up the financial cost to unacceptable levels. There are however two caveats to the use of USD methodology in this way: major conclusions should be backed up by pilot-scale data and the USD methods must be fully verified before the data generated can be used to facilitate regulatory compliance and increase post-approval regulatory process flexibility.

11.3 Validation and regulatory issues

In order for a process or product to be released onto the market it must receive regulatory approval from the relevant authorities in the country of release. In order to achieve approval the product must be shown to be safe and efficacious in humans. The major contribution to this regulatory submission necessary by process development is demonstration of process validation, defined by the FDA as establishing documented evidence which provides a high degree of assurance that a specific process will consistently produce a product meeting its predetermined specifications and quality attributes. In this section, a brief description of the factors and processes that make up a typical validation strategy, as might be applied to the process for antibody fragment production in *E. coli* is given. Secondly, the contribution that USD methodology can make to validation effort is described. Finally, the necessity for assement of the USD methodology itself if it is to make up part of the regulatory submission is stressed, and the means by which this might be achieved explored.

11.3.1 General validation strategies

Process validation can be divided into three approximate stages. Stage 1 involves process pre-qualification, Stage 2 manufacturing qualification, and Stage 3 life-cycle

qualification. Effective planning of process validation is crucial as time and budgetary constraints do not allow for repeating required activities. Therefore the first step towards successful process validation is the creation of a validation master plan (VMP). While not strictly compulsory, a VMP is the first document the regulatory authorities will expect to see during an inspection. A good VMP should be created before validation begins, and be of sufficient detail to include the whole validation process.

11.3.1.1 Stage 1: process pre-qualification

Before the manufacturing process can be validated, all its components must themselves be validated. The facility should be qualified for manufacturing the intended product. It should be verified that procedures are in place for quality systems management such as facility cleaning; gowning; the flow of personnel, equipment and material; environmental monitoring; calibration, change control; and preventive maintenance (Fetterolf, 2007). All production and analytical methods must be validated for consistency. The equipment used must also be validated in a four stage process. Firstly, design qualification (DQ) and installation qualification (IQ) ensures all equipment is calibrated and installed correctly. Operational qualification (OQ) then demonstrates the functionality of the equipment falls within defined limits. Finally performance qualification (PQ) ensures the equipment will work for its intended function. The sources of raw material must be shown to be consistent. Quality control and process monitoring processes must be validated for reliability. Even cleaning protocols for all process and analytical equipment must be fully defined and shown to be capable of reaching a consistent endpoint with all possible challenges. Standard operating procedures must be written for all operations.

11.3.1.2 Stage 2: manufacturing qualification

Stage 2 entails the performance of three consecutive runs at the intended commercial scale (U.S. Food and Drug Administration, 1987). The manufacturing process qualification is performed under a prospective protocol using the appropriate output and results from the stage 1 studies with respect to critical process parameters, in-process controls and specification, and any other criteria specific to the process (Fetterolf, 2007).

11.3.1.3 Stage 3: life-cycle qualification

Process performance must be continuously assessed post-approval. Full batch records must be kept and acceptability criteria outlined in a prospective life-cycle qualification

protocol (Ferenc, 1999). After validation, all changes made to manufacturing process are assessed for impact to the validated process. A non-trivial change may require re-validation, and this is a significant road-block to process evolution as post-approval re-validations are often more costly to implement than the resulting reduction in COGs.

11.3.2 Facilitation of validation by USD methodology

The use of USD methodology either for pre-pilot plant studies before the manufacturing process is finalised or once the manufacturing process is set could ease the regulatory burden in two ways. Firstly, regulators are increasingly encouraging a high degree of understanding of the manufacturing process. Therefore including this information can lead to a more flexible regulatory inspection. Secondly, the knowledge of the whole design space facilitated by USD methodology will lead to greater post-approval flexibility, most notably the potential to make process improvements within the design space without regulatory oversight, but also greater tolerance in batch process deviations can be allowed if these can be shown to fit within the acceptable design space, reducing batch rejection.

11.3.3 Validation of USD methodology

In order to allow inclusion of USD work in any regulatory submission the full range of IQ, OQ, and PQ validation data sets would probably not be needed. However, the methods must be proven to accurately model the performance of the manufacturing scale process. This would require multiple experiments showing comparability between USD and pilot-scale data. The level of reproducibility of the USD mimics must be elucidated. Ideally SOPs and cleaning protocols should be created for each piece of USD equipment.

This requirement clearly represents an obstacle to their uptake by the heavily regulated, inherently conservative pharmaceutical industry. However, the investment made in their verification would be outweighed by the substantial benefits outlined above, especially as more and more small-scale process mimics are adapted by the industry and therefore the regulatory requirements needed become more established.

11.4 Conclusions

Two major applications of USD methodology to industrial process development have been discussed. Firstly, USD methodology could be used in pre-pilot plant studies for

candidate screening and process route-scouting. Secondly, the methodology could be used once the manufacturing process is fixed to allow increased process robustness studies to be undertaken and therefore knowledge of the manufacturing design space to be expanded, facilitating PAT and regulatory confidence. In this role USD could ease validation efforts through increasing process knowledge. Post-approval this increased process knowledge could also be used to justify process changes without extensive re-validation. However, in order for the data produced by the USD methods to be acceptable to the regulatory authorities for this purpose, a separate data set must be obtained that shows comparability between USD and pilot-scale results. This will be a major hurdle to their uptake by the inherently conservative pharmaceutical industry, although the burden would be eased with each subsequent small-scale process mimic that is adapted by the industry.

12. References

Abdel-Salam, H.A., El-Khamissy, T., Enan, G.A., and Hollenberg, C.P. (2001). Expression of mouse anticreatine kinase (MAK33) monoclonal antibody in the yeast *Hansenula polymorpha*. Applied Microbiology and Biotechnology *56*, 157-164.

Abreu, C.R.A., Tavares, F.W., and Castier, M. (2003). Influence of particle shape on the packing and on the segregation of spherocylinders via Monte Carlo simulations. Powder Technology *134*, 167-180.

Al-Rubeai, M. and Emery, A.N. (1996). Flow cytometry applications in cell culture. Marcel Dekker (New York).

Ambler, C.M. (1961). The fundamentals of separation, including Sharples "Sigma value" for predicting equipment performance. Industrial and Engineering Chemistry *53*, 430-433.

Ames, G.F.L., Prody, C., and Kustu, S. (1984). Simple, rapid, and quantitative release of periplasmic proteins by chloroform. Journal of Bacteriology *160*, 1181-1183.

Arbabi-Ghahroudi, M., Tanha, J., and MacKenzie, R. (2005). Prokaryotic expression of antibodies. Cancer and Metastasis Reviews *24*, 501-519.

Bakker, H., Bardor, M., Molthoff, J.W., Gomord, V., Elbers, I., Stevens, L.H., Jordi, W., Lommen, A., Faye, L., Lerough, P., and Bosch, D. (2001). Galactose-extended glycans of antibodies produced by transgenic plants. Proceedings of the National Academy of Science USA *98*, 2899-2904.

Baneyx, F. (1999). *In vivo* folding of recombinant proteins in *Escherichia coli*. In Manual of Industrial Microbiology and Biotechnology, J.E.Davies, A.L.Dermain, G.Cohen, C.L.Hershberger, L.J.Forney, I.B.Holland, W.-S.Hu, J.-H.Wu, D.H.Sherman, and R.C.Wilson, eds. (Washington DC: American Society for Microbiology), pp. 551-565.

Bard, J., Ercolani, K., Svenson, K., Olland, A., and Somers, W. (2004). Automated systems for protein crystallisation. Methods *34*, 329-347.

Barnfield-Frej, A.K., Hjort, R., and Hammarstrom, A. (1994). Pilot-scale recovery of recombinant annexin V from unclarified *Escherichia coli* homogenate using expanded bed adsorption. Biotechnology and Bioengineering *44*, 922-929.

Basu, P.K., Quaadgras, J., Mack, R.A., and Noren, A.R. (1998). Achieve the right balance in pharmaceutical pilot plants. Chemical Engineering Progress *94*, 67-74.

Bauer, H.H. and Fischer, M. (2000). Product life cycle patterns for pharmaceuticals and their impact on R&D profitability of late mover products. International Business Review *9*, 703-725.

Belter, P.A., Cussler, E.L., and Hu, W.-S. (1988). Centrifugation. In Bioseparations: downstream processing for biotechnology, pp. 47-73. John Wiley & Sons (New York).

Bensch, M., Wierling, P.S., von Lieres, E., and Hubbuch, J. (2005). High thoughput screening of chromatographic phases for rapid process development. Chemical Engineering Technology *28*, 1274-1284.

Bermajo, L.L., Welker, N.E., and Papoutsakis, E.T. (1998). Expression of *Clostridium acetobutylicum* ATCC 824 genes in *Escherichia coli* for acetone production and acetate detoxification. Applied Environmental Microbiology *64*, 1079-1085.

Berthold, W. and Kempken, R. (1994). Interaction of cell culture with downstream purification; a case study. Cytotechnology *15*, 229-242.

Better, M., Chang, C.P., Robinson, R.R., and Horowitz, A.H. (1988). Escherichia coli secretion of an active chimeric antibody fragment. Science *240*, 1041-1043.

Betts, J.I. and Baganz, F. (2006). Minature bioreactors: current practices and future opportunities. Microbial Cell Factories *5*, 21.

Bhattacharya, S.K. and Dubey, A.K. (1997). Effects of dissolved oxygen and oxygen mass transfer on overexpression of target gene in recombinant *E. coli*. Enzyme and Microbial Technology *20*, 355-360.

Bizzaro, N. (2007). Antibodies to citrullinated peptides: a significant step forward in the early diagnosis of rhematoid arthritis. Clinical Chemistry and Laboratory Medicine *45*, 150-157.

Blank, G., Zapata, R., Fahrner, R., Milton, C., Yedinak, H., Knudsen, C., and Schmelzer, C. (2001). Expanded bed adsorption in the purification of monoclonal antibodies: a comparison of process alternatives. Bioseparation *10*, 65-71.

Booth, J., Coffman, J., and Kelley, B. High-throughput screening of protein A resin for purification process development. [Downstream processing: High throughput screening in process development]. 2008. http://www.biotwebinar.com/JANUARY112007.html, ACS:BIOT. 11-1-0008.

Bowering, L.C. An engineering study of the design, integration, and control of antibody fragment production processes. 2000. PhD UCL.

Bowering, L.C. 2004. Personal Communication

Bowering, L.C. 2006. Personal Communication

Bowering, L.C., Bracewell, D.G., Keshavarz-Moore, E., Hoare, M., Neil, A., and Weir, C. (2002). Comparison of techniques for monitoring antibody fragment production in *E. coli* fermentation cultures. Biotechnology Progress *18*, 1431-1438.

Boychyn, M., Doyle, W., Bulmer, M., More, J., and Hoare, M. (2000). Laboratory scaledown of protein purification processes involving fractional precipitation and centrifugal recovery. Biotechnology and Bioengineering *69*, 1-10.

Boychyn, M., Yim, S.S.S., Ayazi Shamlou, P., Bulmer, M., More, J., and Hoare, M. (2001). Characterisation of flow intensity in continuous centrifuges for the development of laboratory mimics. Chemical Engineering Science *56*, 4758-4770.

Boychyn, M., Yim, S.S.S., Bulmer, M., More, J., Bracewell, D.G., and Hoare, M. (2004). Performance Prediction of industrial centrifuges using scale-down models. Bioprocess and Biosystems Engineering *26*, 385-391.

Boychyn, R.M. Scale-down principles for the accelerated design of protein purification processes. 2000. PhD. UCL.

Bradford, M.M. (1976). A rapid and sensitive method for the quantification of microgram quantities of protein utilizing the principle of protein-dye binding. Analytical Biochemistry *72*, 248-254.

Brehm-Stecher, B. and Johnston, E. (2004). Single-cell microbiology: tools, technologies, and application. Microbiology and Molecular Biology Reviews *68*, 538-559.

Brinkmann, U., Di Carlo, A., Vasmatiz, G., Kurochkina, N., Beers, R., Lee, B., and Pastan, I. (1997). Stabilization of a recombinant Fv fragment by base-loop interconnection and $V_{H\text{-}VL}$ permutation. Journal of Molecular Biology *268*, 107-117.

Carter, P.J. (2006). Potent antibody therapeutics by design. Nature Reviews: Immunology *6*, 343-357.

Carter, P.J., Kelley, R.F., Rodrigues, M.L., Snedcor, B., Covarrubias, M., Velligan, M.D., Wong, W.L.T., Rowland, A.M., Kotts, C.E., Carver, M.E., Yang, M., Bourell, J.H., Shepare, H.M., and Henner, D. (1992). High level *Escherichia coli* expression and production of a bivalent humanised antibody fragment. Bio/Technology *10*, 163-167.

Chan, G. An ultra scale-down study to understand and predict *E. coli* cell recovery from high-speed discharge centrifuges. 2006. EngD. UCL

Chan, G., Booth, A.J., Mannweiler, K., and Hoare, M. (2006). Ultra scale-down studies of the effect of flow and impact conditions during *E. coli* cell processing. Biotechnology and Bioengineering *95*, 671-683.

Chester, K.A. and Hawkins, R.E. (1995). Clinical issues in antibody design. Trends in Biotechnology *13*, 294-300.

Chhatre, S., Francis, R., O'Donovan, K., Titchener-Hooker, N.J., Newcombe, A.R., and Kesavarz-Moore, E. (2007). A prototype software methodology for the rapid evaluation of bio-manufacturing process options. Biotechnology and applied biochemistry *48*, 65-78.

Chu, C.P. and Lee, D.J. (2001). Experimental analysis of centrifugal dewatering process of poly electrolyte flocculated waste activated sludge. Water Research *35*, 2377-2384.

Cumbaa, C.A., Lauricella, A., Fehrman, N., Veatch, C., Collins, R., Luft, J., DeTitt, G., and Jurisica, I. (2003). Automatic classification of sub-microlitre protein-crystallisation trials in 1536-well plates. Acta Crystallographica. Section D, Biological Crystallography *59*, 1619-1627.

Dainiak, M.B., Kumar, A., Plieva, F.M., Galaev, I.Y., and Mattiasson, B. (2004). Integrated isolation of antibody fragments from microbial cell culture fluids using supermacroporous cryogels. Journal of Chromatography A *1045*, 93-98.

Davies, T.W., Metcalfe, R.A., and Jackson, M.K. The anatomy and impact characteristics of large scale water jets. 15-21. 1980. Fifth international synopsium on jet cutting technology.

De Keyzer, J., Van der Does, C., and Driessen, A.J.M. (2003). The bacterial translocase: a dynamic protein channel complex. Cellular and Molecular Life Sciences *60*, 2034-2052.

Dedhia, N.N., Hottinger, T., and Bailey, J.E. (1994). Overproduction of glycogen in *Escherichia coli* blocked in the acetate pathway improves cell growth. Biotechnology and Bioengineering *44*, 132-139.

Demarest, S.J., Chen, G., Kimmel, B.E., Gustafson, D., Wu, J., Salbata, J., Poland, J., Elia, M., Tan, X., Wong, K., Short, J., and Hansen, G. (2006). Engineering stability into *Escherichia coli* secreted Fabs leads to increased functional expression. Protein Engineering, Design and Selection *19*, 325-336.

DiMasi, J.A., Hansen, R.W., and Grabowski, H.G. (2003). The price of innovation: new estimates of drug development costs. Journal of Health Economics *22*, 151-185.

Donev, A., Cisse, I., Sachs, D., Variano, E.A., Stillinger, F.H., Connelly, R., Torquato, S., and Chaikin, D.M. (2004). Improving the density of jammed disordered packings using ellipsoids. Science *303*, 990-993.

Donovan, R.S., Robinson, C.W., and Glick, B.R. (1996). Optimizing inducer and culture conditions for expression of foreign proteins under control of the *lac* promoter. Journal of Industrial Microbiology *16*, 145-154.

Farid, S., Washbrook, J., and Titchener-Hooker, N.J. (2005). Decision-support tool for assessing biomanufactuing strategies under uncertainty: stainless steel versus disposable equipment for clinical trial material preparation. Biotechnology Progress *21*, 486-497.

Farid, S.S. (2006). Established bioprocesses for producing antibodies as a basis for future planning. Advances in Biochemical Engineering/Biotechnology *101*, 1-42.

Farid, S.S. (2007). Process economics of industrial monoclonal antibody manufacture. Journal of Chromatography B *848*, 8-18.

Ferenc, B.M. (1999). Qualification and change control in validation of pharmaceutical processes., F.Carleton and J.Agalloco, eds, pp. 132-150. Marcell Dekker, Inc. (New York).

Ferris, F.G. and Beveridge, T.J. (1986). Physiochemical roles of soluble metal cations in the outer membrane of *Escherichia coli* K12. Canadian Journal of Microbiology *32*, 594-601.

Fetterolf, D.M. (2007). Developing a sound process validation strategy. Biopharm International *20*, 38-46.

Fischer, E.J. Impacts of separation processes on protein recovery from cells and cell spheroplasts. 1996. PhD. UCL.

Fisher, R., Drossard, J., Emans, N., Commandeur, U., and Hellwig, S. (1999). Towards molecular farming in the future: *Pichia pastoris*-based production of single-chain antibody fragments. Research in Immunology *149*, 589-599.

Forsberg, G., Forsgren, M., Jaki, M., Norin, M., Sterky, C., Enhorning, A., Larsson, K., Ericsson, M., and Bjork, P. (1997). Identification of framework residues in a secreted recombinant antibody fragment that control production level and localization in *Escherichia coli*. Journal of Biological Chemistry *272*, 12430-12436.

Frenken, L.D.J., Hessing, J.G.M., Van den Hondel, C.A.M.J.J., and Verrips, C.T. (1998). Recent advances in the large-scale production of antibody fragments using lower eukaryotic organisms. Research in Immunology *149*, 589-599.

Fuchs, C., Koster, D., Wiebusch, S., Mahr, K., Eisbrenner, G., and Markl, H. (2002). Scale-up of dialysis fermentation for high cell density cultivation of *Escherichia coli*. Journal of Biotechnology *93*, 243-251.

Geisberger, R., Lamers, M., and Achatz, G. (2006). The riddle of the dual expression of IgM and IgD. Immunology *118*, 429-437.

Gibilaro, L.G. (2001). Fluidization-dynamics: The formulation and applications of a predictive theory for the fluidized state. Butterworth-Heinemann (Oxford, UK).

Glennie, M.J. and Johnson, P.W.M. (2000). Review: Clinical trials of antibody therapy. Immunology Today *21*, 403-410.

Glick, B. (1995). Metabolic load and heterologous gene expression. Biotechnology Advances *13*, 247-261.

Glockshuber, R., Malia, M., Pfitzinger, I., and Pluckthun, A. (1990). A comparison of strategies to stabilize immunoglobulin Fv-fragments. Biochemistry *29*, 1362-1367.

Gombert, A.K. and Kilikian, B.V. (1998). Recombinant gene expression in *Escherichia coli* cultivation using lactose as an inducer. Journal of Biotechnology *60*, 47-54.

Gorenflo, V.M., Ritter, J.B., Aescgliman, D.S., Drouin, H., Bowen, B.D., and Piret, J.M. (2005). Characterization and optimization of acoustic filter performance by experimental design methodology. Biotechnology and Bioengineering *90*, 746-753.

Gray, P.P., Dunnill, P., and Lilly, M.D. (1972). The continuous-flow isolation of enzymes. In Fermentation technologies today, G.Terui, ed., pp. 347-351. Society of fermentation technology (Tokyo).

Gutman, G.A. and Hatfield, G.W. (1989). Nonrandom utilization of codon pairs in *Escherichia coli*. Proceedings of the National Academy of Science USA *86*, 3699-3703.

Guzman, L.M., Belin, D., Carson, M.J., and Beckwith, J. (1995). Tight regulation, modulation, and high-level expression by vectors containing the arabinose PBAD promoter. Journal of Bacteriology *177*, 4121-4130.

Hagg,P., de Pohl, J.W., Abdulkarim, F., and Isaksson, L.A. (2004). A host/plasmid system that is not dependant on antibiotics and antibiotic resistant genes for stable plasmid maintenance in *Escherichia coli*. Journal of Biotechnology *111*, 17-30.

Hales, T.C. (1992). The sphere packing problem. Journal of Computational and Applied Mathematics *44*, 41-46.

Harris, L.J., Larson, S.B., Hasel, K.W., and McPherson, A. (1997). Refined structure of an intact IgG2a monoclonal antibody. Biochemistry *36*, 1581-1597.

Hausner, B. (1998). Outsourcing: evaluating alternatives. Pharmaceutical Science and Technology Today *1*, 148-152.

Heckly, R.J. (1985). Principles of preserving bacteria by freeze-drying. Developments in Industrial Microbiology *26*, 379-395.

Hewitt, C.J., Boon, L.A., McFarlane, C.M., and Nienow, A.W. (1998). The use of flow cytometry to study the impact of fluid mechanical stress on *Escherichia coli* W3110 during continuous cultivation in an agitated bioreactor. Biotechnology and Bioengineering *59*, 612-620.

Hewitt, C.J., Nebe-von-Caron, G., Nienow, A.W., and McFarlane, C.M. (1999a). The use of multi-parameter flow cytometry to compare the physiological response of *Escherichia coli* W3110 to glucose limitation during batch, fed-batch and continuous culture cultivations. Journal of Biotechnology *75*, 251-264.

Hewitt, C.J., Nebe-von-Caron, G., Nienow, A.W., and McFarlane, C.M. (1999b). The use of multi-staining flow cytometry to characterise the physiological state of *Escherichia coli* W3110 in high cell density fed-batch cultures. Biotechnology and Bioengineering *63*, 705-711.

Hewitt, C.J., Nebe-von-Caron, G., Axelsson, B., McFarlane, C.M., and Nienow, A.W. (2000). Studies related to the scale-up of high-cell-density *E. coli* fed-batch fermentations using multiparameter flow cytometry: effect of a changing microenvironment with respect to glucose and dissolved oxygen concentration. Biotechnology and Bioengineering *70*, 381-390.

Hewitt, C.J. and Nebe-von-Caron, G. (2004). The application of multi-parameter flow cytometry to monitor individual microbial cell physiological state. Advances in Biochemical Engineering/Biotechnology *89*, 197-223.

Hollander, D.H. and Toyokawa, K. (1956). Variation in sensitivity of *Escherichia coli* to freezing damage during the growth cycle. Proceedings of the Society for Experimental Biology and Medicine *92*, 499-500.

Holms, W.H. (1986). The central metabolic pathways of *Escherichia coli*: relationship between flux and control at a branch point, efficiency of conversion to biomass, and excretion of acetate. Current Topics in Cellular Regulation *28*, 69-105.

Hoogenboom, H.R. (2005). Selecting and screening recombinant antibody libraries. Nature Biotechnology *23*, 1105-1116.

Huang, S.W., Lin, Y.H., Chin, H.L., Wang, W.C., Kuo, B.Y., and Chou, C.P. (2002). Effect of pH on high-temperature production of bacterial penicillin acylase in *Escherichia coli*. Biotechnology Progress *18*, 668-671.

Humphreys, D.P., Heywood, S.P., King, L.M., Bowering, L.C., Turner, J.P., and Lane, S.E. (2004). Engineering of *Escherichia coli* to improve the purification of periplasmic Fab' fragments: changing the pI of the chromosomally encoded PhoS/PstS protein. Protein Expression and Purification *37*, 109-118.

Hutchinson, N., Bingham, N., Murrell, N., Farid, S., and Hoare, M. (2006). Shear stress analysis of mammalian cell suspension for prediction of industrial centrifugation and its verification. Biotechnology and Bioengineering *95*, 483-491.

Irvin, R.T., MacAlister, T.J., and Costerton, J.W. (1981). Tris(hydroxymethyl)aminomethane buffer modification of *Escherichia coli* outer membrane permeability. Journal of Bacteriology *145*, 1397-1403.

Jaeger, H.M. and Nagel, S.R. (1992). Physics of Granular States. Science *255*, 1524.

Jana, S. and Deb, J.K. (2004). Strategies for efficient production of heterologous proteins in *Escherichia coli*. Applied Microbiology and Biotechnology *67*, 289-298.

Janeway, C.A., Travers, P., Walport, P., and Shlomchik, M. (2001). Immunobiology. Garland Publishing (Oxford, UK).

Jefferis, R. and Lund, J. (1997). Glycosylation of antibody molecules: structure and functional significance. Chemical Immunology *65*, 111-128.

Jepras, R.I., Paul, F.E., Pearson, S.C., and Wilkinson, M.J. (1997). Rapid assessment of antiobiotic effects on *Escherichia coli* by *bis*-(1,3-dibutylbarbituric acid) trimethine oxonol and flow cytometry. Antimicrobial agents and chemotherapy *41*, 2001-2005.

Johnson, B.H. and Hecht, M.H. (1994). Recombinant proteins can be isolated from *E. coli* by repeated cycles of freezing and thawing. Bio/Technology *12*, 1357-1360.

Joosten, V., Lokman, C., Van den Hondel, C., and Punt, P.J. (2003). The production of antibody fragments and antibody fusion proteins by yeast and filamentous fungi. Microbial Cell Factories *2*, 1-15.

Katsui, N., Tsuchido, T., Hiramatsu, R., Fujikawa, S., Takano, M., and Shibsaki, I. (1982). Heat-induced blebbing and vesiculation of the outer membrane of *Escherichia coli*. Journal of Bacteriology *151*, 1523-1531.

Kempler, G. and Ray, B. (1978). Nature of freezing damage on the lipopolysaccharide molecule of *Escherichia coli* B. Cryobiology *15*, 578-584.

Keshavarz-Moore, E., Hoare, M., and Dunnill, P. (1990). Disruption of baker's yeast in a high-pressure homogenizer: New evidence on mechanism. Enzyme and Microbial Technology *12*, 764-770.

Kohler, G. and Milstein, C. (1975). Continuous cultures of fused cells secreting antibody of predefined specificity. Nature *256*, 495-497.

Krauss, J. (2003). Recombinant antibodies for the diagnosis and treatment of cancer. Molecular Biotechnology *25*, 1-17.

Kurien, B. and Scofield, K.B. (2006). Western blotting. Methods *38*, 283-293.

Lacki, K.M., Bergander, T., Gronberg, A., and Oberg, K. High throughput process development: Determination of dynamic binding capacity using microtitre plates filled with chromatography resins. [Downstream Processing: High Throughput screening in process development]. 2008. http://www.biotwebinar.com/JANUARY112007.html, ACS:BIOT. 11-1-0008.

Larrick, J.W. and Thomas, D.W. (2001). Producing proteins in transgenic plants and animals. Current Opinion in Biotechnology *12*, 411-418.

Larsen, P.I., Syndes, L.K., Landfald, B., and Strom, A.L. (1987). Osmoregulation in *Escherichia coli* by accumulation of organic osmolytes: Betaines, glutamic acid, and trehalose. Archives of Microbiology *147*, 1-7.

Lee, S.J., Chu, C.P., Tan, R.B.H., Wang, C.H., and Lee, D.J. (2003). Consolidation dewatering and centrifugal sedimentation of flocculated activated sludge. Chemical Engineering Science *58*, 1687-1701.

Lee, S.Y. (1996). High cell density culture of *Escherichia coli*. Trends in Biotechnology *14*, 98-105.

Leung, W.W.-F. (1998). Industrial centrifugation technology. McGraw Hill (New York).

Levin, A.A. and Papageorgiou, L.G. (2004). A hierarchical solution for approach for multi-site capacity planning under uncertainty in the pharmaceutical industry. Computers and Chemical Engineering *28*, 707-725.

Levy, H. and Zamir, A. (1994). Long-term cryoconservation of the halotolerant alga *Dunaliella*. Trends in Genetics *10*, 1-3.

Levy, M.S., Ciccolini, L.A.S., Yim, S.S.S., Tsai, J.T., Titchener-Hooker, N.J., Ayazi Shamlou, P., and Dunnill, P. (1999a). The effects of material properties and fluid flow intensity on plasmid DNA recovery during cell lysis. Chemical Engineering Science *54*, 3171-3178.

Levy, M.S., Collins, I.J., Yim, S.S.S., Titchener-Hooker, N.J., Ayazi Shamlou, P., and Dunnill, P. (1999b). Effect of shear on plasmid DNA in solution. Bioprocess and Biosystems Engineering *20*, 7-13.

Lewis, G., Taylor, I.W., Nienow, A.W., and Hewitt, C.J. (2004). The application of multi-parameter flow cytometry to the study of recombinant *Escherichia coli* batch fermentation processes. Journal of Industrial Microbiology and Biotechnology *31*, 311-322.

Lian, L-Y., Barsukov, I.L., Derrick, J.P., and Roberts, G.C.K. (1994). Mapping the interactions between streptococcal protein G and the Fab fragment of IgG in solution. Nature Structural and Molecular Biology *1*, 355-357.

Lim, A.C., Zhou, Y., Washbrook, J., Titchener-Hooker, N.J., and Farid, S. (2004a). A decisional-support tool to model the impact fo regulatory compliance activities in the biomanufacturing industry. Computers and Chemical Engineering *28*, 727-735.

Lim, H.-K., Kim, S.-G., Jung, K.-H., and Seo, J.-H. (2004b). Production of the kringle fragments of human apolipoprotein(a) by continuous lactose induction strategy. Journal of Biotechnology *108*, 271-278.

Lim, A.C., Washbrook, J., Titchener-Hooker, N.J., and Farid, S. (2006). A computer-aided approach to compare the production economics of fed-batch and perfusion culture under uncertainty. Biotechnology and Bioengineering *93*, 687-697.

Low, D., O'Leary, R., and Pujar, N.S. (2007). Future of antibody purification. Journal of Chromatography B *848*, 48-63.

Luderitz, O., Freudenberg, M.A., Galanos, C., Lehmann, V., Rietschel, E.T., and Shaw, D.H. (1982). Lipopolysaccharides of gram-negative bacteria. Current Topics in Membrane Transport *17*, 79-151.

Madigan, M.T., Martinko, J.M., and Parker, J. (2000). Brock biology of microorganisms., Prentice-Hall International (UK) Ltd., ed. (London).

Malamy, M. and Horecker, B.L. (1961). The localization of alkaline phosphatase in *E. coli* K12. Biochemical and Biophysical Research Communications *5*, 104-108.

Mannweiler, K. and Hoare, M. (1992). The scale-down of an industrial disc-stack centrifuge. Bioprocess Eng. *8*, 19-25.

Manting, E.H. and Driessen, J.M. (2000). *Escherichia coli* translocase: the unravelling of a molecular machine. Molecular Microbiology *37*, 226-238.

Marvin, H.J., Ter Beest, M.B., and Witholt, B. (1989). Release of outer membrane fragments from wild-type *Escherichia coli* and from several *E. coli* lipopolysaccharide mutants by EDTA and heat shock treatments. Journal of Bacteriology *171*, 5262-5267.

Maybury, J.P., Mannweiler, K., Titchener-Hooker, N.J., Hoare, M., and Dunnill, P. (1998). The performance of a scaled down industrial disc-stack centrifuge with a reduced feed material requirement. Bioprocess and Biosystems Engineering *18*, 191-199.

Maybury, J.P., Hoare, M., and Dunnill, P. (2000). The use of laboratory centrifugation studies to predict performance of industrial machines: studies of shear-insensitive and shear-sensitive materials. Biotechnology and Bioengineering *67*, 265-273.

Mazor, Y., Van Blarcom, T., Mabry, R., Iverson, B.L., and Georgiou, G. (2007). Isolation of engineered full-length antibodies from libraries expressed in *Escherichia coli*. Nature Biotechnology *25*, 563-565.

Mazur, P. (1966). Physical and chemical basis of injury in single-celled microorganisms subjected to freezing and thawing. In Cryobiology, H.T.Merryman, ed. (London: Academic Press), pp. 214-315.

Mazur, P. (1970). Cryobiology: the freezing of biological systems. Science *168*, 939-949.

McBroom, A.J. and Kuehn, M.J. (2007). Release of outer membrane vesicles by Gram-negative bacteria is a novel envelope stress response. Molecular Microbiology *63*, 545-558.

McGann, L.E. (1978). Differing actions of penetrating and nonpenetrating cryoprotective agents. Cryobiology *15*, 382-390.

McGann, L.E. (1979). Optimal temperature ranges for control of cooling rate. Cryobiology *16*, 211-216.

McKersie, B.D., Chen, Y., Beus, M.D., Bowley, S.R., Bowler, C., Inze, D., D'Halluin, K., and Botterman, J. (2005). Superoxide dismutase enhances tolerance of freezing stress in transgenic alfalfa (*Medicago sativa L.)*. Plant Physiology *103*, 1155-1163.

Menter, F.R. (1996). A comparison of some recent eddy–viscosity turbulence models. Journal of Fluids Engineering *118*, 514-519.

Menzella, H.G., Ceccarelli, E.A., and Gramajo, H.C. (2003). Novel *Escheichia coli* strain allows efficient recombinant protein production using lactose as an inducer. Biotechnology and Bioengineering *82*, 809-817.

Mergulhao, F.J.M. and Monteiro, G.A. (2004). Secretion capacity limitations of the Sec pathway in *Escherichia coli*. Journal of Microbiolology and Biotechnology *14*, 128-133.

Mergulhao, F.J.M., Summers, D.K., and Monteiro, G.A. (2005). Recombinant protein secretion in *Escherichia coli*. Biotechnology Advances *23*, 177-202.

Micheletti, M. and Lye, G.J. (2006). Microscale bioprocess optimisation. Current Opinion in Biotechnology *17*, 611-618.

Missiakas, D. and Raina, S. (1997a). Protein folding in the bacterial periplasm. Journal of Bacteriology *179*, 2465-2471.

Missiakas, D. and Raina, S. (1997b). Protein misfolding in the cell envelope of *Escherichia coli*: new signalling pathways. Trends in Biochemical Sciences *22*, 59-63.

Molecular Physics Correspondent (1972). What is random close packing? Nature *239*, 488-489.

Morrison, S.L. (1992). *In vitro* antibodies: strategies for production and application. Annual Review of Immunology *10*, 239-265.

Muhlradt, P.F. and Golecki, J.R. (1975). Asymmetric distribution and artifactual reorientation of lipopolysaccharide in the outer membrane bilayer of *Salmonella typhimurium*. European Journal of Biochemistry *51*, 343-352.

Munro, P.A. and Van Til, H.J. (1988). Centrifugal dewatering of acid casein curd: Effect of casein manufacturing and centrifugation variables on curd compression in a laboratory centrifuge. Biotechnology and Bioengineering *32*, 1153-1157.

Murrell, N.J. An engineering study of the recovery of shear sensitive biological materials by high speed disc-stack centrifugation. (1998). PhD. UCL.

Mustafa, M.A., Washbrook, J., Lim, A.C., Zhou, Y.H., Titchener-Hooker, N.J., Morton, P., Berezenko, S., and Farid, S.S. (2004). A software tool to assist business-process decision-making in the biopharmaceutical industry. Biotechnology Progress *20*, 1096-1102.

Naglak, T.J. and Wang, H.Y. (1990). Recovery of a foreign protein from the periplasm of *Escherichia coli* by chemical permeabilisation. Enzyme and Microbial Technology *12*, 603-611.

Nail, S.L. and Searles, J.A. (2008). Elements of quality by design in development and scale-up of freeze-dried parenterals. Biopharm International *21*, 44-52.

Nakano, K., Rischke, M., Sato, S., and Markl, H. (1997). Influence of acetic acid on the growth of *Escherichia coli* K12 during high cell-density cultivation in a dialysis reactor. Applied Microbial Biotechnology *48*, 597-601.

Neal, G., Christie, J., Keshavarz-Moore, E., and Ayazi Shamlou, P. (2003). Ultra scale-down approach for the prediction of full-scale recovery of ovine polycolonal immunoglobulins used in the manufacture of snake venom-specific Fab fragment. Biotechnology and Bioengineering *81*, 149-157.

Nebe-von-Caron, G., Stephens, P.J., Hewitt, C.J., Powell, J.R., and Badley, R.A. (2000). Analysis of bacterial function by multi-colour and single cell sorting. Journal of Microbiology Methods *42*, 97-114.

Nei, T., Araki, T., and Matsusaka, T. (1967). The mechanism of cellular injury by freezing in microorganisms. In Cellular Injury and Resistance in Freezing Organisms, E.Asahina, ed. (Sapporo: Institute of Low Temperature Science), pp. 157-169.

Neu, H.C. and Heppel, L.A. (1964). The release of ribonuclease into the medium when *Escherichia coli* cells are converted to spheroplasts. Journal of Biological Chemistry *239*, 3893-3900.

Neu, H.C. and Heppel, L.A. (1965). The release of enzymes from *Escherichia coli* by osmotic shock and during the formation of spheroplasts. Journal of Biological Chemistry *240*, 3685-3692.

Ngiam, S.-H., Zhou, Y.H., Turner, M.K., and Titchener-Hooker, N.J. (2001). Graphical method for the calculation of chromatographic performance in representing the trade-off between purity and recovery. J. Chrom. A. *937*, 1-11.

Nossal, N.G. and Heppel, L.A. (1966). The release of enzymes by osmotic shock from *Escherichia coli* in exponential phase. Journal of Biological Chemistry *241*, 3055-3062.

Onyeaka, H., Nienow, A.W., and Hewitt, C.J. (2003). Further studies related to the scale-up of high cell density *Escherichia coli* fed-batach fermentations: the additional effect of a changing microenvironment when using aqueous ammonia to control pH. Biotechnology and Bioengineering *84*, 474-484.

Osborn, M.J. and Wu, H.C.P. (1980). Proteins of the outer membrane of gram-negative bacteria. Annual Review of Microbiology *34*, 422.

Packer, E.L., Ingraham, J.L., and Scher, S. (1965). Factors affecting the rate of killing of *Escherichia coli* by repeating freezing and thawing. Journal of Bacteriology *89*, 718-724.

Park, J.I., Grant, C.M., Attfield, P.V., and Dawes, I.W. (2005). The freeze-thaw stress response of the yeast *Saccharomyces cerevsiae* is growth phase specific and is controlled by nutritional state via the RAS-cyclic AMP signal transduction pathway. Applied and Environmental Microbiology *63*, 3818-3824.

Perlmutter, R. (2007). Conquering the innovation deficit in drug discovery. Loews Hotel, Coronado Island, CA, USA, AIChE. SBE's 1st International Conference on Accelerating Bopharmaceutical Development. 19-3-2007.

Persson, J. and Lester, P. (2004). Purification of antibody and antibody-fragment from E. coli homogenate using 6,9-diamino-2-ethoxyacridine lactate as precipitation agent. Biotechnology and Bioengineering *87*, 424-434.

Petrides, D.P., Koulouris, A., and Lagonikos, P.T. (2002). The role of process simulation in pharmaceutical process development and product commercialisation. Pharmaceutical Engineering *22*, Jan/Feb.

Pier, G.B., Lyczak, J.B., and Wetzler, L.M. (2004). Immunology, infection and immunity. ASM Press (Washington, DC).

Pisano, G. and Wheelwright, S.C. (1995). High-tech R&D. Harvard Business Review *73*, 93-105.

Pollock, D.P., Kutzko, J.P., Birck-Wilson, E., Williams, J.L., Echelard, Y., and Meade, H.M. (1999). Transgenic milk as a method for the production of recombinant antibodies. Journal of Immunological Methods *231*, 147-157.

Pugsley, A.P. (1993). The complete general secretory pathway in gram-negative bacteria. Microbiological Reviews *57*, 50-108.

Qiu, J., Swartz, J.R., and Georgiou, G. (1998). Expression of active human tissue-type plasminogen activator in *Escherichia coli*. Applied and Environmental Microbiology *64*, 4891-4896.

Raag, R. and Whitlow, M. (1995). Single chain Fvs. FASEB Journal *9*, 73-80.

Raivio, T.L. and Silhavy, T.J. (2004). Periplasmic stress and ECF sigma factors. Annual Review of Microbiology *55*, 591-624.

Rathore, A.S., Branning, R., and Cecchini, D. (2007). Design space for biotech products. Biopharm International *20*, 36-40.

Ravetch, J.V. and Bolland, S. (2001). IgG Fc receptors. Annual Review of Immunology *19*, 275-290.

Ray, B., Souza, H., and Speck, M.L. (1975). Cryoprotection of *Escherichia coli* by penetrating and nonpenetrating cryopreservatives. Cryobiology *12*, 553.

Reen, D.J. (1994). Enzyme-linked immunosorbent assay (ELISA). Methods in Molecular Biology *32*, 133-140.

Reynolds, T., Boychen, M., Sanderson, T., Bulmer, M., More, J., and Hoare, M. (2003). Scale-down of continuous filtration for rapid bioprocess design: Recovery and dewatering of protein precipitate suspensions. Biotechnology and Bioengineering *83*, 454-464.

Richardson, J.F. and Zaki, W.N. (1954). Sedimentation and fluidisation: Part I. Trans IChemE. *32*, 35-53.

Rietschel, E.T., Galanos, C., Luderitz, O., and Westphal, O. (1982). The chemistry and biology of lipopolysccharides and their lipid A component. In Immunopharmacology and the regulation of leukocyte function, D.R.Webb, ed. pp. 183-229. Marcel Dekker (Basel, Switzerland).

Rodrigues, M.L., Snedcor, B., Chen, C., Wong, W.L.T., Garg, S., Blank, G.S., Maneval, D., and Carter, P.J. (1993). Engineering Fab' fragments for efficient $F(ab)_2$ formation in *Escherichia coli* and for improved *in vivo* stability. Journal of Immunology *151*, 6954-6961.

Rongxiu, L., Dowd, V., Stewart, D.J., Burton, S.J., and Lowe, C.R. (1998). Design, synthesis, and application of a Protein A mimetic. Nature Biotechnology *16*, 190-195.

Roque, A.C.A., Lowe, C.R., and Taipa, M.A. (2004). Review: Antibodies and genetically engineered related molecules: production and purification. Biotechnology Progress *20*, 639-654.

Ruthven, D.M. (1997). Encyclopaedia of separation technology. p. 282. John Wiley and Sons, Inc. (New York).

Ryan, W. and Parulekar, S.J. (1991). Recombinant protein synthesis and plasmid instability in continuous cultures of *Escherichia coli* JM103 harbouring a high copy number plasmid . Biotechnology and Bioengineering *37*, 415-429.

Sachidanandham, R., Gin, K.Y-H., and Poh, C.L. (2005). Monitoring of active but non-culturable bacterial cells by flow cytometry. Biotechnology and Bioengineering *89*, 24-31.

Saier, M.H. (2006). Protein secretion and membrane insertion systems in gram-negative bacteria. Journal of Membrane Biology *214*, 75-90.

Salte, H. Rapid evaluation of options for the primary recovery of antibody fragments expressed in high cell density cultures. 2006. PhD UCL.

Sandee, D., Tungpradabkul, S., Kurokawa, Y., Fukui, K., and Takagi, M. (2005). Combination of Dsb coexpression and an addition of sorbitol markedly enhanced soluble expression of single-chain Fv in *Escherichia coli*. Biotechnology and Bioengineering *91*, 418-424.

Scanziani, E. (1998). Immunohistochemical staining of fixed tissues. Methods in Molecular Biology *31*, 461-466.

Schlichting, H. (1979). Boundary layer theory. Pergamon Press (London).

Shah, N. (2004). Pharmaceutical supply chains: key issues and strategies for optimisation. Computers and Chemical Engineering *28*, 929-941.

Shaw Stewart, P.D. and Baldock, P.F.M. (1999). Practical experimental design techniques for automatic and manual protein crystallization. Journal of Crystal Growth *196*, 665-673.

Shibui, T. and Nagahari, K. (1992). Selection of a functional Fab fragment in *Escherichia coli* and the influence of culture conditions. Applied Microbiology and Biotechnology *37*, 352-357.

Shiloach, J. and Fass, R. (2005). Growing *E. coli* to high cell density - A historical persective on method development. Biotechnology Advances *23*, 345-357.

Shusta, E.V., Raines, R.T., Pluckthun, A., and Wittrup, K.D. (1998). Increasing the secretory capacity of *Saccharomyces cerevisiae* for production of single-chain antibody fragments. Nature Biotechnology *16*, 773-777.

Siddiqi, S.F., Titchener-Hooker, N.J., and Ayazi Shamlou, P. (1996). Simulation of particle size distribution changes occurring during high-pressure disruption of baker's yeast. Biotechnology and Bioengineering *50*, 145-150.

Sidhu, S.S. and Fellouse, F.A. (2006). Synthetic therapeutic antibodies. Nature Chemical Biology *2*, 682-688.

Silber, K.R., Keiler, K.C., and Sauer, R.T. (1992). Tsp: a tail-specific protease that selectively degrades proteins with nonpolar C termini. Proceedings of the National Academy of Science USA *80*, 295-299.

Simmons, L.C., Reilly, D., Klimowski, L., Raju, T.S., Meng, G., Sims, P., Hong, K., Shields, R.L., Damico, L.A., Rancatore, P., and Yansura, D.G. (2002). Expression of full-length immunoglobulins in *Escherichia coli*: rapid and efficient production of aglycosylated antibodies. Journal of Immunological Methods *263*, 133-147.

Skerra, A. and Pluckthun, A. (1988). Assembly of a functional immunoglobulin Fv fragment in Escherichia coli. Science *240*, 1038-1041.

Souza, H. (1980). Studies on the damage to *Escherichia coli* cell membrane caused by different rates of freeze-thawing. Biochemica et Biophysica Acta - Biomembranes *603*, 13-26.

Steen, H.B. (2000). Flow cytometry of bacteria: glimpses from the past with a view to the future. Journal of Microbiology Methods *42*, 65-74.

Steinhaus, I. (1987). The problems of mathematics, pp. 69-82. Oxford University Press (Oxford, UK).

Steponkus, P.L., Stout, D.G., Wolfe, J., and Lovelace, R.V.E. (1985). Possible role of transient electric fields in freezing-induced membrane destabilisation. Journal of Membrane Biology *85*, 191-198.

Sundstrom, H., Wallberg, F., Ledung, E., Norrman, B., Hewitt, C.J., and Enfors, S-O. (2004). Segregation to non-dividing cells in recombinant *Escherichia coli* fed-batch fermentation processes. Biotechnology Letters *26*, 1533-1539.

Sutherland, K. (2005). Centrifuge focus: solids removal - the options. Filtration and Separation *42*, 16-20.

Swamy, K.H.S. and Goldberg, A.L. (1982). Subcellular distribution of various proteases in *Escherichia coli*. Journal of Bacteriology *149*, 1027-1033.

Terryn, C., Michel, J., Kilian, L., Bohomme, P., and Balossier, G. (2000). Comparision of intracellular water content measurements by dark-field imaging and EELS in medium voltage TEM. The European Physical Journal Applied Physics *11*, 215-226.

Thommes, J., Bader, A., Halfar, M., Karau, A., and Kula, M.-R. (1996). Isolation of monoclonal antibodies from cell containing hydridoma broth using a protein A coated adsorbent in expanded beds. Journal of Chromatography A *752*, 111-122.

Thommes, J. and Etzel, M. (2007). Alternatives to chromatographic separations. Biotechnology Progress *23*, 42-45.

Titchener-Hooker, N.J., Zhou, Y.H., Hoare, M., and Dunnill, P. (2001). Biopharmaceutical process development: Part II, Methods of reducing development time. Biopharm Europe *13*, 68-74.

Tsuchido, T., Katsui, N., Takeuchi, A., Takano, M., and Shibaski, I. (1985). Destruction of the outer membrane permeability barrier of *Escherichia coli* by heat treatment. Applied Environmental Microbiology *50*, 298-303.

Tsumoto, K., Nakaoki, Y., Ueda, Y., Ogasahara, K., Yutani, K., Watanabe, K., and Kumagai, I. (1994). Effect of the order of antibody variable regions on the expression of single-chain HyHEL10 Fv fragment in *E. coli* and the thermodynamic analysis of its antigen binding properties. Biochemical and Biophysical Research Communications *201*, 546-551.

U.S. Food and Drug Administration (1987). Guidance for industry: Guidelines on general principles of process validation. (Rockville, MD).

U.S. Food and Drug Administration (2002). www.fda.gov/cder/OPS/PAT.htm. Electronic Citation.

U.S. Food and Drug Administration (2006). Guidance for industry: Q8 pharmaceutical development. (Rockville, MD.

Underdown, B. and Schiff, J. (1986). Immunoglobin A: strategic defense initiative at the mucosal surface. Annual Review of Immunology *4*, 389-417.

Ujam, S.B. A scale-down evaluation of adsorptive process options for the recovery and initial purification of antibody fragments from crude *E. coli* feedstocks. 2007. PhD. UCL.

Vaara, M. (1992). Agents that increase the permeability of the outer membrane. Microbiology Reviews *56*, 295-411.

Van Alphen, L., Verkleij, A., Leunissen-Bijvelt, J., and Lugtenberg, B. (1978). Architecture of the outer membrane of *Escherichia coli* III. Protein-lipopolysaccharide complexes in intramembraneous particles. Journal of Bacteriology *134*, 1089-1098.

Veronese, F.M. and Pasut, G. (2005). PEGylation, successful approach to drug delivery. Drug Discovery Today *12*, 1451-1458.

Viloria-Cols, M.E., Hatti-Kaul, B., and Mattiasson, J. (2004). Agarose-coated anion exhanger prevent cell-adsorbent interactions. Journal of Chromatography A *1043*, 195-200.

Voet, D. and Voet, J.G. (1995). Biochemistry. John Wiley & Sons, Inc. (New York).

Voisard, D., Meuwly, F., Ruffieux, P.A., Baer, G., and Kadouri, A. (2003). Potential of cell retention techniques for large-scale high-density perfusion culture of suspended mammalian cells. Biotechnology and Bioengineering *82*, 751-765.

Von Heijne, G. (1998). Life and death of a signal peptide. Nature *396*, 111-113.

Wallberg, F., Sundstrom, H., Ledung, E., Hewitt, C.J., and Enfors, S.-O. (2005). Monitoring and quantification of inclusion body formation in *Escherichia coli* by multiparameter flow cytometry. Biotechnology Letters *27*, 919-926.

Walsh, G. (2007). Biopharmaceuticals: approval trends in 2006. Biopharm International *20*, 55-67.

Wang, F. and Lee, S.Y. (1998). High cell density culture of metabolically engineered *Escherichia coli* for the production of poly(3-hydroxybutyrate) in a defined medium. Biotechnology and Bioengineering *58*, 325-328.

Wang, Y-H., Yang, B., Ren, J., Gong, M.-L., Liang, D., and Xu, A.-L. (2004). Optimization of medium composition for the production of clavulanic acid by *Streptomyces clavuligerus*. Process Biochemistry *40*, 1161-1166.

Watson, J.P. (1965). Molecular biology of the gene. (New York: W.A. Benjamin).

Weir, A.N.C. and Bailey, N.A. Process for obtaining antibodies using heat treatment. Celltech Therapeutics Limited (Berkshire, UK). (1997). United States Patent 5665866.

Weir, A.N.C. and Mountain, A. (1999). Method for expressing recombinant genes in bacteria in absence of antibiotic selection. United States Patent 5928903.

Wells, D. (1986). The penguin dictionary of curious and interesting numbers. p. 29.: Penguin Books (Middlesex, UK).

Wells, D. (1991). The penguin dictionary of curious and interesting geometry. pp. 237-238. Penguin Books (Middlesex, UK).

Wenger, M.D., DePhillips, P., Price, C.E., and Bracewell, D.G. (2007). An automated microscale chromatographic purification of virus-like particles as a strategy for process development. Biotechnology and applied biochemistry *47*, 131-139.

Wierling, P.S., Bogumil, R., Knieps-Grunhagen, E., and Hubbuch, J. (2007). High-throughput screening of packed-bed chromatography coupled with SELDI-TOF MS analysis: Monoclonal antibodies versus host cell protein. Biotechnology and Bioengineering *98*, 440-450.

Williams, N. (2000). Immunoprecipitation procedures. Methods in Cellular Biology *62*, 449-453.

Williams, S.R. and Philipse, A.P. (2003). Random packings of spheres and spherocylinders simulated by mechanical contraction. Physical Review *E67*.

Willoughby, N., Martin, P., and Titchener-Hooker, N.J. (2005). Extreme scale-down of expanded bed adsorption: purification of an antibody fragment directly from recombinant *E. coli* culture. Biotechnology and Bioengineering *87*, 641-647.

Wolfe, J. and Bryant, G. (2001). Cellular cryobiology: thermodynamic and mechanical effects. International Journal of Refrigeration *24*, 438-450.

Wong, H.W., Kim, Y.C., Lee, S.Y., and Chang, H.N. (1997). Effect of post-induction nutrient feeding strategies on the production of bioadhesive protein in *Escherichia coli*. Biotechnology and Bioengineering *60*, 271-276.

Wright, A. and Morrison, S.L. (1997). Effect of glycosylation on antibody function: implications for genetic engineering. Trends in Biotechnology *15*, 26-32.

Yanaida, K. and Ohasi, A. Flow characteristics of water jets. A3-A39. 1978. Fourth international symposium on jet cutting technology.

Yim, S.S. and Shamlou, P.A. (2000). The engineering effects of fluids flow on freely suspended biological macro-materials and macromolecules. Advances in Biochemical Engineering/Biotechnology *67*, 83-122.

Yu, L.X. Implementation of quality-by-design: Question based review. Drug Information Association 2nd Annual Meeting. 2006.

Zapata, G., Ridgway, J.B.B., Mordenti, J., Osaka, G., Wong, W.L.T., Bennett, G.L., and Carter, P.J. (1995). Engineering linear $F(ab)_2$ fragments for efficient production in *Escherichia coli* and enhanced antiproliferative activity. Protein Engineering *8*, 1057-1062.

Zhang, H., Kong, S., Booth, A.J., Boushaba, R., Levy, M.S., and Hoare, M. (2007). Prediction of shear damage of plasmid DNA in pump and centrifuge operations using an ultra scale-down device. Biotechnology Progress *23*, 858-865.

Zhou, Y.H. and Titchener-Hooker, N.J. (1999). Visualizing integrated bioprocess designs through "windows of operation". Biotech. Bioeng. *65*, 550-557.

Zierold, K. (1988). Methods in microbiology. Academic Press (London, UK).

Zimmermann, J.J.F., Oddie, K., Langer, R., and Cooney, C.L. (1991). The release of heparinase from the periplasmic space of *Flavobacterium heparinum* by three step osmotic shock. Applied Biochemistry and Biotechnology *30*, 137-148.

Appendix A1: Bacterial growth rate calculations

The specific growth rates (μ) presented were calculated as follows.

The number of cells at any point (B) is dependent upon the number of cells at time zero (B_0) and a constant (μ, the specific growth rate), i.e.:

$$B = \mu.B_0 \qquad \text{[A1-1]}$$

The change in cell number over time (t) is shown in Equation A1-2:

$$\frac{dB}{dt} = \mu.B \qquad \text{[A1-2]}$$

Therefore to determine μ:

$$\int \frac{1}{B} dB = \int \mu dt \qquad \text{[A1-3]}$$

This gives:

$$\ln B = \mu t + C \qquad \text{[A1-4]}$$

Thereby the gradient of a plot of ln B over t will determine the specific growth rate. In this Chapter 3 B has been assumed to be proportional to the optical density at 600 nm and also the DCW. An example of a typical growth rate determination is given in Fig. A1-1.

The generation time, or doubling time (t_d), is the time required for the cell population to double. This can be calculated from the specific growth rate as shown in Equation A1-5.

$$t_d = \frac{\ln 2}{\mu} \qquad \text{[A1-5]}$$

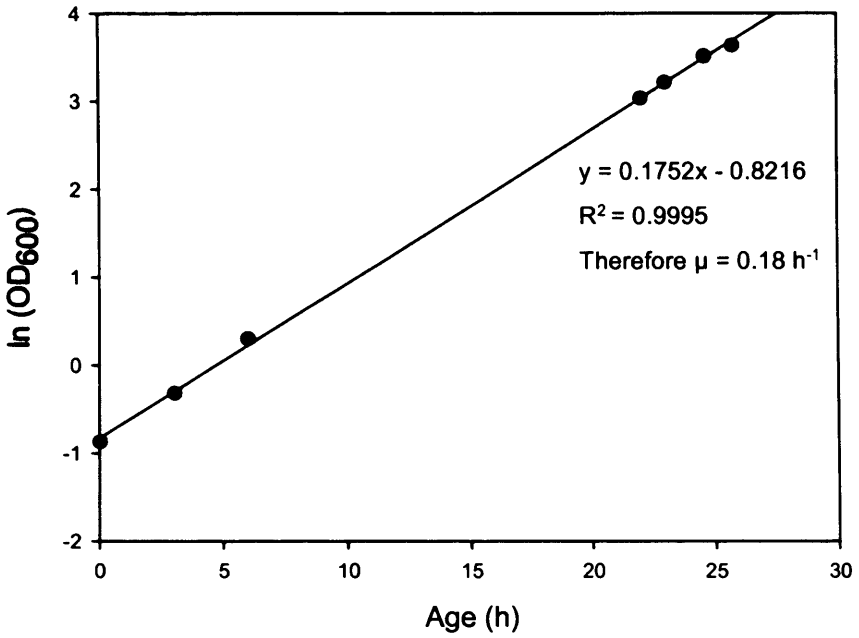

Fig. A1-1: The determination of the initial growth rate as part of the IPTG-induced process characterisation detailed in section 3.3.2. The specific growth rate, μ, is equal to the gradient of a plot of the natural log of the cell number against fermentation time. Note that pre-induction OD_{600} is used to estimate cell number.

Appendix A2: Relative centrifugal force

The spin speed, N (rps), and the corresponding RCF value at which a centrifuge is operated are related by the following equations:

$$RCF = \frac{r\omega^2}{g} \qquad \text{[A2-1]}$$

Where r is the centrifugal radius and ω is the angular velocity (rad/s), given by:

$$\omega = 2\pi N \qquad \text{[A2-2]}$$

Appendix A3: MATLAB code and curve-fit equations used to create process model

In this section full details are given of the process model created in Chapter 8 relating the upstream post-induction glycerol feed rate to Fab' yield after initial DSP.

A3.1 Curve fit equations

The equations of the curves fit to the experimental data in Figures 8-2, 8-5, 8-6 and 8-9 are given below.

A3.1.1 Fig. 8-2 Equations

The effect of post-induction glycerol feed rate upon Fab' yield during the fermentation:

$$Yield(fermentation) = 12109x - 4277.2x^2 - 7459.8 \quad \text{[A3-1]}$$

A3.1.2 Fig. 8-5 Equations

The effect of post-induction glycerol feed rate upon clarification efficiency during centrifugal cell harvest, determined at pilot (Eqn. A3-2) and USD (Eqn. A3-3) scale.

$$\%Clarification(pilot) = 99.878x - 38.526x^2 + 34.628 \quad \text{[A3-2]}$$

$$\%Clarification(USD) = 94.567x - 36.275x^2 + 36.364 \quad \text{[A3-3]}$$

A3.1.3 Fig. 8-6 Equations

The effect of post-induction glycerol feed rate upon % Fab' extraction during periplasmic extraction procedure, determined at pilot (Eqn. A3-4) and USD (Eqn. A3-5) scale.

$$\%Extraction(pilot) = 42.301x + 8.4288 \quad \text{[A3-4]}$$

$$\%Extraction(USD) = 16.178x^2 - 11.202x + 53.489 \quad \text{[A3-5]}$$

A3.1.4 Fig. 8-8 Equations

The effect of post-induction glycerol feed rate upon dewatering yield during centrifugal spheroplast removal, determined at pilot (Eqn. A3-6) and USD (Eqn. A3-7) scale.

$$Yield(pilot) = 1.042 - 0.0464x \qquad [A3\text{-}6]$$

$$Yield(USD) = 1.0359 - 0.0478x \qquad [A3\text{-}7]$$

A3.2 MATLAB code

In the following pages the code used to generate the process model presented in Chapter 8 is displayed.

A3.2.1 Pilot-scale model

```
function Yield = Summary(Flowrate)
%%%%%%%%%%%%%%%%%%%%%%%%%%%%%%%%%%%%%%%%%%%%%%%%%%%%%%%%%%%%%%%%%%%%%%
%
%This is the hub of my pilot-plant model. Here we determine the total
%amount of Fab that will be produced at the end of the 2nd
centrifugation step for an input of a range of flowrates over the
whole process. This model only calculates the output for a harvest
time of 36hrs. Note that this model gives total Fab produced NOT fab
productivity.
%%%%%%%%%%%%%%%%%%%%%%%%%%%%%%%%%%%%%%%%%%%%%%%%%%%%%%%%%%%%%%%%%%%%%%
%
%First calculate the amount of Fab that the Flowrate would produce.
FermenterYield=Fermentation2(Flowrate);
%Again note that this is for a 36 hr harvest time. Also, flow rate is
%inputed in amount of 80% (w/w) Glycerol per h per L of starting broth
%Next calculate how much of this will survive the first centrifugation
Centrifuge1Yield=Centrifugation2(Flowrate);
Step1Yield=FermenterYield.*Centrifuge1Yield;
%Note that we have assumed that centrifuge yield directly correlates
with %
%clarification which may not be the case.
%Next calculate how much of this will survive the Lysis
LysisYield=Lysis2(Flowrate);
Step2Yield=Step1Yield.*LysisYield;
%next calculate how much of this will survive the second centrifuge
step
```

```
Centrifuge2Yield=Dewatering2(Flowrate);
Step3Yield=Step2Yield.*Centrifuge2Yield;
%No more steps are in our model therefore...
Yield=Step3Yield;
```

A3.2.2 USD model

```
function Yield = SummaryUSD(Flowrate)
%%%%%%%%%%%%%%%%%%%%%%%%%%%%%%%%%%%%%%%%%%%%%%%%%%%%%%%%%%%%%%%%%%%%%%%%
%
%This is the hub of my USD model. Here we determine the total
%amount of Fab that will be produced at the end of the 2nd
centrifugation step for an input of a range of flowrates over the
whole process. This model only calculates the output for a harvest
time of 36hrs. Note that this model gives total Fab produced NOT fab
productivity.
%%%%%%%%%%%%%%%%%%%%%%%%%%%%%%%%%%%%%%%%%%%%%%%%%%%%%%%%%%%%%%%%%%%%%%%%
%First calculate the amount of Fab that the Flowrate would produce.
FermenterYield=Fermentation2(Flowrate);
%Again note that this is for a 36 hr harvest time. Also, flow rate is
%inputed in amount of 80% (w/w) Glycerol per h per L of starting broth
%Next calculate how much of this will survive the first centrifugation
Centrifuge1Yield=Centrifugation2USD(Flowrate);
Step1Yield=FermenterYield.*Centrifuge1Yield;
%Note that we have assumed that centrifuge yield directly correlates
with %
%clarification which may not be the case.
%Next calculate how much of this will survive the Lysis
LysisYield=Lysis2USD(Flowrate);
Step2Yield=Step1Yield.*LysisYield;
%next calculate how much of this will survive the second centrifuge
step
Centrifuge2Yield=Dewatering2USD(Flowrate);
Step3Yield=Step2Yield.*Centrifuge2Yield;
%No more steps are in our model therefore...
Yield=Step3Yield;
```

A3.2.3 M-Files

A.3.2.3.1 Fermentation

```
function A=Fermentation2(Flowrate)
sizeofflowrate=size(Flowrate);
sizeofflowrate2=sizeofflowrate(1,2);
A=[];
```

```
for counter=1:1:sizeofflowrate2;
      A=[A,Fermentation(Flowrate(counter))];
end

function Fab = Fermentation(Flowrate)
%Here we calculate the amount of Fab inside the cells (i.e.
%[Fab]total-[Fab]supernatant for each flowrate
Result=12109*Flowrate-7459.8-(Flowrate.^2)*4277.2;
%As this is a polynominal will bring up negative values of [Fab].
Solving
%the polynominal (and from experimental data) we can see that if
Flowrate
%is >20, [Fab] will =0 (as can't produce negative Fab). Likewise, if
%Flowrate is less than 6, [Fab]=0, as here the graph goes negative as
well.
%Therefore...
if Result < 0
      Result=0;
end
Fab=Result;
```

A.3.2.3.2 Centrifugal cell harvest

A.3.2.3.2.1 Pilot-scale

```
function B=Centrifugation2(Flowrate)
sizeofflowrate=size(Flowrate);
sizeofflowrate2=sizeofflowrate(1,2);
B=[];
for counter=1:1:sizeofflowrate2;
      B=[B,Centrifugation(Flowrate(counter))];
end

function CY = Centrifugation(Flowrate)
%Here we calculate the % yield of the first centrifugation step
%Note this is for pilot-scale data only
Value2=99.878*Flowrate-38.526*(Flowrate.^2)+34.628;
%Correct for recoveries > 0 or < 100
if Value2 < 0
      Value2=0;
elseif Value2 > 100
      Value2=100;
end
%render into a ratio from a percentage
```

```
CY=(Value2/100);
%Centrifugation2 mat file continues this to adapt for matrices
```

A.3.2.3.2.2 USD

```
function B=Centrifugation2USD(Flowrate)
sizeofflowrate=size(Flowrate);
sizeofflowrate2=sizeofflowrate(1,2);
B=[];
for counter=1:1:sizeofflowrate2;
      B=[B,CentrifugationUSD(Flowrate(counter))];
end

function CY = CentrifugationUSD(Flowrate)
%Here we calculate the % yield of the first centrifugation step
%Note this is for pilot-scale data only
Value2=94.567*Flowrate-36.275*(Flowrate.^2)+36.364;
if Value2 < 0
      Value2=0;
elseif Value2 > 100
      Value2=100;
end
%render into a ratio from a percentage
CY=(Value2/100);
%Centrifugation2 mat file continues this to adapt for matrices
```

A.3.2.3.3 Periplasmic extraction

A.3.2.3.3.1 Pilot-scale

```
function C=Lysis2(Flowrate)
sizeofflowrate=size(Flowrate);
sizeofflowrate2=sizeofflowrate(1,2);
C=[];
for counter=1:1:sizeofflowrate2;
      C=[C,Lysis(Flowrate(counter))];
end

function LY = Lysis(Flowrate)%Here we calculate the ratio of Fab
inside the cells that is released by%lysis.
Value=42.301*Flowrate+8.4288;
%We must correct incase the equation gives over 100% release
if Value > 100
      Value=100;
end
```

```
%render into a ratio from a percentage
LY=(Value/100);
%Fermentation2 mat file continues this to adapt for matrices
```

A.3.2.3.3.2 USD

```
function C=Lysis2USD(Flowrate)
sizeofflowrate=size(Flowrate);
sizeofflowrate2=sizeofflowrate(1,2);
C=[];
for counter=1:1:sizeofflowrate2;
      C=[C,LysisUSD(Flowrate(counter))];
End

function LY = LysisUSD(Flowrate)
%Here we calculate the ratio of Fab inside the cells that is released
by%lysis.
Value=53.489+(Flowrate.^2)*16.178-11.202*Flowrate;
% Note that the quadratic will not give a value of less than 0.
%However, we must correct incase the equantion gives over 100% release
if Value > 100
      Value=100;
end
%render into a ratio from a percentage
LY=(Value/100);
%Fermentation2 mat file continues this to adapt for matrices
```

A.3.2.3.4 Centrifugal spheroplast removal

A.3.2.3.4.1 Pilot-scale

```
function D=Dewatering2(Flowrate)
sizeofflowrate=size(Flowrate);
sizeofflowrate2=sizeofflowrate(1,2);
D=[];
for counter=1:1:sizeofflowrate2;
      D=[D,Dewatering(Flowrate(counter))];
end

plot(Flowrate,D)
function DY=Dewatering(Flowrate)
%Here we calculate the yield of the dewatering step.
% Note this is for Pilot-scale data
Value3=1.042-0.0464*Flowrate;
%Note that this is a linear equation for determining the YIELD of the
```

```
%dewatering step. I have already converted %D into a YIELD
if Value3 > 100
      Value3=100;
elseif Value3 < 0
      Value3=0;
end
DY=Value3;
```

A.3.2.3.4.2 USD

```
function D=Dewatering2USD(Flowrate)
sizeofflowrate=size(Flowrate);
sizeofflowrate2=sizeofflowrate(1,2);
D=[];
for counter=1:1:sizeofflowrate2;
      D=[D,DewateringUSD(Flowrate(counter))];
end

plot(Flowrate,D)
function DY=DewateringUSD(Flowrate)
%Here we calculate the yield of the dewatering step.
% Note this is for Pilot-scale data
Value3=1.0359-0.0478*Flowrate;
%Note that this is a linear equation for determining the YIELD of the
%dewatering step. I have already converted %D into a YIELD.
if Value3 > 100
      Value3=100;
elseif Value3 < 0
      Value3=0;
end
DY=Value3;
```

Appendix A4: Publication

The paper 'Adapted Ultra Scale-Down Approach for Predicting the Centrifugal Separation Behaviour of High Cell Density Cultures' by Tustian et al. (2007), published in 'Biotechnology and Bioengineering', is printed overleaf.

Appendix A5: Conference Presentations

A selection of the work presented in this thesis has been presented at the following international conferences:

- Tustian, A.D., Bowering, L.C., Hoare M., Baganz, F. and Titchener-Hooker, N.J. (2007) An engineering study of key interactions within the process for antibody fragment production. *2nd Singapore biologics manufacturing conference.* Singapore 28-30 March.

- Tustian, A.D., Bowering, L.C., Baganz, F., Hoare, M. and Titchener-Hooker, N.J. (2007). The use of ultra scale-down approaches to enable rapid investigation and characterization of the initial downstream process for antibody fragment production in *E. coli*. Oral presentation in *society of biological engineering's first conference on accelerating biopharmaceutical development*, Coronado Island, California, USA. 19-22 March.

- Tustian, A.D., Bowering, L.C., Baganz, F., Hoare, M. and Titchener-Hooker, N.J.,. (2007). Development of ultra scale-down mimics for high cell density recovery operations. *Society of biological engineering's first conference on accelerating biopharmaceutical development.* Coronado Island, California, USA, 19-22 March.

- Tustian, A.D. (2006). Rapid ultra scale-down approach for predicting the dewatering of cellular sediments in industrial centrifuges. *Annual bioProcessUK conference 2006.* Edinburgh, UK, 29-30 November.

The research posters displayed at the '2nd Singapore Biologics Manufacturing Conference' and the 'Society of Biological Engineering's First Conference on Accelerating Biopharmaceutical Development (Fig. A5-1), and also at the 'Annual bioProcessUK Conference 2006' (Fig. A5-2) are displayed overleaf.

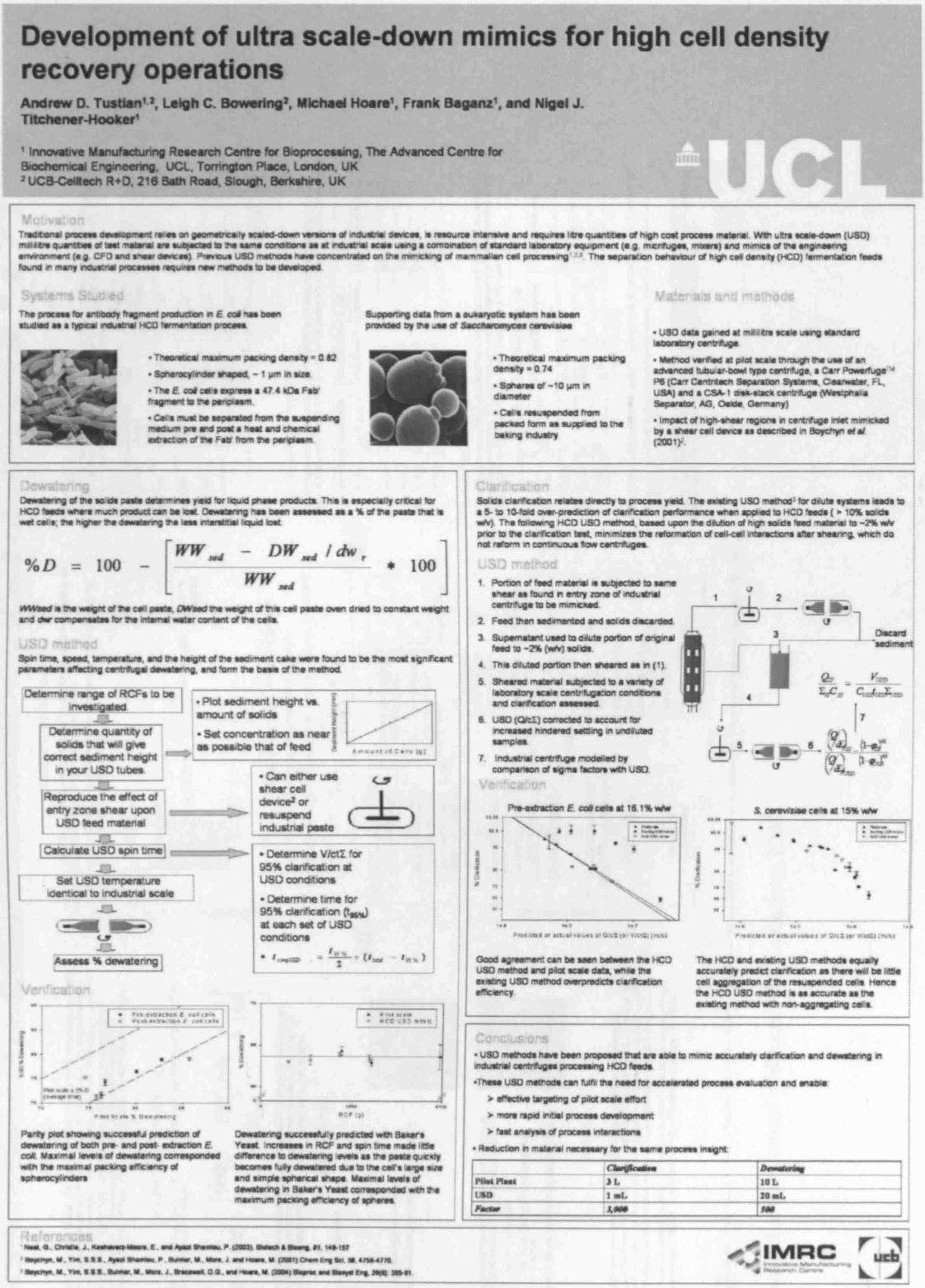

Fig. A5-1: Poster presented at '2nd Singapore Biologics Manufacturing Conference' and the 'Society of Biological Engineering's First Conference on Accelerating Biopharmaceutical Development'.

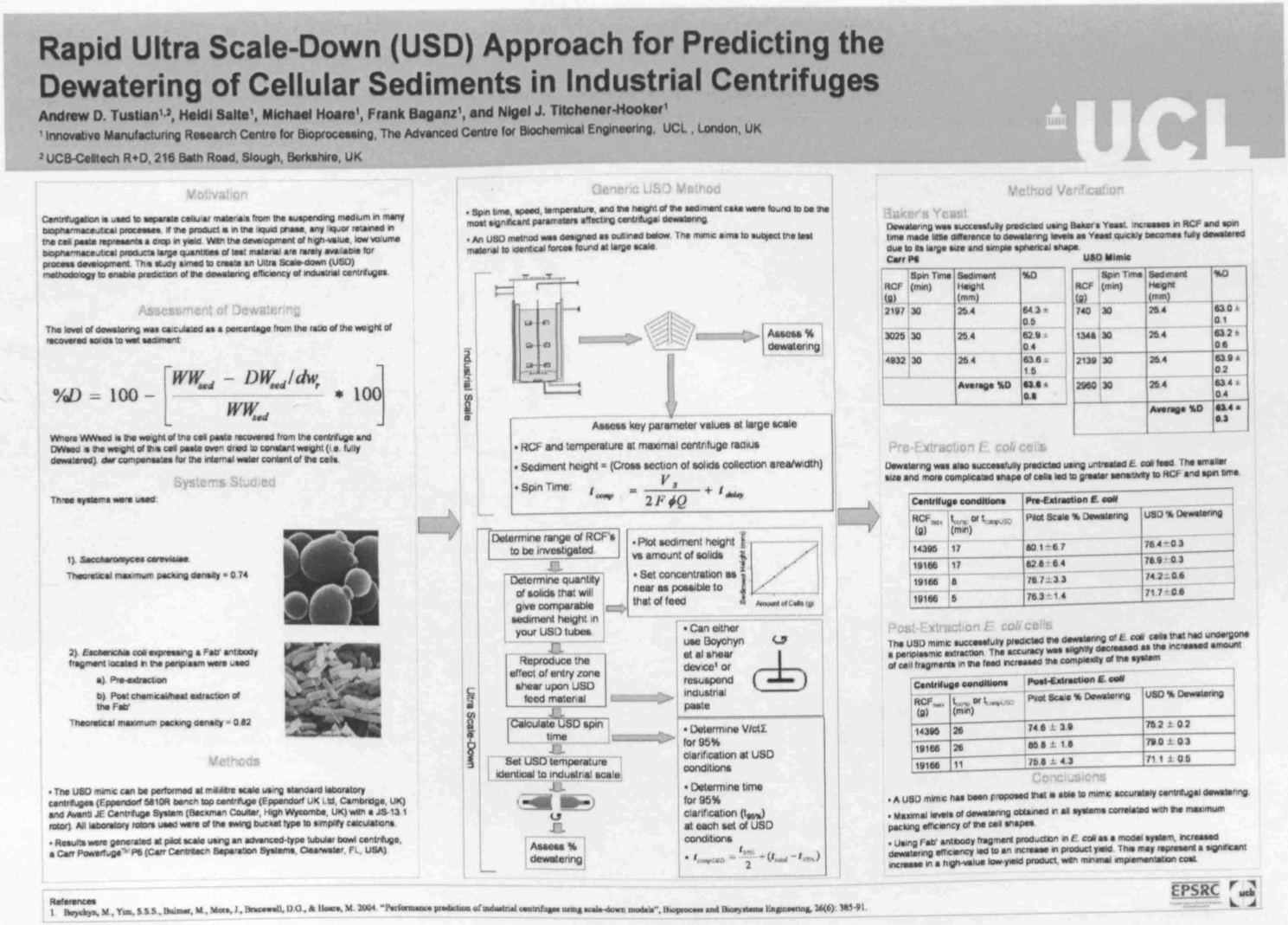

Fig. A5-2: Poster presented at the 'Annual bioProcessUK Conference 2006'.